

Mechanisms of Host Defense to Influenza Virus Infection

Jeffrey Downey

Meakins-Christie Laboratories

Department of Pathology

McGill University, Montreal, Quebec, Canada

August 2020

A thesis submitted to McGill University in partial fulfillment of the requirements for the
degree of Doctor of Philosophy

© Jeffrey Downey, 2020

ABSTRACT

Influenza viruses cause severe, recurrent respiratory infections that have afflicted humans since at least the Middle Ages. Despite this long evolutionary period, today, clinicians are still hampered by limited prophylactic and therapeutic treatments for the lethal complications of influenza infection. Virus-encoded virulence factors and immune evasion strategies that efficiently dampen and subvert the host's immune response, as well as an incomplete understanding of the mechanisms that comprise an effective immune response all hinder development of clinical interventions against influenza. Thus, studies that provide greater insight into pulmonary host-pathogen interactions during influenza infection are of urgent need.

It has been demonstrated that host defense to infectious diseases is comprised of two arms: 1) host resistance that directly inhibits pathogen replication at the site of infection and 2) disease tolerance, which mitigates collateral tissue damage caused by the inflammatory response and/or pathogen virulence factors. While anti-influenza drugs that block viral egress by inhibiting neuraminidase protein function are available, the antiviral efficacy and disease amelioration of these drugs are minimal, as a result of emerging resistant strains and general ineffectiveness of these drugs. Moreover, seasonal influenza vaccines are widely deployed and attempt to generate antibody-mediated memory responses against surface hemagglutinin viral-proteins to block entry of the virus. Yet, they also exhibit variable efficacies, due in part to high viral mutation rates. Collectively, the currently available therapeutic interventions that directly affect viral replication and conventional vaccine strategies specific to influenza are clinically imperfect. Thus, the central hypothesis of this thesis is that targeting both host resistance and disease tolerance are required for generating fully effective immunotherapeutic and vaccine strategies against influenza viruses. As such, it was the goal of this body of work to better understand the nature of host-influenza interactions and to provide targetable pathways for future influenza therapies.

The first part of the thesis emphasizes upon host resistance and describes receptor-interacting serine/threonine protein kinase 3 (RIPK3) as a critical component of macrophage antiviral immunity to influenza infection. RIPK3 had been primarily described in the

necroptotic pathway of cell death, which was known to have potent antiviral characteristics to certain viral infections. However, we found that rather than regulating macrophage necroptosis, RIPK3 activated multiple antiviral pathways in macrophages to promote IFN-I responses in response to influenza virus infection. Correspondingly, mice lacking RIPK3 were more susceptible to infection, exhibiting reduced pulmonary IFN-I levels and elevated viral titres that were abrogated by exogenous administration of IFN- β . Thus, agonists of RIPK3 are interesting prospects in enhancing host resistance to influenza infection.

The second part of this thesis focuses on disease tolerance, where we define an essential role for mitochondrial cyclophilin D (CypD) in regulating immunopathology during influenza infection. In contrast to RIPK3 deficiency, *CypD*^{-/-} mice were more susceptible to infection due to enhanced pulmonary tissue damage, rather than impaired host resistance. A reduction in the production of the epithelial regenerative cytokine IL-22 by NK cells was responsible for the elevated tissue damage in *CypD*^{-/-} mice. Concordantly, intranasal administration of IL-22 assisted in pulmonary tissue repair and improved survival of *CypD*^{-/-} mice, without modulating host resistance to influenza infection. Thus, activation of the CypD/IL-22/NK cell axis is indispensable upon infection, which underscores the importance of disease tolerance in immunity to influenza.

In the last part of this thesis, we focus on *unconventional* approaches to influenza vaccines. Conventional influenza vaccines generate highly specific adaptive memory responses but are often mismatched to circulating strains and, thus, are not fully effective. As the vast majority of species rely solely on innate immunity for host defense, it stands to reason that a critical evolutionary trait like immunological memory would have evolved in this primitive branch of our immune system. While the concept of the innate memory response (termed trained immunity) is “unconventional”, there is ample evidence that vaccines such as the Bacillus Calmette-Guerin (BCG) induce trained immunity to provide protection against TB as well as other pathogens. Yet, the exact mechanisms of “off-target” BCG protection remain unclear. To better understand this phenomenon, we dissected the cellular and molecular mechanisms of hematopoietic stem cells in generating or impairing trained immunity. Finally, using the inducers of trained immunity BCG and β -Glucan, we investigated their potential as unconventional vaccines against

influenza. Both BCG- and β -Glucan-vaccinated mice were remarkably protected against influenza, by enhancing host resistance and disease tolerance mechanisms, respectively. These data indicate that trained immunity can provide heterologous protection against influenza virus, which has important implications in future vaccine design.

Taken together, this thesis outlines novel pathways of host resistance and disease tolerance to influenza infection that can be targeted for host immunotherapy and offers trained immunity as a promising unconventional vaccine strategy.

RÉSUMÉ

Les virus de l'influenza sont responsables d'infections respiratoires sévères et récurrentes qui affectent les humains depuis au moins le Moyen-Âge. Malgré cette longue période évolutive, les options thérapeutiques et prophylactiques des cliniciens pour protéger contre les potentielles complications fatales des infections grippales sont toujours limitées à ce jour. Les facteurs de virulence encodés par le virus et les stratégies d'évasion de la réponse immunitaire qui atténuent et subvertissent la réponse de l'hôte, ainsi qu'un manque de connaissances des mécanismes qui conduisent à une réponse immunitaire efficace, ralentissent le développement de nouvelles thérapies pour lutter contre les virus de l'influenza. C'est pourquoi des études améliorant notre compréhension des interactions hôte-pathogènes durant les infections pulmonaires par le virus de l'influenza sont requises.

Il a été démontré qu'une réponse immunitaire efficace face aux infections repose sur deux stratégies: 1) la résistance de l'hôte, qui inhibe directement la réplication du pathogène sur le site de l'infection et 2) la tolérance à la maladie, qui atténue les dommages tissulaires collatéraux causés par la réponse inflammatoire et/ou les facteurs de virulence des pathogènes. Bien que des médicaments anti-influenza bloquant la sortie du virus en inhibant la fonction de la protéine neuraminidase soient disponibles, leur efficacité antivirale et leur effet sur l'amélioration des symptômes sont limités dû à une augmentation de la résistance des virus et à une inefficacité générale. De plus, même si les vaccins contre la grippe saisonnière sont largement administrés et visent à générer une réponse mémoire médiée par les anticorps ciblant les protéines de surface hémagglutinines pour bloquer l'entrée du virus, ils présentent une efficacité variable due en partie à une fréquence de mutation élevée du virus. Ces données suggèrent que les interventions thérapeutiques qui affectent directement la réplication du virus et les stratégies de vaccination conventionnelles spécifiques aux virus influenza sont cliniquement imparfaites. Ainsi, l'hypothèse centrale de cette thèse est qu'il est nécessaire de cibler à la fois la résistance de l'hôte et la tolérance à la maladie pour générer des immunothérapies et des stratégies vaccinales efficaces contre les virus de l'influenza. L'objectif de ces travaux de thèse est de mieux comprendre les interactions hôte-pathogène dans les

infections grippales afin d'identifier de nouvelles approches pour le développement de futures thérapies contre les virus de l'influenza.

La première partie de cette thèse est portée sur la résistance de l'hôte et décrit la protéine sérine/thréonine kinase interagissant avec des récepteurs 3 (RIPK3) comme un élément essentiel de l'immunité antivirale des macrophages dans les infections par le virus de l'influenza. RIPK3 a principalement été décrite pour ses fonctions dans la nécroptose, un mode de mort cellulaire qui participe à l'immunité antivirale lors de certaines infections. Cependant, nos travaux montrent qu'indépendamment de la régulation de la nécroptose des macrophages, RIPK3 active de multiples voies antivirales des macrophages pour favoriser la production d'interféron de type I (IFN-I) après infection par le virus influenza. En conséquence, les souris déficientes pour RIPK3 sont plus susceptibles à l'infection par le virus influenza, présentant une réduction des niveaux pulmonaires d'IFN-I et une augmentation de la réplication virale, pouvant être corrigée par l'administration d'IFN- β exogène. Ainsi, l'utilisation d'agonistes de RIPK3 ouvre des perspectives intéressantes pour augmenter la résistance de l'hôte lors d'infections grippales.

La deuxième partie de cette thèse s'intéresse à la tolérance à la maladie et définit le rôle essentiel de la protéine mitochondriale cyclophiline D (CypD) dans la gestion de l'immunopathologie pulmonaire dans les infections grippales. Contrairement à la déficience en RIPK3, les souris déficientes pour la protéine CypD sont plus sensibles à l'infection par le virus influenza, non pas à cause d'une résistance de l'hôte défectueuse, mais à une augmentation des dommages tissulaires pulmonaires due à un défaut de production de la cytokine IL-22 par les cellules NK, impliquée dans la régénération de l'épithélium. En conséquence, l'administration intranasale d'IL-22 recombinante améliore la survie des souris *CypD*^{-/-} en favorisant la réparation des tissus pulmonaires, sans affecter la résistance de l'hôte. Ainsi, l'activation de l'axe CypD/IL-22/cellule NK est indispensable après infection et souligne l'importance de la tolérance à la maladie dans l'immunité contre les infections par le virus influenza.

Dans la dernière partie de cette thèse, nous nous sommes concentrés sur les approches *non conventionnelles* de vaccination contre le virus de l'influenza. Les vaccins conventionnels qui génèrent des réponses immunitaires mémoires hautement spécifiques ne sont pas toujours

en adéquation avec les souches d'influenza en circulation et ne sont donc pas complètement efficaces. Comme la plupart des espèces repose uniquement sur l'immunité innée pour la défense de l'hôte, il semble probable qu'un trait évolutif critique comme la mémoire immunologique ait évolué au sein de cette branche primitive de notre système immunitaire. Bien que le concept de réponse mémoire innée (appelée immunité entraînée) soit « non conventionnel », il existe de nombreuses indications que le vaccin Bacillus Calmette-Guérin (BCG) induit l'immunité entraînée qui confère une protection contre la tuberculose ainsi que d'autres pathogènes. Cependant, les mécanismes précis impliqués dans ce processus ne sont pas encore élucidés. Pour mieux comprendre ce phénomène, nous avons disséqué les mécanismes moléculaires et cellulaires des cellules souches hématopoïétiques impliqués dans la génération ou l'altération de l'immunité entraînée. Enfin, nous avons analysé le potentiel du BCG et du β -glucane, des inducteurs de l'immunité entraînée, comme vaccins non conventionnels contre le virus influenza. Les souris vaccinées par le BCG ou le β -glucane sont protégées de l'infection par le virus influenza, et présentent une augmentation des mécanismes de résistance de l'hôte et de la tolérance à la maladie, respectivement. Ces résultats indiquent que l'immunité entraînée peut conférer une protection croisée contre le virus influenza avec d'importantes implications pour le développement de futurs vaccins.

Collectivement, les travaux de cette thèse décrivent de nouveaux mécanismes de résistance de l'hôte et de tolérance à la maladie qui peuvent être ciblés pour l'immunothérapie de l'hôte et présentent l'immunité entraînée comme une stratégie de vaccination non conventionnelle prometteuse.

ACKNOWLEDGEMENTS

I must begin, first and foremost, by extending my sincerest gratitude to my supervisor Dr. Maziar Divangahi. Since our first fateful meeting on the volleyball court nearly a decade ago, all the way through to the final days of this thesis submission, it has been a pleasure to learn from you and grow both personally and scientifically. It has been quite a run, full of many successes and failures, but what has remained constant through both extremes has been your support. It is this committed and caring mentorship that has made it a pleasure to be a part of your laboratory for the last several years. I appreciate you taking a chance on me and I will be forever grateful for this opportunity. I look forward to the future and our continued collaboration together.

I would also like to thank all the members of the Divangahi lab over the years that helped contribute to this fun and invigorating environment. You have each contributed uniquely to my experiences here and I could not be more grateful to have met you all. A particular thank-you to Dr. François Coulombe who helped pave the way for Ph.D students in the lab and worked tirelessly with me from the beginning to train and mould me from a fledgling to more independent scientist. I equally acknowledge Dr. Nargis Khan, whose experimental precision, indefatigable attitude towards science and cheerful personality never fail to inspire me. A very special thank-you to Dr. Erwan Pernet, who has undoubtedly transcended the realm of scientific colleague to that of close friend. Thank-you for your help with this thesis and all that you have done on my behalf over the years. To other students that kept science enjoyable along the way, including Laura Mendonca, Jonathan Dunn, Alissa Rutman, Jessika Royea and Michael O’Sullivan, I appreciate you all. I extend my gratitude to all my collaborators over the years, both internal and external, including my committee members Dr. Carolyn Baglole and Dr. Simon Rousseau for their insight during meetings, as well as our close and constant collaborators: Dr. Irah King, Dr. James Martin, and Dr. Martin Richer—who have often likely unwittingly provided strong productive influence on my studies.

Additionally, I offer my heartfelt appreciation to my family and friends outside of the laboratory. To my parents for their boundless support, you have made everything attainable through your sacrifice and dedication. Thanks to my brothers: David, for being a role model

and an endless source of good times, and Dr. Michael Downey for motivating me to pursue continued studies in academia and providing an endless familial mentor. Finally, to my many friends stemming directly or indirectly from the 2009-2010 McGill volleyball team, it has been an absolute delight throughout and I'm certain the good times are just getting started. I cannot describe how valuable all your friendships are to me; although certainly, I am happy to remain "Team Quebec" forever. To Ryan Brant, here's to a prosperous year...

TABLE OF CONTENTS

ABSTRACT	ii
RÉSUMÉ	v
ACKNOWLEDGEMENTS	viii
TABLE OF CONTENTS	x
CONTRIBUTION TO ORIGINAL SCIENTIFIC KNOWLEDGE	xiv
CONTRIBUTION OF AUTHORS	xvi
LIST OF ABBREVIATIONS	xvii
CHAPTER 1:	xxiv
INFLUENZA: AN INTRODUCTION TO THE DISEASE AND HOST-INFLUENZA INTERACTIONS IN THE LUNG	xxiv
1.1: Introduction	xxv
1.2: The influenza virus: a threatening pulmonary pathogen.....	xxvi
1.2.1: Overview of influenza viruses.....	xxvi
1.2.2: Influenza virus genome and structure	xxviii
1.2.3: Influenza virus replication.....	xxix
1.2.4: Anti-influenza pharmaceuticals.....	xxxi
1.2.5: Influenza as a disease	xxxii
1.2.6: Virulence factors of influenza viruses.....	xxxiv
1.2.7: Secondary bacterial pneumonia following primary influenza infection	xxxvii
1.2.8 The mouse model of IAV infection.....	xxxviii
1.3: Epidemiology of influenza infections and a century of pandemics	xli
1.3.1: Seasonal epidemic influenza infections	xli
1.3.2: Pandemic influenza infections.....	xlii

1.4: The immune response to influenza virus infection	xlvii
1.4.1: The lung as a unique entry point for influenza viruses and other pathogens	xlvii
1.4.2: The immune system.....	xlvii
1.4.3: Pulmonary host defense mechanisms.....	xliv
1.4.4: Mechanical and chemical responses in the lung	1
1.4.5: Host resistance mechanisms to IAV.....	li
1.4.6: Mechanisms of Disease tolerance to influenza virus infection	lxv
1.4.7: The bone marrow as the control centre for hematopoiesis and immune regulation..	lxix
1.5: Vaccination as a strategy against IAV	lxxxiii
1.5.1: Conventional influenza vaccination	lxxxiii
1.5.2: Potential universal influenza vaccinations	lxxv
1.5.3: Unconventional vaccination: Trained innate immunity	lxxvii
1.5.4: The bone marrow as the critical site for trained immunity	lxxxviii
1.5.5: Moving towards a more effective influenza vaccine.....	lxxxix
1.6: Rationale	lxxxix
1.6.1: Main hypotheses.....	lxxxix
1.6.2: Major objectives	lxxxix
PREFACE TO CHAPTER 2	lxxxiii
CHAPTER 2:.....	lxxxiv
RIPK3 interacts with MAVS to regulate type I IFN-mediated immunity to Influenza A Virus infection.....	lxxxv
2.1 Abstract	lxxxvi
2.2 Author Summary.....	lxxxvii
2.3 Introduction	lxxxviii

2.4 Results	xc
2.5 Discussion	xcv
2.6 Materials & Methods.....	xcix
2.7 Acknowledgements	cvi
2.8 Figures.....	cvii
PREFACE TO CHAPTER 3	cxii
CHAPTER 3:.....	cxiii
Cyclophilin D promotes disease tolerance to influenza A virus infection by licensing NK cell development and function	cxiv
3.1: Summary	cxv
3.2: Abstract	cxvi
3.3: Introduction.....	cxvii
3.4: Results.....	cxx
3.5: Discussion	cxxix
3.6: Materials & Methods	cxixiii
3.7: Acknowledgements	cxixix
3.8: Figures.....	cxl
PREFACE TO CHAPTER 4	cxlv
CHAPTER 4:.....	cxlvi
<i>M. tuberculosis</i> reprograms HSCs to limit myelopoiesis and impair trained immunity via a type I IFN/iron axis.....	cxlvii
4.1: Highlights.....	cxlviii
4.2: Abstract	cxlix
4.3: Introduction.....	cl

4.4: Results	cliii
4.5 Discussion	clxix
4.6: Materials & Methods	clxxiv
4.7: Acknowledgements	cxciv
4.8: Figures.....	cxcv
PREFACE TO CHAPTER 5	ccii
CHAPTER 5:.....	cciii
Trained immunity as a vaccination strategy against influenza A virus infection.....	cciv
5.1: Summary	ccv
5.2: Abstract	ccvi
5.3: Introduction.....	ccvii
5.4: Results & Discussion	ccix
5.5: Materials & Methods	ccxiv
5.6: Acknowledgements	ccxvii
5.7: Figures.....	ccxviii
CHAPTER 6:.....	ccxxi
DISCUSSION, MAIN CONCLUSIONS AND FUTURE DIRECTIONS	ccxxi
6.1: Phases of the immune response: resistance versus tolerance.....	ccxxii
6.2: Harnessing the power of immune training in vaccination against influenza	ccxxix
6.3: Concluding remarks	ccxxxiii
BIBLIOGRAPHY:.....	ccxxxiv
APPENDICES:.....	cclxxii

CONTRIBUTION TO ORIGINAL SCIENTIFIC KNOWLEDGE

The results section of this thesis is comprised of chapters 2-5 and represents novel additions to the collective scientific knowledge. The thesis is submitted in accordance to the standards set out by McGill University and the Department of Pathology and is presented here in a “manuscript-based” format.

Chapter 2: In this published manuscript (1), we demonstrate that RIPK3 promotes host resistance to influenza by enhancing IFN-I responses by pulmonary macrophages and protecting against severe disease.

1. RIPK3 promotes IFN-I production in the lungs and airways of influenza infected mice by inhibiting pulmonary viral replication
2. RIPK3 specifically mediates IFN-I responses by influenza infected macrophages (both resident and recruited) to control viral replication within macrophages
3. RIPK3 acts transcriptionally to reduce IFN- β mRNA expression by interacting with MAVS and antagonizing RIPK1-mediated activation of the MAVS/TBK1/IRF3 IFN- β pathway
4. RIPK3 acts post-transcriptionally to stabilize IFN- β mRNA by activating PKR and preserving the Poly-(A) tail to specifically promote IFN- β translation
5. RIPK3-dependent necroptosis is not observed in macrophages following influenza infection

Chapter 3: In this submitted manuscript (submitted to *Journal of Experimental Medicine*, 2020), we elucidate a novel axis of disease tolerance to influenza infection. We demonstrate that mitochondrial Cyclophilin D (CypD) protects the epithelium of influenza infected mice by promoting IL-22 production by recruited NK cells, independently of viral replication.

1. CypD protects against influenza infection by minimizing pulmonary tissue damage, without altering viral titres
2. CypD licences NK cell maturation and activation in influenza infected mice to promote effector function

3. CypD restricts p53-associated cell death of NK cell progenitors during lymphopoiesis
4. CypD increases the production of epithelial protective IL-22 by NK cells to resolve pulmonary tissue damage
5. Specific transfer of CypD-sufficient NK cells protects mice against influenza-dependent pathology in an IL-22-dependent manner.

Chapter 4: In this published manuscript (2), we uncover that BCG and *Mtb* differentially reprogram hematopoietic stem cells in the bone marrow to confer beneficial or detrimental trained macrophage responses, respectively, to subsequent *Mtb* infection.

1. BCG and *Mtb* equally access the bone marrow, but uniquely reprogram HSCs for at least one-year post-exposure
2. Bone marrow-derived macrophages from *Mtb* infected mice are impaired in their anti-mycobacterial capacity both *in vivo* and *in vitro* via an IFN-I/iron axis
3. *Mtb* promotes lymphopoiesis at the expense of myelopoiesis by causing RIPK3-dependent necroptosis in committed myeloid, but not lymphoid, progenitors
4. Stem cells from *Mtb*-infected mice are severely compromised in their long-term reconstitution capacity

Chapter 5: In this manuscript in preparation, we highlight non-specific unconventional vaccine strategies against influenza A virus infection and provide evidence for trained immune responses in this observed heterologous protection.

1. BCG protects against lethal influenza A virus infection and enhances antiviral immune responses
2. Live BCG vaccination generates a unique subset of effector memory $\alpha\beta$ T-cells that express CX₃CR1 and enter the lung parenchyma to potentially combat influenza infection
3. Macrophages from BCG-vaccinated mice are trained and produce more inflammatory and antiviral cytokines upon *in vitro* infection
4. Dectin-1 agonist β -Glucan provides protection against subsequent influenza A virus infection by promoting disease tolerance

CONTRIBUTION OF AUTHORS

The work described in this thesis was completed under the direction of Dr. Maziar Divangahi. In this section, authors are denoted by their initials (e.g. Jeffrey Downey, JD). Their respective contributions to each chapter are detailed below:

Chapter 1: The literature review was written by JD. Some portions of the introduction are adapted from the invited review “Dissecting host cell death programs in the pathogenesis of influenza” published in *Microbes & Infection* and written by JD, EP, FC and MD (3).

Chapter 2: JD, EP and MD wrote the manuscript and designed experiments. JD performed all *in vivo* experimentation, while the majority of *in vitro* experiments were performed by EP. Additional experimentation was done by FC, BA, IM, JJ, SQ, DCV, JGM and PJ provided technical support, expertise and reagents as required.

Chapter 3: JD performed all experimentation with assistance from EP. JD analyzed data. JD and MD designed experiments and wrote the manuscript.

Chapter 4: JD and NK completed the majority of experiments. Genetic analyses were conducted by JS with assistance from AP, under the direction of LBB. NK performed all experiments involving *Mtb* and JD performed most experiments with Poly (I:C), β -Glucan and the ferritin-deletion model. BB generated the ferritin *lox/lox* mouse and performed some pilot experiments with SC, under the supervision of MPS. EA performed Imagestream experiments. EP and EK performed additional experimentation. AN, BM, CS, MPS, LBB provided expertise and reagents. MD conceived and supervised the project. JD, NK and MD designed experiments and wrote the manuscript.

Chapter 5: JD designed and completed all experiments and wrote the manuscript, under the direction of MD.

Chapter 6: JD wrote the discussion.

LIST OF ABBREVIATIONS

ADCC: Antibody-dependent cell mediated cytotoxicity

AEC: Alveolar epithelial cell

AIDS: Acquired immunodeficiency syndrome

Akt: Protein kinase B

AM: Alveolar macrophage

APC: Antigen presenting cell

ARDS: Acute respiratory distress syndrome

ASC: Apoptosis-associated speck-like protein containing a CARD

ATP: Adenosine triphosphate

BAL: Bronchoalveolar lavage

BCG: Bacillus Calmette-Guérin

BcL-xL: B-cell lymphoma-extra large

BCR: B-cell receptor

BM: Bone marrow

BMDM: Bone marrow-derived macrophage

CARD: Caspase activation and recruitment domain

CBF β : Core Binding Factor Beta

CCL: Chemokine (C-C motif) ligand

CD: Cluster of differentiation

CLP: Common lymphoid progenitor

CLR: C-type lectin receptor

cMoP: Ccommon monocyte progenitor

CMP: Common myeloid progenitor

COVID-19: Coronavirus disease 2019

CPSF: Cleavage and polyadenylation specificity factor

cRNP: Complementary ribonucleoprotein

CryoET: Electron cryotomography

CXCL: Chemokine (C-X-C motif) ligand

CypD: Cyclophilin D

DAI: DNA-dependent activator of IFN regulatory factors

DAMP: Danger/damage associated molecular pattern

DC: Dendritic cell

DMEM: Dulbecco's Modified Eagle Medium

DNA: Deoxyribonucleic acid

ECMV: Encephalomyocarditis virus

EID/TCID: Egg/tissue culture infectious dose

EPO: Erythropoietin

FDR: False discovery rate

Fe: Iron

Fth: Ferritin heavy chain

GAPDH: Glyceraldehyde 3-phosphate dehydrogenase

GAS: γ -activated sequences

GFP: Green fluorescence protein

GISRS: Global Influenza Surveillance and Response System

GM-CSF: Granulocyte-macrophage colony-stimulating factor

GMP: Granulocyte-monocyte progenitor

GO: Gene ontology

GP: Granulocyte progenitor

GSEA: Gene Set Enrichment analyses

H&E: Hematoxylin and eosin

H₂O₂: Hydrogen peroxide

HA: Hemagglutinin

HIV: Human immunodeficiency virus

HPAI: Highly pathogenic avian influenza

IAV: Influenza A virus

IBV: Influenza B virus

ICV: Influenza C virus

IDV: Influenza D virus

IFITM: IFN-inducible transmembrane protein

IFNAR: IFN-I receptor

IFNGR: Interferon-gamma receptor

IFN-I/II/III: Type I, II, or III interferon

IFNLR: IFN-lambda receptor

Ig: Immunoglobulin

IKK: IκB kinase

IL: Interleukin

ILC: Innate lymphoid cell

IM: Interstitial macrophage

IMM: Inflammatory monocyte/macrophages

iNOS: Inducible nitric oxide synthase

IRF: Interferon regulatory factor

ISG: Interferon stimulated gene

ISRE: Interferon-sensitive response elements

iv: Intravenous

JAK: Janus family kinases

LAIV: Live attenuated influenza vaccines

LCMV: Lymphocytic choriomeningitis virus

LD₅₀: Lethal dose of 50% of the population

LDH: Lactate dehydrogenase

LKS: Lineage⁻ cKit⁺ Sca-1⁺

LPS: Lipopolysaccharide

LTB₄: Lipid mediator leukotriene B₄

LT-HSC: Long-term hematopoietic stem cell

MAIT: Mucosal-associated invariant T cells

MAVS: Mitochondrial antiviral-signaling protein

MCMV: Murine cytomegalovirus

MDA5: Melanoma differentiation-associated gene 5

MDCK: Madin Darby Canine Kidney

MDP: Monocyte dendritic cell progenitor

MDP: muramyl dipeptide

MEM: Minimum essential medium

MGL: Macrophage galactose type C-type lectin

MHC: Major histocompatibility complexes

MLKL: Mixed lineage kinase domain like pseudokinase

mLN: Mediastinal lymph node

MMP-1: Matrix Metalloproteinase-1

MMR: Macrophage mannose receptor

Mpge1: Microsomal prostaglandin E synthase-1

MPP: Multipotent progenitor

MRSA: Methicillin-resistant *Staphylococcus aureus*

Mtb: *Mycobacterium tuberculosis*

Mx1: Myxovirus resistance protein 1

Mφ: Macrophage

NA: Neuraminidase

Nec-1: Necrostatin-1

NET: Neutrophil extracellular trap

NF-κB: Nuclear factor kappa-light-chain-enhancer of activated B cells

NK cell: Natural killer cell

NKP: NK cell progenitor

NLR: Nucleotide-binding oligomerization domain-like receptors

NP: Nucleoprotein

NS: Non-structural protein

OAS: Oligoadenylate synthetase

PAMP: Pathogen associated molecular pattern

PBS: Phosphate buffered saline

pDC: plasmacytoid dendritic cell

PFU: Plaque forming units

PGE₂: Prostaglandin E 2

PI3K: Phosphatidylinositol 3-kinases

PKR: Protein Kinase R

Poly (I:C): Polyinosinic:polycytidylic acid

Poly(A)-tail: 3' polyadenylation

Ppif: Peptidyl-prolyl isomerase F

PR8: influenza A/Puerto-Rico/8/34

PRR: Pattern recognition receptor

QC: Quality control

qPCR: Quantitative polymerase chain reaction

QVLP: Quadrivalent influenza vaccine replication

RAG: Recombination activating gene

RD-1: Region of difference 1

RIG-I: Retinoic acid-inducible gene I

RIPK1/3: Receptor-interacting serine/threonine protein kinase 1 or 3

RLR: RIG-I-like receptor

RNA: Ribonucleic acid

RNase-L: Ribonuclease L

ROS: Reactive oxygen species

RSV: Respiratory syncytial virus

RT-PCR: Reverse transcription polymerase chain reaction

S1P: Sphingosine-1-phosphate

SAR: Systemic acquired resistance

STAT: Signal transducer and activator of transcription

ST-HSC: Short-term hematopoietic stem cell

TBK1: TANK-binding kinase 1

TCR: T-cell receptor

T_{EM}: T effector memory cell

TGF- β : Transforming growth factor beta

T_h: T helper

tipDC: TNF/iNOS-producing dendritic cell

TLR: Toll-like receptor

TNF: Tumour necrosis factor

TRAIL: TNF-related apoptosis-inducing ligand

vRNP: Viral ribonucleoprotein

WT: Wild type

ZPB1: Interferon-inducible protein Z-DNA binding protein 1

β -Glucan: Beta-Glucan

CHAPTER 1:

**INFLUENZA: AN INTRODUCTION TO THE DISEASE AND
HOST-INFLUENZA INTERACTIONS IN THE LUNG**

1.1: Introduction

“There is a constant struggle going on throughout nature between the instinct of the one to escape its enemy and of the other to secure its prey”

-Charles Darwin: *Essay on Instinct* from *Mental Evolution in Animals* (4)

The near constant exposure of humans to invading infectious agents puts continual pressure on the immune system to evolve mechanisms that defend the host against invasion and dispel the pathogen. Collectively referred to as “**host defense**” strategies (5), these processes are essential in ensuring survival and returning the infected and inflamed tissue to homeostasis. However, adaptation is not only limited to the infected host, as it is equally important for the pathogen to evolve immune subversion mechanisms that support pathogen persistence and repeated transmission at the cost of host fitness (6). This essential, never-ending cycle of evolution/counter-evolution by host and pathogen has been termed an “evolutionary arms race” between organisms (7) As an important example of this continual arms race, infections with influenza viruses (**Figure 1.1**) have occurred since at least the 16th century, if not ancient times, and they remain the most common source of recurrent respiratory infections and hospitalizations today (8, 9). Despite yearly vaccination programs and approved anti-influenza drugs, influenza causes unwavering seasonal epidemics and sporadic, stochastic pandemics that occur at significant cost to humanity. In fact, since the beginning of the 20th century, four such pandemics have occurred and there remains continued risk of the arrival of a novel pandemic strain, likely arising from avian influenza sources (10). Thus, influenza’s success as a pathogen for centuries, without eradication or significant decline in annual morbidity, intimates at this arms race between host and pathogen, while underscoring the importance of better understanding host-influenza interactions in the lung. It was the goal of this body of work to delineate previously unappreciated mechanisms of immunity against influenza virus infection and propose novel strategies of protection outside of conventional antiviral therapies or vaccination. In light of

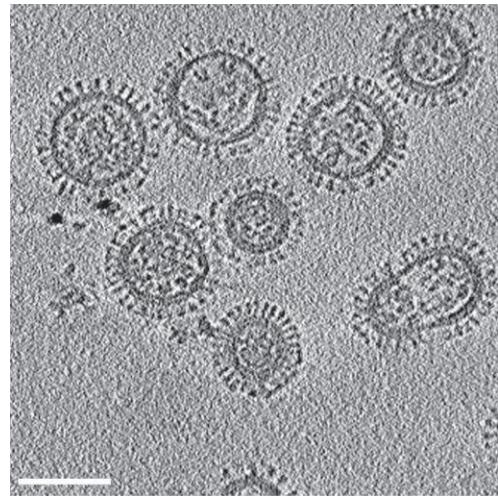


Figure 1.1: Influenza A Virus. Electron cryotomography (CryoET) image. Typical spherical morphology of influenza virions. Budding projections on the virion membrane are surface proteins Hemagglutinin and Neuraminidase, which facilitate virus entry and egress, respectively, as well as provide strain classification (*i.e.* H1N1). Scale bar represents 100 nM. Taken from (8).

our efforts, we suggest that immunomodulatory strategies that target the host's own immune response, in addition to those that target the virus directly, are promising avenues for future clinical intervention.

To begin, in chapter one, we review important concepts of influenza viruses, infections and the subsequent immune response in the lung. These immunological concepts focus on previously appreciated mechanisms of the host defense pathway, which helped guide this work and have evolved biologically, in part, from the continued immunological stress of the influenza virus on its human host.

1.2: The influenza virus: a threatening pulmonary pathogen

1.2.1: Overview of influenza viruses

Influenza viruses comprise 4 out of 6 genera of the *Orthomyxoviridae* viral family. Members of the family are enveloped viruses with a negative-sense, segmented RNA genome. Until recently, influenza viruses were thought to be comprised of three subtypes: A, B and C, of which all could infect humans (11). Recently, a fourth subtype influenza D was isolated from clinically ill swine (12). The ability of influenza D to infect humans has been suggested by antibody seroprevalence (13), yet its ability to cause symptomatic disease appears negligible (14). Influenza C virus infections produce only mild illness, while influenza B virus (IBV) infections can cause significant respiratory disease and occasional epidemics. Yet, importantly, B viruses cannot cause pandemics. Conversely, influenza A viruses (IAV) are by far the most threatening respiratory pathogen of the family to humans, being responsible for widespread seasonal epidemics and intermittent, devastating pandemics (15). Because influenzas B and C are almost exclusively confined to humans, with minimal spillover infections in animals and no known zoological reservoirs, they lack strain diversity and the high mutation rates needed to cause pandemics. On the other hand, the natural reservoir for IAV is the gastrointestinal and respiratory tracts of aquatic birds and IAV readily infects many different types of animals, thereby substantially increasing strain diversity and imparting pandemic-causing potential (16), as we will see in **section 1.2.6**.

Viruses of the influenza A genus are further defined by expression of hemagglutinin (HA) and neuraminidase (NA) glycoprotein subtypes on the surface of their virions. Although 16 unique HA and 9 NA subtypes have been isolated in avian hosts, only 3 HA and 2 NA readily infect and spread through humans.

Therefore, they are the ones capable of causing sustainable human disease and pandemics (11). Other rare HA/NA combinations of infections arising from birds have occasionally been observed in humans,

often causing severe, life-threatening illness. However, they are not able to readily transmit from human to human. These infectious strains are referred to as highly pathogenic avian influenzas (HPAI) and the most common subtypes seen in humans are H5N1 and H7N9, although infections from H7N3, H7N7, H9N2 and H10N8 have caused recorded deaths. The hazard of these viruses is that they will retain their pathogenicity, while mutating to allow for successful human transmission. Thus, HPAI strains remain an omnipresent pandemic risk.

As detailed in **section 1.3.2**, there have been four pandemics since the start of the 20th century, each marking the emergence of a new dominant human strain (**Figure 1.2**). In 1918, the devastating Spanish Flu was caused by an emergent H1N1 strain. The 1918 Spanish Flu exhibited incredible pathogenicity and transmissibility, being responsible for 50-100 million deaths. Descendants of this strain circulated until 1957, when they disappeared and were replaced by the Asian Influenza pandemic-causing H2N2 strain. In 1968, a novel reassortment H3N2 strain emerged in humans, leading to the third pandemic: The Hong Kong Flu. Surprisingly, strains stemming from pre-1957 H1N1 period re-emerged in 1977, circulating alongside H3N2 strains. Finally, the first pandemic of the 21st century occurred in 2009 following the appearance of an unrelated H1N1 that jumped directly from swine to humans, replacing old H1N1 strains. Since 2009, relatives of the Hong Kong H3N2 and Swine Flu H1N1 viruses have co-circulated in humans, each causing significant annual morbidity and mortality (17).

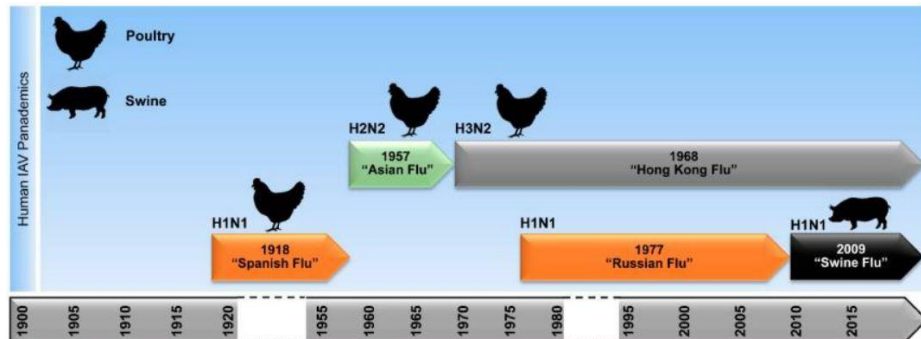


Figure 1.2: IAV subtypes in humans since 1918. Timeline of emerging IAV strains since the Spanish Flu pandemic. Since 1900 two unique H1N1, as well as one H2N2 and H3N2, strains have circulated in humans, causing pandemics. The animal of origin is indicated next to each subtype and year of origin. Taken from (16).

To better understand how these infections occur, manifest and transmit in humans, in the ensuing sections, we will explore the replicative cycle of influenza, the disease it causes and its virulence factors, focusing predominantly on the most threatening IAV.

1.2.2: Influenza virus genome and structure

All influenza viruses are composed of an anti-sense, segmented RNA genome. IAV and IBV viruses have 8 different segments, while ICV and IDV have 7, as the H and the N proteins are combined into a single protein and genomic segment (11). The 8 segments of

IAV and IBV viruses are numbered in decreasing length and encode for 10 essential proteins present within the virions, as well as up to several additional strain-specific proteins that have been identified (**Figure 1.3**) (16). Segments 1, 2 and 3 encode for the virus polymerase proteins PB2, PB1 and PA, respectively, and in some A viruses, segment 2 can also encode for the virulence factor protein PB1-F2 (18), while segment 3 can encode PA-X (19)

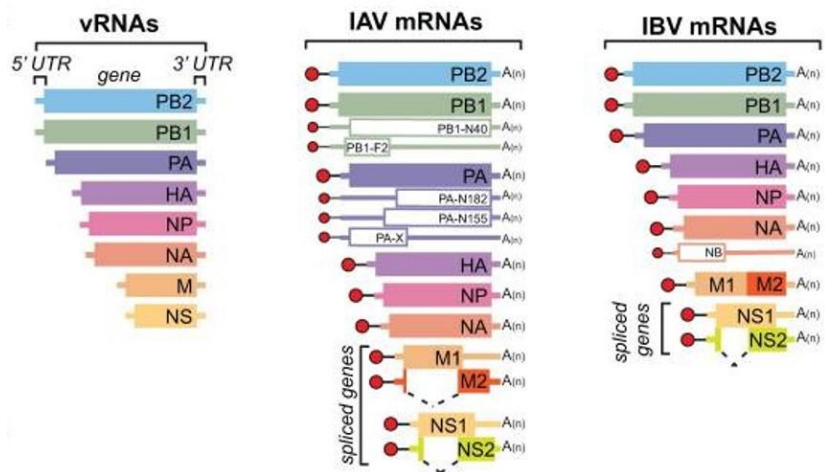


Figure 1.3: Genetic segments of influenza viruses. The 8 segments of influenza A and B viruses numbered by length and named by encoded proteins (left). The resulting mRNA products from each gene segment for IAV (centre) and IBV (right). Note the discrepancies between viral proteins arising from segments 2 and 3, which add virulence to IAV but are absent from IBV. Taken from (15).

from alternative reading frames. No known analogues of PB1-F2 or PA-X exist in B, C or D viruses, providing one reason for their decreased virulence (11). In IAV, the surface proteins HA, NA and M2 are translated from segments 4, 6 and 7, and functionally they facilitate viral entry, in the cases of HA and M2, and egress, in the case of NA, from cells. HA is the most prevalent protein on the virion surface, followed by NA at a 1:4 ratio and M2 at a roughly 1:100 ratio. Segment 7 additionally gives rise to the M1 protein by alternative splicing and M1 underlies the viral envelope and provides structure to the virion. Viral nucleoprotein (NP) is encoded on segment 5 and it is packaged into a hairpin structure, along with the genomic viral RNA (vRNA) and the polymerase proteins, collectively known as the viral ribonucleoprotein

or vRNP. Finally, segment 8 gives rise to two proteins: non-structural protein 1 (NS1) and 2 (NS2), both of which are present in very low amounts in virions, but are upregulated dramatically in infected cells (20). NS1 has many functions and is the chief virulence factor of influenza viruses (21), as it strongly manipulates host immune responses by predominantly interfering with IFN-I and cell death pathways. The role of NS2 is not as well-studied; however, it is known to facilitate export of vRNP segments from the nucleus, which is critical for viral replication (22). In IBV there are 4 surface proteins: HA, NA, and, rather than M2, NB and BM2. C and D viruses replace the HA and NA proteins with a single surface protein and also express a minor matrix protein similar to M2 (11).

Morphologically, IAV and IBV virions can exist in spherical or filamentous forms, with spherical being the most prevalently recovered from patients, while ICV and IDV can only be spherical. Although the exact consequence of filamentous virions is not understood, recent evidence suggests they enhance viral spread and persistence within the lungs *in vivo* (23). Importantly, in laboratory-passaged IAV strains using Madin-Darke Canine Kidney (MDCK) cells, the filamentous form is almost entirely lost, due to enhanced rigidity of the M1 protein that shapes the virion (16). Thus, it is important to consider that some biological relevance of filamentous IAV virions may be lost experimentally, as a consequence.

1.2.3: Influenza virus replication

Influenza viruses enter the human respiratory system through contact with infected surfaces, large virus-containing respiratory droplets or, most effectively, through small aerosols (24). The major site of productive replication for IAV is epithelial cells lining the respiratory tract, so early infection is maintained in upper airway epithelial cells, such as those found in the nose and nasopharynx. IAV replication is a multi-step process that requires both the cellular machinery of the host and virus-encoded proteins (**Figure 1.4**). Infection is initiated by interactions between IAV HA and terminal sialic acid residues on the plasma membrane surfaces of susceptible host cells (**step 1**). Sialic acids are bound to carbohydrates primarily through two linkages: $\alpha(2,3)$ or $\alpha(2,6)$ (25). HA specificity for 2,3 or 2,6 linkages is critical in determining pathogenicity and species tropism of IAV. Human influenza viruses recognize $\alpha 2,6$ linkages, while avian and equine viruses recognize $\alpha 2,3$ linkages. Interestingly, swine influenzas indistinguishably recognize either linkage and this makes them ideal mixing-pots for multiple IAV strains.

Following interaction between HA and the sialylated glycans, viral entry occurs mainly via receptor-mediated clathrin-dependent endocytosis for spherical influenza forms, or macropinocytosis for

filamentous influenza virions (26) (**step 2**). Once intracellular, the endosome is further acidified to ~pH 5 and this prompts a conformational change in the HA protein that exposes a fusion domain that permits fusion of the viral envelope with the endosome. Endosomal acidity is species-dependent; thus, this biological factor provides an additional mechanism of viral tropism (27). For human viruses, this fusion is facilitated by the cleavage of HA at a single arginine site by extracellular trypsin-like proteases that cleave the HA into activated HA1 and HA2 subunits. Presence of hydrogen ions within the acidic milieu of the endosome causes the opening of the M2 ion channel that transverses the viral envelope to acidify the virion. Virion acidification triggers the loss of its structural integrity by freeing vRNPs from their scaffolding on the M1 protein and releases them into the cytoplasm of the host cell (16) (**step 3**).

Once the vRNPs have accessed the cytoplasm, their movement to the nucleus for replication is entirely dependent upon the nuclear transport system of the host. Each protein of the viral polymerase subunit contains a nuclear localization signal and import is mediated by the host α/β -importin system into the nucleoplasm (16). Upon entry to the nucleus, viral PB1, PB2 and PA proteins “snatch” the 5’ caps of endogenous mRNA, effectively hiding the existence of viral mRNA from the host, while enhancing positive-sense transcription by providing the necessary primers. This 5’ “cap-snatching” is an essential component of influenza pathogenesis and a quintessential example of a host subversion strategy. 3’

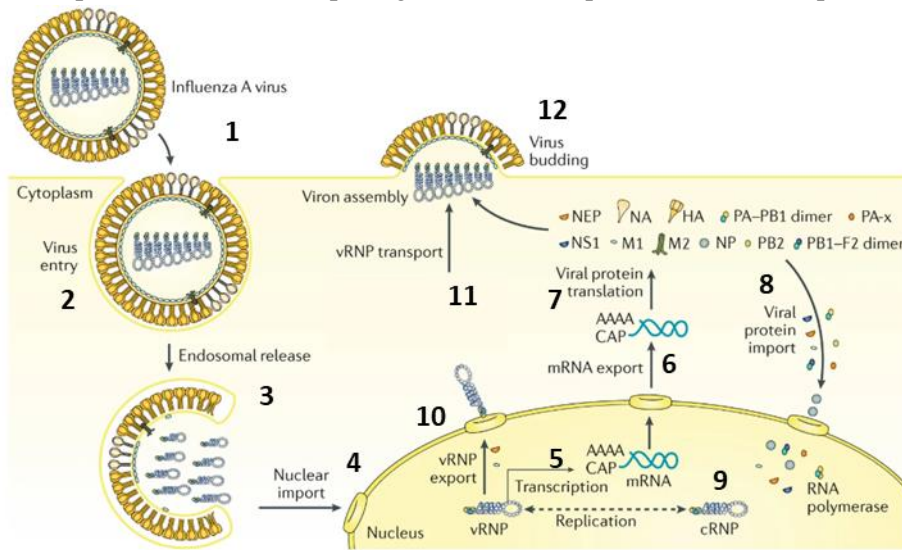


Figure 1.4: Influenza replication cycle. Influenza replication requires both host and viral machinery and proceeds through several steps as marked by the numbers in black and detailed in the text. Replication occurs in the nucleus, which is rare amongst RNA viruses. Adapted from (26)

polyadenylation (poly(A)-tail) then occurs through “stuttering” transcription by the viral polymerase, due to uracil repeats encoded within the viral genome (**step 5**). The transcribed viral mRNA is then exported and spliced akin to host mRNA transport and splicing mechanisms (**step 6**).

Translation then proceeds using host ribosomal machinery (16) (**step 7**).

Following translation, HA, NA and M2 are trafficked to and embedded within the cell membrane through the Golgi Apparatus, while the remaining viral proteins are transported back into the nucleus to generate

additional antisense copies of the vRNP (28) (**step 8**). Viral polymerases replicate genomic antisense vRNP from positive-sense complementary RNP (cRNP) intermediates that are slowly and inefficiently generated, because this process proceeds in the absence of primers (**step 9**). Complete vRNP replication, furthermore, requires the incorporation of newly synthesized viral NP returning from the cytoplasm (29). Thus, the transition away from viral mRNA transcription (early stage) towards the generation of new vRNPs (late stage) necessarily occurs at later timepoints post-infection, as it requires translation of the NP protein in the cytosol and translocation back into the nucleus, as well as the inefficient and slow creation of cRNPs from unprimed polymerase reactions. Once complete vRNPs are formed, they are exported from the nucleus using a combination of the host's nuclear export machinery and the viral M1 and NS2 proteins that expediate this process (**step 10**) (11). Importantly, this replication of influenza vRNP in the nucleus, rather than the cytoplasm, is exceedingly rare amongst RNA viruses, with *retroviridae* being the only other family of RNA viruses known to do this (16).

Following vRNP exit from the nucleus, they are transported to the cell membrane, where they interact with the HA, NA and M2 proteins that have accumulated there. In conjunction with the viral surface proteins, the envelope of the virus is generated using incorporation of the host's lipid membrane. The M2 protein specifically packages completed vRNPs into the virion and HA-mediated interactions with surface sialic acid residues are again formed (**step 11**). Mature and infectious progeny then bud off of the cell surface and, finally, sialic acid interactions are cleaved by the NA protein to release the infectious viral progeny (**step 12**). The cycle then repeats itself (28).

1.2.4: Anti-influenza pharmaceuticals

As detailed above, extensive study of the replicative cycle of influenza viruses has led to the generation of anti-influenza drugs. Initial classes of drugs, known as amantadines targeted the M2 protein, because of its importance in viral entry. Amantadines block M2 channel activity and prevent envelope uncoating. However, the M2 protein is not present on IBV, thus restricting amantadine usage to IAV infections—a distinction not immediately clear upon diagnosis. Moreover, the vast majority of circulating IAV strains are now completely resistant to current amantadines; therefore, their usage is precluded (11).

To overcome the restrictions of amantadines, currently prescribed and widely deployed anti-influenza drugs, such as Oseltamivir and Zanamivir, target the final step of the replication cycle by inhibiting neuraminidase activity, rather than entry. By acting as a sialic acid analogue, they bind the active

site of the neuraminidase protein and render it incapable of cleaving host-virus sialic acid interactions necessary for viral spread. Importantly, because these drugs target NA proteins, they are viable options against both IAV and IBV (11). Despite showing considerable efficacy in murine and *in vitro* studies, effects in humans are more controversial. Collectively, they show limited to no protection in the majority of cases and are only beneficial when delivered at early stages of infection, before symptoms develop (30, 31). Moreover, although resistance is currently low, emergent, highly-resistant strains have been noted and are expected to continually rise (32). Intriguingly, a novel drug that targets the “cap-snatching” mechanism of influenza replication has recently been developed and approved for usage in the United States in 2018 (33). The drug, Baloxavir Marboxil, inhibits the endonuclease activity of the PA viral protein to prevent the “snatching” of the 5’ cap of host mRNA to inhibit viral replication. Although its efficacy in practice is still unknown, it is thought to potentially prevent severe symptoms by only about 1 day. *It is, therefore, evident that past, current and emerging antiviral drugs are insufficient to combat influenza and novel therapeutic strategies are required.*

1.2.5: Influenza as a disease

Upon infection, IAV exhibits a short incubation period of 1-2 days, before a replicative burst causes a spectrum of disease severity, ranging from asymptomatic to fulminant. Clinically, the disease presents systemically with fever, chills, myalgia and general malaise, coupled with respiratory symptoms such as non-productive cough, sneezing, and sore throat or upper chest pain (8). Seasonal and mild influenza illnesses typically exhibit a fever that lasts 3 days, with a range of 2-8 days. Malaise and cough, on the other hand, can persist for weeks following the fever’s resolution (34). Experimentally, it has been noted that following sublethal infection in mice, pulmonary inflammation does not fully subside until over 4 weeks post-infection (35, 36). This suggests that long-term pulmonary remodelling occurs after influenza infection, which may have unappreciated effects on the progression of other infectious or inflammatory diseases of the lung. In line with this, IAV infections are strongly correlated with worsened allergic disease in mouse models (37) and asthma exacerbations in humans (38). Influenza infection, therefore, modulates pulmonary homeostasis far beyond acute viral-induced inflammation.

Because uncomplicated influenza clinically presents similarly to many respiratory infections, symptoms are, alone, insufficient to confirm diagnosis. Adequate confirmation of a suspected influenza infection is achieved as a balance between sensitivity and speed. Presently, three major classes of diagnostics exist, each with its associated pros and cons. These three classes are: viral culture, RT-PCR,

and rapid antigen detection assays. Classically, influenza viral culture was the gold-standard and it has near-perfect sensitivity; however, it is laborious and slow, originally requiring up to 10 days for results (27). The onset of rapid viral culture using centrifugation decreased the time dramatically to a few days, yet it is accompanied with a minor drop in specificity (70-90%) and is still relatively slow, with confirmation after about 3 days (8). RT-PCR is highly sensitive and specific, provides deep sequencing of viral variants and manufactures results in a few hours. Yet, it requires highly trained technicians and access to specialized equipment, so its use is limited as a point-of-care diagnostic. Conversely, modern point-of-care rapid antigen detection assays (that detect either the viral genome or nucleoprotein (27)) can be done on-site with results in approximately 15 minutes. These tests, though, are expensive, exhibit high technical expertise and have wildly variable sensitivities, ranging from 63% for seasonal infections and <40% during the 2009 pandemic (39). Thus, accurate detection of influenza infections remains a considerable hurdle that is further confounded by many co-circulating strains and pervasiveness of other respiratory viral infections (34).

Epithelial cells have long been appreciated as the major source of influenza virus replication and culturable virus can be retrieved from the upper and lower airways of infected individuals (40). The observation that the trachea, bronchi and alveoli epithelia represent the major sites of replication was first suggested by Winternitz and colleagues in 1919 (41) and immunofluorescence experiments, started during the 1957 H2N2 pandemic, confirmed presence of the virus within alveolar and tracheobronchial epithelial cells (42). Interpandemic and low virulence IAV strains fail to penetrate past the upper airways and sickness is, therefore, usually uncomplicated and mild in healthy individuals. Conversely, pandemic, avian and highly virulent seasonal infections can progress to primary viral pneumonia, as a result of translocation of the virus into the lower airways, with the most nefarious cases rapidly resulting in acute respiratory distress syndrome (ARDS). ARDS has a mortality rate of approximately 40% and manifests as a result of predisposing host and viral factors (34). Autopsies beginning with the 1889 pandemic, and cemented during the 1918 pandemic, supported this notion of epithelial tropism and increased severity with lower airway involvement, as histopathological observations of severe tracheitis, pharyngitis, tracheobronchitis and alveolitis were nearly ubiquitously described (43).

The near-universal occurrence of secondary bacterial infection in the early pandemics made demarcation between primary viral histopathological changes and secondary bacterial sequelae nearly impossible. However, today, with the onset of antibiotics and improved hygiene, viral pneumonia and ARDS are the primary causes of influenza-induced mortality (44). The major histological changes associated with severe disease are necrotizing alveolitis and bronchiolitis, coupled with hyalination of the alveoli, pulmonary hemorrhaging, wide-spread epithelial sloughing and complete denudation of the basement membrane (45) (**Figure 1.5**). Epithelial cell necrosis equally activates the vascular endothelium to increase permeability and cytokine release from pulmonary immune and structural cells (known as the “cytokine storm”) that is intimately linked to the onset of ARDS. Moreover, the breakdown of the epithelial-endothelial barrier compromises gas exchange and disrupts the osmotic pressure barrier that typically prevents pulmonary edema. As a result, respiratory insufficiency, stemming from edema and extensive alveolar hemorrhaging, is a major contributor to mortality (39).

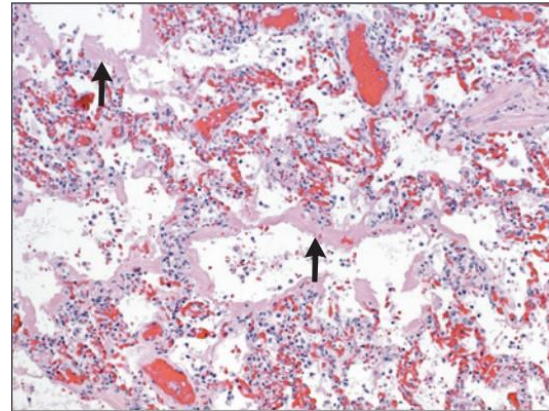


Figure 1.5: Histology from an autopsy of a 13-year-old boy during the 2009 pandemic. Hematoxylin and eosin staining of a lung section. Histological changes are as explained in the text and constitute massive inflammatory cell influx, pulmonary hemorrhaging and hyaline membrane formation (arrows). Death followed a seven-day clinical course and was likely caused by respiratory failure. Taken from (43).

1.2.6: Virulence factors of influenza viruses

Influenza viruses are ever-changing, and this persistent mutation drives continued influenza pathogenicity and yearly endemics. Mutation of influenza viruses is mediated by two distinct phenomena: antigenic drift and antigenic shift. Antigenic drift occurs in both IAV and IBV, but only IAV can mutate via antigenic shift. The surface proteins HA and NA contribute to the antigenic characterization of influenza viruses and antigenic drift results from point mutations in these genes. These small changes minimally affect the appearance of the HA or NA protein to the immune system, yet this drift is sufficient to compromise antibody or T-cell recognition, especially when multiple mutations are accumulated over time (46). Much of this form of mutation occurs within a singularly-infected human host, as antigenic drift appears as a by-product of the error-prone viral polymerase and indirectly due to the selection pressure of the host’s immune system during the host-pathogen arms race (46).

IAV can, furthermore, undergo antigenic shift. Antigenic shift occurs when an IAV strain acquires a completely different HA or NA gene segment and, as a result, the human population has no pre-existing protective immunity. This reassortment can occur only when a cell is infected with multiple IAV strains of different origins, such as human and avian. Although all influenza viruses have a segmented genome that permits antigenic shift, because IAV is the only influenza species with animal reservoirs and zoonotic infections, it is the only one capable of antigenic shift. Animals such as the swine are ideal vessels for antigenic shift, as they are equally and readily infected by avian, human and porcine IAV strains. Novel strains generated following antigenic shift are pandemic-causing strains and are, thus, the most dangerous as emergent strains (11, 27).

On an infection level, the major determinant of influenza severity is the ability of the virus to penetrate the upper airways and translocate to the lower airways. The majority of seasonal strains fail to do so and, as a result, cause mild, resolving illness. Pandemic and HPAI infections, on the other hand, exhibit an altered tropism and viral replication is often seen in the lower airways, resulting in a more severe prognosis (**Figure 1.6**). This movement is facilitated in part by the affinity of HA proteins for various sialic acid residues on the surface of epithelial cells. Avian influenza strains recognize with higher affinity $\alpha(2,3)$ linkages, while human strains utilize $\alpha(2,6)$ residues. Although both $\alpha(2,6)$ and $\alpha(2,3)$ linkages are found throughout the entirety of the human lung, HA that bind $\alpha(2,3)$ receptors preferentially infect the lower airways, due to a higher frequency of those receptors in the more distal portions of the lung. Importantly, although HPAI strains easily infect the lower airways and cause severe disease, this movement limits their infectious capacity. Human strains, conversely, replicate effectively in the upper airways to generate highly infectious virus-containing droplets that transmit rapidly between hosts. It is this alveolar tropism that enhances HPAI lethality, but severely limits human-to-human transmission. Interestingly, swine viruses equally recognize $\alpha(2,6)$ and $\alpha(2,3)$ linkages. Thus, pandemic strains, such as the 2009 virus that mutated in the swine host, can exhibit pronounced infiltration of the lower airways, which causes enhanced pathogenicity, while maintaining high levels of human transmission (47). In addition to HA sialic acid tropism, glycosylation sites on the HA protein are inversely correlated to pathogenicity. Heavily glycosylated viruses, like those commonly seen in seasonal infections, are more effectively trapped and expelled by the ciliary beat of the upper airways, while poorly glycosylated viral

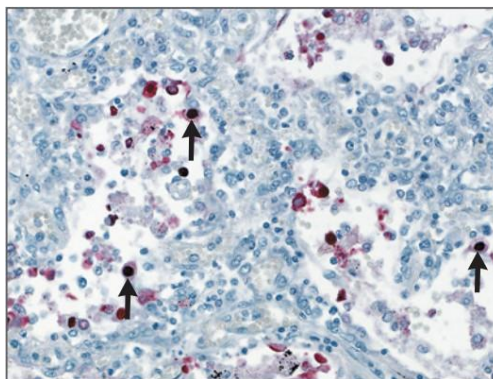


Figure 1.6: Histology from an autopsy of a 55-year-old woman during the 2009 pandemic. Arrows indicate the presence of IAV NP in the nuclei of alveolar type I and II pneumocytes. Staining is naphthol fast-red substrate and hematoxylin counterstain using an anti-IAV NP antibody. Taken from (43).

variants are able to penetrate distal pulmonary areas. In support of this, the HA protein of the 1918 virus exhibited a single glycosylation site (48). Frighteningly, a recent study showed that a single amino acid substitution in the HA of an H7N9 IAV strain was sufficient to confer human receptor preference and that this mutation also led to a loss of a glycosylation site, underscoring the pandemic potential of avian strains (49).

Studies using recombinant viruses expressing 1918 (50) or 2009 (47) HA and NA proteins on a seasonal IAV backbone, conclusively showed that expression of these proteins conferred pathogenicity, presumably in part through the mechanisms described above. Generally, HA from human strains must be cleaved by extracellular trypsin-like proteases present only in the respiratory and gastrointestinal tracts to infect cells, as human IAV HA expresses only a single cleavage site. This restrains replication to the lungs. Discordantly, HPAI strains possess several basic cleavage sites on their HA; thus, they are readily cleaved by ubiquitous furin-proteases found intracellularly in the Golgi network. This allows viral dissemination outside of the respiratory tract and is the underlying mechanism for systemic viral infection seen in cases of HPAI infection. Incredibly, the 1918 HA did not require trypsin for its infectivity and this likely explains why cases of multi-organ failure and systemic tissue involvement were reportedly observed during the Spanish Flu pandemic (50, 51). This peculiarity has not been noted again in human strains and likely underlies much of the astonishing pathogenicity of this virus.

Further to surface proteins as virulence factors of IAV, several other proteins encoded in their genome contribute substantially to virulence. The most extensively described virulence factor is the NS1 protein (21). Viruses engineered to not express NS1 show heavily attenuated virulence (52). NS1 antagonizes cellular responses at many different levels and is primarily studied for its role in inhibiting antiviral IFN-I/III responses. IFN-I induction following IAV infection occurs initially by activation of the RIG-I pathway through interactions with the 5'-triphosphate of viral ssRNA. RIG-I then translocates to mitochondria and interacts with the mitochondrial antiviral signaling protein (MAVS) to activate transcription factors IRF3 and NF- κ B, resulting in IFN-I and inflammatory cytokine production, respectively (53). NS1 initially blocks the induction of IFN-I by binding RIG-I and preventing its activation of MAVS (54). NS1 is also a potent repressor of translation of IFN genes by inhibiting host pre-mRNA 3' polyadenylation via interaction with the Cleavage and Polyadenylation Specificity Factor (CPSF) protein. This broadly suppresses mRNA transport and subsequent translation in the cytosol (55). Interestingly, viral mRNA is saved from this inhibition, as its polyadenylation is facilitated directly by the viral polymerase, independently of the host. Finally, NS1 also acts on the IFN pathway post-translationally. NS1 binds antiviral PKR, a major repressor of translation, to facilitate viral mRNA translation (56). It also blocks the

activation of the canonical interferon-stimulated gene (ISG) OAS, which is heavily upregulated following IFN-I signalling. OAS activates the otherwise latent RNA-L to degrade IAV RNA. The mechanism of this inhibition of OAS by NS1 appears to be indirect and occurs via sequestration of RNA away from OAS (57). The newly discovered PA-X protein also strongly suppresses host gene expression by inhibiting translation, through poorly understood mechanisms (58).

IAV also manipulates the immune response and enhances its virulence through regulation of cell death pathways. As we reviewed in (3), cell death manipulation by IAV is biphasic and variable depending on cell type. First IAV blocks early host-driven induction of apoptosis, which would remove its replicative niche. In addition to inhibiting IFN-I responses, initial expression of NS1 in infected cells equally activates the pro-survival PI3K/Akt pathway to permit early viral replication (59). Later during infection, NP expression and late-phase NS1 expression activate cell death pathways to promote viral dissemination (60). Moreover, the PB1-F2 protein expressed solely in IAV strains homes to the mitochondria, specifically within monocyte/macrophages, and induces the intrinsic pathway of apoptosis via cytochrome c release (61), which indirectly blunts IFN-I production by reducing macrophage numbers (62). Influenza viruses, therefore, disrupt host responses to infection at several different levels. These highly specific and effective mechanisms of antagonism intimately highlight the forever escalating arms-race of host versus pathogen. Further insight into the pathways of this antagonism is essential to combat highly lethal emergent IAV strains and generate more effective therapies.

1.2.7: Secondary bacterial pneumonia following primary influenza infection

Historically, the prevalence of secondary bacterial infection following influenza infections was nearly 100%. Yet, today bacterial pneumonia is present in as low as 10% of fatal cases (63). While certainly the usage of antibiotics and improved hospital and hygiene practices are primarily responsible for this reduction, it is unclear whether current circulating strains of influenza are also inherently less capable of promoting secondary bacterial infection. The frequency of secondary bacterial pneumonia is also IAV strain dependent, with circulating H3N2 strains having a higher propensity than H1N1 strains (64). The majority of bacterial pneumoniae result from *Streptococcus pneumoniae* or *Staphylococcus aureus* overgrowths and a minority of cases from other bacteria, such as *Haemophilus influenzae*. Currently, there are decreasing rates of *S. pneumoniae* infections, due in large part to vaccination, and an increase in *S. aureus* infections for which there is no vaccine and a steady rise in methicillin-resistant (MRSA) strains (64). Indeed, MRSA infections are of considerable concern in combatting influenza, particularly amongst elderly populations.

The mechanisms of secondary bacterial invasion are complex, and dependent upon host, bacterial and viral factors. In the upper airways, IAV infection disrupts the ciliary beat that typically prevents bacteria from entering the lower airways, causing it to slow and beat irregularly, limiting its ability to control bacterial invasion (48). Sloughing of the epithelium induced as a by-product of viral replication, reduces the effectiveness of mucus adherence to the epithelium and also enhances receptor availability for bacteria to bind. Similarly, the cleavage of sialic groups on the surface of epithelial cells during viral egress is associated with greater bacterial penetrance and adherence. Expression of NA by some strains of bacteria including subsets of *S. pneumoniae* further compounds this phenomenon. Additionally, the lower airways and kinetics of infections play critical roles in the progression of bacterial pneumonia. Influenza infection must precede bacterial infection for enhanced virulence, not vice versa (65), as IAV depletes the residential immune cell of the lower airways, alveolar macrophages (AM), shortly following infection. As AM are strongly bactericidal, this elimination by IAV dramatically impairs clearance of secondary bacterial infection (62, 66, 67). Moreover, the anti-inflammatory milieu required for wound healing and return to homeostasis at later time points post-IAV infection, indirectly provides a niche for bacterial invasion. For example, IFN-I signalling in the later stages of IAV infection is chiefly anti-inflammatory and synergizes with IL-10 to permit bacterial overgrowth in the lower airways, because of a broadly dampened immunological state and loss of pathogen recognition ability (48, 68). *Therefore, IFN-I, although critical in its antiviral capacity, additionally promotes secondary bacterial infection, highlighting the importance pathogen-specific responses and tight immune regulation.* Taken together then, both the inflammatory and anti-inflammatory environment promoted sequentially by IAV infection, as well as upper and lower respiratory involvement, contribute to the pathogenicity of influenza and the development of secondary bacterial pneumonia.

1.2.8 The mouse model of IAV infection

Animal models remain the best technique to study the immune response to influenza infection. Many animals can be infected experimentally, with ferrets and mice being the most commonly researched, followed by swine. Each animal model comes with its respective benefits and drawbacks, depending on the nature of the research question. Ferrets are predominately used because their pulmonary architecture is homologous to humans, as is clinical disease progression, including fever. Human IAV can readily infect ferrets, due to a prevalence of $\alpha(2,3)$ sialic linkages in the ferret lung and, critically, ferrets can transmit infectious virions from an infected host to an uninfected host through their sneeze reflex and nasal

secretions. They also support HPAI replication and extrapulmonary infection, as has been noted in humans. Thus, they are integral in understanding transmission and disease pathogenesis of circulating human or HPAI IAV strains. Because of their ability to transmit IAV, they are also extensively used to model vaccination efficacy. Unfortunately, in comparison to mice, housing is more expensive and ferrets lack reagents and genetic manipulation tools (i.e. knockout ferrets) that limit their overall use (69).

Mice, on the other hand, are small, inexpensive and have a vast repertoire of technical reagents and knockouts. Importantly, unlike ferrets, human strains do not readily infect mice and, thus, circulating IAV strains must be serially passaged multiple times to “adapt” them to the mouse. The most commonly used adapted laboratory strain, and the one utilized for the vast majority of this thesis, is the influenza A/Puerto-Rico/8/34 (H1N1), abbreviated as PR8. Other viruses are routinely used, such as IAV WSN, as an additional example of H1N1 viruses, X31 as a model of H3N2 infection or the IBV Flu B, all of which exhibit milder prognoses compared to the PR8 virus. Disease progression in the mouse is similar to humans, where viral loads peak at around 3 days post-infection and are often cleared by 10 days post-infection, when signs of morbidity become most evident. Inflammation is similarly observed for multiple weeks following infection. Infected C57BL/6 mice exhibit many similar symptoms to humans, such as anorexia, weight loss and lethargy, while additionally manifesting ruffled fur; rapid, shallow breathing; reduced posture and hypothermia. Based on the infecting dose, cachexia and mortality can result (70). Laboratory infectious doses are often described as lethal or sublethal, on the basis of the lethal dose of 50% of the population (LD_{50}) or the egg/tissue culture infectious dose (EID; TCID), as the allantoic fluid of chicken eggs or MDCK cell culture is used to propagate the virus in the laboratory. Although they vary dramatically from laboratory to laboratory, in our studies, the LD_{50} is ~90 plaque forming units (PFU) and the sublethal dosage (no mortality in male C57BL/6 mice) is 50 PFU. In all our studies, infections are performed intranasally with mice under anesthesia, although in some studies by other groups intratracheal infections are performed. However, intratracheal infections completely bypass replication in the upper airways, which deviates dramatically from natural infections and may alter results, correspondingly.

Histological changes following PR8 infection in mice are similar to those observed in humans during lethal infection, including severe alveolitis, epithelial necrosis, as well as pulmonary hemorrhaging and edema. Virally infected epithelial cells are present all down the respiratory tract. Moreover, the immune system and its response to pulmonary viral infection is evolutionarily highly conserved between mice and humans. *Thus, PR8 infection in the mouse accurately mirrors the inflammatory response and disease progression of life-threatening primary viral pneumonia in humans.* The major drawback to the mouse model is, however, that it ineffectively maps uncomplicated seasonal IAV infections, which represent the

majority of disease in humans. Furthermore, mice do not readily produce infectious secretions of IAV, so their usage is precluded from transmission studies (71). Thus, increased combination of ferret and mouse models, as a more complete surrogate of human disease, is an important research strategy to more comprehensively investigate both immunity to and transmission of IAV.

1.3: Epidemiology of influenza infections and a century of pandemics

“Influenza killed more people in a year than the Black Death of the Middle Ages killed in a century; it killed more people in twenty-four weeks than AIDS has killed in twenty-four years.”

- John M. Barry: *The Great Influenza: The Story of the Deadliest Pandemic in History* (72)

1.3.1: Seasonal epidemic influenza infections

Although influenza infections are thought to subsist in human hosts at low levels throughout the entire year, there is a marked increase during “flu season”, which occurs during winter months in temperate climates, like those experienced in Canada and the United States. Seasonal influenza epidemics appear locally suddenly, peak for 2 to 3 weeks and linger for anywhere from 5 to 10 weeks (73). In North America this period of time is typically between November to March, while in the southern hemisphere the season generally runs from May to September. In tropical zones, influenza infections are equally prevalent as in temperate climates; however, the degree of seasonality and the predictability of infection is much less defined, which poses significant challenges in vaccination strategy and public health initiatives (74). The exact reason for the seasonality of influenza epidemics in temperate climates is incompletely understood, yet likely represents a myriad of factors that includes changes in host behaviour in colder, darker months (75, 76) and apparent atmospheric factors, such as humidity and temperature, on viral transmission (77-79) as well as fluctuations in the host’s immune response (80).

In non-pandemic years, it is estimated that influenza causes approximately 1 billion infections globally *per annum*, which result in 3-5 million cases of severe illness and upward of 500 000 deaths. At particular risk are those under the age of two, aged individuals over 65 and immunocompromised individuals, including pregnant women (8, 27, 81). In fact, it is estimated that individuals over 65 represent greater than 90% of all influenza-caused hospitalizations during interpandemic years and roughly 2 out of 3 deaths were in individuals younger than two (27, 81). Moreover, in 2007, in the United States alone, these cases of severe illness and hospitalizations heavily burden the healthcare system, costing \$10.4 billion dollars in direct medical fees and \$16.3 billion dollars in economic losses (27). Thus, seasonal influenza epidemics are a major determinant of global health and remain a consistent infectious threat.

1.3.2: Pandemic influenza infections

Beyond yearly epidemics, the greatest hazard of influenza is its ability to cause markedly deadly periodic pandemics, which cause substantially more morbidity and mortality, as well as cumbersome financial burden. Compared to epidemic strains, pandemic influenza strains also exhibit reduced seasonality and greatly enhanced lethality in typically low-risk middle-aged populations (82). Fortunately, they remain rare. Since the start of the 1900s, there have been four influenza pandemics. The first, in 1918 was the worst single pandemic in recorded history. Since then, three more have arisen: first in 1957 (Asian Influenza), then 1968 (Hong Kong Influenza) and, finally, most recently, in 2009 (Swine Flu). Today, highly pathogenic avian-derived influenza strains (e.g. H5N1, H7N9) exhibit high pandemic potential and are thought of as the prime candidates for an upcoming pandemic. Although avian strains currently have limited infectivity of humans and minimal human-to-human transmission capabilities, they mutate rapidly and have mortality rates in excess of 30% (10, 83). *Critically, what exactly causes a pandemic strain to evolve and what permits their signature infectivity and lethality are poorly understood. Moreover, the ability to predict the arrival of future pandemics is completely lacking.* Greater understanding of the mechanisms acquired by pandemic influenza strains will, therefore, assist in the preparation for future pandemics and should remain at the forefront of investigation. In the next subsections, we will revisit a century of IAV pandemics, beginning with the one of 1918.

A) 1918 H1N1 Spanish Influenza Pandemic

Despite spuriously referred to as the “Spanish Influenza”, the origin of the 1918 influenza pandemic is unknown and the exact reason for its exceptional pathogenicity remains a major unanswered question (84). Total infection rates reached 1/3 of all individuals worldwide and with fatal cases ranging between 50 to 100 million, it is the single deadliest event in human history, killing approximately 3% of the world’s

population. So dramatic was the effect on human life, the Spanish Influenza caused a ~10 year drop in life expectancy in the United States (**Figure 1.7**) (85). Histopathological analyses of lung sections revealed near ubiquitous presence of complicating secondary bacterial infection (48, 86) and “pneumonia with acute hemorrhagic edema” (83) with firsthand accounts describing, “Thoracic cavities of victims contained varying amounts of light brown or yellow to dark red fluid. Dark, bloody, frothy fluid often poured out when lungs were sectioned” (87): findings that were not similarly observed in future pandemics. What caused this dramatic pathology is unclear, though studies using reconstructed influenza viruses (88) with a 1918 protein backbone (50) directly show that viral proteins from the 1918 virus are intrinsically more virulent and capable of causing severe viral pneumonia (89). Fortunately, antibiotics dramatically dampened mortality via secondary bacterial infection in coming influenza pandemics; however, intrinsic viral virulence remains an unfettered problem (43).

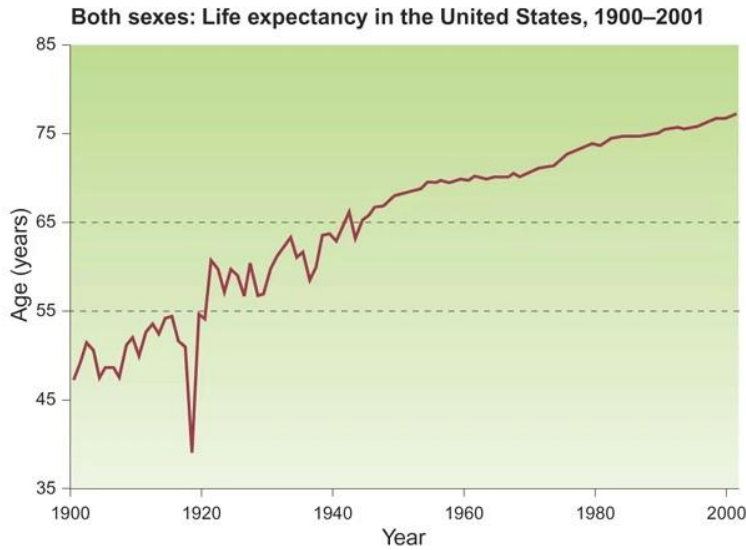


Figure 1.7: United States life expectancy in the 20th century. Despite exhibiting a consistent rise, a dramatic decade-drop in life expectancy in 1918 is attributed to the deadliest pandemic in human history. Taken from (84)

hemorrhagic edema” (83) with firsthand accounts describing, “Thoracic cavities of victims contained varying amounts of light brown or yellow to dark red fluid. Dark, bloody, frothy fluid often poured out when lungs were sectioned” (87): findings that were not similarly observed in future pandemics. What caused this dramatic pathology is unclear, though studies using reconstructed influenza viruses (88) with a 1918 protein backbone (50) directly show that viral proteins from the 1918 virus are intrinsically more virulent and capable of causing severe viral pneumonia (89). Fortunately, antibiotics dramatically dampened mortality via secondary

bacterial infection in coming influenza pandemics; however, intrinsic viral virulence remains an unfettered problem (43).

Another defining feature of the 1918 pandemic is a dramatic W-shaped mortality curve, where an additional highly susceptible population is observed in the ages between 25 and 45, rather than the traditional U curve of less severe pandemic and epidemic strains (**Figure 1.8**). In fact, 99% of deaths occurred in those younger than 65 with 50% of all deaths being in those between 20 and 40 (43, 82). This mortality rate in young individuals has not been experienced since. Why this occurred is unknown, but it is suggested some cross-protection to the 1918 influenza was observed in individuals older than 65, due immunological memory from previous influenza infections at the end of the 19th century, which was not afforded to younger, as-of-yet unborn individuals.

B) 1957 H2N2 Asian Influenza Pandemic and 1968 H3N2 Hong Kong Influenza Pandemic

The Asian Influenza pandemic began in February of 1957 in China with first infections being detected in the United States in the summer of 1957. Similar to the 1918 pandemic, but to a much smaller magnitude, individuals under 40 were at considerable risk, with those younger than 65 accounting for 36% of lethality. In total, excess mortality rates over endemic years reached 69 800 (83). The third pandemic of the 20th century surfaced in Hong Kong in 1968 and initial viral isolates were obtained in the United States in the winter of 1968. Although severe in some regions, it is thought that the relatively attenuated nature of this pandemic in many

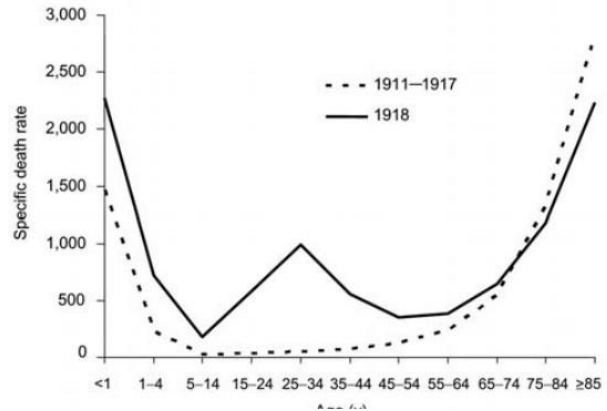


Figure 1.8: Mortality curve of the 1918 Spanish Flu. Differing from seasonal influenzas and other pandemics, the Spanish Flu caused significant death in young populations. The cause of this is not entirely understood. Taken from (81).

areas of the world was due to cross-protection induced by the same neuraminidase protein from the 1957 pandemic, adding strength to observations from the 1918 pandemic of protection in older individuals, stemming from immunological memory. Again, young people were disproportionately affected by the pandemic, with those under 65 accounting for nearly 50% of the mortality (43). Mortality associated with secondary bacterial infection was still prevalent, yet significantly reduced in comparison to the 1918, and was similar to interpandemic years in some cases, hovering around 45% (86). Thus, the enhanced mortality of the pandemic strains compared to seasonal strains, despite equal levels of bacterial coinfection, suggests intrinsic pathogenic factors of these viruses.

C) 2009 H1N1 Swine Flu

The most recent influenza pandemic began in April 2009, when the infecting virus was isolated in Mexico and the United States (90). The World Health Organization declared a pandemic in early June 2009 (91). An ancestor of the 1918 pandemic strain, it was the second H1N1 pandemic strain since 1900. Although the relative mortality of the 2009 strain hovered only around 1%, therefore barely differing than seasonal strains, its transmission rate was highly augmented and replication within experimentally infected animals (92, 93) and humans (94) was elevated, suggesting enhanced intrinsic virulence. In addition, those 60 and above were relatively saved and a substantial burden of mortality was in younger individuals, often

without predisposing factors (95). Critically, bacterial coinfections were no longer seen in the majority of cases of severe illness or mortality for the first time (44, 96). In all, bacterial coinfections were observed in an average of only 26-38%, and reported as low as 10%, of fatal cases and did not vary substantially from seasonal years (96).

Importantly, 2009 infections also marked the first time neuraminidase antiviral resistance was detected during a pandemic, after beginning to appear in seasonal strains in 2007. Near complete resistance to adamantane M2 inhibitors was initially observed during the pandemic and as a result, their usage was discontinued (97). The neuraminidase inhibitor Oseltamivir was the drug chiefly deployed. Resistant viruses were detected in approximately 2% of tested viruses in over 27 000 samples (91). The majority of these viruses were confined to immunocompromised patients, or those receiving oseltamivir treatment; however, this was not true of all cases (91) and treatment efficacy was highly contentious (44). Interestingly, although viral replication was enhanced, the 2009 pandemic virus exhibited no known mutations associated with enhanced virulence. Thus, unknown pre-disposing host factors may have been the major determinants of mortality.

D) Considering future pandemics

Although it is currently impossible to predict when and which strain will cause the next pandemic, future pandemics are inevitable and predictive efforts should be maintained (10). Undoubtedly, mutation of circulating strains or re-emergence of other human strains are an unwavering threat to develop into a pandemic strain. However, much of the current evidence supports the emergence of HPAI strains as the next pandemic-causing virus (98). Although lethal and readily transmittable in certain birds, current HPAI infections are rare and limiting in humans, and it is uncertain if *bona fide* human-to-human transmission is possible. Despite this, when they occur, HPAI infections are coupled with incredibly high mortality (often >50%) that transpires rapidly following infection, often due to ARDS (45). ARDS was extensively documented in both the 1918 and 2009 pandemics, almost exclusively independent of secondary bacterial infection (43, 44). It is this concept that HPAI viruses could undergo antigenic shift in a susceptible animal species that would increase the strain's preference for human sialic acid linkages while maintaining enhanced pathogenicity of an HPAI strain, which makes them prime candidates as the future cause of pandemics. The observation that the 2009 virus caused notable mortality in younger populations, with infrequent bacterial coinfection and no known virulence mutations in the viral genome, suggests that future pandemics will be lethal based on inherent predisposing host factors, such as variations in the immune

response. Rising viral resistance and limited effectiveness of antivirals in preventing severe disease strongly advocate for a greater understanding of the pathogenesis of influenza and the discovery of novel host-driven therapies. *Thus, as we will see in the upcoming sections, efforts to gain better insight into host immune pathways that protect against highly virulent influenza strains is strongly warranted.*

1.4: The immune response to influenza virus infection

1.4.1: The lung as a unique entry point for influenza viruses and other pathogens

As mentioned, circulating human influenza strains are confined to replicate in the lungs, as human IAV requires extracellular trypsin proteases that cleave surface HA proteins to enable infection. Although HPAI strains can disseminate, the respiratory tract is still the initial site of infection. Thus, the lungs are the critical tissue for influenza (29). While most vital organs are protected from the environment by structural components, the lungs are constantly exposed to ambient air, as they perform the essential task of gas exchange. Specific aspects of pulmonary biology, then, make the respiratory tract a unique niche for invading pathogens and an ideal entry point. This function of gas exchange, although essential, leaves the lung susceptible to infection, due to its intimate contact with the external environment. On average, an adult human inhales 11 000 litres of air and breathes roughly 25 000 times per day (99). Although the vast majority of air inspired is composed of innocuous debris and particulate matter, this is not always the case, and the substantial burden of gas exchange obligates frequent exposure to infectious microbes (100). *Thus, host defense responses in the lung must be **extremely well regulated** to protect against pathogens that threaten host fitness, while equally avoiding hyperactivation to non-injurious exposures that compromise lung function via immunopathology.* This balancing act of host resistance and disease tolerance mechanisms that expel pathogens and maintain tissue integrity, respectively, will be highlighted in the following sections.

1.4.2: The immune system

Upon infection, the immune system uncovers the nature of the invading pathogen and responds accordingly. In the lung, immunity is achieved through a carefully regulated stratum of effector mechanisms that conceptually deploys sequentially, based on location within the lungs and specificity of the response (101). Initially, constitutive mechanical responses work to repel the pathogen without activation of the immune system. If the pathogen manages to subvert the non-specific physical barriers of the lung, then immune activation results. Broadly, the immune system is grouped into two branches: the innate and adaptive systems. The innate immune system responds rapidly and recognizes pathogen associated molecular patterns (PAMPs), expressed by the invading microbe, or damage associated molecular patterns (DAMPs), released by the host in response to cellular stress or death, via pattern recognition receptors (PRR). Different families of PRRs exist, including toll, NOD, RIG-I, -like and C-type lectin receptors (TLR,

NLR, RLR, CLR) with the specificity of the PRR to a particular PAMP or DAMP helping the immune system recognize the type of pathogen to orchestrate an appropriately targeted inflammatory response (102, 103). In the case of IAV infection, initial recognition of the virus is done by infected epithelial cells of the respiratory tract as well as the tissue-resident macrophage of the airways, the alveolar macrophage (AM), that patrols the epithelial/endothelial barrier of alveoli. AM and epithelial cells are potent producers of chemokines and cytokines. Engagement of these cells by IAV is then complemented by the recruitment and/or activation of resident interstitial macrophages of the lung parenchyma, neutrophils, inflammatory monocytes, NK cells, innate lymphoid cells (ILCS) and dendritic cells (DCs) that bolster the response. The recruited cells extravasate into the parenchyma and airways in response to chemokines produced by AM and infected epithelial cells; such as CCL2/CCL5, CXCL1 and CXCL3 that recruit monocytes, neutrophils and NK cells, respectively. Later, trafficking of viral antigen to the lymph nodes via DCs initiates antigen presentation and the adaptive immune response, with the antigen specific cells then returning to the lung to aid in viral clearance, resolution and immune memory.

The adaptive immune arm is further subdivided into two branches: the cellular response (primarily virus-specific CD4⁺ and CD8⁺ T-cells), which kills infected cells by apoptosis, and the humoral response (virus-specific antibodies coming from plasma cells of the B-cell lineage) that neutralizes the virus prior to entry into a cell or during egress (104). Adaptive responses are highly specific, yet lag significantly behind innate immunity during primary infection, appearing in the lungs beginning at approximately a week post-infection. However, following resolution of the primary infection, immunological memory is formed by cells of the adaptive system that affords a speedier and more robust response upon secondary exposure to IAV, which dramatically decreases disease severity and morbidity during subsequent infections. Classically, in contrast to the adaptive arm, the innate immune response was thought to have no memory, responding similarly to the same pathogen after successive infections and with equal intensity. Recently, this dogma has been challenged and it is now understood that innate immunity can, in fact, be anamnestic, exhibiting enhanced responses to successive heterologous challenges, following certain stimuli. This broad non-specific innate memory is termed “trained innate immunity” (105). This emerging immunological concept has radically changed our understanding of the immune response and is a burgeoning field of discovery. This concept is further explored in **section 1.5.3** and greater comprehension of its mechanisms served as the impetus for our studies in Chapters 4 and 5.

1.4.3: Pulmonary host defense mechanisms

Collectively, the protective immune mechanisms to infection are referred to as **host defense** mechanisms. The intricate array of host defense mechanisms is vast and continually being reshaped as greater understanding of the immune system develops. Classically, investigation centred almost exclusively upon discovering immune factors that act directly against IAV to halt its replication and dispel it from the lung. These are referred to as **host resistance** mechanisms. Insufficient host resistance results in a longer disease course, augmented viral shedding, worsened pulmonary necrosis and impaired gas exchange, all of which contribute substantially to IAV-induced morbidity and mortality. Thus, elucidating anti-IAV host resistance mechanisms is valuable and this need set the groundwork for our study in Chapter 2. Conventional thinking suggested that the greater the magnitude of host resistance responses the more effective the immune response. Now, however, it is becoming known that host resistance comes with a steep inflammatory cost responsible for substantial tissue damage and immunopathology, in addition to damage induced by the pathogen. Thus, immune mechanisms must be in place to restrain host resistance responses, preserve tissue integrity and return the inflamed site to homeostasis, without direct impact on the pathogen. This host defense strategy is known as **disease tolerance** (106). While initially largely ignored, recent study has discovered the importance of disease tolerance during IAV infection. Indeed, the majority of IAV mortality can be attributed to immunopathology caused by overly zealous host resistance mechanisms that compromise disease tolerance, rather than direct cytopathic effects of the virus. Our study in Chapter 3 uncovers a novel pathway in disease tolerance to influenza infection.

Although, conceptually, as we will discuss in chapter 6, it is appealing to suggest that shortly following IAV infection a wave of host resistance mechanisms is deployed, followed subsequently by a wave of disease tolerance mechanisms, it is, in fact, more likely that disease tolerance mechanisms are evoked at the onset of the inflammatory response. Thus, the interplay between the magnitude of host resistance responses and regulation by disease tolerance mechanisms is a crucial area of investigation, as a break in either branch contributes to the susceptibility of the host

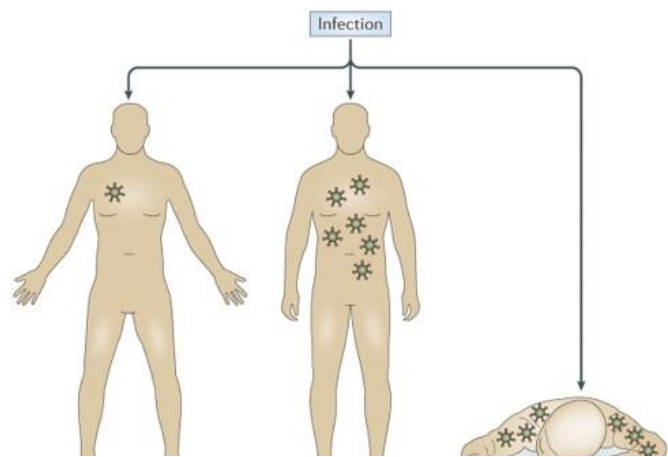


Figure 1.9: Host defense mechanisms. Upon infection, the immune response can be broken into two broad arms, host resistance and disease tolerance. Host resistance mechanisms eliminate the pathogen, while disease tolerance mechanisms reduce the inflammatory cost associated with the inflammatory response. If either branch fails, the host is susceptible. Taken from (106).

(Figure 1.9) (107). Taken together, the lung is a unique organ that requires an intricate and highly regulated immune response to patrol it. In the coming sections, we will investigate the nature of this response and discuss the mechanisms of host defense against IAV, beginning with physical barrier responses in the lung and then more specifically at the known mechanisms of host resistance and disease tolerance.

1.4.4: Mechanical and chemical responses in the lung

Chemical and mechanical features of the lung afford constitutive non-specific protection against invading microbes, including IAV. Although the branching network of bronchioles and the constantly diminishing size of the airways are formidable barriers for larger pathogens such as bacteria, IAV virions are typically too small to be trapped. However, filamentous IAV virions can exist on the micron scale and, thus, may be caught and expelled (11). In the upper airways, closing of the trachea by the epiglottis forms an impenetrably seal of the lung and particulates are then either swallowed or exhaled back into the environment, while cough generation creates turbulent forces that allow for the removal of debris and mucus deposits, without cellular activation (108). More distally, mucus generated by goblet cells coats ciliated epithelial cells and chemical properties of the mucus trap pathogens, while the coordinated ciliary beat, known collectively as the mucociliary escalator, moves infected mucus back up the airways for expulsion (109). In addition to trapping pathogens, mucus and respiratory secretions have an intrinsic antimicrobial capacity, as first described by Alexander Fleming almost 100 years ago, in 1922 (110). Thus, mucus furthermore provides the necessary microenvironment to activate these antimicrobial peptides. For example, collectins form a large family of proteins that bind carbohydrates on the surface of microbes, such as IAV. Some of these collectins, including surfactant protein D and mannose-binding lectin, bind HA, and inhibit its activity, effectively blocking viral entry (111). Also within this milieu are so-called “natural” IgM Abs, constitutively produced by B-cells even in the absence of infection, of which a small subset can relatively non-specifically bind a variety of IAV strains to activate the immune system via complement or expel the virus directly (112). Important to note, the vast majority of potential infectious agents are dispelled by these constitutive factors, without immune involvement; however, when these non-specific defenses are breached, then the immune system must become activated and more specific anti-IAV responses result.

1.4.5: Host resistance mechanisms to IAV

Host resistance is the most intensely researched branch of the immune response to IAV. Resistance mechanisms act directly on the virus to halt its replication and attenuate its pathogenicity. When important host resistance factors are missing, increased mortality results, hallmarked by enhanced viral loads and cytopathic effects in the lung.

A) Interferons

The most extensively studied mediators of viral host resistance are the interferon cytokine pathways. Interferons are pleotropic cytokines that belong to 3 known families: IFN-I, II, III, with IFN-I and III being the most substantially described antiviral cytokines. The anti-IAV capacity of IFN-I was described over 60 years ago by Isaacs and Lindenmann in a pair of seminal 1957 studies (113, 114). 50 years later IFN-III was described as a similarly antiviral protein, initially described following ECMV infection (115, 116). IFN-I comprises a diverse family of proteins; including 13 IFN- α subtypes, a single IFN- β , IFN- ϵ , IFN- κ , IFN- ζ (mice) and IFN- ω (humans). Despite this diversity at the protein level, all IFN-I bind the IFN-I receptor (IFNAR): a heterodimeric receptor containing IFNAR1 and IFNAR2 subunits. IFNAR signalling occurs in an autocrine or paracrine manner, due to the rapid usage of the protein. Expression of IFNAR is ubiquitous, being expressed by all nucleated cells and this hints at the widespread action of IFN-I. Interestingly, despite the fact that every subtype binds the same receptor and high redundancy of downstream responses is appreciated, clear differences still exist in cellular responses to different IFN-I subtypes (117). Although the exact mechanisms underlying the differential responses are unknown, variation in subtype receptor affinity (IFNAR1 versus IFNAR2) and alterations in the promotor sequence of different IFN-I subtypes are thought to contribute to this phenomenon (118). Ligand binding leads to the recruitment of the Janus family kinases (JAKs), Tyk2 and Jak1, that phosphorylate each other and the receptor to recruit signal transducer and activator of transcription 1 and 2 (STAT1 and STAT2). pSTAT1 and pSTAT2 heterodimers partner with interferon regulatory factor 9 (IRF9) to form the ISGF3 complex that enters the nucleus and promotes transcription of hundreds of ISGs by interacting with the interferon-sensitive response elements (ISRE) in their promoters. These ISGs then function through diverse mechanisms to restrict viral replication and modulate the immune response (118). In addition to STAT1 and STAT2 heterodimers, STAT1 homodimers are also formed and interact with γ -activated sequences

(GAS) in the promoters of certain ISGs, akin to IFN-II. Finally, non-canonical signalling through STAT1 and STAT3 heterodimers occurs following ligation of IFNAR by certain α -subtypes. STAT3 activation negatively regulates further IFN-I signalling and attenuates inflammatory ISGs, thus having a more immunomodulatory, rather than, antiviral role. This STAT3-dependent mechanism-of-action of IFN-I will be introduced further in the section on disease tolerance (**Section 1.4.6**) (119). Signalling through other STATs, such as STAT4-6, has been reported; however, the effect of these pathways during IAV infection is unknown (118, 120).

IFN-I signalling is essential in host resistance to IAV, with *Ifnar1*^{-/-}, *Ifnar2*^{-/-} and *Ifnb*^{-/-} mice being highly susceptible to infection by both human (H1N1) (121-124) and avian (H5N1) (125) IAV. These mice exhibit enhanced viral loads at early time points post-infection (122, 123) that ultimately return to WT levels at later time-points (123, 126), confirming the importance of IFN-I in host resistance to IAV, but also suggesting that IFN-I-independent effects complete viral clearance at later times post-infection. *Stat1*^{-/-} mice are even more susceptible to infection than IFNAR-deficient mice, succumbing quickly to a fulminant systemic infection, likely due to the fact that STAT1 contributes to many additional signalling pathways beyond IFN-I (127). Initial production of IFN- β leads to signalling through IFNAR and causes upregulation of ISGs, including IRF7. IRF7 functions as the transcription factor for all IFN- α subtypes, except α 4. Thus, IFN-I production occurs in biphasic waves of **IFN- β (antiviral)** and **IFN- α (immunomodulatory)** to protect against viral infection (128). The importance of the upregulation of ISGs in host resistance to IAV has been appreciated for over 30 years with the discovery of the Myxovirus resistance protein 1 (Mx1). Mx1 is undetectable in resting cells, but is highly upregulated specifically downstream of ISGF3/IRE binding (129). It is now understood that Mx1 interacts with IAV vRNPs in the nucleus to prevent replication (130) and protect against IAV infection. Today, several more ISGs have been shown to be of critical importance in inhibiting IAV replication at every stage of its replicative cycle. IFN-inducible transmembrane (IFITM) protein family members inhibit IAV replication at early stages of infection, by blocking the fusion of the viral membrane with the endosome. Mice lacking IFITM3, therefore, succumb rapidly to IAV infection and have impaired host resistance (131). In the cytosol, Protein Kinase R (PKR) halts IAV replication through phosphorylation of the translation initiation factor eIF2 α , effectively repressing translation of host and viral proteins. Correlatingly, PKR-deficient cells exhibit enhanced viral replication and *Pkr*^{-/-}

mice are highly susceptible to several viral infections, including IAV. Moreover, PKR enhances the longevity and magnitude of IFN- β responses by promoting the stability of IFN- β mRNA through the maintenance of its poly(A)-tail (132). Finally, the 2'-5'-oligoadenylate synthase 1 (OAS1) senses viral RNA in the cytosol to activate ribonuclease L (RNase-L), which degrades host and viral ssRNA to restrict viral replication and protect against IAV infection (133). *Critically, the vast majority of inbred mouse strains are highly susceptible to influenza infection when compared to wild mice, due to an absence of a functional Mx1 gene, including C57Bl/6 mice used in all of our studies. Therefore, most ISG knockout studies need to be, in effect, considered double knockout studies (Mx1 and the gene of interest) and, as such, great care must be taken in interpretation of the results* (107). Given that humans express Mx1 homologues, further study using Mx1-sufficient mice should be emphasized (134).

IFN-II, in both mice and humans, is composed of a single member IFN- γ that signals through the complex of IFNGR1 and IFNGR2. IFN-II signals through both JAK1 and 2 and utilizes STAT1 homodimers to interact with GAS and induce transcription of responsive genes (135). Thus, there is significant overlap in cellular responses to both IFN-I and II through mutual interaction with GAS elements (136). However, IFN-II does not induce transcription of genes solely with ISREs; thus, some specificity does exist. For example, OAS-1 is exclusively upregulated by ISRE engagement and, therefore, is not induced by IFN-II. On the other hand, IFITM1 is regulated by all IFNs, while IRF1 shows a higher responsiveness to IFN-II (120). NK cells and NK T-cells are the primary innate producers of IFN-II, while effector CD4⁺ T-cells are mostly responsible on the adaptive side to promote Th1 polarization of the immune response. Additionally, while IFNAR is expressed on all nucleated cells, IFNGR is mostly confined to leukocytes and hematopoietic cells, suggesting an immunomodulatory role for IFN-II. IFN-II acts most strongly to activate macrophages to kill intracellular pathogens and promote cytotoxic T and NK cell responses (135). Strangely, despite transcriptional overlap with IFN-I signalling, significant production of IFN-II following IAV infection and expression of IFNGR on many immune cells in the lung, the role of IFN-II in resistance to primary IAV infection is controversial. Studies have equally shown a protective (137), detrimental (138), or redundant (139) role for IFN-II signalling during IAV infection. The reason for these discrepancies is not entirely known, but may be due to differences in experimental design, infectious strain of IAV, or background of mice. Thus, the exact nature of IFN-II and its contribution to host resistance to IAV immunity is unknown. Given the critical requirement for IFN-II in other viral infection models (140), further study on the function of IFN-II during IAV infection is warranted. Greater understanding of

the kinetics and regulation of the IFN-II response, as well as its role in the recall response (141), may help rectify these uncertainties.

Finally, IFN-III is composed of four IFN- λ s (IFN- λ 1-4) in humans, where in mice only IFN- λ 2-3 are produced. Similarly to IFN-I, IFN-III induces formation of the ISGF3 complex, downstream of its receptor and its induction occurs just as IFN-I. However, the receptor for IFN-III is uniquely IFNLR, composed of two subunits IFNLR1 and IL10R β .

IL10R β also serves as a receptor subunit for other members of the IL-10 family of cytokines, such as IL-10 and IL-22 (142) (**Figure 1.10**). As with IFN-I, IFN-III signalling is essential in immunity to IAV, contributing to host resistance by limiting viral replication in epithelial cells (143). Interestingly though, IFNLR activation leads to a more specific transcriptional program of ISGs than IFN-I. This subset is less inflammatory and has different kinetics, exhibiting a lower but more prolonged induction of ISGs than IFN-I. Moreover, the expression of the IFNLR is much more cell-specific than IFNAR, as receptor expression is restricted to epithelial cells and a small subset of lowly-expressing leukocytes, including monocytes and some DCs (117). This collectively suggests that regardless of similarly activating ISRE-encoding

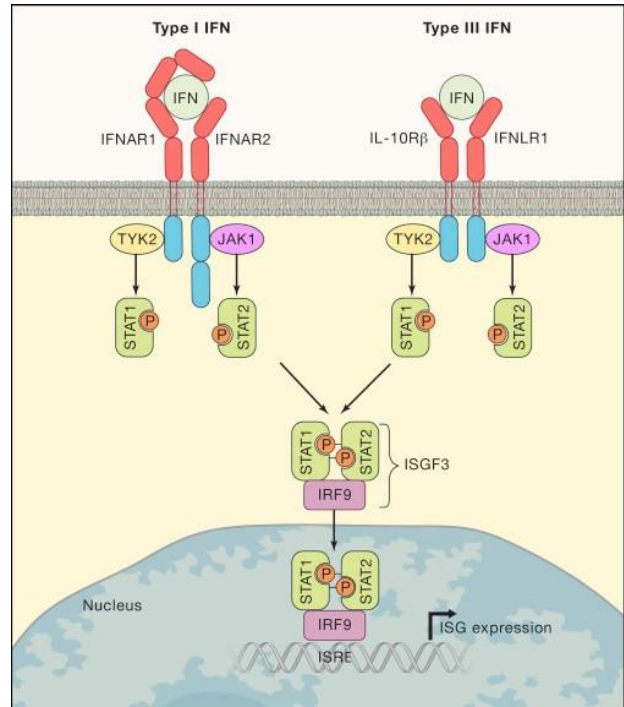


Figure 1.10: Type I and III Signalling. Both type I and type III interferons activate similar signalling pathways but use different receptors. Despite pathway homology, IFN-III activates a different subset of ISGs. Taken from (116).

genes and protecting against IAV infection by enhancing host resistance, the specific roles of IFN-I and IFN-III may differ, but complement *in vivo* (117). In line with this, there is accumulating evidence suggesting that IFN-III is preferentially and more quickly produced by epithelial cells of the upper airways to control mild infection and limit transmission, **without inducing inflammatory cytokine production by leukocytes** (144). However, upon more severe infection, there is a loss of IFN-III control in the upper airways and the virus escapes more distally, necessitating activation of the **inflammatory and antiviral cascade** of IFN-I that ultimately protects in the lower airways, at considerable inflammatory cost (145). Thus, it appears the host has evolved sequential and compartmentalized IFN responses to counter viral replication in the upper versus lower airways, each of which balances antiviral and inflammatory magnitudes to maintain host resistance to IAV, without dramatically jeopardizing host fitness. Assuredly,

further study into the regulatory mechanisms of IFN-I versus IFN-III induction is an intriguing avenue of future investigation.

B) RLRs

Production of IFN-I/III occurs through similar pathways following recognition of IAV. The sensors responsible for their induction are varied and highly cell-specific (146). In structural cells (e.g. fibroblasts and pneumocytes), conventional DCs (cDC) and M ϕ , sensing of the virus by the cytosolic RLR RIG-I is critical in the production of IFNs. Although RIG-I was initially discovered as a sensor of dsRNA, it is now known to also recognize 5'-triphosphates of ssRNA (54). Recognition of these phosphates by RIG-I is critical for the initial sensing of replicating IAV, within antiviral stress granules in the cytoplasm (147), and RIG-I-signalling is essential in viral clearance (148). ATP-dependent conformational changes of RIG-I then lead to recruitment to the mitochondrial antiviral signalling protein (MAVS; also known as VISA, Cardif, IPS-1) through the caspase activation and recruitment domain (CARD). Another RLR, melanoma differentiation-associated gene 5 (MDA5), equally interacts with MAVS, yet it is activated by longer ssRNA segments and is, therefore, dispensable in IAV sensing (149). RLR/MAVS pathway-defective M ϕ (150), cDCs (151) and mice (134) all fail to produce IFN- β , and *Mavs*^{-/-} mice exhibit enhanced viral loads and susceptibility to IAV, primarily through an inability to upregulate of Mx1 (134). Interestingly, MAVS is located on the mitochondrial membrane as well as the surface of peroxisomes. At the mitochondrion, MAVS is phosphorylated by TANK-binding kinase 1 (TBK1). This phosphorylation recruits and activates transcription factor IRF3 via phosphorylation by TBK1, facilitating subsequent dimerization and translocation to the nucleus for the induction of IFN- β (152). Moreover, mitochondrial MAVS leads to inflammatory cytokine production by the IKK/NF κ B axis. On the other hand, peroxisomal MAVS signaling proceeds independently of IRF3, instead requiring IRF1 to specifically induce IFN- λ , without activating NF κ B (153). Thus, localization of MAVS provides a cellular mechanism for specific IFN-I versus IFN-III production and the lack of an inflammatory cytokine signature observed in IFN-III-rich niches. As epithelial cells (144) and macrophages (150, 154) represent the major sources of IFN-III and IFN-I, respectively during IAV infection, it is intriguing to suggest that in addition to location within the

lung, the intracellular balance between levels of peroxisomes and mitochondria may dictate preferential production of IFN-I versus IFN-III.

C) TLRs

In addition to RIG-I, endosomal TLRs 3 and 7 contribute to IFN-I responses during IAV infection. TLR7 recognizes ssRNA within the endosome during initial infection and, thus, signals without the need for IAV replication. TLR7 signals through the adaptor protein MYD88 to activate inflammatory cytokine production and IFN-I/ISGs through NF κ B and IRF7, respectively. The role of TLR7 and its signaling components in immunity to IAV during primary infection is complex and appears to be strain-, dose- and time-dependent (134, 155-157), which is further complicated by the fact that the majority of studies use TLR7-deficient mice were coupled with RIG-I- or TLR3-signaling deficiencies. Taken together, however, evidence primarily supports the role of TLR7 signaling in the protective production of IFN-I and enhancement of host resistance to IAV. Moreover, despite uncertainty in innate immune responses, multiple studies have consistently shown a role for TLR7 in promoting humoral responses to IAV, but not T cell responses, that are important in vaccination efficacy (107, 151), suggesting TLR 7 may play a larger role in the establishment of immunological memory, rather than *bona fide* innate responses. Interestingly, in contrast to cDCs, M ϕ and structural cells, plasmacytoid DCs (pDCs) produce large quantities of IFN- α exclusively through TLR signalling, rather than RIG-I-pathways. This unique feature of pDC biology is due to high constitutive levels of IRF7 expression, which acts as the major transcription factor for most IFN- α subtypes (158). Despite being professional IFN- α producers, the role of pDC is again controversial during primary IAV infection. One study has shown a redundant role for pDCs following H1N1 infection (159), while another found a critical role for TLR7 signaling in pDCs in early viral clearance following H7N7 infection, in an Mx1-sufficient environment (160). Correlating to the latter study, an *IRF7*^{-/-} deficient human showed impaired IFN- α production by pDCs and suffered life-threatening ARDS following primary pandemic 2009 H1N1 infection (161). Thus, the protective input of pDCs appears to be primarily Mx1 family dependent.

Contrasting to TLR7, TLR3 recognizes IAV in apoptotic bodies that are taken up by efferocytosis (the uptake of apoptotic bodies) by phagocytes, thereby, contributing to later stages of IFN-I production, following replication. Unique amongst TLRs, TLR3 signals exclusively through the adaptor TRIF to promote IFN-I production in an IRF3-dependent manner and inflammatory cytokines downstream of NF κ B. Interestingly, *tlr3*^{-/-} mice exhibit elevated viral loads due to a loss of IFN-I production and a reduction of CD8⁺ T cells; yet, they are more resistant to IAV, in part because of reduced immunopathology (157). However, humans with a *TLR3*^{-/-} phenotype are highly susceptible to IAV, perhaps due to an impaired adaptive response as well as structural cell responses (162). Therefore, TLR3 is essential in humans in response to IAV, contrasting murine study.

In sum, members of the RLR and TLR family synergize to promote host resistance to IAV, principally through the production of IFN-I and IFN-III, which is largely supported by experimental data and case studies of humans. However, it is evident that our knowledge of the exact contributions of each individual receptor, as well as crosstalk between pathways for the instruction of the adaptive arm, and the relative importance of RLRs versus TLRs in protection against IAV, is still lacking and further granularity is still needed.

D) NLRs and CLRs

The nucleotide-binding oligomerization domain-like receptors (NOD-like receptors; NLRs) are a diverse family of primarily myeloid-expressed receptors that are activated by a variety of PAMPs and DAMPS to instruct the immune response. The human genome encodes 22 NLRs, of which few have known functions. However, recent work has uncovered that multiple NLRs contribute to host resistance against IAV as well as disease tolerance. NLR family member NOD2 was initially described as a cellular sensor for peptidoglycan-derived muramyl dipeptide (MDP) (163) and was shown to be involved in immunity to *Mtb* (164). However, it also senses ssRNA of IAV in fibroblasts and BMDM to promote IFN- β responses in a MAVS/IRF3-dependent manner to protect against IAV infection (165). Moreover, in epithelial cells NLRC5 interacts with RIG-I to stabilize its activation of MAVS and this function potentiated IFN- β production and dampened

viral replication (166). In fact, NLRC5 also contributes to host resistance to IAV by promoting MHC-I expression and subsequent generation of CD8⁺ cytotoxic T cell responses that enhance viral clearance *in vivo* (167), although its expression was not associated with significant changes in morbidity/mortality. Thus, it appears that NLRC5 is inessential in immunity to IAV, despite promoting host resistance. Moreover, the exact PAMP responsible for NLRC5 remains unknown. Finally, NLRX1 is a mitochondrial protein that has had many reported roles in response to IAV and other viral infections. Initial work suggested that NLRX1 negatively regulated MAVS signaling at the mitochondria following IAV infection to dampen inflammatory and antiviral responses (168). However, this has since been refuted by us (62) and others (169). As mentioned earlier, we showed that NLRX1 interacts with IAV-expressed PB1-F2 specifically in the mitochondria of infected macrophages to disarm its pro-apoptotic potential and maintain the IFN- β -producing pulmonary M ϕ pool to counter viral replication (62). Thus, NLRs contribute to host resistance to IAV infection and mitochondria appear to be critical in IFN-I production through both antiviral signaling (MAVS) and cell death (NLRX1).

C-type lectin receptors (CLRs) are well-established PRRs in protection against fungi, due to their recognition of carbohydrates expressed on the fungal surface (170). Interestingly, although still incompletely appreciated, various CLR members, including the macrophage mannose receptor (MMR) and macrophage galactose type C-type lectin (MGL), have been shown to be alternative receptors for IAV entry in M ϕ and DC, independent of sialic acid residues (171). Also, a recent study found that the CLR SIGN-R1 plays an important role in host resistance to IAV. SIGN-R1 was found to be expressed early post-infection in the trachea on the surface of monocyte-derived inflammatory DCs. SIGN-R1 recognized and interacted with glycosylated carbohydrates on IAV virions and promoted viral clearance through the recruitment of active NK cells to the site of infection (172). The homing of these cells to the trachea, and not more distal airways, is consistent with the notion that glycosylated viruses are less capable of penetrating the upper airways. Therefore, recognition of glycans by CLR-expressing cells is advantageous there. CLRs appear to represent a previously underappreciated family of antiviral PRRs, as well as receptors for IAV to infect myeloid cells.

Innate Immune Cells

E) Alveolar Macrophages

Although airway epithelial cells (AEC) represent the major replicative cell all down the respiratory tract, in the alveoli during severe infection, resident AM are infected *in vivo* (173) and they are thought to serve as the first immune cells to encounter the virus. Although infection of macrophages by most strains of IAV is primarily abortive (174), AMs appear to act as a sink for infection, with this interaction with the virus being essential for activation and coordination of robust anti-IAV responses. AMs highly express the receptors discussed above and they act as major producers of cytokines and chemokines shortly after infection. Likely due to their importance in immunity to infection, IAV has evolved mechanisms to induce cell death in AM shortly following infection, which enhances viral loads (62) and secondary bacterial overgrowth (66). Correlatingly, depletion of AM, either by loss of GM-CSF ($Csf2^{-/-}$) (175, 176)—which is the critical maintenance cytokine for AM at steady-state—or by genetic deletion of Core Binding Factor Beta (CBF β) (177), renders mice highly susceptible to IAV infection. These mice exhibit elevated viral replication and succumb to respiratory insufficiency (175, 177). Intriguingly, AM are also a major source of IFN-I, following IAV (154) and RSV infection (178). Thus, preservation of AM function is critical for anti-IAV immunity and protection against ARDS, at least in part due to IFN-I production, and IAV targets AM cell death pathways to facilitate its replication and compromise host resistance (67).

F) Other Innate Leukocytes

Early pulmonary M ϕ and AEC responses serve primarily to halt viral replication and recruit other innate leukocytes to the site of infection to aid in the antiviral effort. Neutrophils rapidly accumulate in the airways as early as one-day post-infection and peak at 3 days in response to CXCL1 in mice, or IL-8 in humans. Despite this pronounced recruitment, the role of neutrophils in host defense to IAV is unclear. Neutrophils can be non-productively infected by IAV and are capable of producing ROS and defensins that can contribute to killing and neutralization of IAV (179). Nevertheless, neutrophilic ROS and extracellular traps (NETs) contribute substantially to immunopathology (180) and may be more beneficial in the prevention of secondary bacterial infection, rather than direct anti-IAV effects (181).

Inflammatory monocytes, recruited in a CCR2-dependent manner, extravasate and reach peak levels in the lung shortly following neutrophils, where they differentiate into inflammatory monocyte-

derived macrophages (IMM) and TNF/iNOS producing DCs (tipDCs). CCR2-derived cells contribute to antiviral immunity through inflammatory cytokine production (182, 183), yet enhance susceptibility through their proinflammatory “cytokine storm” profile, such that *Ccr2*^{-/-} mice show increased survival (182-184). However, the importance of these cells may be masked by solely exploring primary infection models, as tipDCs present antigen to CD8⁺ T-cells *in situ* (185) and IMM promote the proliferation of tissue-resident CD8⁺ memory T-cells (184), suggesting that immunological memory and recall responses may be severely compromised in *Ccr2*^{-/-} mice.

NK cells are innate cytotoxic lymphocytes that contribute importantly to host resistance to IAV. When in proximity to an infected cell, perforin housed in secretory lysosomes of NK cells creates aqueous pores within the membrane of the cell. Granzymes are then released to enact cell death through apoptosis. Importantly, in contrast to adaptive lymphocytes this process is not MHC-mediated and is, thus, in effect, faster and less specific (186). Sialylated activating receptors NKp44 and NKp46 on NK cells directly interact with HA expressed on the surface of IAV-infected cells through α 2,6 linkages, causing direct cell lysis (187). Correspondingly, mice lacking NKp46 exhibit enhanced mortality (188) and NK cell-depletion studies using an anti-Asialo GM1 antibody also report increased susceptibility, as well as elevated viral loads (189, 190), confirming the role of NK cells in host resistance to IAV. In addition to NK cells, non-NK innate lymphoid cells 1 (ILC1s) display anti-IAV effects in an ILC1-deficient adoptive transfer model (191). Unconventional T-cell populations have also been suggested to contribute to IAV resistance, although the exact mechanisms of these responses are unclear. NK T-cells are so named due to their expression of markers of both conventional T- and NK- cells and they recognize glycolipid antigens via their $\alpha\beta$ TCR and the non-classical MHC molecule CD1d. Intranasal administration of the NK T-cell superagonist α -galactosylceramide boosted resistance to pandemic H1N1 infection in swine, presumably by activating NK T-cell effector functions (192), which are vast and combine components of the innate and adaptive systems (193). Finally, $\gamma\delta$ T-cells are a unique subset of T-cells that express $\gamma\delta$ subunits of the TCR, rather than $\alpha\beta$. $\gamma\delta$ T-cells are not restricted by MHC; however, the antigens that activate them remain elusive. $\gamma\delta$ T-cells are innate-like lymphocytes that are most heavily studied in the protection of mucosal barriers and as early producers of IL-17 (194). However, a recent study associated a high fat, low carbohydrate ketogenic diet with augmented resistance to IAV infection, due to enhanced $\gamma\delta$ T-cell accumulation and responses in the lung (195), emphasizing the importance of lifestyle in the regulation of protective anti-IAV immune responses. Therefore, ILCs and innate lymphocytes are emerging as critical mediators of resistance to IAV. Greater emphasis on the mechanistic basis of their protective capacities will be instrumental in potentially harnessing them for future therapies.

G) Adaptive Immune Cells

The adaptive system is composed of T- and B- cells that differ from innate cells in that their responses are highly restricted to specific antigens. Antigen specificity is determined by molecular sequences in the T- or B- cell receptor (TCR; BCR) generated during hematopoiesis and reflect conserved sequences of self and foreign peptides. B-cells can recognize their cognate antigen either in its native form or membrane bound form on the major histocompatibility complexes (MHC) of antigen presenting cells (APCs). T-cells, on the other hand, must be presented their cognate antigen on MHC molecules. Antigen presentation is initiated in secondary lymphoid organs and during IAV infection the major site is the lung-draining mediastinal lymph node (mLN), continuing within the lung parenchyma later-on to enhance the response and seed the tissue with long-lived memory cells (185). Migratory DCs are the principal APC due to their high expression of MHC and motility. Therefore, DCs represent the bridge between the innate and adaptive arms of the immune response. MHC molecules are broadly defined as either class I or class II. All nucleated cells express MHC-I and CD8⁺ T-cells are presented antigen of intracellular origin via MHC-I to confer their cytolytic capacity against intracellularly infected cells. Thus, CD8⁺ cells are critical in viral immunity (196). Antigen loaded on MHC-I has two sources: 1) direct infection of DCs by IAV leading to viral antigen presentation or 2) cross-presentation. The capability to cross-present is restricted to a small subset of APCs and affords the ability to present exogenously-derived antigens (i.e. those obtained via efferocytosis) on MHC-I molecules, thereby stimulating a strong CD8⁺ T-cell response, without compromising APC effector functions caused by direct viral infection (197). Conversely to MHC-I, only APCs express MHC-II and these interact with helper CD4⁺ T-cells, which help mould the inflammatory milieu through the production of families of cytokines. IAV biases strongly towards a Th1 response, such that CD4⁺ T-cells produce high levels of IFN- γ in response to IL-12 released by DCs to activate CD8⁺ T-cells and M ϕ to kill IAV intracellularly. Classically, MHC-II epitopes were thought to be exclusively of extracellular origin, processed through the endosomal pathway; however, a recent study has indicated that endogenous MHC-II antigens are far more immunogenic during IAV infection than exogenous (198), indicating that alternative pathways for antigen processing are critical for a robust MHC-II-restricted T-cell response following IAV infection.

The adaptive lymphocyte response is comprised of three phases: 1) initial activation and effector responses, 2) contraction via cell death and 3) the induction of memory cells. Central memory cells home to the mLN, while effector memory cells remain in the tissue, and both are activated very quickly upon re-exposure to their cognate antigen during secondary IAV infection. So robust is this protection afforded by the adaptive memory response, that experimentally, homologous secondary infections of 5 log higher

infectious doses cause only a small percentage of morbidity/mortality with far fewer viruses collected from the lungs (148). This phenomenon is fully dependent on the adaptive memory, as *Rag*^{-/-} (mice lacking T- and B- cells) exhibit no protection (199). This memory response is primarily facilitated by cytolytic IAV-experienced CD8⁺ T-cells in the airways, as well as anti-IAV IgA and IgG Abs, secreted in the upper respiratory tract mucosa or serum, respectively (200). However, although the hallmark of adaptive immunity is the memory response, it contributes substantially to host resistance during primary infection as well. During primary infection, *Rag*^{-/-} mice are unable to clear the virus and succumb to infection when compared to WT mice (201). As *Rag*^{-/-} mice broadly lack all T- and B- cells, understanding which cellular compartment is most responsible for this phenotype is refractory. To this point, mice deficient specifically in CD8⁺ T-cells clear the infection and survive, albeit with slightly delayed kinetics (202). CD4⁺ T-cell-deficient mice also show delayed viral clearance, but similar mortality (203). This seems to be primarily attributed to a loss of B-cell responses, as B-cell-deficient mice are more susceptible to infection, while mice lacking B and CD8⁺ cells, but sufficient in CD4⁺ T-cells, equally cannot clear the virus and die (204). Thus, the individual components of the adaptive response are highly interconnected, combining to assist in late-stage host resistance, rather than the early innate responses. Interestingly, although effector T-cells are major producers of TNF- α and IFN- γ , these cytokines seem to contribute minimally to the protection afforded by these cells (196).

As mentioned previously, DCs represent the bridge between innate and adaptive immunity through their antigen presentation and translocation to the draining LNs. In the lung, two known subsets of migratory DCs exist, namely CD103⁺ DCs and CD11b⁺ DCs, and recruitment to the mLN is dependent on CCR7 expression. Although their exact contributions to host resistance to IAV and establishment of memory is not fully delineated, it is clear that each plays an important role, seemingly through different mechanisms (197). CD103⁺ DCs accumulate in the mLN quickly, appearing as early as 2 days post-infection, and they are critical in shaping initial effector CD8⁺ T-cell responses. These CD103⁺ DCs highly express the transcription factor BATF3, which is essential for cross-presentation (205). CD11b⁺ DCs enter the LN as the second wave of DCs, arriving between 6-8 days post-infection. They, on the other hand, do not express BATF3, and are, thus, precluded from cross-priming T-cells, instead being directly infected by IAV as the source of endogenous antigen (206). They are also considered the primary MHC-II APCs (207), while both migratory subsets, as well as LN-resident DCs, have been shown to promote memory responses (197). Following the acquisition of antigen specificity and expansion in the LN, the antigen specific T-cells migrate through the bloodstream back to the lung to exact their effector functions. It is becoming increasingly clear that proliferation continues at the site of infection, due to continued interactions with non-migratory DC subsets that are derived from monocytes (184, 185). Deletion of these cells following

infection reduces immunopathology; however, it also severely compromises viral clearance and increases mortality (208).

Fascinatingly, IFN-I also contributes extensively to the maintenance and generation of adaptive responses. In addition to its previously highlighted role in innate immunity, IFN-I production in the LN facilitates antigen presentation by providing necessary co-stimulatory signals (209). Moreover, in the lung, IFN-I signalling primes CD103⁺ DC for cross-presentation, while protecting them from direct IAV infection through the upregulation of antiviral ISGs, prior to migration (205). Finally, direct signalling of IFN-I on B-cells critically regulates the induction of humoral immunity to IAV (210).

H) Cell Death Programs

Arguably, manipulation of cell death programs during infection represents ground-zero of the host/pathogen evolutionary arms-race. Cell death is intimately linked to the pathogenesis of many, if not all, pathogens, including chronic infections such as HIV (211) or *Mtb* (212), and acute infections like *S. enterica* (213) or IAV (3). Additionally, cell death plays a critical role in human development and homeostasis, with an estimated 100 to 200 billion cells dying by apoptosis daily in an adult. A paramount feature of apoptosis is the fact that it proceeds in an immunologically silent manner to prevent continual activation of the immune system. Perhaps as a result of its profound importance at steady-state, the apoptotic machinery is highly conserved in multicellular eukaryotes. Therefore, it is not surprising that pathogens encode both pro- and anti- apoptotic proteins to manipulate cell death.

The observation that IAV infection induces epithelial cell death has been made since at least the 1918 pandemic, with the extent of apoptosis positively correlated to disease severity and strain virulence (214). Apoptosis is broadly divided into intrinsic and extrinsic pathways and both are activated following IAV infection. Intrinsic apoptosis represents a culmination of apoptotic stimuli mediated directly by IAV replication and is defined by caspase 9 activation downstream of cytochrome c release by mitochondria. Alternatively, extrinsic apoptosis proceeds indirectly of viral replication and is initiated by death ligand-signaling pathways via caspase 8. FasL, TRAIL and IFN- β ligation have all been implicated in the induction of extrinsic apoptosis. Both pathways then culminate on effector caspases, such as caspase 3 or 7 (215). While intrinsic apoptosis is mostly modulated by IAV factors, extrinsic apoptosis is primarily mediated by the immune system and can contribute substantially to immunopathology (182, 216). Importantly, caspase 3 activation is essential in the manufacture of new IAV virions (217), underscoring the intimate relation of

viral propagation and host cell death. As mentioned in **section 1.2.6**, apoptosis during IAV infection is biphasic: first being blocked by the viral NS1 protein to promote replication and then being induced by NP and PB1-F2 proteins to facilitate viral spread. Thus, blockade of apoptosis emerges as a potential enhancer of host resistance. In this vein, inhibition of caspase 3 (217), pro-apoptotic pathways (218), or TRAIL (219) decreased cellular viral loads. Additionally, blocking of FasL-signalling in mice *in vivo* lowered viral titres and protected against lethal IAV infection (220). Inhibition of apoptosis may, therefore, be an appealing immunomodulatory IAV therapy.

Diverging from apoptosis, which is highly conserved and programmed, necrosis was thought to be a passive form of cell death that was strongly pro-inflammatory and occurred unregulated in response to significant cellular stress. Now, however, it is well-established that many forms of necrosis are, in fact, programmed, with necroptosis being the most thoroughly described. Necroptosis is a pro-inflammatory form of cell death whereby the necroptotic cell releases DAMPs that activate neighbouring cells. During times of caspase inhibition, necroptosis occurs via phosphorylation of the receptor-interacting serine/threonine protein kinase 3 (RIPK3) and family member RIPK1. RIPK3 then phosphorylates the mixed lineage kinase domain like pseudokinase (MLKL), which induces necroptosis by a combination of the assembly of a pore-forming complex at the plasma membrane and as a platform for Ca²⁺-mediated necrosis (221). Although uncontrolled non-necroptotic necrosis of the epithelium is strongly associated with mortality linked to respiratory insufficiency and ARDS (214), stromal cell necroptosis is antiviral and protective, presumably through destruction of the replicative niche. *Ripk3*^{-/-} mice are more susceptible to IAV, and fibroblasts, epithelial cells and lungs all have enhanced IAV titres, due to an inability to undergo necroptosis (222). **However, as we will see in Chapter 2, the role of RIPK3 in macrophages and other leukocytes during the immune response to IAV infection was completely unknown.**

Necroptosis can only occur when caspase 8 activity is compromised. Therefore, necroptosis is traditionally inhibited by the action of extrinsic apoptosis. While apoptosis has conserved eukaryotic cellular machinery, necroptosis is poorly conserved, and the pathway is only known to have evolved at all in higher-order animals. Intriguingly, as discussed, IAV has evolved several mechanisms to modulate host apoptotic pathways to promote its replication cycle, including caspase inhibitors. Yet, no known necroptotic inhibitors are expressed by IAV. Collectively, this suggests that the host necroptotic pathway may have evolved relatively recently, as an additional antiviral strategy, in part due to the immense exploitative evolutionary pressure put on the apoptotic pathway by pathogens.

1.4.6: Mechanisms of Disease tolerance to influenza virus infection

Contrasting to the large canon of research conducted on host resistance mechanisms to IAV infection, relatively little is known about disease tolerance as a host defense strategy to IAV. Having been a well-established component of plant immunity for approximately 150 years; disease tolerance has only been appreciated in humans and other animals in the last decade and a half (223). However, as previously highlighted, mammalian host resistance mechanisms are inherently immunopathological and inflammatory during IAV infection. Sometimes this associated inflammation is even collectively detrimental to the host—despite some loss of antiviral capacity, as is the case in TLR3- and CCR2-deficiencies. Thus, there must be a wide network of mechanisms in place to tolerate this associated antiviral inflammatory cost. Indeed, although still in its infancy, appreciation for understanding disease tolerance mechanisms to IAV infection is rapidly growing. There is considerable overlap in the families of molecules that mediate tolerance versus resistance, albeit with different mechanisms. Therefore, it seems that divergent resistance and tolerance functions of the same immune mediators may have appeared as a result of a necessary evolutionary compromise in host defense (224). *Interestingly, the majority of IAV-related deaths stem from immune dysregulation, rather than direct viral effects, indicating that a break in disease tolerance is the principal driver of susceptibility to IAV and not, counterintuitively, an inability to inhibit viral replication* (225). In this section, we will look at these known mechanisms of disease tolerance that protect the host by mitigating pulmonary damage and returning the lung tissue to homeostasis, without directly affecting viral fitness.

A) Interferons

As with host resistance, IFN-I is critically involved in disease tolerance responses. PRR activation causes an initial wave of IFN- β , followed by a subsequent wave of IFN- α subsets, downstream of IFN- β ligation of IFNAR. Where IFN- β is chiefly antiviral, IFN- α signaling is more appreciated for its immunomodulatory effects and serves to dampen PRR-mediated inflammatory cytokine production and cell proliferation (226). In the context of IAV infection, it has been refractory to delineate the specific role of IFN-I in disease tolerance, as mice constitutively lacking IFN-I signaling have enhanced viral loads and neutrophilia (122, 123). Thus, it is possible that the loss of host resistance led to a break in disease tolerance, rather than a direct function of IFN-I in promoting disease tolerance. However, we recently showed that signaling of the bioactive lipid mediator leukotriene B₄ (LTB₄) specifically promoted IFN- α production by CX3CR1-expressing interstitial macrophages (IM) to suppress the proliferation of inflammatory monocyte-derived cells, without affecting IFN- β responses or antiviral immunity. Thus, a reduction in IFN- α via loss

of LTB₄ signalling confirmed a specific disease tolerance function of IFN-I (150). Moreover, IFN-I signaling leads to the production of the canonical anti-inflammatory cytokine IL-10, through a STAT3-dependent manner, which ameliorates immunopathology (119) during IAV infection (122). Currently, there are no known disease tolerance mechanisms for IFN-II or IFN-III in the context of IAV infection.

B) Alveolar Macrophages and Barrier Responses

As AM are frequently bombarded by particulate matter and potentially injurious exposures due to their location at the epithelial/endothelial barrier of the lung, they exhibit a highly tolerant phenotype as to not be constantly activated and immunopathological. Several reasons exist for this, including poor antigen presentation skills stemming from a lack of costimulatory molecules, reduced phagocytic capacity compared to tissue macrophages, and constitutive production of the anti-inflammatory cytokines like TGF- β that maintain regulatory lymphocyte populations and protect the epithelium (227). In fact, a major determinant of what turns AM from regulatory to inflammatory is the disruption of the neighbouring epithelium/endothelium. To this end, AM remain in contact with type II AECs and endothelial cells through CD200R/CD200 interactions. Notably, following IAV infection, a loss of this interaction via physical disruption or using CD200^{-/-} mice led to massive tissue damage with minimal effects on viral burden, dominated by a heightened inflammatory profile of AM (228). The importance of barrier maintenance is further appreciated by the expression of the matrix metalloproteinase-1 (MMP-1) following IAV infection by myeloid cells, including AM, that lyses the extracellular matrix and aggravates tissue damage (229). Endothelial cells also contribute to barrier rupture, through inflammatory cytokine amplification when sphingosine-1-phosphate (S1P) signalling is lost. Thus, agonism of this pathway promotes disease tolerance (230). Finally, it has been suggested that the driving cause of IAV-driven susceptibility to secondary bacterial infection is also pulmonary destruction that can be prevented through administration of the tissue-regenerative protein amphiregulin (65). Amphiregulin has also been shown to boost protective disease tolerance in a primary model of IAV infection, being released by ILC2 (231) and this was critically dependent upon IL-33 produced by AM and NKT cells (232). Thus, AMs and the maintenance of the epithelial/endothelial barrier are important regulators of resistance and tolerance.

C) Other Innate Responses

Other innate immune mediators have been implicated in maintenance of disease tolerance responses. Yet, seemingly contradictory conclusions in different studies investigating similar models underscore the fine-line between protective tolerance responses that attenuate immunopathology and overly-tolerant responses that allow for enhanced disease progression. For example, TNF- α , an inflammatory hallmark of PRR activation, exerts pleotropic functions, causing both cell survival and death based on its signalling pathway. Prophylactic inhibition of TNF- α ameliorated IAV-induced tissue damage and elongated survival, without affecting viral clearance (233). However, complete germline loss of TNF- α signalling aggravated epithelial injury and delayed disease resolution (35). Similar observations have been in regard to IL-17, which is produced almost exclusively by $\gamma\delta$ T-cells early post-IAV infection. In neonatal mice, a $\gamma\delta$ T-cell/IL-17/IL-33 axis protected against lethal infection, without affecting viral loads, and a correlation of IL-17 levels in nasal secretions and reduced disease severity was observed in human children (234). Although in adult mice, IL-17 was also shown to be responsible for off-target gastrointestinal pathology (235) and exacerbated disease severity in the lung (236). Mucosal-associated invariant T (MAIT) cells are another unconventional subset of T-cells, expressing a semi-invariant $\alpha\beta$ TCR that recognizes metabolites of the riboflavin biosynthetic pathway. They are a burgeoning field of research due to their high frequency in human peripheral blood, as well as their diverse effector functions that are important in infection and antitumor immunity (237). Murine MAIT cells have been shown to protect against IAV infection by preventing pulmonary epithelial damage, independent of viral clearance (238). A similar response is thought to exist in humans (239). However, the exact mechanisms of their protection in mouse and humans require greater investigation.

As previously highlighted, NK cells can recognize IAV-infected cells through HA/NKp46 interactions to assist in host resistance. Interestingly, pulmonary NK cells are equally necessary in disease tolerance. IL-22 is a member of the IL-10 family of cytokines and its receptor is expressed almost exclusively on structural cells at mucosal sites. Initially recognized for its importance in maintaining gut homeostasis (240), it is now appreciated that IL-22 acts on lung epithelial cells to protect against IAV-dependent cytolysis and induce beneficial epithelial hyperplasia during both primary IAV (241-243) and secondary bacterial (244, 245) infections, without altering pathogen burdens. As such, *Il-22*^{-/-} mice succumb to infection with markedly enhanced epithelial barrier destruction. Several cellular sources can contribute to the IL-22 response during IAV infection, including NKT cells (246) and $\gamma\delta$ T-cells (245). Yet, it appears that conventional NK cells represent the primary protective source of IL-22 in response to IAV (242, 243). **As we investigated in Chapter 3, despite the substantial evidence supporting a critical role for an NK**

cell/IL-22 cascade in disease tolerance to IAV, the exact cellular pathways involved remained obscure.

D) Adaptive Immune Cells

Although the adaptive system is indispensable in the late stages of viral clearance, its high effector state contributes to immunopathology. Thus, a unique subset of CD4⁺ T-cells known as T_{regs}, denoted further by their expression of the transcription factor Foxp3 and CD25, serves to rein in effector T-cell responses through the inhibition of T-cell proliferation and the production of IL-10. T_{regs} represent a ubiquitous strategy of adaptive system regulation that is far from singular to IAV infection. Interestingly though, T_{reg} responses during IAV infection precede effector responses in the lung and serve to set a tolerant tone prior to the arrival of antigen-specific cytotoxic responses (247). Moreover, highly activated cytotoxic CD8⁺ T-cells and, to a lesser degree, Th₁-polarized CD4⁺ T-cells can also contribute IL-10 to balance the magnitude of the inflammatory response (248).

E) Cell Death Programs

Pyroptosis is a rapid inflammatory form of cell death that is characterized by a loss of membrane integrity and DNA damage, which acts as a DAMP for neighbouring cells to sustain inflammation. Pyroptotic cell death is dependent upon caspase-1, NLRP3—a member of the NOD-like receptor family—and the adaptor ASC. Upon interaction, these proteins collectively form the inflammasome. NLRP3 is highly expressed in myeloid cells and activation of the inflammasome leads to release of IL-1 family cytokines (e.g. IL-1 β , IL-18), as well as pyroptosis. Interestingly, inflammasome activation requires two signals: signal 1 is mediated by TLR signalling and it induces expression of pro-IL-1 β and pro-IL-18 proteins, while signal 2 is provided by cell stressors that activate NLRP3 and caspase-1. Synergy of the two signals causes cleavage of the pro-forms of the cytokines into their active states and ultimately pyroptosis (249). IAV has been shown to activate NLRP3 through multiple ways, including interaction of viral NP/PB1 with the newly discovered myeloid innate sensor: interferon-inducible protein Z-DNA binding protein 1 (ZPB1) (250).

Although inflammasome activation and pyroptosis are potentially inflammatory, in immunity to IAV, they have been shown to protect the host without contributing substantially to viral clearance until very late

time-points post-infection. Mice lacking caspase-1, ASC, or ZBP1 all succumb to lethal infection, exhibiting reduced cell recruitment as well as unfettered apoptosis and necrosis. Thus, the inflammasome activation primarily contributes to disease tolerance (250, 251). The minor contribution of the inflammasome to late-stage viral elimination can likely be attributed to its role in promotion of the adaptive response (252). Lastly, although the inflammasome is incontrovertibly linked to IL-1 β and IL-18 release following IAV infection, whether or not IAV induces *bona fide* pyroptosis has not been properly elucidated, as pyroptosis induction is difficult to measure. Interestingly, on the other hand, one study has suggested that in the immunosuppressed elderly population, pyroptosis detrimentally compromises disease tolerance by promoting neutrophilia and NETosis (134). Certainly, further research of pyroptosis in IAV pathogenesis is warranted.

Finally, just as overly exuberant cell death can dysregulate disease tolerance to IAV, so too can cells that are protected against IAV-induced cell death. Club cells are small ciliated epithelial cells that line bronchioles. Interestingly, they have been shown to be highly responsive to IFN-I signalling, such that IAV infection is unable to lyse the cell and disseminate, despite significant replication. As a result, club cells clear IAV, yet contribute to long-standing immunopathology due to sustained inflammatory cytokine release, such as CXCL10 and CCL5 in both murine and human models (253). However, although this phenomenon confers susceptibility to primary IAV infection, the heightened antiviral ISG signature bestows non-specific protection against subsequent heterologous IBV infection (254), coupling transient loss of disease tolerance to longer-lasting enhanced host resistance.

1.4.7: The bone marrow as the control centre for hematopoiesis and immune regulation

As infections with human IAV strains are almost exclusively confined to the respiratory tract, fittingly the majority of research has focused on responses in the lung. Yet, it has long been established that the bone marrow represents the initial source of all blood cells in humans, which then circulate through the vasculature and seed the tissues, hinting at the importance of bone marrow/periphery axes during inflammation. The idea that marrow sustained the blood and bone has been around since antiquity, during the time of Hippocrates (255). However, it was not until the observations by Osler and his contemporaries in the 19th century that the bone marrow was properly recognized as the seedbed of the blood (256). Today,

it is known that at steady-state the bone marrow produces 200 billion red blood cells, 400 billion platelets and 10 billion leukocytes daily—numbers that can be augmented dramatically during inflammation or stress (255). Thus, the central actions of the bone marrow are of critical importance during times of peripheral inflammation, including IAV infection, where increased demand of leukocytes is necessitated.

The generation of blood cells is a process termed hematopoiesis, coming from the Greek words *haima* (blood) and *poiēsis* (to produce something).

Hematopoiesis proceeds in a tightly regulated fashion from pluripotent progenitors with high dormancy and self-renewal capacity, denoted by their expression of CD150, (CD150⁺ CD48⁻ long-term hematopoietic stem cells; LT-HSCs, followed by CD150⁺ CD48⁺ short-term HSCs; ST-HSCs) to CD150⁻ CD48⁺ multipotent progenitors (MPPs), collectively referred to as lineage⁻ cKit⁺ Sca-1⁺ (LKS) cells, before differentiating into increasingly lineage-restricted progenitors that are more active, but have lost their self-renewal capabilities (**Figure 1.11**) (257, 258). An important bifurcation occurs just downstream of the MPP, where progenitor cells become destined to give rise to either cells of the myeloid/erythroid or lymphoid lineages, but not both. MPPs differentiate into cells of the myeloid/erythroid lineage through the common myeloid progenitor (CMP) and the lymphoid lineage through the common lymphoid progenitor (CLP) (259). From there, hematopoiesis continues through gradually more restricted progenitors where the ability to give rise to multiple cell types is progressively lost, until, ultimately, mature effector leukocytes are generated. For example, monopoiesis progresses downstream of the LKS to the CMP and then through the granulocyte-monocyte progenitor (GMP; loss of erythroid potential), followed by the common monocyte progenitor (cMoP; loss of granulocyte potential), before finally giving rise to mature Ly6c^{hi} and Ly6c^{lo} monocytes that egress into the peripheral blood (260). As an exploding field of

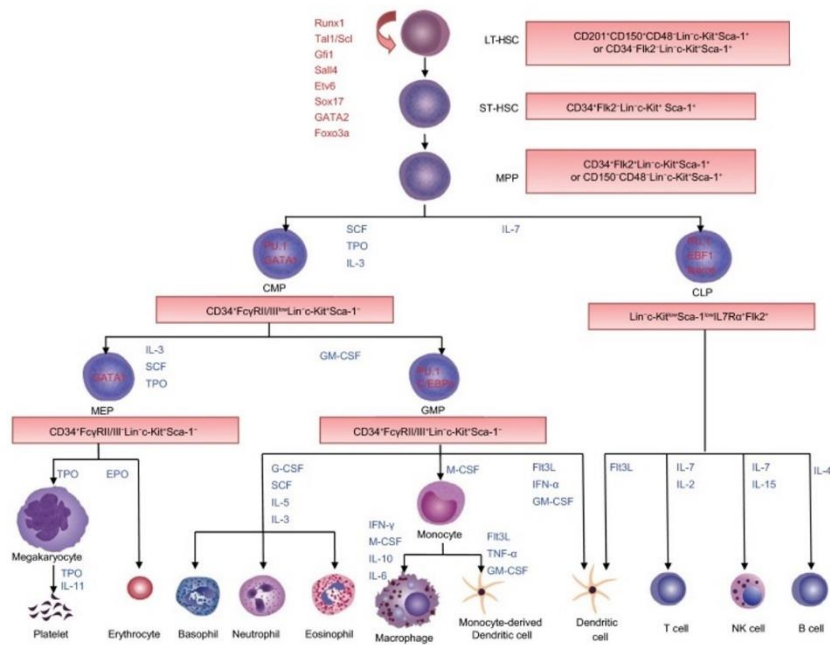


Figure 1.11: Hematopoietic hierarchy. Hematopoiesis progresses through a series of differentiation steps from pluripotent stem cells to committed effector cells. With each step, differentiating lineage potential is progressively loss, but cellular activation is enhanced. The two major lineages (myeloid and lymphoid) bifurcate downstream of the MPP. In red are the associated known markers for each cell type and in blue are the cytokines or growth factors required for differentiation. Taken from (257).

research, discrete progenitor populations for each effector leukocyte, and the markers for them, are constantly being elucidated. In this vein, it was initially thought that hematopoiesis progressed in this rigorous stepwise fashion with lineage-restriction decisions occurring strictly downstream of LKS cells, such that LKS cells possessed unbiased pluripotent differentiation patterns. However, an abundance of evidence has refuted this, and it is becoming increasingly understood that lineage biasing is progressive and begins very early during differentiation. This begins at the level of HSCs, where higher expression of CD150 confers myeloid lineage bias (261) and continues at the level of MPPs, with MPP3 (CD34⁺ Flt3⁻) and MPP4 (CD34⁺ Flt3⁺) subsets biasing towards the myeloid or lymphoid lineage, respectively (262). Thus, programming of HSC lineage determination during infection could fundamentally impact the magnitude and nature of the inflammatory response.

The signals involved in interrupting HSC quiescence and in lineage determination are complex and, despite their importance in shaping the immune response, remain incompletely understood. It is known that specific transcription factor expression is needed to differentiate into particular lineages, such as PU.1 of the myeloid lineage or Notch signalling during T-cell development (257). However, their expression does not directly affect HSC lineage commitment decisions. Cytokine signalling, alternatively, plays a direct, integral role in stem cell activation and proliferation. Recently, TNF- α was shown to promote HSC survival (263), as was IL-6 (264). IFNs, additionally, appear to be critical mediators. At steady-state, IFN-II is essential for maintaining stem cell quiescence and survival (265), but chronic exposure to either IFN-I (266, 267) or IFN-II (268) causes excessive proliferation and exhaustion of the HSC compartment. Interestingly, above stem cell maintenance, IFN signalling can directly regulate lineage commitment through modulation of cell death pathways in HSCs and subsets of committed progenitors. For example, IFN-I-dependent osteopontin production (269) promotes lymphopoiesis via inducing myeloid progenitor apoptosis (270), while IFN-I-dependent necroptosis of HSCs blunts myelopoiesis during bacterial infection (271). The effects of lineage commitment biasing of HSCs on the subsequent peripheral immune response, though, and whether this biasing could be exploited by pathogen virulence factors, were unknown. **As we will see in Chapter 4, lineage biasing in the bone marrow is an underappreciated regulatory mechanism of the immune response, as the balance between myelopoiesis and lymphopoiesis has critical effects on host defense to highly pathogenic microbes.**

In contrast to chronic viral (272) and bacterial (268) infections, where it is well-established that continually heightened requirement for leukocytes causes stem cell exhaustion and bone marrow collapse, very little investigation of the bone marrow compartment has occurred following acute infections like IAV. However, some study into the long-distance effects of IAV infection on the bone marrow exists. Seminal

work by Seo *et al.* highlighted that in addition to critically promoting an antiviral state in the lung, IFN-I signalling in the bone marrow also protected against IAV by acutely modulating hematopoiesis. Following infection, *Ifnar1*^{-/-} mice exhibit neutrophilia, due to an inability to generate Ly6C^{hi} monocytes, instead producing Ly6C^{int} monocytes, not found in WT mice, that produce substantial levels of KC in the lung to fuel neutrophil chemotaxis and immunopathology (123). Additionally, recruited monocytes arrive in the lung tissue with a pre-emptive antiviral state, due to pulmonary-derived IFN-I signalling in the bone marrow that confers resistance to infection and contributes to viral clearance (273). Thus, the protective role of acute IFN-I in the bone marrow against IAV is at least two-fold. Finally, a prophylactic fibre-rich diet has recently been shown to promote monopoiesis that prevents neutrophilic immunopathology and boosts cytotoxic CD8⁺ T-cell responses following IAV infection (274). Certainly, the protective responses of the bone marrow in immunity to IAV remain an exciting outstanding area of research.

Over the course of the previous sections, the complexity of immunity to influenza virus infections has been made evident. Many cellular components of both the innate and adaptive systems have been implicated in protection against influenza, either via direct viral clearance (Host Resistance) or by safeguarding the lung tissue against immunopathology (Disease Tolerance). Although vast research efforts have been expended on understanding the exact immunologically mechanisms in a beneficial versus detrimental immune response, many unanswered questions linger. Moreover, it has been highlighted that effective immunomodulatory, rather than antiviral, therapeutic strategies are, as of yet, still entirely lacking. Acknowledging this pitfall in existing clinical interventions, the next section will overview the current vaccine as the only partially protective preventative strategy against influenza.

1.5: Vaccination as a strategy against IAV

As previously stated, anti-IAV drugs are routinely administered when infection is suspected, yet their efficacy has been consistently challenged (31). Rising resistance rates and ineffectiveness when prescribed following symptom-onset add to the inadequacies of antivirals. To combat this, prophylactic therapies such as vaccination are appealing, in that they prevent, rather than fight, disease. Indeed, the only chance for disease eradication depends on a highly protective vaccine and the best approach in preventing influenza infection remains the vaccine. However, as evidenced below, the current vaccination strategy is equally fraught with shortcomings and, as such, better understanding of what constitutes a protective response to vaccination and how that can be harnessed in building a more effective influenza vaccine is warranted.

1.5.1: Conventional influenza vaccination

Current vaccines invariably target the adaptive system and their effectiveness is dependent upon a combination of memory T- and, primarily, B- cells, which robustly responds following re-exposure to conserved antigens. Thus, the candidate vaccine's efficacy at preventing disease is principally measured experimentally by levels of neutralizing antibodies in the serum (IgG) and T-cell responses upon *ex vivo* restimulation, thereby primarily ignoring potential contributions from other cells. In the case of influenza, vaccination is thought to principally protect through the generation of neutralizing IgG antibodies that target the globular head of the HA protein (275). Although these prevent infection of cells and, thus, disease, the head of the HA protein is highly variable and harbours strong mutagenic potential from antigenic drift. Because antigen-specific responses of the host are highly conserved, but the viral HA that these responses recognize is not, in contrast to other more effective vaccines against other pathogens, influenza vaccines are necessarily administered annually to maintain their protection (276).

Despite this annual vaccination program, antigenic mismatch often still occurs. As mismatch causes low vaccine efficacy, global surveillance by the WHO of circulating influenza strains transpires year-round to map mutations in the circulating strains, in hopes of generating proper vaccination strains for upcoming epidemics. Biannual meetings for each the northern and southern hemispheres are conducted by the WHO's Global Influenza Surveillance and Response System (GISRS) to select which strains will be incorporated, based on antigenic information of infecting strains and epidemiological data of over 130 national influenza centres in 100 countries across the globe. Unfortunately, due to the length of time required to generate

appropriate amounts of vaccine stocks, strain decisions are made at least 6 months prior to the flu season in either hemisphere, increasing the likelihood for antigen mismatch (276). Pandemic strains that emerge via antigenic shift render the vaccine completely ineffective due to evasion of memory responses, heavily compounding efficacy issues. All taken together, over the last decade-and-a-half, adjusted influenza vaccine effectiveness has varied substantially but invariably suboptimal, ranging anywhere from 10 to 60% (**Figure 1.12**) (277).

Administered influenza vaccines contain either three (trivalent) or four (quadrivalent) strains. Quadrivalent vaccines combine two IAV strains: an H1N1 strain descended from the 2009 pandemic and an H3N2 strain descended from the 1968 pandemic, as well as two IBV strains: Yamagata and Victorian.

The trivalent vaccine, on the other hand, immunizes against both IAV strains and a single IBV strain based on WHO recommendations (275). The majority of influenza vaccines are inactivated influenza vaccines (IIV) in which the virion has been disrupted by fixatives (whole virus) or ethers (split virus), but temperature-dependent live attenuated influenza vaccines (LAIV) are also available in North America and much of

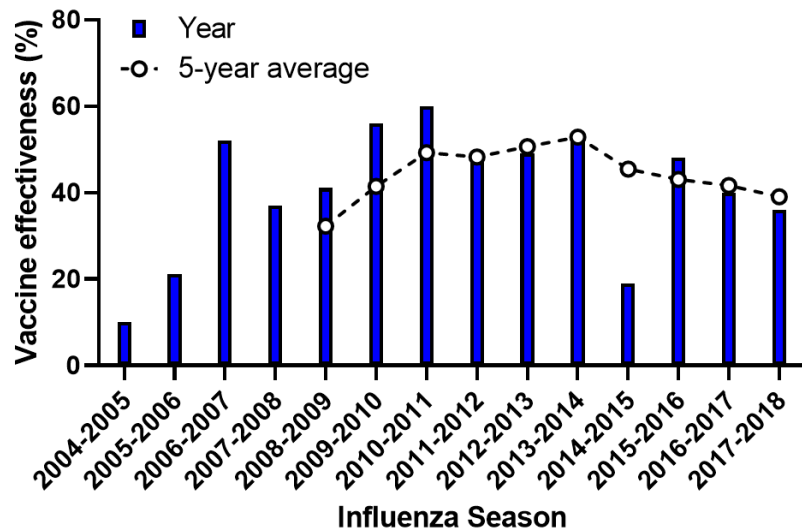


Figure 1.12: Annual vaccine effectiveness in the United States. Influenza vaccine effectiveness since 2004, varying from 60% to 10%. The high mutagenic rate of the HA head of the virus is primarily to blame. The dashed line indicates 5-year rolling average. Adapted from (276)

Europe. Of the IIV subtypes, split virus vaccines are more common and effective, due to exposure of all viral proteins rather than just those on the surface. Interestingly, although less immunogenic when compared to IIV, LAIV more closely mimics a natural infection, therefore conferring a broader adaptive response that comprises cell-mediated immunity and mucosal-associated IgA responses in the upper respiratory tract, in addition to conventional IgG responses (278). To generate, both vaccine types are predominantly propagated in embryonated chicken eggs, which afford high viral titres. Discouragingly, forced viral replication within eggs causes selective egg-adapted changes of the HA protein that lower immunogenicity and lead to antigenic mismatch. This phenomenon is especially evident with the current H3N2 strain that replicates poorly in eggs and, thus, requires several passages to obtain suitable titres,

increasing the occurrence of these egg-adapted changes (279). Adding to these issues is that HPAI strains remain refractory to conventional vaccination strategies, as they are highly pathogenic in embryonated chicken eggs (275).

To partially overcome these shortcomings, novel strategies have been brought forth. Recombinant HA vaccines are approved for use in the United States and are manufactured using recombinant protein-expressing insect cells or viruses (280). As the recombinant HA vaccine does not use replicating virions or eggs, it does not induce egg-adapted mutations, could be used for HPAI vaccines and can also be produced to large volumes within 2 months. However, it only induces immunity to HA and, therefore, is highly dependent on exact strain match. It also exhibits low immunogenicity, being only suitable for healthy individuals between 18-49 as a result (276). IIV and LAIV propagation has been equally done in cell culture (e.g. MDCK cells) to avoid egg-adapted mutations, yet viral replication is reduced when compared eggs and high titres are not sufficiently reached to become a viable option. Intriguingly though, recent work has been undertaken that utilizes the *Nicotiana benthamiana* plant as a vector for quadrivalent influenza vaccine replication (QVLP), which limits propagating strain mutations. Experimentally, QVLPs were shown to be more immunogenic than the split-virion vaccine, inducing both a balanced T- and B- cell response (281). In ongoing Phase II clinical trials, QVLPs were shown to be safe and immunogenic in both young and aged populations (282), suggesting that plant-derived vaccines may be better than current egg-based strategies.

1.5.2: Potential universal influenza vaccinations

Modifications to the current vaccine such as the vector used, route of administration, or initial virus source show promise in improving influenza vaccine efficacy. Yet, due to the fact that current vaccines preferentially induce the generation of neutralizing IgG antibodies that recognize the head of the HA protein, which exhibits rapid mutation rates, all are highly susceptible to viral antigenic drift/shift and poor seeding strain decisions. Thus, the current vaccination strategy is inherently limited in its efficacy by such factors, and, therefore, much of the current vaccine research has shifted towards finding a so-called universal vaccination that is broadly cross-protective. If successful, these universal vaccines would repeal the requirement for yearly vaccination and elongate the protective period, regardless of the dominant circulating IAV, IBV, or, even, HPAI strain. Continuing to target the adaptive arm of immunity, the majority of work has centred around generating neutralizing immunity to more conserved viral epitopes.

Unlike the head domain, the stalk region of the HA protein is antigenically much more conserved. Antibodies that target the HA-stalk are produced during infection, but their numbers are significantly lower than those targeting the head and the stalk is of relatively low immunogenicity. Additionally, they are not naturally neutralizing by preventing viral fusion, as are the anti-HA head antibodies, serving instead to enhance antibody-dependent cell mediated cytotoxicity (ADCC), prevent the HA conformational change in the endosome, or by activating complement, showing activity against a broad range of heterologous influenza infections (283, 284). Enhanced production of these stalk-recognizing antibodies following vaccine is achieved by using an engineered fragmented or headless HA protein to force immunogenicity of the stalk region to both IAV and IBV strains (275, 284). In a similar vein, surface influenza NA proteins have been shown to be quite conserved and in animal studies injection of anti-NA antibodies from immunized animals exhibited heterologous strain protection; however, antibodies against NA have never been formerly quantified in current human vaccines. Excitingly, recent study has elucidated human NA-specific antibodies that offer broadly neutralizing effects against all tested IAV strains of human, swine and avian origins, as well as some IBV strains are generated during vaccination (285). Ongoing study is needed to determine how to enhance the levels of anti-NA antibodies following infection or vaccination, although important proof-of-concept now exists. Similarly, due to its equally conserved nature, the transmembrane M2 protein has been extensively investigated for use in a universal vaccine, having been formally tested in early-phase clinical trials (286). Despite exhibiting safety and some efficacy, no such vaccine has been marketed and greater effort is needed to enhance immunogenicity.

Vaccine efficacy tends to decline in elderly individuals through not well understood mechanisms, which is particularly true in the case of current influenza vaccines. Interestingly, it has been suggested that current influenza vaccines that bolster humoral responses while only weakly promoting cell-mediated responses may be poor candidates for a universal vaccine, as robust vaccine effect has been observed in aged populations in the absence of a humoral response, but with a strong cell-mediated response (287). Furthermore, the immunodominant antigen of cytotoxic T-cells is derived from the NP protein, which is highly conserved within influenza strains, suggesting that T-cell-mediated immunity may play an important role in the cross-protection of a universal vaccine. Similarly, a pox virus vaccine engineered to express conserved internal IAV NP and M1 proteins enhanced T-cell mediated immunity in experimentally infected humans, and decreased disease severity and viral shedding (288). Intriguingly, the previously mentioned plant-derived vaccines also significantly elevated T- as well as B-cell responses (281), suggesting plant produced vaccines may be more protective through a number of mechanisms.

As cytotoxic T-cell responses require infection to occur, they can only limit disease severity, while antibodies can neutralize viruses prior to infection to prevent disease entirely. *Thus, it is expected that a true universal influenza vaccine candidate will synergize cell-mediated and humoral responses, and, as we will explore in the following section, likely involve contributions from the innate system as well, potentially by exploiting an expanding immune concept known as trained immunity.*

1.5.3: Unconventional vaccination: Trained innate immunity

As discussed previously, conventional thinking branched the immune system into the amnestic innate system and the anamnestic adaptive system. The adaptive system is poorly conserved evolutionarily,

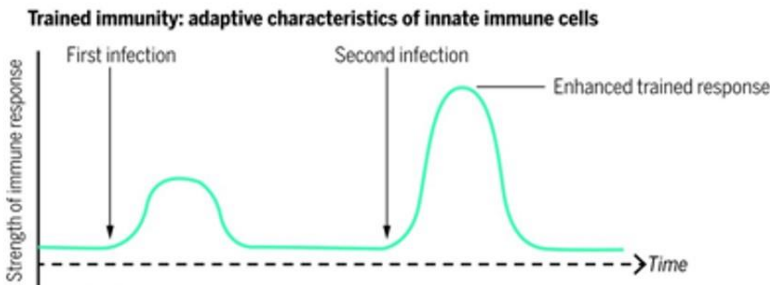


Figure 1.13: Schematic of trained immune responses. Following a trained stimulus, innate immune cells exhibit enhanced inflammatory responses to subsequent stimuli. Taken from (104).

only being found in upper order vertebrates, while all other organisms with an immune system have only an innate compartment or signalling mediators. Thus, it was thought that immune memory was an important immunological step that emerged with the evolution of complex orders of life. However, dating back to the

early 20th century (289), a concept known as systemic acquired resistance (SAR) in plants had been appreciated, where infected portions of plants could relay resistance mechanisms to uninfected portions of plants, akin to vaccination in vertebrates, despite lacking formal immune cells (290). This argued the capacity for immune memory exists outside of the adaptive response. Since then, this capacity has been extensively described in invertebrates, where enhanced resistance to secondary infection was mediated by innate cells (291), and more recently beginning in the 1980s in vertebrates, including humans and other mammals.

In 2011 this phenomenon was coined innate trained immunity (292), where initial inflammatory stimuli could train innate cells (e.g. monocyte/macrophages and NK cells) to respond more robustly to subsequent infections similar or dissimilar to the initial inflammatory cue in comparison to naïve cells (**Figure 1.13**) (105). This boosting of the secondary inflammatory response is mediated by epigenetic (293, 294) and/or metabolic (295, 296) reprogramming induced by the initial stimulus. Effector molecules and

indicators of trained immunity are vast, but research has focused on enhanced release of inflammatory cytokines such as IL-1 β and IL-6 in comparison to untrained cells (105). Very recently, trained immunity has been extended to non-bone marrow-derived cells, such as embryonically-derived lung resident alveolar macrophages (297) and structural cells (298). Although trained immunity has been shown extensively to be protective against infectious diseases, it can manifest itself deleterious during inflammatory disorders such as atherosclerosis and neuropathies (299). **As we highlight in chapter 4, more insight into the signature of protective versus detrimental trained immunity of innate cells imprinted by pathogens is required before it can be harnessed therapeutically.**

Although inducers of trained immunity are still being discovered and likely numerous, two have already been extensively described, one a live bacterium and the other a PRR ligand (105):

1. *Bacillus Calmette-Guérin (BCG): A live attenuated form of the bacterium Mycobacterium bovis, used for over a century as the vaccine against Mycobacterium tuberculosis (Mtb) (300).*
2. *β -Glucan: A polysaccharide PAMP found on the surface of fungi and bacteria that acts as the ligand for the PRR Dectin-1. Dectin-1 is highly expressed on the surface of myeloid cells (301).*

1.5.4: The bone marrow as the critical site for trained immunity

The initial ability of BCG to train cells was described in mature bone marrow-derived monocyte/macrophages of humans and mice through recognition by NOD2 (302). With the half-life of innate immune cells being short, roughly 24 hours for monocytes at steady-state (303), a trained phenotype confined to innate cells shows limited promise in immunity to chronic diseases or as a vaccination strategy. However, as introduced in **section 1.4.7**, bone marrow HSCs give rise to all circulating leukocytes throughout the entirety of an organism's life. Recently, our laboratory showed the importance of the route of delivery in the longevity of trained immunity. By delivering BCG intravenously, which granted BCG

access to the bone marrow, rather than subcutaneously, which did not, bone marrow HSCs became programmed in an IFN-II-dependent manner, which conferred long-lived training to progeny cells and,

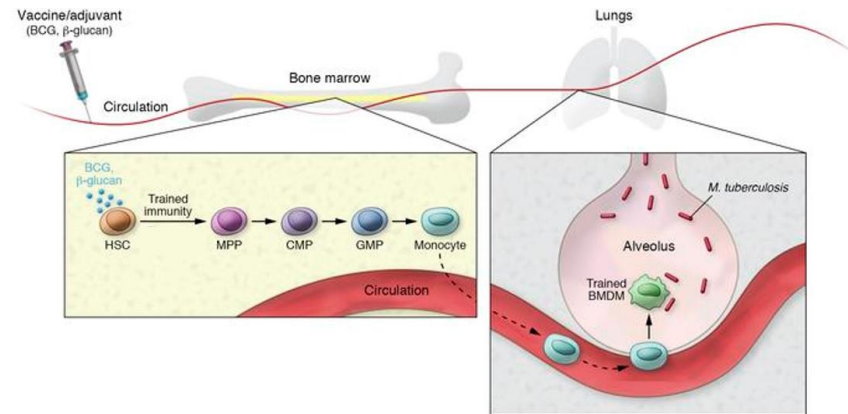


Figure 1.14: Targeting the bone marrow to generate long-term trained immune responses. Initial findings of trained immunity were hampered by the fact that monocytes were short-lived. By gaining access to the bone marrow, BCG programs stem cells, such that all downstream progeny exhibit a trained phenotype that allows them to traffic to the lung and more effectively combat *Mtb*. Taken from (304).

ultimately, to monocyte-derived macrophages via epigenetic and transcriptional changes. This training afforded enhanced antimycobacterial responses of BMDM against subsequent *Mtb* infection for upwards of 5 months in a murine model (304). Thus, by targeting HSCs through intravenous administration, elevated protection can be observed

downstream (**Figure 1.14**) (305). Evidence for the enhanced efficacy of intravenous administration of BCG against *Mtb* has since been extended to non-human primates (306).

1.5.5: Moving towards a more effective influenza vaccine

Taken together, current vaccination strategy is insufficient to protect against seasonal and pandemic influenza infections, in part due to vaccine production drawbacks and the fact it primarily generates highly strain-specific anti-HA-head antibodies. Recent work focusing on the generation of universal vaccines by creating a cross-protective and broadly neutralizing humoral response against more highly conserved antigens such as the HA-stalk, as well as a robust cytotoxic T-cell response have shown considerable promise experimentally. However, as of yet, nothing has fully materialized into a marketable vaccine. Interestingly, innate immune responses, until recently thought to be amnesiac in mammals, are now known to exhibit memory-like responses, called trained immunity, that can provide long-term heterologous protection through HSC reprogramming in the bone marrow. As mentioned, two potent inducers of trained macrophage-mediated immunity are already approved for use in humans and widely deployed: the vaccine for *Mtb*, BCG, and the ligand for the PRR Dectin-1, β -Glucan. Equally, the TLR3 agonist Poly (I:C:LC) has been prophylactically administered intranasally to provide protection against several IAV strains, and

other viruses, alone for up to one month prior (307-309), or as an adjuvant along with the classical influenza vaccine (310), by inducing IFN-I. Recent early results in humans also show promise (311). **Finally, as we will see in chapter 5, these immunomodulators and inducers of trained immunity are appealing candidates as unconventional universal vaccines for IAV due to the non-specific and long-term protection conferred by them.**

1.6: Rationale

It is evident that despite at least a century of intensive clinical, epidemiological, immunological and molecular study, our understanding of the host response to influenza infection remains incomplete. The first influenza pandemic of the 20th century, the 1918 Spanish Flu, was the single deadliest pandemic in human history. Although influenza mortality has dramatically declined to approximately 500 000 deaths per year, much of this can be attributed to the arrival of hygienic practices and the age of antibiotics that curtailed secondary bacterial pneumonia, rather than effective influenza interventions (i.e. antivirals and immunomodulators) or prophylactics (i.e. vaccination). Thus, our ability to effectively combat influenza is still lacking, at least in part due to our imperfect comprehension of the mechanisms underlying a successful immune response.

As highlighted in Chapter 1, it is now appreciated that, upon infection, host defense to influenza can be broadly divided into two branches: host resistance mechanisms which restrict viral replication and disease tolerance mechanisms that counter the tissue damage caused by the inflammatory response. If these branches are appropriately regulated, influenza is dispelled from the lungs, tissue damage is resolved and the host returns to homeostasis. However, if one branch is compromised, immune dysregulation occurs and the host succumbs to infection, either via unsustainable levels of viral replication or an intolerable magnitude of lung pathology. Vaccination can pre-emptively boost both host resistance and disease tolerance mechanisms to ameliorate disease severity, or even prevent infection. Yet, current influenza vaccines fail to provide reliable protection by targeting traditional adaptive memory responses, arguing that alternative strategies of vaccination may yield higher efficacy. Trained immunity represents an appealing mechanism of a universal influenza vaccine, as it can provide non-specific heterologous protection. However, effectors of protective trained immunity *in vivo* are based on hitherto unknown mechanisms, converging on the bone marrow. Thus, the fundamental reason for our study was to carefully interrogate protective pathways of host resistance and disease tolerance to provide therapeutic targets, as well as to better understand the mechanisms of protective trained immunity to harness its potential in future vaccine design.

1.6.1: Main hypotheses

- 1) *Host resistance and disease tolerance mechanisms both critically protect against IAV infection*
- 2) *Differential manipulation of bone marrow hematopoiesis (i.e. myelopoiesis versus lymphopoiesis) is a critical pathogen virulence strategy that manipulates effector leukocyte responses*
- 3) *Protective trained immunity can be utilized as universal vaccination strategies against IAV*

1.6.2: Major objectives

- 1) *To investigate the potential role of RIPK3 in host resistance to IAV*
- 2) *To determine the potential role of CypD in disease tolerance to IAV*
- 3) *To investigate how related mycobacteria BCG and Mtb manipulate hematopoiesis and their effects on trained innate immunity*
- 4) *To harness the power of trained immunity as potential vaccines against IAV*

PREFACE TO CHAPTER 2

Cell death is intimately involved in both host defense to infection, as well as IAV pathogenesis. Extensive work by us (62, 154) and others (312) had previously investigated the role of apoptosis in anti-influenza immunity and disease pathogenesis. However, other cell death pathways remained less thoroughly scrutinized. Interestingly, a novel form of programmed cell death known as RIPK3-dependent necrosis, or necroptosis, in structural cells contributed to host resistance following vaccinia (313) and IAV (222) infections. Yet, macrophage necroptosis following *Mtb* (314) and *S. enterica* (213) infections facilitated bacterial dissemination, suggesting that necroptosis following infection could be either protective or detrimental, depending on the cell type or pathogen. What role necroptosis had in macrophages following IAV infection was completely unknown, but given the critical role of macrophages in immunity to IAV (175, 176), we initially hypothesized that RIPK3-deficiency would conserve macrophage viability and function post-infection to protect against IAV. In fact, unexpectedly, our results outlined a role for RIPK3 in IFN-I production by macrophages that crucially contributed to host resistance to IAV, without affecting macrophage cell death. Thus, the contribution of RIPK3 to IAV resistance is at least two-fold: the control of viral replication through structural cell necroptosis and by IFN-I production by pulmonary macrophages.

CHAPTER 2:

**RIPK3 interacts with MAVS to regulate type I IFN-mediated
immunity to Influenza A virus infection**

RIPK3 interacts with MAVS to regulate type I IFN-mediated immunity to Influenza A Virus infection

Jeffrey Downey^{1*}, Erwan Pernet^{1*}, François Coulombe¹, Benoit Allard¹, Isabelle Meunier¹, Joanna Jaworska¹, Salman Qureshi¹, Donald C. Vinh¹, James G. Martin¹, Philippe Joubert², and Maziar Divangahi¹.

1. Department of Medicine, Department of Pathology, Department of Microbiology & Immunology, McGill University Health Centre, McGill International TB Centre, Meakins-Christie Laboratories, McGill University, 1001 Decarie Boulevard, Montreal, Quebec, H4A 3J1, Canada.
2. Department of Pathology, Quebec Heart and Lung Institute, 2725 Chemin Sainte-Foy, Quebec, Quebec G1V 4G5, Canada

*These authors equally contributed to this work.

Corresponding Author:

Maziar Divangahi, Ph.D.

Assistant Professor of Medicine

RI-MUHC, Centre for Translational Biology

Meakins-Christie Laboratories

1001 Decarie Blvd,

Block E (EM3.2248)

Montreal, Quebec H4A 3J1

Tel: (514) 934-1934 Ext. 76431

email: maziar.divangahi@mcgill.ca

***Plos Pathogens.* 13 (4), e1006326 2017 Apr 14. 10.1371/journal.ppat.1006326**

2.1 Abstract

The type I interferon pathway plays a critical role in both host defense and tolerance against viral infection and thus requires refined regulatory mechanisms. RIPK3-mediated necroptosis has been shown to be involved in anti-viral immunity. However, the exact role of RIPK3 in immunity to Influenza A Virus (IAV) is poorly understood. In line with others, we, herein, show that *Ripk3*^{-/-} mice are highly susceptible to IAV infection, exhibiting elevated pulmonary viral load and heightened morbidity and mortality. Unexpectedly, this susceptibility was linked to an inability of RIPK3-deficient macrophages (M ϕ) to produce type I IFN in the lungs of infected mice. In M ϕ infected with IAV *in vitro*, we found that RIPK3 regulates type I IFN both transcriptionally, by interacting with MAVS and limiting RIPK1 interaction with MAVS, and post-transcriptionally, by activating protein kinase R (PKR)—a critical regulator of IFN- β mRNA stability. Collectively, our findings indicate a novel role for RIPK3 in regulating M ϕ -mediated type I IFN anti-viral immunity, independent of its conventional role in necroptosis.

2.2 Author Summary

Influenza A virus (IAV) is a pulmonary pathogen that presents a significant threat to human health through seasonal epidemics and occasional, highly lethal pandemics. Type I IFN is an essential component of anti-viral immunity to influenza infection and pulmonary macrophages are the major source of type I IFN. Recently, we have shown that programmed macrophage cell death (apoptosis) plays a key role in immunity to influenza infection. Interestingly, another cell death program, termed necroptosis, has been implicated in control of viral infection via receptor-interacting serine/threonine protein kinase 3 (RIPK3). In the present study, we define a novel role of RIPK3 in regulating the type I IFN pathway to protect against lethal IAV infection, which is independent of necroptosis. RIPK3 regulates type I IFN signaling at both the transcriptional and post-transcriptional levels to sequester viral replication and protect the host against influenza infection. Thus, manipulation of the RIPK3 pathways poses a novel avenue in the development of anti-IAV treatments.

2.3 Introduction

Pulmonary macrophages (M ϕ) reside in the unique extraepithelial environment of the lower airways and are the main source of one of the key components of host anti-viral immunity: type I IFN (primarily IFN- α and β) (178, 315, 316). However, many highly pathogenic viruses, including IAV, have evolved to reach the lower respiratory tract and effectively sidestep the type I IFN pathway in M ϕ . Initial recognition of IAV-ssRNA occurs by the cytosolic RNA helicase retinoic acid-inducible gene I (RIG-I) that interacts with the mitochondrial anti-viral-signaling protein (MAVS) to activate the interferon regulatory factor 3 (IRF3)-mediated type I IFN pathway, upstream of the TANK-binding kinase 1 (TBK1) (152). Subsequent binding of type I IFNs to their heterodimeric receptor (IFN α R) leads to activation of the JAK/STAT pathway and the transcription of IFN-inducible genes (ISGs), such as the double-stranded RNA-dependent protein kinase R (PKR), which is critical in controlling viral replication, by regulating proteins involved in inhibiting both host and viral translation (317) as well as IFN- β mRNA integrity (132).

Resident alveolar M ϕ are the first immune cells to encounter IAV in the airways and orchestrate the immune response (175). While both the frequency and number of resident alveolar M ϕ are constant shortly after infection (318), the frequency and total cell number of bone marrow derived-monocytes, recruited in a CCR2-dependent manner, are significantly increased and represent the major source of M ϕ in the lungs during IAV infection (154, 184). We, and others, have shown that the induction of type I IFN by pulmonary M ϕ is indispensable during IAV infection (154, 178, 315). Thus, it is not surprising that IAV has evolved several strategies to inhibit the type I IFN axis, including encoding the virulence factor PB1-F2, which specifically targets mitochondria to induce early apoptosis in M ϕ (18, 319) to limit the production of type I IFN (62). Interestingly, the receptor interacting serine/threonine protein kinase (RIPK) family members (RIPK1 and RIPK3) regulate necroptosis (a form of programmed necrosis) and play a critical role in immunity to viral infections. For example, RIPK3-mediated necroptosis was shown to be important in the host defense against vaccinia virus (313), murine cytomegalovirus (MCMV) (320), as well as IAV (222). Additionally, a cell death-independent role for RIPK1 and RIPK3 in inflammation has also been described in myeloid cells. In models of LPS-induced inflammation using bone marrow-derived M ϕ (BMD-M ϕ) (321), or bone marrow-derived dendritic cells (DC)

(322), RIPK3-deficient cells failed to release pro-inflammatory cytokines (323, 324). Consistent with these studies, it has been also demonstrated that RIPK1 regulates the production of potent inflammatory cytokines, including TNF- α (325). Importantly, it has recently been shown that RIPK3 confers enhanced viral clearance and protection to IAV by modulating apoptotic and necroptotic cell death in infected lung structural cells (222), while its expression moderately affects the pro-inflammatory and anti-viral signature of fibroblasts (326). However, the function of RIPK3 in lung immune cells, which contribute significantly to immunity to IAV infection has not been well understood.

In this report, we sought to further delineate the role of RIPK3 in immunity to pulmonary IAV infection. As previously shown, herein, we define RIPK3 as an essential component of host defense against IAV infection. Surprisingly, RIPK3-deficient mice were extremely susceptible to IAV infection due to a significant reduction in type I IFN. Pulmonary M ϕ from RIPK3-deficient mice failed to mount an effective type I IFN response to IAV. Mechanistically, we demonstrated that RIPK3 was upregulated in IAV-infected M ϕ and its induction was required for optimal production of type I IFN at two steps: via interaction with MAVS to regulate IFN- β transcription and via activation of PKR to stabilize IFN- β mRNA. Notably, the loss-of-function in RIPK3 has no effect on cell death responses to IAV-infected M ϕ , both *in vitro* and *in vivo*, indicating a new cell-death independent function for this kinase in innate anti-viral responses.

2.4 Results

RIPK3-deficient mice are highly susceptible to IAV infection and exhibit a heightened pulmonary viral load

To examine a potential role for RIPK3 in immunity to IAV infection, wild-type (WT) and *Ripk3*^{-/-} mice were infected with a low dose (50 pfu) of IAV. *Ripk3*^{-/-} mice exhibited significant morbidity as shown by increased weight loss (Fig 1A) as well as mortality (Fig 1B) compared to WT mice. Similar data were obtained using a higher dose of (90 pfu \approx LD₅₀) of IAV infection (S1A-B Fig). This increase of mortality was associated with a significantly increased pulmonary viral load (Fig 1C) and decreased levels of active type I IFN in both the airways and the lungs (Fig 1D and 1E, respectively) and reduced levels of IFN- β in the lungs (S1C Fig). Corresponding to the increased pulmonary viral load (Fig 1C), *Ripk3*^{-/-} lungs had a higher percentage of viral nucleoprotein (NP)⁺ cells in both epithelial cells (Non-leukocytes, CD45⁻ NP⁺) as well as leukocytes (CD45⁺ NP⁺) (Fig 1F). Interestingly, the percentage of NP⁺ pulmonary M ϕ (CD45⁺ F4/80⁺ CD19⁻) was higher in the lung (S1D Fig) and BAL (Fig 1G) of *Ripk3*^{-/-} mice, indicating RIPK3-deficient M ϕ are more susceptible to IAV infection *in vivo*. The initial control of virus propagation is a major determinant of an adequate host immune response, allowing elimination of the pathogen with minimal immunopathology. In line with this, the significant increase in viral load in *Ripk3*^{-/-} mice correlated with markedly enhanced inflammation (Fig 1H, S2A-B Fig) and immunopathology (Fig 1I and S1E Fig) as well as reduced pulmonary function (Fig 1J). Collectively, these data indicate that RIPK3 plays an indispensable role in immunity to IAV infection by regulating host pulmonary anti-viral responses and reducing pulmonary immunopathology.

RIPK3 is required for optimal induction of type I IFN in M ϕ infected with IAV

During the steady state, the pulmonary compartment is primarily comprised of resident alveolar M ϕ (AM ϕ). However, after pulmonary infection the recruitment of monocyte/M ϕ from the bone marrow is critical for host defense to infection (123). Since M ϕ are the primary source of type I IFN in response to pulmonary viral infections (154, 178, 315, 316) and *Ripk3*^{-/-} mice elicited

attenuated type I IFN responses to IAV, we next determined whether *Ripk3*^{-/-} Mφ are impaired in their ability to produce type I IFN *in vitro*. Consistent with the significant reduction of type I IFN and increased viral load in the lungs of RIPK3-deficient mice, a significant reduction of total active type I IFN and IFN-β was observed in IAV-infected *Ripk3*^{-/-} BMD-Mφ (Fig 2A-B), AMφ (S3A Fig), but not BMDC (S3B Fig). In addition, RIPK3-deficient BMD-Mφ were more permissive to IAV infection, as evaluated by qPCR for IAV NS1 transcripts (Fig 2C), flow cytometry for NP protein (Fig 2D), or standard plaque assay (S3C Fig). Similarly, WT BMD-Mφ treated with the selective inhibitor of RIPK3 activity (GSK ‘843) also exhibited less active type I IFN upon IAV infection (Fig 2E) with a higher viral load (Fig 2F). Finally, we sought to extend the role of RIPK3 in immunity to IAV in human monocyte-derived Mφ. Using monocyte-derived Mφ generated from peripheral blood mononuclear cells (PBMC) obtained from healthy donors and infected with a human strain of IAV (H3N2), RIPK3-inhibited PBMC released significantly less type I IFN (Fig 2G) and exhibited an elevated viral load (Fig 2H). These data collectively indicate that RIPK3 regulates the induction of type I IFN in murine and human Mφ infected with IAV.

As necroptosis has been shown as a mechanism involved in cytokine release (e.g. IL-1) (323), and RIPK3 is a key player in this cell death pathway, we initially hypothesized that RIPK3-mediated necroptosis is required for the secretion of type I IFN from IAV-infected BMD-Mφ. Consistent with other experimental models using LPS (327), which show that the addition of the pan-caspase inhibitor (zVAD-FMK) is required for the induction of necroptosis (S3D Fig), we also found that inhibition of caspases via zVAD increased necroptosis in IAV-infected BMD-Mφ (Fig 2I). In these experimental models, the induction of necroptosis was RIPK1- and RIPK3-dependent, as necroptosis was completely abrogated by addition of necrostatin-1 (Nec-1) or the loss-of-function of RIPK3 (Fig 2I and S3D Fig). However, in the absence of zVAD, using the LDH assay (Fig 2J), Annexin V/7-AAD staining (S3E Fig), or viability dye (S3F Fig), we found no difference in the cell death program between groups of IAV-infected BMD-Mφ at any time points of infection. In agreement with these *in vitro* observations, the levels of pulmonary Mφ death were not altered in the BAL of WT and *Ripk3*^{-/-} mice infected with IAV (S3G Fig). Thus, the use of pan-caspase inhibitors to reveal necroptosis in the majority of experimental models may mask the other biological functions of RIPK1/RIPK3 in natural settings. Together, these results

indicate that the lack of type I IFN responses by *Ripk3*^{-/-} BMD-Mφ is not coupled to cell death outcomes in IAV-infected Mφ.

RIPK3 interacts with MAVS, mediating type I IFN signaling in BMD-Mφ infected with IAV

As the induction of the type I IFN pathway is critically mediated by RIG-I/MAVS signaling during IAV infection in BMD-Mφ (S4A Fig), we next assessed whether RIPK1 and RIPK3 are involved in regulation of this pathway. Following IAV infection of WT BMD-Mφ, we observed an upregulation of RIPK3 (Fig 3A). We found that prior to IAV infection, RIPK3 is primarily localized in the cytoplasm (Fig 3B-C). However, following IAV infection of WT BMD-Mφ, the levels of cytoplasmic RIPK3 markedly decreased, while there was an increase in RIPK3 translocation to the mitochondria (Fig 3B-C). Interestingly, we also found that RIPK3 interacted with MAVS (Fig 3D and S4B Fig) and surprisingly, in IAV-infected *Ripk3*^{-/-} BMD-Mφ, there was a robust interaction between RIPK1 and MAVS (Fig 3E and S4B-C Fig) at the mitochondria (Fig 3F). This enhanced interaction between RIPK1/MAVS led to a significantly increased level of phosphorylation of the downstream mediators of MAVS signalling, TBK1 and the transcription factor IRF3 (Fig 3G-H). A similar trend was also observed in stimulation of *Ripk3*^{-/-} Mφ with the RIG-I ligand, 5'triphosphate (ppp) dsRNA, which led to increased levels of interaction between RIPK1 and MAVS, increased phosphorylation of IRF3, as well as IFN-β transcripts (S4D-F Fig). To test whether RIPK1 directly mediates TBK1 activation, we next inhibited RIPK1 using Nec-1 and demonstrated that TBK1 activation was completely abolished in IAV-infected *Ripk3*^{-/-} BMD-Mφ (Fig 3H and S4G Fig). Furthermore, inhibition of RIPK1 by Nec-1 significantly decreased the levels of IFN-β mRNA after IAV infection (Fig 3I). These data collectively indicate that in the absence of RIPK3, there is increased activation of the RIPK1-dependent RIG-I/MAVS signaling pathway. Thus, these findings support RIPK3 as a negative regulator of RIPK1-mediated activation of type I IFN signaling pathways during IAV infection.

RIPK3 activates the PKR pathway in BMD-M ϕ infected with IAV, increasing the integrity of IFN- β transcripts and promoting protection

Given the increased activation of TBK1/IRF3 signaling in *Ripk3*^{-/-} BMD-M ϕ , we next investigated whether this leads to an upregulation at the transcriptional level of IFN- β . In line with the increased TBK1/IRF3 signaling, IFN- β transcripts were elevated in IAV-infected RIPK3-deficient BMD-M ϕ (Fig 4A). Similarly, the levels of IFN- β transcripts were also significantly elevated in the lungs of *Ripk3*^{-/-} mice after 3 and 6 days of IAV infection (Fig 4B). These results were surprising as the levels of IFN- β protein were significantly reduced in both IAV-infected *Ripk3*^{-/-} BMD-M ϕ (Fig 2A-B) and lungs (Fig 1D-E and S1C Fig). To address the disparity between the transcription and translation of IFN- β in RIPK3-deficient BMD-M ϕ and lungs, we next investigated the mechanism involved in IFN- β post-transcriptional regulation. Protein kinase R (PKR) is an important player in the host response to viral infections mainly via phosphorylating the α subunit of the translation initiation factor eIF2 (eIF2 α) that inhibits both host and viral mRNA translation, thus suppressing viral propagation (317, 328). Additionally, several studies also demonstrate that PKR plays a key role in augmenting type I IFN responses to viral infection (132, 329). This mechanism can occur at a translational level through activation of eIF2 α kinase (330) or at a post-transcriptional level by preserving the integrity of IFN- β mRNA, via the maintenance of its poly(A)-tail (132). We found that during IAV infection there was no difference in phosphorylation of eIF2 α in *Ripk3*^{-/-} or WT BMD-M ϕ (Fig 4D). However, after IAV infection, activation of PKR was markedly reduced in *Ripk3*^{-/-} BMD-M ϕ , compared to the WT as assessed by confocal microscopy (Fig 4C) or western blot (Fig 4D), and no significant effects were observed in the total PKR protein (S5A Fig). Correlating to these *in vitro* findings, we also found a significant reduction of PKR phosphorylation in the lungs of IAV-infected *Ripk3*^{-/-} mice, compared to infected WT mice (Fig 4E). Furthermore, the reduction of PKR activation in IAV-infected *Ripk3*^{-/-} BMD-M ϕ correlated with diminished IFN- β mRNA stability, as evaluated by the levels of IFN- β mRNA after synthesis of cDNA with oligo(dT) primers, compared to hexamer primers (Fig 4F). Comparable to another viral model (132), this effect was specific to IFN- β mRNA, as the levels of GAPDH (S5B Fig) and IL-6 (S5C Fig) mRNA did not differ following synthesis with either hexamer or oligo(dT) primers. In agreement with the loss of IFN- β mRNA integrity, confocal analysis confirmed the reduction of intracellular IFN- β protein levels within *Ripk3*^{-/-} IAV-

infected BMD-M ϕ (Fig 4G-H). These data collectively indicate that in RIPK3-deficient M ϕ and mice infected with IAV, PKR activation is profoundly compromised, leading to reduced IFN- β mRNA stability and thus IFN- β production.

Finally, to directly address whether the reduced anti-viral function of *Ripk3*^{-/-} BMD-M ϕ *in vitro* translated to an impaired control of IAV replication *in vivo*, we adoptively transferred (intratracheally) BMD-M ϕ from either *Ripk3*^{-/-} or WT mice into *Rag1*-deficient mice (lacking B and T cells), which were then infected intranasally with IAV (Fig 4I). At day 3 post IAV-infection, the *Rag1*^{-/-} mice that received *Ripk3*^{-/-} BMD-M ϕ showed a significantly increased pulmonary viral titre in comparison to the *Rag1*^{-/-} mice that received WT BMD-M ϕ (Fig 4J). Finally, to provide the direct link between reduction of type I IFN in RIPK3-deficient mice and susceptibility to IAV infection, we reconstituted IFN- β in the lungs of *Ripk3*^{-/-} mice and showed that there was a significant reduction in pulmonary viral load, which was comparable to the viral load in infected WT mice (Fig 4K). Taken together, our data provide the first evidence that RIPK3 intrinsically regulates anti-viral immunity in M ϕ , independent of its conventional role in necroptosis, by driving PKR activation and the IFN- β anti-viral effector program.

2.5 Discussion

In the present study, we define a novel and critical role of RIPK3 in host defense against IAV. Our findings provide strong evidence that in IAV-infected M ϕ , RIPK3 regulates type I IFN production at both the transcriptional level, via interaction with the RIG-I/MAVS signaling pathway, as well as the post-transcriptional level, via activation of PKR (**Fig 5**).

RIPK3 was initially identified as a master regulator of necroptosis (221). Genetic studies have undoubtedly shown the critical physiological role of RIPK1/3 dependent necroptosis in embryonic development (331, 332). Moreover, accumulating evidence indicates that RIPK1/3 are also key players in host defense. Several viral infections have been shown to initiate RIPK1/3 mediated necroptosis, which contributes to host immunity against the infection (313, 320, 333). While a previous study suggested that the protection and survival of RIPK3-deficient mice is comparable to WT mice following IAV infection (334), here we have demonstrated that RIPK3-deficient mice are remarkably susceptible to pulmonary IAV infection, which is also in line with a recent study by Balachandran's group (222). The exact nature of this difference is unknown, but we speculate that the strain of IAV, as well as the low dose of IAV (~0.4 LD₅₀), which was weight-adjusted, may potentially explain these differences. Additionally, following IAV infection, it was shown that RIPK3 was critical in the production of IL-1 β by M ϕ via the NLRP3 inflammasome (333). Although, the *in vivo* consequences of this deficiency were not investigated in that study, activation of the NLRP3 inflammasome was previously shown to be crucial in immunity to IAV infection (251).

RIPK3 deficient mice are fully resistant to murine cytomegalovirus (MCMV) (320), murine hepatitis virus (335) and lymphocytic choriomeningitis virus (336), but they are particularly susceptible to vaccinia virus (313). The susceptibility of RIPK3-deficient mice to vaccinia has been directly linked to necroptosis in a RIPK1-dependent manner (313), while their resistance to MCMV—despite their inability to induce necroptosis—was RIPK1-independent (320). These differences might be the reflection of a dual regulatory role of RIPK1 in the transcription of cytokines, as well as cell death. For instance, RIPK1 was shown to be essential in inducing inflammatory cytokines (IL-6, IL-1 β , TNF- α) in response to bacterial (337) and viral infections (338). This pro-inflammatory role may be explained by its ability to trigger NF- κ B

activation via a TLR3/TRIF-dependent pathway (339, 340). In the case of type I IFN, during dsRNA responses (338) and following VSV or Sendai virus infection (341), RIPK1 has been shown to be involved in upregulation of type I IFN signaling and can interact with the RIG-I/MDA5/MAVS complex (152, 342, 343). Similar to these studies, our data indicate that during IAV infection, in the absence of RIPK3, there is a markedly increased interaction between RIPK1 and MAVS compared to WT that leads to enhanced activation of TBK1/IRF3 and transcription of IFN- β mRNA in M ϕ . Interestingly, others have previously reported that RIPK3 negatively regulates the TRIF-RIPK1-induced NF- κ B pathway (339). Our data suggest a potentially similar mechanism in which the interaction of RIPK3 with MAVS limits its interaction with RIPK1 to dampen TBK1/IRF3 activation. Whether RIPK3 directly inhibits RIPK1 recruitment to RIG-I/MAVS, or recruitment of other partners in the complex, requires further investigation. Taken together, our data support the function of RIPK1 as an activator of host immunity, while RIPK3 serves to limit RIPK1 activity, regulating the inflammatory response at the signaling level during the “tug-of-war” between host defense and tolerance.

Several recent reports (321, 322, 333, 344) describe the functional role of RIPK3 in regulating pro-inflammatory cytokines, independent of necroptosis. Herein, we showed that RIPK3 controls IFN- β production at the mRNA level, by regulating the stability of IFN- β transcripts through the activation of PKR. It is well established that PKR-deficient cells are impaired in type I IFN production following viral infections. Interestingly, a study by Schulz and colleagues revealed that PKR activation is indispensable in the production of IFN- β to MDA5-mediated viruses (e.g. ECMV) but dispensable for RIG-I-mediated viruses (e.g. Sendai virus, Δ NS1-IAV) in infected DC. However, another study indicated that the optimal production of type I IFN in pulmonary macrophages infected with IAV was dependent on activation of PKR (216). Similarly, we also found that PKR plays an indispensable role in the stability of IFN- β mRNA by maintaining the poly(A) tail in IAV-infected BMD-M ϕ , rather than controlling IFN- β production through eIF2 α kinase activation. How RIPK3 regulates PKR activation and which molecular mechanisms are involved upstream of RIPK3 in this process need further investigation.

Interestingly, the DNA-dependent activator of IFN regulatory factors (DAI) is a recently characterized sensor of IAV that modulates both cell death responses (345) and inflammation

(250). In the study by Thapa et al., DAI was shown to promote apoptosis and necroptosis upstream of RIPK3 in IAV-infected fibroblasts, supporting DAI as an activator of RIPK3. Moreover, DAI was first identified as an activator of TBK1/IRF3 in the type I IFN response to herpes simplex virus 1 (346). These studies are intriguing and may reveal the differential role of RIPK3 in regulating type I IFN production via sensing IAV genomic RNA and the RIG-I/MAVS axis versus necroptosis via DAI/MLKL axis. Potentially, the differential expression of RIG-I versus DAI in different cell types can dictate the functional role of RIPK3 in immune cells (e.g. macrophages) versus structural cells (e.g. fibroblasts or epithelial cells). Furthermore, the replicative capacity of IAV and the levels of cytosolic IAV genomic RNA in each cell type may preferentially activate one axis versus the other. Certainly, this is a very exciting area of research and further investigation is required to determine the mechanisms regulating innate immunity to IAV infection.

Moreover, although in the current study we demonstrate that the function of RIPK3 is dispensable in M ϕ death modality during IAV infection, the contribution of RIPK3 in pathogenesis of IAV *in vivo* is certainly more complex and we cannot exclude its potential role as a death kinase in other immune cells or structural cells. In this context, a recent publication highlighted the critical role of RIPK3-mediated necroptosis in promoting immunity to IAV in fibroblasts (222). Interestingly, they also showed that the levels of type I IFN, although modest, were significantly reduced in RIPK3-deficient fibroblasts after infection with IAV (326). However, fibroblasts contribute substantially less to type I IFN production than macrophages, which have been demonstrated to be the main producer of type I IFN during IAV infection (154). Both our study, as well as Balachandran's studies indicate that RIPK3 has evolved to promote viral clearance through distinct mechanisms in immune (macrophages) and lung structural cells (fibroblasts). Furthermore, the function of RIPK3 also appears to differ among immune cells. For instance, RIPK3-deficient DC were impaired in the production of pro-inflammatory cytokines following LPS stimulation, while M ϕ were not (322). Our data also support this notion since the production of type I IFN was only impaired in M ϕ but not DC. Thus, the mechanisms underlying the differential activation of RIPK3 is certainly cell, as well as pathogen specific.

Pulmonary M ϕ convert into highly active cells following detection of IAV viral particles by PRRs and become the major source of type I IFN (154). As the initial control of virus

propagation through type I IFN is a major determinant of an adequate host immune response that eliminates the pathogen with minimal immunopathology, IAV has evolved multiple strategies to subdue M ϕ type I IFN pathways. We have recently demonstrated that the mitochondrial PRR belonging to the NOD-like family (NLRX1) plays a critical role in M ϕ by maintaining mitochondrial fitness and preventing IAV-induced cell death to maximize type I IFN production (62). IAV's strategies for suppressing type I IFN in M ϕ is not limited only to PRRs, as they also target M ϕ eicosanoid pathways (154). In line with this, one may envision a scenario where IAV evolved a strategy to upregulate RIPK3 to dampen RIPK1/MAVS-mediated TBK1/IRF3/type I IFN production to facilitate its replication. However, the host may have counter-evolved to promote a secondary role of RIPK3 in activating PKR and eliciting type I IFN responses through mRNA stability. Additional studies are required to address this unique function of RIPK3 in regulating type I IFN responses, following infection with other strains of IAV or pathogens.

In summary, we provide conclusive *in vivo* evidence showing that the lack of RIPK3 limits the production of type I IFN, which results in enhanced IAV propagation, early excessive host inflammatory responses that contribute to pulmonary tissue and vasculature damage/dysfunction and, ultimately, enhanced mortality. The integrity of type I IFN pathways is essential in anti-viral immunity and identification of molecular mechanisms that are involved in maintaining this will undoubtedly provide new opportunities for targeted therapy of highly pathogenic strains of IAV.

2.6 Materials & Methods

Mice

Six- to ten-week-old C57BL/6 mice were purchased from Jackson Laboratories. *Ripk3*^{-/-}, kindly provided from Vishva Dixit (Genentech, San Francisco), and *Mavs*^{-/-}, a kind gift from Dr. Salman Qureshi (McGill University), were bred at McGill University. Experiments were performed using age- and sex-matched mice.

Isolation and Culture of Primary Macrophages and Cell Lines

Murine Bone Marrow-Derived Macrophages (BMD-M ϕ) were isolated following aseptic flushing of tibiae and femurs of eight- to ten-week-old mice. Macrophages were differentiated from bone marrow precursors for 7 days in RPMI-1640 supplemented with 30% (vol/vol) L929 cell- [American Type Culture Collection (ATCC)] conditioned medium, 10% (vol/vol) FBS, 2 mM L-glutamine, 1 mM sodium pyruvate, 1% essential and nonessential amino acids, 10mM HEPES and 100 U/mL penicillin/streptomycin. To generate BMDC, bone marrow was cultured in RPMI-1640 supplemented with 10% (vol/vol) FBS, 2 mM L-glutamine, 1 mM sodium pyruvate, 1% nonessential amino acids, 100 U/mL penicillin/streptomycin and 0.35% B-mercaptoethanol, containing 20 ng/ml of GM-CSF as described previously (347). Alveolar macrophages (AM ϕ) were collected by bronchoalveolar lavage of naïve mice using cold, sterile PBS. AM ϕ were cultured in RPMI-1640 supplemented with 10% (vol/vol) FBS, 2 mM L-glutamine, 10mM HEPES and 100 U/mL penicillin/streptomycin. After 1h adhesion, AM ϕ were washed with PBS and placed in fresh media. Madin-Darby Canine Kidney cells (MDCK) were obtained from ATCC and maintained in Dulbecco's Modified Eagle Medium (DMEM) enriched with 10% (vol/vol) FBS, 2mM L-glutamine, and 100 U/mL of penicillin/streptomycin. To generate human monocyte-derived macrophages, peripheral blood mononuclear cells (PBMCs) were isolated from healthy donors using Ficoll-Paque PLUS (GE Healthcare, Burlington, ON, Canada), according to the manufacturer's protocol. PBMCs were then cultured in RPMI with 2% human serum with 20ng/mL of human M-CSF. Monocytes were differentiated for 7 days with fresh media added

every second day. All reagents and supplements pertaining to cell culture were purchased from GIBCO. Cells were seeded at a density $0.5-1.5 \times 10^6$ cells/well of a 6-well plate.

Viruses and Infections

All *in vitro* and *in vivo* infections were performed using influenza A/Puerto Rico/8/34 (H1N1) virus (IAV), kindly provided by Dr. Jonathan A. McCullers (St. Jude Children Research Hospital), except for *in vitro* infections of human cells that were performed using the clinical strain H3N2 A/Hong-Kong/1/68. Mice were challenged intranasally (in 25 μ L PBS) with IAV at a sublethal dose of 50 pfu or a lethal dose of 90 pfu. *In vitro*, BMD-M ϕ were seeded in tissue culture plates the day before infection, unless indicated otherwise, and infections were performed in fresh medium lacking L929 cell-conditioned medium with 1, or 5 multiplicities of infection (MOI) of virus. Viruses were propagated and isolated from MDCK cells and titrated using standard plaque assay in MDCK cells (348).

Flow Cytometry

BAL were collected by cannulating the trachea with a 22-gauge cannula, then washing the lungs with 3 x 800 μ L of cold, sterile PBS. The total volume of the recovered lavage after 3 washes was ~2mL. Cells were initially surface stained with anti-CD16/32 (BD Bioscience) in 0.5% BSA/PBS solution to block non-specific AB interaction with Fc receptors. Cells were then surface-stained with different combinations of PE-conjugated anti-Siglec-F, PE-Cy7-conjugated anti-F4/80, APC-conjugated anti-CD11c, APC-Cy7 anti-CD11b, FITC-conjugated anti-Gr1, PE-Cy5.5-conjugated anti-CD115 (All from BD Biosciences). For NP staining, cells were fixed and permeabilized using BD CytoFix/CytoPerm (BD #554714) before intracellular staining with FITC-conjugated anti-NP (Abcam #ab20343). Flow cytometry was performed using BD LSR II (BD Biosciences) with FACSDiva Software Version 6.1.2 (BD Biosciences). Analysis was performed using FlowJo Software Version 10.0.6 (Tree Star).

Histopathological analysis

Lungs were inflated and fixed for at least 24 hours with 10% formalin, and then embedded in paraffin. 5 μ m sections were cut and stained with hematoxylin-eosin. Slides were scanned at a resolution of 200X magnification (Nanozoomer scanner, Hammamatsu, Japan) and pictures were taken using NDPI viewer (Hammamatsu, Japan).

Analysis of Pulmonary Function

Airway responses to methacholine were evaluated using a small animal ventilator (flexiVent apparatus and flexiVent 5.1 software) as previously described (349).

Cell Death Analysis

LIVE/DEAD Fixable Violet Dead Cell staining was implemented to determine cell viability following viral infection (Molecular Probes). Necrosis and apoptosis levels *in vitro* and *in vivo* were assessed using the PE-AnnexinV and 7-amino-actinomycin D (7-AAD) Apoptosis Detection Kit I (BD Biosciences) according to the manufacturer's instructions and analyzed by flow cytometry. Lactate dehydrogenase (LDH) release in culture supernatants of IAV-infected BMD-M ϕ was quantified using the CytoTox 96 Non-Radioactive Cytotoxicity Assay (Promega), as per the manufacturer's recommendations.

BMD-M ϕ Stimulation and Cytokine Quantification

BMD-M ϕ were stimulated with 100ng/mL of LPS (Sigma-Aldrich) for 24 hours or with 1 μ g/mL of 5'triphosphate (ppp) dsRNA (InvivoGen) for different lengths of time. Secretion of total active type I IFN (both IFN- α and IFN- β) in BAL fluid, lung homogenates and cell culture supernatants was assessed using B16-blue IFN α/β reporter cell line (InvivoGen), according to the specifications

of the manufacturer. IFN- β levels in culture supernatants were measured using Verikine Mouse IFN- β ELISA kit (PBL Assay Science #42400-1). When indicated, BMD-M ϕ were pre-treated with a combination of necrostatin-1 inhibitor (Nec-1, 10 μ M, Sigma-Aldrich), zVAD-FMK (zVAD, 25 μ M, R&D) for 1 hour before infection with IAV. In some experiments, BMD-M ϕ were pre-treated with the selective RIPK3 inhibitor GSK'843 (kindly provided by GSK) (10 μ M) (350). Samples were then collected for further analysis.

RNA Isolation and RT-qPCR.

RNA from BAL of IAV-infected mice or from BMD-M ϕ was extracted using Qiazol reagent (Qiagen) according to manufacturer's instructions. Five hundred ng of RNA was reverse transcribed using the Quantitect Reverse Transcription kit (Qiagen), as directed by the manufacturer. cDNA was generated by qPCR using EvaGreen SYBR Green (Biorad) and the following primers : *GAPDH*-forward: 5'-GGTCCTCAGTGTAGCCCAAG-3'; *GAPDH*-reverse: 5'-AATGTGTCCGTCGTGGATCT-3'; *Ifn- β* -forward: 5'-AGACTATTGTTGTACGTCTCC-3'; *Ifn- β* -reverse: 5'-CAGTAATAGCTCTTCAAGTGG-3'; *IL-6*-forward: 5'-CACAAAGCCAGAGTCCTTCAGAGA-3'; *IL-6*-reverse: 5'-CTAGGTTTGCCGAGTAGATCT-3'-forward. Viral *NSI*-forward: 5'-AGAAAGTGGVAGGCCCTCTTTGTA-3'. Viral *NSI*-reverse: 5'-GGGCACGGTGAGCGTGAACA-3'. Cq values obtained on CFX96 PCR System (Biorad) were analyzed using the formula $2^{-\Delta Cq}$ formula normalizing target gene expression to *GAPDH*. In some experiments oligo dT primers (0.4 μ g/mL, Qiagen) were used in place of random hexamer primers to generate cDNA targeting specifically the poly(A)-tail of the mRNA. For the experiments involved in mRNA stability, the fold difference in gene expression was calculated by using the formula $2^{-\Delta Cq}$, where $\Delta Cq = Cq\text{-target gene}_{\text{wild-type}} - Cq\text{-target gene}_{\text{Ripk3}^{-/-}}$.

Western Blot

Cells obtained from BAL of WT or *Ripk3*^{-/-} mice at day 3 post-infection or BMD-Mφ were lysed in lysis buffer (1% Triton X-100, 150mM NaCl, 20mM Hepes pH7.5, 10% glycerol, 1mM EDTA, supplemented with anti-protease and anti-phosphatase cocktails, Roche) and protein concentration was determined using BCA assay (Pierce). 20 μg of protein were resolved by SDS-PAGE and transferred onto PVDF membranes (Biorad). Membranes were blocked and incubated overnight at 4°C with gentle agitation with primary antibodies. The following primary antibodies were used: anti-RIPK3 (1:1000, Proscience #2283), anti-phospho-PKR (1:200, Santa Cruz Biotechnology #sc-101784), anti-PKR (1:200, Santa Cruz Biotechnology #sc-1702), anti-RIPK1 (1:1000, Cell Signaling Technology #3493), anti-phospho-IRF3 (1:500, CST #4947), anti-IRF3 (1:1000, CST #4302), anti-phospho-eIF2α (1:1000, CST #3597), anti-eIF2α (1:1000, CST #5324), anti-MAVS (1:1000, CST #4983), anti-TBK1 (1:1000, CST #3504), anti-pTBK1 (1:1000, CST #13498), anti-CYPD (1:1000, Calbiochem #AP1035) and anti-actin (1:10000, Sigma-Aldrich #2066). Primary antibodies were followed by HRP-conjugated secondary antibodies and signal was detected using Clarity ECL kit (Biorad) and acquired on Chemidoc MP System (Biorad). Densitometry analyses were performed using ImageJ software (NIH).

Mitochondria isolation.

Mitochondrial and cytosolic fractions from IAV-infected or uninfected WT BMD-Mφ were extracted using Qproteome Mitochondria Isolation Kit (Qiagen) following manufacturer's instructions. Purified mitochondria were lysed with RIPA buffer and further analysed by western blot using antibodies against RIPK3, CYPD, MAVS and actin.

Immunoprecipitation

Protein (250-500μg) from whole-cell extracts lysed in lysis buffer (1% Triton X-100, 150mM NaCl, 20mM Hepes pH7.5, 10% glycerol, 1mM EDTA, supplemented with anti-protease cocktail,

Roche) were incubated with anti-RIPK3 or anti-RIPK1 or rabbit IgG overnight at 4°C with gentle agitation. Protein G beads were then added for an additional 2 hours incubation at room temperature. Immunoprecipitates were washed 3 times with lysis buffer (2500g, 3min, 4°C), eluted by boiling in 2x Laemmli buffer and analyzed by western blot using antibodies against MAVS, RIPK3 or RIPK1.

Confocal Microscopy

BMD-M ϕ were seeded in a media chamber of a glass microscopy slide (Nunc Labtek II). Cells were infected with IAV-PR8 for the indicated period of time and then fixed in 4% (vol:vol) paraformaldehyde for 15 min. When indicated, mitochondria were stained using Mitotracker Orange CMTMRos (200nM, Life Technologies #M7510) for 30 minutes at 37°C and then fixed with PFA. Cells were then permeabilized by incubating with 0.1% Triton X-100 in PBS for 15 min. Samples were blocked with 1% milk in PBS Tween 0.1% for 1h and then incubated with a specific rabbit polyclonal anti-IFN- β (1:50, #PA5-20390, ThermoFisher), anti-RIPK3 (1:50), anti-RIPK1 (1:50) or anti-pPKR (1:50) overnight at 4°C. Cells were incubated for 1 hour with secondary antibody Alexa Fluor 488- or Alexa Fluor 555-conjugated goat anti-rabbit (1:1000, Invitrogen) and nuclei were stained with Hoechst (1:2000, Molecular Probes). Coverslips were mounted (ProLong Gold Anti Fade, Invitrogen) onto microscope slides. Images were acquired using a Zeiss LSM 700 laser-scanning confocal microscope.

Adoptive Transfer Model of Infection

BMD-M ϕ from Wild Type and *Ripk3*^{-/-} mice were generated as described previously. On day 7 of differentiation, BMD-M ϕ were harvested and resuspended at a density of 1 x 10⁶ cells per 50 μ L. BMD-M ϕ were then transferred by the intratracheal route into naïve *Rag1*^{-/-} mice. After 2 hours, *Rag1*^{-/-} were intranasally infected with 500 PFU of IAV. Lungs were harvested and processed as previously described for viral load analysis.

Interferon- β treatment.

Recombinant murine interferon- β was purchased from R&D Systems (#8234-MB-010). Mice were intranasally infected with 50 pfu of IAV. On day 2 post-infection, mice were given intranasally either PBS or IFN- β (2000U). Mice were euthanized on day 3 post-infection and lungs were harvested and processed to determine pulmonary viral load as previously described.

Statistical analysis

Data are presented as mean \pm SEM. Statistical analyses were performed using GraphPad Prism v6.0g software (Graphpad). Statistical differences were determined using log-rank test (survival studies: Fig 1B and S1B Fig), Kruskal-Wallis followed by Dunn's multiple comparison test (Fig 4K), two-way ANOVA followed by Bonferroni's multiple comparison test, or Mann-Whitney test, with significance expressed as follows: * $p < 0.05$, ** $p < 0.01$, *** $p < 0.001$, **** $p < 0.0001$.

Ethics Statement

All experiments involving animals were approved by McGill (Permit # 2010-5860) in strict accordance with the guidelines set out by the Canadian Council on Animal Care. Human blood samples were collected from healthy donors following informed consent for the McGill University Health Centre (MUHC) institutional review board-approved research protocol GEN10-256.

2.7 Acknowledgements

The authors would like to thank Dr. Shantelle LaFayette for confocal microscopy assistance and Dr. Michaela Zago for reagents and technical help.

2.8 Figures

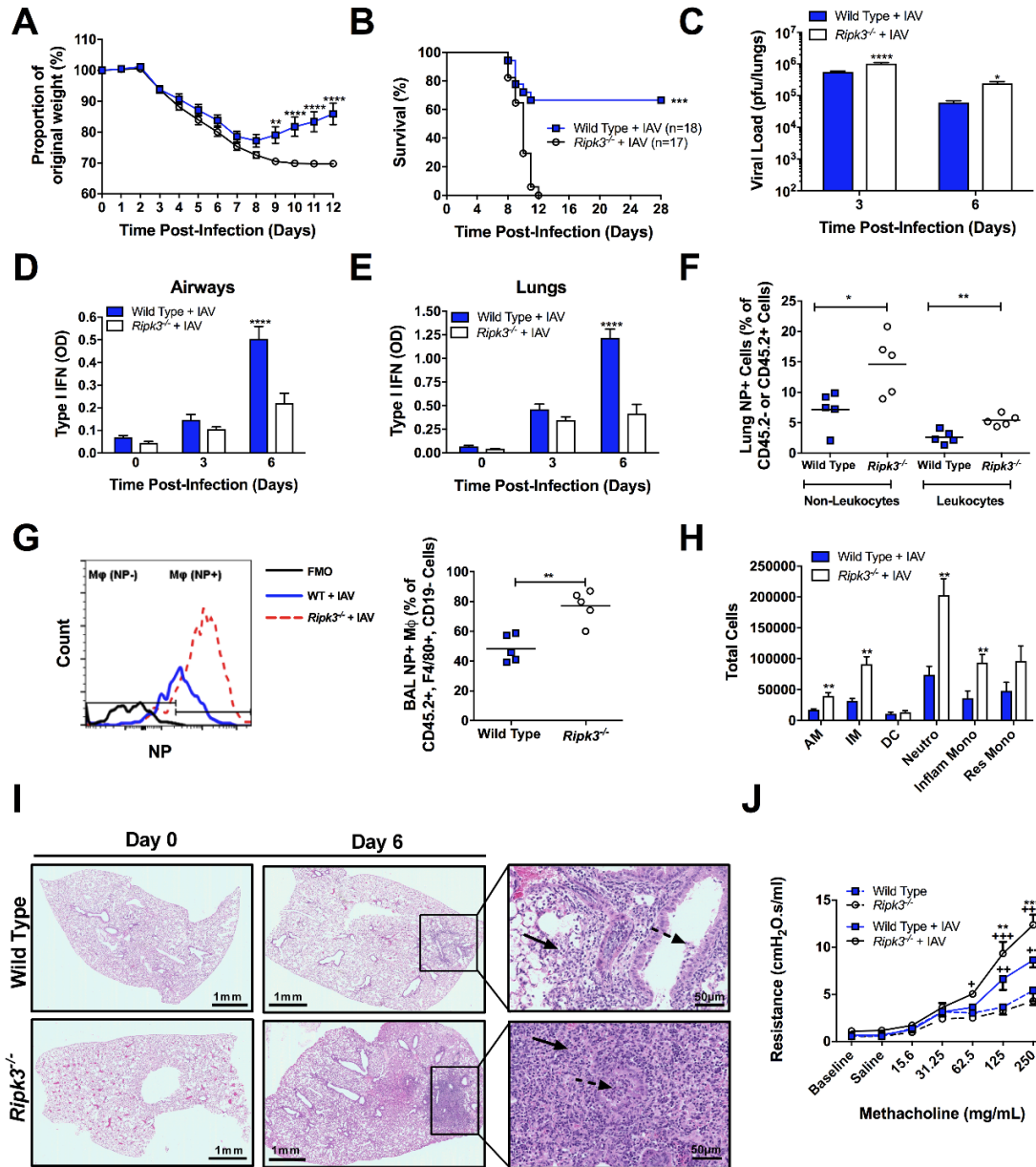


Fig 2.8.1. RIPK3 restricts early viral replication and prevents excessive inflammation, morbidity, and mortality during IAV infection. (A-J) WT and *Ripk3*^{-/-} mice were infected with a sublethal dose (50 pfu) of IAV and morbidity, as a percentage of original weight (A), and survival (B) were assessed. Pulmonary viral loads (C) and total active type I IFN (α and β) via B16-blue reporter cells in the bronchoalveolar lavage (BAL) (D) or lung parenchyma (E) were measured at various times post-infection. (F-G) At 3 days post-infection lungs and BAL from WT and *Ripk3*^{-/-} mice were collected and cells were intracellularly stained for IAV NP protein. (F) Percentage of NP+ non-leukocytes and leukocytes in the lung. (G) Representative histogram (left panel) of NP protein levels in M ϕ (CD45.2⁺ F4/80⁺ CD19⁻ cells) of the BAL and the frequency of NP⁺ M ϕ (right panel). (H) Number of alveolar M ϕ (AM), interstitial M ϕ (IM), dendritic cells (DC), neutrophils (Neutro), Gr1⁺ inflammatory monocytes (Inflam Mono), and Gr1⁺ resident monocytes (Res Mono) present in the BAL at day 3 post-infection. At low power, inflammation is absent in both Wild Type and *Ripk3*^{-/-} (day 0). At high power, the inflammatory infiltrate is composed of lymphocytes, histiocytes and neutrophils within the alveolar space (solid arrow) and bronchiolar lumen (dotted arrow), shown at 6 days post-infection. Scale bar represents 1mm (low magnification) and 50 μ m (higher magnification). Using flexivent, total respiratory resistance (J) of uninfected or IAV-infected mice was measured following methacholine challenge at day 6 post-infection. Data are represented as mean \pm SEM. * p <0.05, ** p <0.01, *** p <0.001, **** p <0.0001 between genotypes as indicated, in J, † indicate significant differences over baseline parameter readings of the same genotype. Except in A and B (as indicated), n =4-8 animals per group per time point.

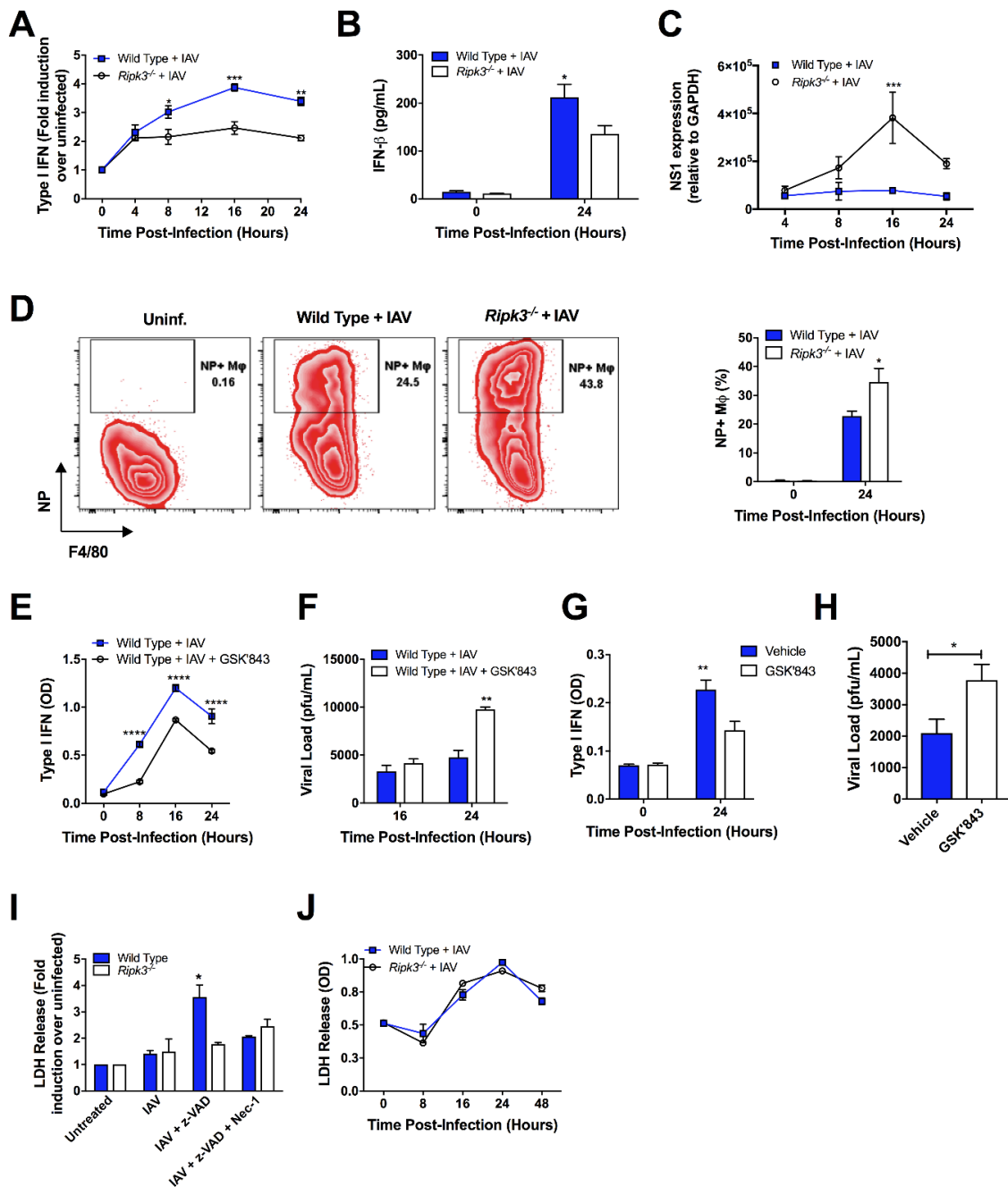


Fig 2.8.2. RIPK3-deficient BMD-Mφ are impaired in anti-viral immunity, independent of the necroptosis pathway. (A-F, I-J) BMD-Mφ from WT and *Ripk3*^{-/-} mice were generated and infected with IAV at MOI 1. Total active type I IFN (α and β) was assessed in supernatants (A) and IFN- β by ELISA (B). (C) The relative levels of viral NS1 mRNA were determined via qPCR. (D) BMD-Mφ from WT and *Ripk3*^{-/-} mice were infected with IAV and the level of viral protein NP was analyzed by flow cytometry. Zebra plots (left panel) are representative of the 24h time-point and numbers adjacent to the gates indicate percent of NP⁺ Mφ as quantified in the right panel. Level of total active type I IFN in cell culture supernatants (E) and viral load (F) in BMD-Mφ from WT mice treated, or not, with the selective RIPK3 inhibitor GSK'843 (10 μ M) and infected with IAV. (G-H) Human monocyte-derived Mφ treated, or not, with the selective RIPK3 inhibitor GSK'843 (10 μ M) were infected with IAV H3N2. Levels of active type I IFN (G) and viral load (H) were assessed in culture supernatants 24h after infection. (I) BMD-Mφ from WT and *Ripk3*^{-/-} mice were generated and treated with various combinations of zVAD-FMK (zVAD, 25 μ M) and necrostatin-1 (Nec-1, 10 μ M) for 1h and then were infected with IAV. Necroptosis was assessed by lactate dehydrogenase (LDH) assay after 24h of IAV infection. (J) LDH was measured in BMD-Mφ cell culture supernatants following IAV infection at various time points. Data are representative of the mean \pm SEM of triplicate wells and are representative of at least 3 experiments. *p<0.05, **p<0.001, ***p<0.001, ****p<0.0001

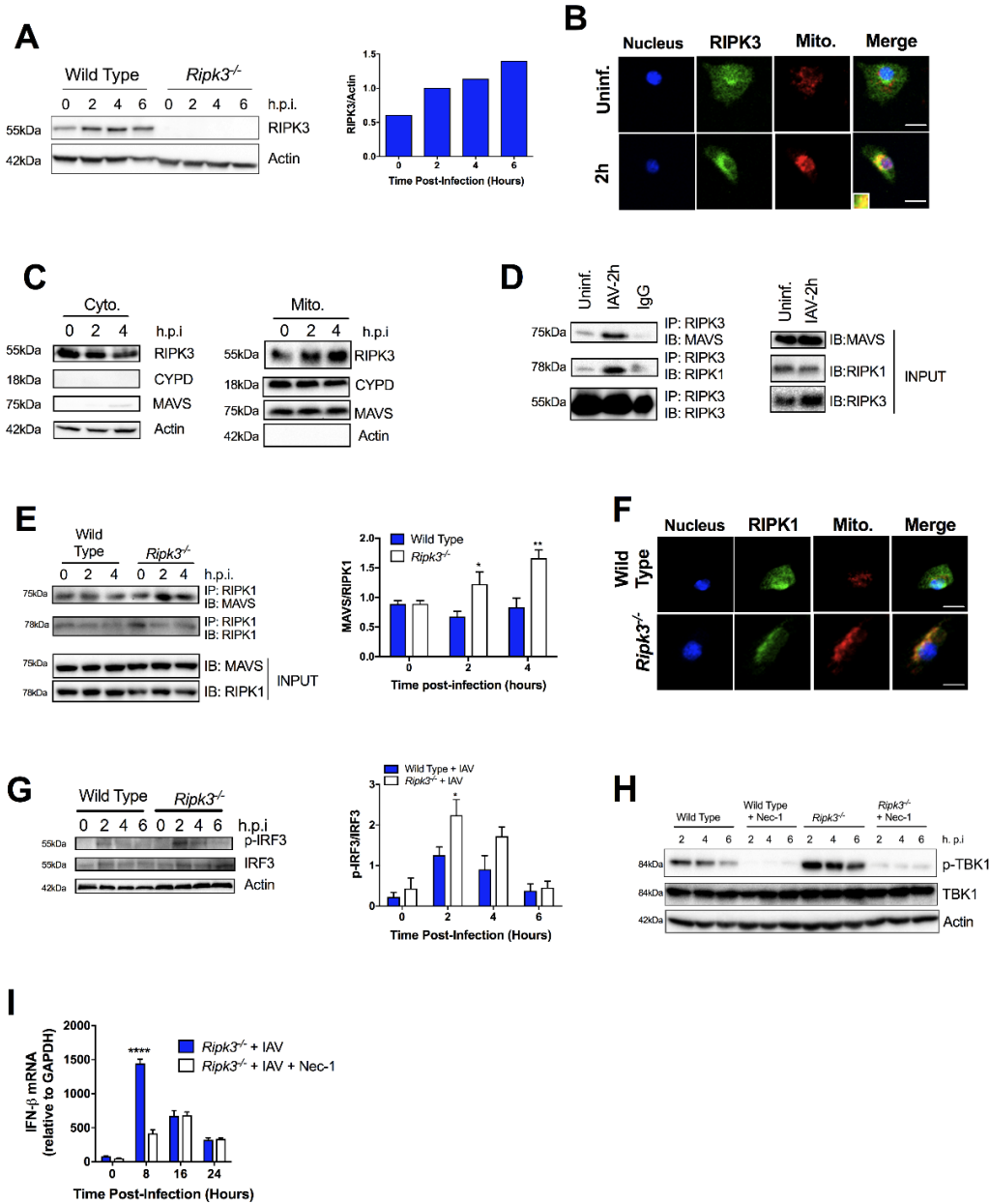


Fig 2.8.3 RIPK3 interacts with MAVS in IAV-infected BMD-Mφ regulating TBK1 and IRF3 phosphorylation. BMD-Mφ were infected with IAV at an MOI of 5 (A-H) or 1 (I). (A) Western blot analysis of RIPK3 expression at various times post-IAV infection in WT BMD-Mφ. Densitometry analysis to quantify ratio of RIPK3 to β-actin is shown in the right panel. (B) Immunofluorescence analysis of co-localization of RIPK3 (green) and mitochondria (red) in WT BMD-Mφ infected or not with IAV. Yellow regions are the areas of RIPK3 and mitochondria colocalization. Nuclei were stained with Hoechst (blue). The scale bars represent 10μm. (C) BMD-Mφ lysates were collected at 0, 2 and 4 hours post-IAV infection. Cytosolic and mitochondrial fractions were isolated and analyzed by western blot for RIPK3 and MAVS. Actin and mitochondrial protein CYPD were used as loading controls and to ensure purity of the fractions. (D-E) BMD-Mφ lysates were collected at 0, 2 (D-E) and 4 (E) hours post-IAV infection and immunoprecipitation was performed with anti-RIPK3 (D) or anti-RIPK1 (E). Samples were then analyzed by immunoblotting for MAVS or RIPK1. (E, right panel) Densitometry analysis to quantify the interaction between MAVS and RIPK1 is shown, representative blot in left panel (n=3). (F) Immunofluorescence analysis of co-localization of RIPK1 (green) and mitochondria (red) in WT and *Ripk3*^{-/-} BMD-Mφ 2 hours post IAV-infection. Nuclei were stained with Hoechst (blue). The scale bars represent 10μm. (G) Representative blot (left panel) of phosphorylated IRF3 in WT and *Ripk3*^{-/-} BMD-Mφ infected, or not, with IAV at various times post-infection. Densitometry analysis to quantify ratio of phosphorylated IRF3 to total IRF3 is shown in the right panel (n=3). (H-I) WT and *Ripk3*^{-/-} BMD-Mφ were pretreated with/without necrostatin-1 (Nec-1, 10μM) for 1h and then were infected, or not, with IAV. Representative blot of the phosphorylation of TBK1, determined by western blot as in B. (I) Total RNA was extracted and the expression of IFN-β mRNA was determined by qPCR. Data are expressed as mean ± SEM representative of at least three independent experiments. *p<0.05, **p<0.001, ***p<0.0001.

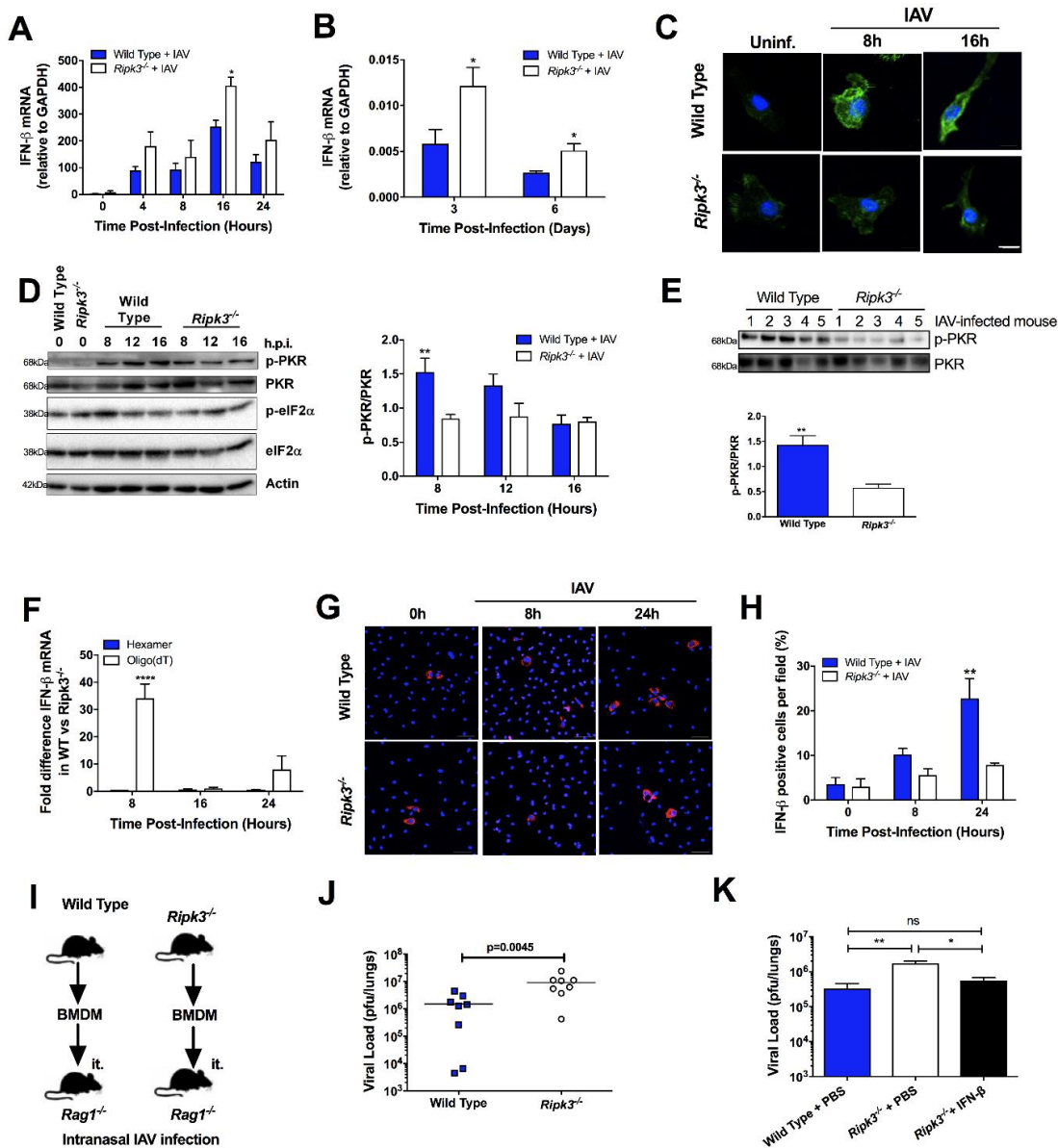


Fig 2.8.4. RIPK3 regulates IFN-β mRNA integrity through activation of PKR. Total RNA was extracted from IAV-infected BMD-Mφ (MOI 1) (A) or cells of the BAL (50 pfu) (B) and the expression of IFN-β mRNA was determined by qPCR. (C) Phosphorylation of PKR (green) was analyzed by immunofluorescence in WT and *Ripk3*^{-/-} BMD-Mφ at different time point post IAV-infection. Nuclei were stained with Hoechst (blue). The scale bars represent 10μm. (D) Phosphorylated and total forms of PKR and eIF2α in whole-cell lysates were analysed by immunoblotting. β-Actin was used as a loading control. One representative blot is shown (left panel). Densitometry analysis to quantify the ratio of phosphorylated PKR relative to total PKR (n=4, right panel). (E) Cells were harvested from the BAL of infected (50 pfu) WT or RIPK3-deficient mice and levels of phosphorylated and total PKR were determined by western blot (top panel). Densitometry analysis to quantify the ratio of phosphorylated PKR relative to total PKR (n=4, bottom panel). (F) Difference in the expression of IFN-β mRNA between WT and *Ripk3*^{-/-} BMD-Mφ infected with IAV. Gene expression was analyzed by qPCR following cDNA generation using random hexamers (blue bars) or oligo(dT) primers (white bars). (G) Confocal images showing IFN-β production in IAV-infected BMD-Mφ. Cells were stained with a rabbit polyclonal antibody specific for IFN-β (red) as well as nuclear dye Hoechst (blue). (H) Percentage of cells positive for IFN-β stain per random field. The scale bars represent 50μm. (I) BMD-Mφ (1x10⁶ cells) from WT and *Ripk3*^{-/-} mice were adoptively transferred (i.t.) into naïve *Rag1*^{-/-} mice, which were then infected with 500 PFU of IAV 2h post-transfer. (J) Viral load was assessed 3 days after IAV-infection (n=8, compilation of 2 experiments). (K) Wild Type and *Ripk3*^{-/-} mice were infected with 50 pfu of IAV. After 2 days, mice were intranasally administered PBS or 2000U of IFN-β. Viral load was determined at day 3 post-infection by standard plaque assay (n=7-8 mice/group, compilation of 2 experiments). *p<0.05 **p<0.01, ****p<0.0001, ns=not significant.

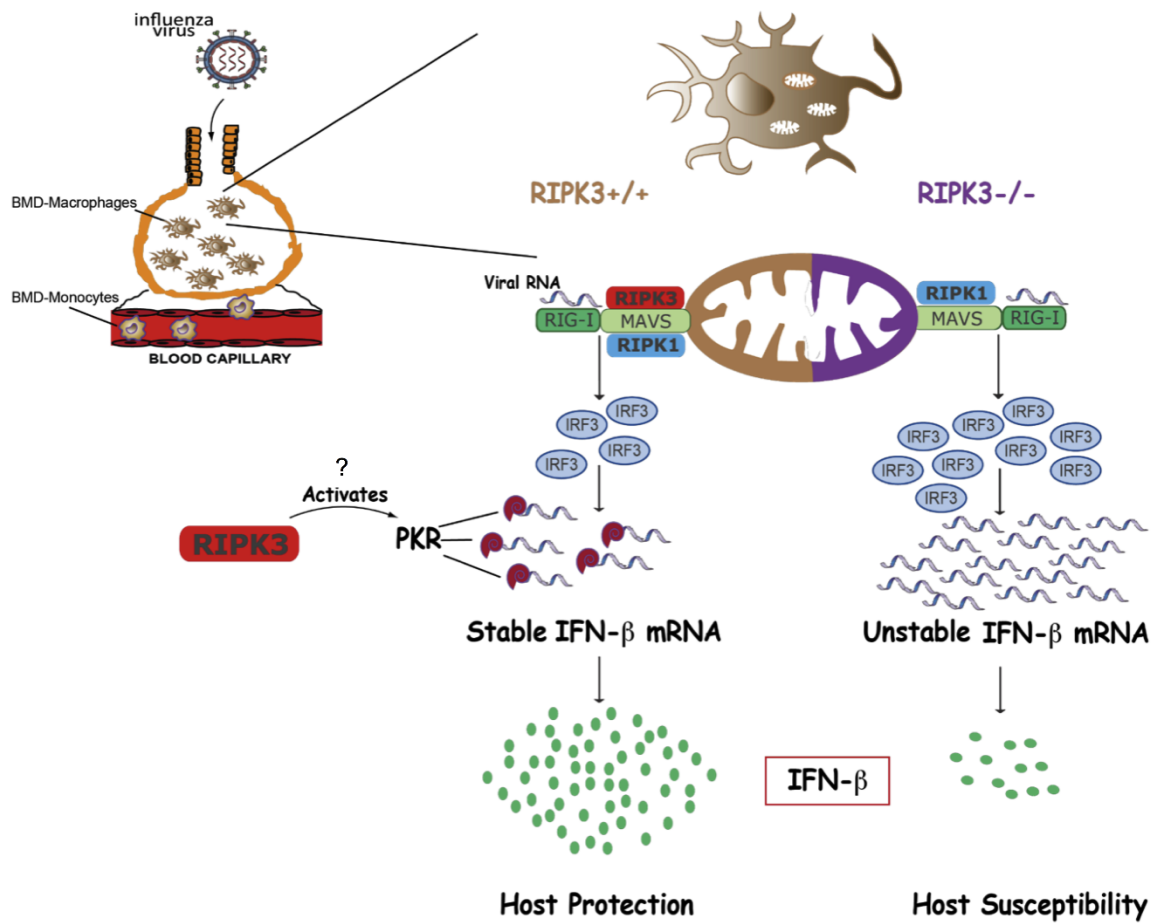


Fig 2.8.5. RIPK3 enhances innate anti-viral immunity against Influenza A virus.

Pulmonary infection by IAV triggers the recruitment of monocytes from the bone marrow that differentiate into macrophages. IAV encounters and infects those macrophages, where viral RNA activates the RIG-I/MAVS pathway, leading to production of the key anti-viral cytokine IFN-β. IAV-induced RIPK3 interaction with MAVS at the mitochondria and may represent an immune evasion strategy to decrease IFN-β production. In the absence of RIPK3, there is increased RIPK1/MAVS interactions, which enhance downstream signaling, resulting in higher TBK1/IRF3 activation and IFN-β mRNA levels. However, this mechanism is counteracted by the RIPK3-mediated activation of PKR. PKR stabilizes IFN-β mRNA through the poly(A) tail, leading to increased IFN-β protein production and, ultimately, host protection.

PREFACE TO CHAPTER 3

As explored in chapter 1, disease tolerance is an integral component of protective immunity to IAV (351), yet it remains substantially less understood than resistance mechanisms such as the antiviral macrophage/IFN-I axis we investigated in chapter 2. Despite this, respiratory insufficiency secondary to a break in pulmonary disease tolerance underlies the majority of mortality caused by IAV in humans, particularly in the absence of confounding bacterial co-infections (44), strongly arguing in favour of greater investigation of disease tolerance mechanisms. Interestingly, a previous study of ours highlighted a critical function for the mitochondrial protein CypD in disease tolerance to chronic *Mtb* infection, through the regulation of T-cell responses (352). Thus, we sought to delineate the role of CypD during acute viral infection, hypothesizing that, in contrast to chapter 2, CypD would be more susceptible to IAV infection due to increased pulmonary damage. In line with our hypothesis, we found *CypD*^{-/-} mice were highly susceptible to IAV, without any defect in viral clearance. Using a series of reconstitution and adoptive transfer experiments, we showed that CypD is essential for IL-22 production by pulmonary NK cells that protects the lung epithelium from damage and promotes disease tolerance to IAV.

CHAPTER 3:

**Cyclophilin D promotes disease tolerance to influenza A virus
infection by licensing NK cell development and function**

Cyclophilin D promotes disease tolerance to influenza A virus infection by licensing NK cell development and function

Jeffrey Downey¹, Erwan Pernet¹ and Maziar Divangahi¹

1. Department of Medicine, Department of Pathology, Department of Microbiology & Immunology, McGill University Health Centre, McGill International TB Centre, Meakins-Christie Laboratories, McGill University, 1001 Decarie Boulevard, Montreal, Quebec, H4A 3J1, Canada.

Corresponding Author:

Maziar Divangahi, Ph.D.

Associate Professor of Medicine

RI-MUHC, Centre for Translational Biology

Meakins-Christie Laboratories

1001 Decarie Blvd,

Block E (EM3.2248)

Montreal, Quebec H4A 3J1

Tel: (514) 934-1934 Ext. 76431

e-mail: maziar.divangahi@mcgill.ca

Submitted to *Journal of Experimental Medicine*, 2020

3.1: Summary

Influenza A virus (IAV) is a principal cause of global infections, with cases ranging from asymptomatic to fatal, but the immune correlates that underlie this spectrum of severity remain incompletely known. In this study, we show that NK cell-derived IL-22, induced in a CypD-dependent manner, protects the lung epithelium following lethal infection to protect mice without an effect on antiviral resistance. Greater insight into mediators of disease tolerance to IAV will fuel next generation therapies.

3.2: Abstract

An effective immune response to influenza A virus (IAV) requires two arms: host resistance, which restricts viral replication, and disease tolerance that limits tissue damage caused by the immune response to IAV. Interestingly, fatal influenza infections are more often associated with dysregulated inflammation, rather than an inability to control viral replication, highlighting the importance of mechanisms involved in disease tolerance to IAV. Here, we show that cyclophilin D (CypD), a mitochondrial protein known to regulate cell death and cytokine production, protects against IAV infection through disease tolerance. Mice deficient in CypD (*CypD*^{-/-}) exhibit enhanced susceptibility to IAV infection, despite comparable myeloid immune responses and intact antiviral immunity. Instead, *CypD*^{-/-} susceptibility was due to pulmonary tissue damage, caused by a lack of the cytokine IL-22 that protects the lung epithelium. We found the critical source of IL-22 following IAV infection to be conventional natural killer (NK) cells that failed to reach the airways of infected CypD-deficient mice, as a result of dysregulated lymphopoiesis in the bone marrow. Importantly, following infection, a single administration of recombinant IL-22 in the airways abrogated pulmonary damage and rescued *CypD*^{-/-} mice. Thus, the CypD/IL-22/NK cell axis is critical in immunity to IAV by promoting disease tolerance, limiting lung tissue damage and maintaining pulmonary function.

KEYWORDS: Influenza, Disease Tolerance, Cyclophilin D, IL-22, NK cells, Lymphopoiesis

3.3: Introduction

In response to infection, host resistance mechanisms inhibit replication to prevent loss of pathogen control. These resistance mechanisms are a critical component of host defense to infection, yet they come with a considerable inflammatory cost that paradoxically threatens host fitness through immunopathology. Thus, immune mechanisms of disease tolerance exist to mitigate tissue damage, restore organ function and counter the cost of anti-microbial inflammation (106, 223, 224). Influenza A viruses (IAV) cause consistent and recurrent respiratory infections, responsible for approximately half a million deaths per annum globally, while also causing unpredictable and devastating pandemics. Severe and fatal IAV infections are more often characterized by a “cytokine storm”, which contributes to a break in disease tolerance characterized by destruction of the pulmonary epithelial/endothelial barrier and respiratory insufficiency, rather than ineffective antiviral resistance responses (44, 225, 353). Additionally, an average of 16% of influenza infections are estimated to be asymptomatic, suggesting certain individuals, via unknown mechanisms, are highly tolerant to IAV and do not require robust host resistance responses (354). Yet, despite these findings, our knowledge of the underlying mechanisms of disease tolerance to IAV remains incomplete. Similar observations have been made clinically during the 2020 COVID-19 pandemic, caused by the novel SARS-CoV-2 virus—a member of the RNA viral family *Coronaviridae*— which through the first six months was responsible for over 10 million infections, 500 000 deaths and incalculable socioeconomic losses. Like influenza, deaths due to COVID-19 seem to be often associated with a loss of disease tolerance as asymptomatic individuals appear to harbour similar viral titres to symptomatic individuals (355). Thus, understanding mechanisms of disease tolerance and uncovering targetable pathways may provide conserved front-line therapies to combat pandemics by a variety of acute respiratory pathogens.

IAV infections are short-lived and usually self-resolving within approximately 7-10 days, though inflammation can persist for weeks post-infection. The early inflammatory response is marked by an influx of innate leukocytes into the lung parenchyma and airways through a combination of distal recruitment from the bone marrow/vasculature and local *in situ* proliferation. Cells of the myeloid lineage, such as neutrophils and inflammatory CCR2⁺ monocyte-derived

macrophages (IMM), play important roles in early restriction of viral replication (180, 184) and priming of the adaptive response (185), yet contribute substantially to immunopathology, such that *Ccr2*^{-/-} mice exhibit elevated viral loads, but enhanced survival (182, 183). Mechanistically, our group recently highlighted the importance of the bioactive lipid leukotriene B₄ (LTB₄) in inhibiting *in situ* proliferation of monocyte-derived IMM by specifically potentiating immunomodulatory IFN- α signalling to conserve pulmonary epithelial integrity (150). Equally, reduction of extracellular matrix (ECM) turnover, to which the lung epithelium is anchored, by inhibiting membrane type I matrix metalloprotease (MT1-MMP) activity during IAV infection protected mice by conserving epithelial structure (229). Thus, maintenance of the pulmonary architecture appears to be an essential component of a protective immune response to IAV.

In addition to myeloid cells, innate lymphocytes, such as natural killer (NK) cells accumulate in the lung shortly upon infection, beginning as early as 2 days post-infection (356). NK cells express a variety of activating and inhibitory receptors that perform diverse context- and tissue-specific functions, including well-described roles in the killing of tumour or virally infected cells in a non-MHC-restricted manner through production of IFN- γ and expression of perforin and granzymes (357). In the context of IAV infection, NK cells contribute to host resistance by recognizing sialylated hemagglutinin (HA) proteins (187, 358) on the surface of IAV infected cells to facilitate lysis and enhance viral clearance (188-190). Beyond their role in host resistance during IAV infection, NK cells are equally critical in disease tolerance by secreting the epithelial protective cytokine IL-22. IL-22 is a member of the IL-10 family of cytokines that maintains mucosal barriers by inducing survival and proliferation of epithelial cells, where the IL-22 receptor (a heterodimeric receptor composed of an IL-22R1 and a IL-10R2 subunit) is exclusively expressed, being absent from hematopoietic cells (359). Although several cell types are capable of producing IL-22 following IAV infection, including NKT cells, $\gamma\delta$ T-cells, ILCs and $\alpha\beta$ T-cells (245, 246), NK cells have been suggested to be the major source (242), especially at later time-points (243). Importantly, *Il22*^{-/-} mice exhibited enhanced epithelial damage and pulmonary pathology, following infection with IAV (241, 243, 245), although this may be dose-dependent (242). What molecular mediators may be involved in the production of IL-22 from NK cells upon infection, however, have not been elucidated.

Cyclophilin D (CypD), nuclearly encoded by the *Peptidyl-prolyl isomerase F (Ppif)* gene, is a member of the cyclophilin family of isomerases that resides within the mitochondrial matrix. CypD is well-established as an essential modulator of the mitochondrial permeability transition pore (MPTP) and, thus, is required for the induction of necrosis (360, 361). CypD-dependent necrosis is involved in numerous pathologies, including neurological disorders (362, 363) and we highlighted a role for it in *Mycobacterium tuberculosis (Mtb)*-induced macrophage necrosis (314). However, independent of its role in macrophage necrosis, we recently showed that CypD critically promoted immunity to *Mtb* through the regulation of T-cell metabolism and contraction (352), without altering bacterial burden, adding a previously unappreciated requirement for CypD in disease tolerance to chronic bacterial infections, while it enhanced T-cell responses to LCMV infection in a cell extrinsic manner (364). However, the role of CypD during IAV infection is unknown.

Given the important regulatory role of CypD in macrophage necrosis (314, 361) and the importance of conserved macrophage viability/function in immunity to IAV (3, 62, 66), we initially hypothesized that the inhibition of CypD-mediated necrosis would enhance macrophage viability and, thus, protection to infection. Surprisingly, in contrast to our expectations, CypD-deficient mice were highly susceptible to IAV infection without aberrations in host resistance mechanisms or leukocyte necrosis. We found that a lack of IL-22 production by NK cells in the infected airways of *CypD*^{-/-} mice was the major cause of the susceptibility and exogenous reconstitution of IL-22 into the airways of *CypD*^{-/-} abrogated their heightened mortality. Phenotyping analyses by flow cytometry revealed that *CypD*^{-/-} mice had altered NK cell kinetics and maturation in comparison to WT mice and this was due to enhanced cell death of NK cell-specific progenitors in the BM. Thus, our findings elucidate an essential role for CypD in immunity to IAV infection and in conjunction with our previous work (352, 364) hint at a potentially broad importance of CypD in response to infection. In addition to antivirals and vaccination programs, greater insight into mechanisms of disease tolerance to IAV will be pivotal in development of novel therapies.

3.4: Results

CypD is dispensable for host resistance to influenza A virus infection, but is critical in the maintenance of disease tolerance

Given the role of CypD in certain forms of necrosis (360, 361) and the intimate relationship between influenza A virus (IAV) pathogenesis and cell death (3), we postulated that *CypD*^{-/-} mice would have reduced leukocyte necrosis following infection that would enhance immune responses and dampen disease severity. Using our established IAV model to investigate this, we began by infecting wild type (WT) and *CypD*^{-/-} mice with a sublethal 50 PFU dose of PR8 IAV and, unexpectedly, found no differences in necrotic cell death (**Fig. S1A**), as measured by lactate dehydrogenase (LDH) levels in the BAL over the course of infection. Despite this, *CypD*^{-/-} mice were highly susceptible to an LD₅₀ (90 pfu) dose of IAV, exhibiting increased mortality (**Fig. 1A**) and morbidity (**Fig. 1B**). Interestingly, the enhanced mortality of *CypD*^{-/-} mice was not due to differences in host resistance, as *CypD*^{-/-} mice had similar viral loads (**Fig. 1C**) and levels of active type I IFN (IFN-I) in the lung (**Fig. 1D**) and BAL (**Fig. 1E**), as well as equal amounts of antiviral IFN-β (**Fig. S1B-C**). In light of these findings, we then hypothesized that the susceptibility was linked to dysregulated disease tolerance responses. Therefore, we assessed the levels of tissue damage and pulmonary inflammation in *CypD*^{-/-} mice compared to WT mice following infection. As hypothesized, CypD-deficient mice exhibited impaired disease tolerance, evidenced by enhanced pulmonary edema (**Fig. 1F**), as well as protein and erythrocyte influx into the BAL (**Fig. 1G-H; Fig. S1D**). Additionally, using a fluorescently-labelled dextran molecule delivered into the airways of mice at 7 days post-IAV infection, there was reduced fluorescence in *CypD*^{-/-} lungs, indicative of enhanced epithelial/endothelial damage compared to WT mice due to greater diffusion of the dextran across this otherwise impermeable barrier (**Fig. 1I**). Finally, we also noted elevated inflammatory cell accumulation in the parenchyma (**Fig. 1J**) and airways (**Fig. 1K**) of *CypD*^{-/-} lungs, beginning at 7 days post-infection, which coincided with the onset of enhanced tissue damage in these mice. This correlated with histological H&E staining at 7 days post-infection, with no inflammation observed in either group at steady-state (**Fig. 1L**). Thus, CypD is essential in immunity to IAV by regulating disease tolerance, rather than host resistance, to protect against immunopathology.

The hematopoietic compartment confers susceptibility of *CypD*^{-/-} mice to IAV and CypD-deficient NK cells exhibit altered kinetics and are phenotypically immature

Mechanisms of disease tolerance are numerous and can be mediated by either structural or hematopoietic compartments (106, 224, 365). To delineate which cellular compartment was primarily responsible for the increased tissue damage in *CypD*^{-/-} mice, we generated bone marrow chimeric mice, wherein the hematopoietic compartment of lethally irradiated CD45.1 WT mice was reconstituted with CypD-deficient (CD45.2) (*CypD*^{-/-} → WT) bone marrow (BM) and vice versa (WT → *CypD*^{-/-}). At 10-12 weeks post-reconstitution, reconstitution efficiency was greater than 95% (data not shown). Mice were then infected for 7 days to correlate with the peak of lung damage in the CypD-deficient mice and pulmonary damage was assayed as before. *CypD*^{-/-} → WT mice showed a statistically significant increase in erythrocytes in the BAL and pulmonary inflammation when compared to WT (**Fig. 2A-B**), as well as elevated inflammatory cell influx into the BAL (**Fig. S2A**). Although the WT → *CypD*^{-/-} mice showed a small increase over the WT control in each experiment, this was never significant. Thus, the lack of disease tolerance is mediated primarily by the hematopoietic compartment of CypD-deficient mice.

To elucidate which cell(s) of the hematopoietic compartment may be responsible for the increased lung damage, we extensively phenotyped innate immune cells by flow cytometry (**full gating strategy Fig. S1 E-F**) at various time points post-infection in the lung parenchyma and airways. As we have previously shown the importance of regulating IMM numbers upon infection to maintain disease tolerance (150), we initially characterized IMM kinetics in the BAL and found similar frequencies and numbers in WT and *CypD*^{-/-} mice (**Fig. 2C**), as were the frequency and number of Ly6C^{hi} monocytes (**Fig. 2D**). As with IMM, pulmonary neutrophilia is correlated with increased immunopathology and a poorer prognosis during IAV infection (180). Yet, we found a reduced frequency, but similar number, of neutrophils in the BAL of *CypD*^{-/-} mice at day 5 p.i. with no differences at other timepoints, suggesting neutrophils could not explain the exacerbated lung injury in these mice (**Fig. 2E**). Of note, however, we discovered altered kinetics of NK cells in the airways of CypD-deficient, such that *CypD*^{-/-} mice had an elevated frequency at day 5 p.i. but a reduction 7 days p.i. when differences in pulmonary damage became apparent (**Fig. 2F**). No differences in any of the cell populations assessed were observed in the lung parenchyma (**Fig.**

S2B-E), perhaps hinting at the importance of spatial regulation of immune responses (i.e. parenchyma versus airways) during IAV infection.

NK cells are required in protection to IAV through both resistance and tolerance responses (188, 243). Moreover, a recent study suggested that lower ratios of NK cells to inflammatory monocytes may underlie individual susceptibility to IAV, without affecting early viral loads (366), leading us to hypothesize that they may be responsible for the exacerbated lung damage observed in *CypD*^{-/-} mice. Thus, we sought to further interrogate their phenotype post-infection. NKp46/IAV HA interactions elicit cell lysis via perforin and granzyme to kill virally infected cells (187, 188). However, *CypD*-deficient and WT NK cells expressed similar levels of perforin and granzyme B (**Fig. 2G-H**), suggesting the lytic capacity of *CypD*-deficient NK cells was intact correlating with similar viral loads in these mice. The maturation and accumulation of effector functions in NK cells is known to be dependent on downregulation of CD27 and upregulation of CD11b, which gives rise to four populations of NK cells (CD27⁻ CD11b⁻, CD27⁺ CD11b⁻, a transitory CD27⁺ CD11b⁺, CD27⁻ CD11b⁺) (367-369). Unbiased single cell analysis has confirmed the importance of these different populations in determining effector function of NK cells in mice (370). Intriguingly, *CypD*^{-/-} NK cells exhibited a significantly higher frequency and number of immature (CD27⁺ CD11b⁻) cells and significantly less fully mature (CD27⁻ CD11b⁺) cells when compared to WT in both the BAL (**Fig. 2I-L**) and lung (**Fig. S2F-J**) at different timepoints post-infection. Similar results were obtained in splenic NK cells (**Fig. S2K-M**), although a total increase of NK cells was observed at day 7 post-infection in the *CypD*^{-/-} mice. To assess the potential for a direct role of *CypD* in NK cells, we purified splenic NK cells from WT and *CypD*-deficient hosts and verified significant expression of *CypD* in WT, but not *CypD*^{-/-} cells (**Fig. 2M**), which aligns with data publicly available from ImmGen (371).

Taken together, our results show that *CypD*-deficient mice have reduced accumulation of NK cells in the airways at the time of peak immunopathology and the cells present have altered surface level expression of critical maturation markers, suggesting an alteration in their effector function.

CypD promotes NK cell hematopoiesis to generate mature peripheral NK cells post-IAV infection

The lack of developmentally mature NK cells in the airways of *CypD*^{-/-} mice following IAV infection could be explained by a variety of mechanisms, including perturbations in local proliferation and/or cell death. To investigate these possibilities, we analyzed markers of proliferation (Ki67) and cell death (active caspase 3) by flow cytometry on NK cells in the BAL and found no differences (**Fig. 3A-B**). In addition to proliferation and cell death, aberrant recruitment or chemotaxis into the airways could be responsible. CCR2, along with CCR5, expression on NK cells is known to specifically facilitate migration of NK cells into the airways, without affecting extravasation into the lung, which is instead mediated by CX3CR3 (356, 372). As previously reported (372), we observed a high frequency of CCR2 expressing NK cells in the BAL at 5 days p.i. that decreased with time, while expression on parenchymal NK cells was low throughout, supporting the notion that CCR2 is required for NK cell accumulation in the BAL, but is dispensable for translocation into the lung from the vasculature. Nevertheless, the frequency of CCR2⁺ NK cells was indistinguishable between WT and *CypD*^{-/-} mice in the BAL, lung and blood (**Fig. 3C; Fig. S3A-B**), confirming CCR2-mediated migration of NK cells into the airways is not dependent on CypD expression.

Although continual on-demand egress of NK cells from the BM into the blood to supply peripheral tissues is well-described, it is now known that an additional population of long-lived tissue-resident NK cells exists in several peripheral tissues that can be differentiated by expression of CD49a rather than CD49b (373). This population is most prevalent in the uterus, liver and skin, but can be found in a variety of other sites including the lung (374). To see if this population of tissue-resident NK cells was altered in our model, we investigated expression of CD49a versus CD49b on the surface of NK cells from WT and *CypD*^{-/-} mice. As expected (374), the vast majority of NK cells from the BAL and lungs of both groups of mice were CD49b⁺ CD49a⁻, indicative of a predominantly blood-derived population, and this frequency was the same between both groups (**Fig. 3D; Fig. S3C**). Thus, differences in blood-derived versus resident NK cells could not explain the changes in accumulation and effector states observed in *CypD*^{-/-} mice. Interestingly, the frequency of NK cells in the peripheral blood was decreased in CypD-deficient mice (**Fig. 3E**).

Those cells displayed a less activated profile at day 5 post-infection, but not at steady-state or day 7 post-infection (**Fig. 3F-G; Fig. S3D-E**).

The reduction of NK cells in the blood and peripheral tissue led us to speculate that there was a defect in the generation of NK cells in the BM of *CypD*^{-/-} mice and subsequent recruitment via the peripheral blood. NK cell generation occurs through a stepwise progression of progenitors, ultimately giving rise to fully mature effector NK cells that are released into the bloodstream. Downstream of the pluripotent LKS cells, a major bifurcation exists that separates out cells of the lymphoid lineage and those of the myeloid/erythroid lineage, through the common lymphoid progenitor (CLP; Lin⁻ CD127⁺ cKit^{lo} Sca1^{lo}) and the common myeloid progenitor (CMP; Lin⁻ CD127⁻ cKit⁺ Sca1⁻ CD34⁺ CD16/32⁻), respectively. Deriving from the CLP, NK cells are generated first from the pre-NK progenitor (pre-NKP; Lin⁻ CD127⁺ CD27⁺ CD122⁻ CD244.2⁺), then the NKP (Lin⁻ CD127⁺ CD27⁺ CD122⁺ CD244.2⁺), which represents what is thought to be the first fully committed cell of the NK lineage, and finally *bona fide* NK cells that then begin to express Nkp46, CD49b and CD11b (375). To investigate any potential aberrations in NK cell development between WT and *CypD*^{-/-} mice, we phenotyped the BM precursors beginning at the LKS population and working towards more committed progenitors during homeostasis and upon infection. We observed no differences in the frequency or number of LKS cells between groups (**Fig. 4A; Fig. S4A**), nor in the CLP (**Fig. 4B; Fig. S4B**). Additionally, there were similar levels of the CMP and granulocyte-monocyte progenitor (GMP) in WT and *CypD*-deficient mice (**Fig. S4C-D**), correlating with equal levels of myeloid cells in the lung/BAL. However, beginning at the NK cell-specific progenitors, we noted a decrease in pre-NKP (Lin⁻ CD27⁺ CD127⁺ CD244.2⁺ CD122⁻) and NKP (Lin⁻ CD27⁺ CD127⁺ CD244.2⁺ CD122⁺) populations (**Fig. 4C-E**). This reduction of NK cell progenitors led to a lower frequency of fully mature CD11b⁺ CD27⁺ expressing NK cells in the BM (**Fig. 4F; Fig. S4E**). Thus, *CypD* mediates NK cell hematopoiesis and an inability to progress through the NK cell lineage aligns with a lack of mature NK cells in the periphery.

***CypD*^{-/-} NK cell progenitors express higher levels of p53 and undergo enhanced cell death, leading to their reduction in the BM**

Looking to extend on our observation of a reduction of NK cell output due to a lack of NK cell progenitor production in *CypD*^{-/-} mice, we investigated the reason for the reduction. Both at steady-state and upon infection, CypD expression had no effect on proliferation of NK cell progenitors, as determined by intracellular Ki67 expression (**Fig. S4F-G**). Because we observed no differences in progenitor proliferation, we next hypothesized that cell death may be responsible, as it has been shown to be a critical mediator of hematopoiesis and the biasing of myelopoiesis versus lymphopoiesis (263, 271). Interestingly, p53, a central regulator of cell growth arrest and cell death in a variety of cell types (376), has recently been demonstrated to interact with CypD in mitochondria to facilitate necrosis of structural cells (377), while also antagonizing p53-dependent growth arrest in a tumour model, suggesting that CypD-deficiency could increase p53 function (378). Moreover, enhanced expression or activity of p53 halts lymphopoiesis, causes cell death specifically in the lymphoid lineage and leads to lymphopenia (379, 380). Thus, we investigated the level of p53 in NK cell progenitors and found an elevation in p53 protein in *CypD*^{-/-} pre-NKP (**Fig. 4G**) and NKP progenitors (**Fig. 4H**), but not in effector NK cells in the BM (**Fig. S4H**) or BAL (**Fig. S4I**). Using differential expression of AnnexinV/NucSpot (a 7-AAD analogue), the upregulation of p53 correlated with an enhanced percentage of dead (AnnexinV⁺ NucSpot⁺) NKP cells (**Fig. 4I**), but not in pre-NKP cells (**Fig. 4SJ**). Collectively, our results indicate that CypD antagonizes p53 function and likely prevents p53-mediated cell death to conserve NK cell lymphopoiesis and the generation of mature effector NK cells.

Mice deficient in CypD are more susceptible to IAV due to a lack of IL-22 production by conventional NK cells

Having established dysregulated NK cell hematopoiesis in the BM led to decreased output/accumulation of mature NK cells in the airways of infected mice, we next wanted to determine if *CypD*^{-/-} NK cells were functionally different and, if so, if these functional differences were responsible for the observed susceptibility of these mice. As our previous results indicated

that cytolytic markers were equally expressed in both WT and *CypD*^{-/-} mice (**Figure 2G-H**), we instead wondered whether the cytokine profiles differed between mice. NK cells are a well-known source of IFN- γ during IAV infection (381, 382). However, the role of IFN- γ in response to IAV infection is controversial (137-139) and a potential role in disease tolerance is not well-described. Nevertheless, we noted a significant decrease in the levels of IFN- γ in the BAL of infected *CypD*^{-/-} mice at day 7 p.i., correlating with the increased pathology (**Fig. 5A**). Utilizing *ex vivo* stimulation of cells with PMA/ionomycin, we confirmed by intracellular cytokine staining (ICS) that CD49b⁺ NK cells from the BAL and spleen were substantial sources of IFN- γ and that a significantly lower frequency of *CypD*^{-/-} NK cells was IFN- γ ⁺ at 5 days post-IAV infection (**Fig. 5B; Fig. S5A**). However, as suggested by a previous study (139), using *Ifngr*^{-/-} mice, we found no role for IFN- γ signalling in disease tolerance to IAV, with mice exhibiting similar levels of protein and number of erythrocytes in the BAL (**Fig. S5B-C**), although a significant increase in total leukocytes was noted (**Fig. S5D**). To completely rule-out that the reduction in IFN- γ was responsible for the damage in the CypD-deficient mice, we reconstituted the airways of WT and *CypD*^{-/-} mice with 100ng of IFN- γ intranasally (i.n.), or PBS, at 5 days p.i. and collected the BAL at 7 days post-IAV and characterized pulmonary barrier damage. As expected, we observed a significant increase in erythrocytes and protein in the BAL of CypD-deficient mice that received PBS compared to control WT mice, but there was no amelioration in either group that received IFN- γ (**Fig S5E-F**). Collectively, these data confirm that despite a reduction of NK cell-derived IFN- γ in CypD-deficient airways post-IAV infection, this does not explain the lack of disease tolerance observed in these mice.

An emerging protective role for NK cells is as an important source of IL-22—a promoter of epithelial cell survival and proliferation at barrier sites—and a critical correlate of immunity to IAV (241, 243). Thus, we postulated that a lack of IL-22 production from CypD-deficient NK cells was underlying the susceptibility of these mice. To assess this hypothesis, we began by confirming previous work (241) that IL-22-deficient mice had enhanced protein and cell accumulation in the BAL, as well as pulmonary inflammation by histology at 7 days post-IAV infection (**Fig. S5G-I**), indicative of impaired disease tolerance. Next, we assayed IL-22 in the BAL of WT and *CypD*^{-/-} mice at various time points p.i. and found a significant reduction in *CypD*^{-/-} mice at 7 days p.i. (**Fig. 5C**). Moreover, as with IFN- γ , we identified NK cells as an important source of IL-22 and

there was a specific reduction of IL-22⁺ NK cells in both the BAL and spleen of CypD-deficient mice compared to WT at 5 days post-IAV (**Fig. 5D**; **Fig. S5J**). These data collectively confirm the importance of CD49b⁺ blood-derived conventional NK cells in IL-22 production following IAV infection.

Because of the observation that IL-22 is critical in promoting disease tolerance to IAV and that *CypD*^{-/-} mice lacked IL-22 in the airways, we wanted to investigate whether or not reconstitution of CypD-deficient airways with IL-22 could protect against IAV infection in a disease tolerance manner. At 5 days post-lethal IAV infection, we intranasally reconstituted the airways of WT and *CypD*^{-/-} mice with 100ng of IL-22 or PBS and assessed mortality. As expected, *CypD*^{-/-} mice that received PBS were significantly more susceptible than WT mice that received PBS. Yet, we noted that CypD-deficient mice given exogenous IL-22 were significantly less susceptible to IAV compared to *CypD*^{-/-} PBS controls and their survival was comparable to WT mice (**Fig. 5E**). This improvement in survival could be completely correlated to improved disease tolerance and not host resistance, as the elevated erythrocyte influx was abrogated in the CypD-deficient mice by cell counts and histology (**Fig. 5F-G**), with no effect on viral loads (**Fig. 5H**). No improvement was seen in WT mice receiving IL-22 compared to those receiving PBS, suggesting that increased levels of IL-22 may not protect an already IL-22-sufficient host.

Finally, having established the role of IL-22 in enhancing disease tolerance in *CypD*^{-/-} mice, as well as an inability of CypD-deficient NK cells to produce IL-22, we sought to directly assess the capacity of WT versus *CypD*^{-/-} NK cells to protect against tissue damage in an IL-22-deficient environment. To do this, we purified NK cells from naïve spleens of WT and CypD-deficient hosts, then transferred 1x10⁵ cells, or control PBS, intratracheally into infected *IL-22*^{-/-} hosts at 5 days post-IAV infection, as to not affect early viral replication or the onset of tissue damage. At 7 days p.i. (2 days post-transfer), we collected the BAL and lungs and assayed damage and viral loads. We found that IL-22-deficient mice that received WT NK cells exhibited statistically significantly enhanced disease tolerance, as assessed by attenuated protein and erythrocyte accumulation in the BAL, while no improvement was noted in mice receiving *CypD*^{-/-} NK cells compared to PBS controls (**Fig. 5I-J**). Furthermore, no differences in viral load between any group could be delineated; thus, disease tolerance, rather than host resistance, was responsible for the reduced

airway damage (**Fig. 5K**). As the cells from both groups displayed the same purity prior to transfer (>85%, data not shown) and they were transferred into the same IL-22-deficient microenvironment, the inability of *CypD*^{-/-} NK cells to promote disease tolerance in this scenario must be due to an intrinsic inability to produce IL-22. Therefore, NK cell-derived IL-22 is dependent upon CypD expression and is essential in the establishment of disease tolerance following IAV infection.

3.5: Discussion

The immune response to influenza virus must be tightly regulated at both the innate and adaptive branches. Shortly following infection, resident immune cells coordinate early innate leukocyte infiltration to inhibit IAV replication and clear it from the lung, through host resistance responses. Host resistance to IAV is well studied (101) and current influenza antivirals, such as oseltamivir, aid in these pathways by directly acting on the virus to inhibit replication/egress (27). Although insufficient host resistance can be lethal (383, 384), the majority of IAV-related deaths stem from dysregulated immune responses and immunopathology (44, 225). Thus, it is essential to understand the mechanisms that promote disease tolerance to IAV. As an immune mechanism, disease tolerance was initially observed in plants (385) and has since been extended to mammals (106, 224). While our understanding of mechanisms of disease tolerance is accumulating during chronic infections, such as helminths or *Mycobacterium tuberculosis* (305, 386), following acute infections like IAV, it remains incomplete. However, our group and others have suggested that pulmonary barrier integrity is a fundamental component (150, 229). In the current study, we extend this observation and find that CypD protects against IAV by limiting tissue damage to promote disease tolerance.

The unique location of CypD within the mitochondrial matrix places it at the epicentre of PRR signaling, cell death and metabolism during response to infection. For example, in mature leukocytes, the mitochondrial antiviral signalling protein (MAVS) is anchored to the outer mitochondrial membrane and is essential for the induction of IFN-I in response to several viruses, including IAV. Although activation of the cytosolic PRR RIG-I by viral RNA is the major initiator of MAVS-mediated responses, mitochondrial heat shock proteins, fission proteins and mitochondria-derived ROS all regulate MAVS function (387). Additionally, IAV-encoded PB1-F2 localizes to the mitochondria and induces early intrinsic apoptosis to temper antiviral responses, which is combatted by the host PRR NLRX1 within the mitochondrial matrix (62). During LCMV infection, enhanced mitochondrial oxidative phosphorylation promotes antiviral immunity by pDCs (388), while our recent study highlighted the importance of CypD-dependent metabolic changes in T-cell contraction to promote disease tolerance to *Mtb* (352). Thus, mitochondria are

critical orchestrators of both resistance and tolerance mechanisms in ways that are cell and pathogen specific.

Although the majority of previous work has focused on mitochondria in mature leukocytes, this study also revealed a role for mitochondrial CypD in regulating lymphopoiesis and p53-associated progenitor cell death. In structural cells, p53, an essential regulator of cell survival and death, was previously shown to translocate to the mitochondrial matrix and interact with CypD, resulting in cell necrosis (377). Interestingly, enhancement of p53 activity specifically within lymphocyte progenitors has been shown to induce cell death and skewing of hematopoiesis towards myelopoiesis (379, 380). Our results uncovered a hitherto unappreciated inhibition of p53 by CypD in NK cell progenitors to promote lymphopoiesis, akin to the role previously described for Mym1 and Mdm2 (379, 380). Importantly, hematopoietic progenitor cell death is emerging as a master regulator of lymphopoiesis versus myelopoiesis (270, 271). Though no direct protein-protein interaction experiments between p53 and CypD were attempted in our study, it is intriguing to speculate that a balance between pro-lymphopoiesis versus pro-myelopoiesis signals in progenitors may alter the outcome of p53/CypD interactions in the mitochondria, either by promoting or antagonizing p53-dependent lymphoid progenitor cell death, as leukocyte requirements change in the periphery. Certainly, more study is required to fully delineate the contributions of CypD and p53 to hematopoiesis, as well as other known regulators such as Mym1 and Mdm2.

In addition to our results in the bone marrow, we equally identified a function for CypD in mature NK cells that promotes their activation and function. NK cells are well-known for their role in host resistance by killing virally infected cells, through an “innate” non-MHC restricted manner, which differs from cytotoxic antigen-specific T-cells (357). Specifically during IAV infection, complete genetic ablation of NK cells (via knockout of the transcription factor *Nfil3*; *Nfil3*^{-/-} mice) (190), loss of the HA interacting receptor NKp46 (*Nkp46*^{-/-}) (188), or depletion using an anti-asialo GM1 antibody (189), all result in lethality and elevated viral titres in the lung. Although one finding suggested that NK cells contribute to IAV pathogenicity, this is likely due to the high dose used, as this result was not obtained at medium or low doses (389). Furthermore, an additional role for NK cells in IL-22 production has been shown to be critical in disease

tolerance to IAV (243). Here we show that CypD regulates this IL-22 production from NK cells (**Fig. 5D**), while the components of host resistance (e.g. viral loads (**Fig. 1C**) and NK cell expression of perforin and granzyme B (**Fig. 2G-H**)) are not regulated by CypD expression. Therefore, the importance of NK cells in the immune response to IAV is varied and involves both resistance and tolerance functions.

Early NK cell responses, beginning at approximately 2 days post-IAV infection appear to be mediated by NKp46 and are primarily concerned with restricting viral replication by killing infected cells. Thus, studies using mice that lack NK cells or NKp46 expression prior to the onset of infection show enhanced mortality coupled with increased viral loads (188-190). However, following viral containment, the function of NK cells appears to shift from host resistance to disease tolerance, as marked by enhanced production of IL-22. Our results suggest that the early phase of NK cell function is CypD-independent, while the later stages are CypD-dependent. In this vein, several lymphocyte subsets have been identified as sources of IL-22 in response to IAV, including NK cells, NKT cells, ILCs and conventional $\alpha\beta$ T-cells. Studies investigating the early phase of IAV infection (i.e. 2 and 4 days p.i.) elucidated NKT and ILCs as the major sources (245, 246), while our work and another study (243) at later timepoints reveal conventional NK cells as the primary source of IL-22. Collectively, these results suggest that early IL-22 production is dominated by NKT cells and ILCs, while NK cells are performing their antiviral function, before NK cell function shifts to disease tolerance via the production of IL-22. Undoubtedly, further insight into the kinetics of IAV infection and how leukocyte function changes over time is required to more completely understand this complex phenomenon.

Our study also outlines an important bone marrow/lung/NK cell axis that is differentially regulated by varying roles of CypD. The exact molecular mechanisms of differential CypD function in progenitors versus mature lung NK cells is unknown and requires further investigation. Intriguingly, mounting evidence suggests that progenitors may be imprinted in the bone marrow and that this signature may affect the function of terminally differentiated effector cells in a process termed “trained innate immunity” (390). Thus, NK cells in the periphery of *CypD*^{-/-} mice may be imprinted with an immature phenotype because of the lack of CypD function in bone marrow NK cell progenitors. We have recently described BCG, the vaccination against *Mtb*, delivered

intravenously imprints hematopoietic stem cells to promote myelopoiesis and generate more protective macrophage responses to subsequent *Mtb* infection (304). Interestingly, NK cells have equally been shown to be “trained” by BCG (391) and memory NK cells are generated following IAV infection (190). Thus, it is possible that CypD may play a role in protective NK cell imprinting in the bone marrow. The potential for trained immune responses to IAV is currently unknown.

In conclusion, influenza infections are responsible for yearly seasonal epidemics that result in approximately 1 billion infections and between 300 000-500 000 deaths worldwide each year, as well as sporadic pandemics (27). Past IAV pandemics as well as the current COVID-19 pandemic have highlighted how an incomplete understanding of the immune response to acute respiratory infections hinders the generation of efficacious vaccines or antiviral therapies. Our study in eicosanoids and IAV, and now IL-22, has outlined the potential for combinatory immunomodulatory and antiviral therapies to combat IAV (150, 154) in both experimental (229) and clinical settings (32). The emerging observation that disease tolerance is equally critical in immunity to SARS-CoV-2 (392, 393), offers promise that immunomodulatory therapies targeting disease tolerance may provide more universal benefit to a variety of infections. Thus, investigating novel pathways of disease tolerance is required to combat current and next generation respiratory viruses.

3.6: Materials & Methods

Mice

Six- to ten-week-old C57BL/6, CD45.1, *Ifngr*^{-/-} mice were purchased from Jackson Laboratories. *CypD*^{-/-} mice were provided by M. Fortin (Oregon Health and Science University, Portland, OR, USA) and *Il22*^{-/-} mice were a gift from I. King (McGill University, Montreal, Canada). All animals were housed and inbred at the animal facility of the Research Institute of McGill University. Experiments were performed using age- and sex-matched mice.

Viruses & Infection

All *in vivo* infections were performed using mouse adapted influenza A/Puerto Rico/8/34 (H1N1) virus (IAV), kindly provided by Dr. Jonathan A. McCullers (St. Jude Children Research Hospital). Mice were challenged intranasally (in 25 μ L PBS) with IAV at a sublethal dose of 50 PFU or a lethal dose (LD₅₀) of 90 PFU. 90 PFU was used for the survival experiments in **Fig. 1A** and **Fig. 5F**. For all other experiments, 50 PFU was used. During survival experiments mice were monitored twice daily for signs of duress and weighed daily. Mice reaching 75% of original body weight were considered moribund and sacrificed. Viruses were propagated and isolated from Madin-Darby Canine Kidney (MDCK) cells and titrated using standard MDCK plaque assays. MDCK cells were obtained from the American Type Culture Collection and maintained in Dulbecco's modified Eagle medium enriched with 10% (v/v) FBS, 2 mM L-glutamine and 100 U ml⁻¹ penicillin/streptomycin.

Protein in the BAL

BAL were collected by cannulating the trachea with a 22-gauge cannula, then washing the lungs with 3 \times 1 ml of cold, sterile PBS. The total volume recovered after lavage was \sim 0.7 ml. Samples were spun down (1,500 r.p.m.; 10 min) and the total protein content was assessed by Pierce BCA Protein assay (Thermo Fisher Scientific).

Texas Red-Dextran Lung Permeability

WT and *CypD*^{-/-} were infected for 7 days with 50 PFU. On day 7, mice were delivered 25µL of 50mg/mL (1.25mg) Texas Red-Dextran (10 000 MW) intranasally. 1 hour later mice were sacrificed and lungs were carefully excised without damaging. Lungs were imaged using the In Vivo Xtreme (Bruker) using fluorescence capture. Resulting images were then analyzed for total fluorescent intensity of lung images using ImageJ software (National Institutes of Health). During the 1 hour of incubation Texas Red-Dextran molecules diffused into the blood of infected mice, due to the loss of epithelial/endothelial barrier integrity. Therefore, lower fluorescence is indicative of increased damage and compromised barrier integrity.

Generation of chimeric mice

CD45.1⁺ B6 mice or *CypD*^{-/-} mice were lethally irradiated with 9 Gy following 3 days of antibiotic treatment (0.5g Enrofloxacin (Bayer) per litre of drinking water). 16 hours later, the BM compartment was reconstituted with 4x10⁶ nucleated cells from either CD45.1⁺ mice (*CypD*^{-/-} recipient) or *CypD*^{-/-} mice (CD45.1⁺ recipient) and antibiotic treatment was maintained for 2 additional weeks. Between 10-12 weeks post-injection, reconstitution was validated by flow cytometry and was >95%. Mice were then infected for downstream assays.

Flow Cytometry

Lung tissues were perfused with 10 mL of PBS, harvested and minced before collagenase digestion (150 U mL

⁻¹) for 1 h at 37 °C. Lungs were passed on a 40 µm nylon mesh, and red blood cells were lysed. For bone marrow staining, cells were isolated following aseptic flushing of the tibiae and femurs, and red blood cells were lysed. BAL were collected as previously described, spun down and red blood cells lysed. Spleens were aseptically removed, crushed on a 40 µm nylon mesh, and red blood cells were lysed. Then total cell counts were determined with a haemocytometer, and two to three million cells were used for staining. In some experiments BAL were counted prior to red blood cell lysis to enumerate erythrocyte influx into the airways and then red blood cells were

lysed. For peripheral blood staining, the blood was collected by cardiac puncture in a BD Microtainer tube and stained extracellularly; red blood cells were then lysed.

Cells were initially stained with eFluor-506 viability dye in PBS (eBioscience; 20 min; 4 °C), washed and surface stained with anti-CD16/32 (BD Biosciences) in 0.5% BSA/PBS solution to block non-specific antibody interactions with Fc receptors (10 min; 4 °C). Cells were then surface stained with combinations of PE-CF594-conjugated anti-SiglecF, BUV395-conjugated anti-CD11b, PerCP-eFluor780-conjugated anti-Ly6G, fluorescein isothiocyanate (FITC)- or allophycocyanin (APC)-conjugated anti-Ly6C, APC-eFluor780-conjugated anti-F4/80, BV421-conjugated anti-CD11c, FITC- or BUV395-conjugated anti-CD45.2 or APC-conjugated anti-CD45.1, Pe-Cy7-conjugated anti-CD3, BV786-conjugated anti-CD127, APC- or BUV737-conjugated anti-NKp46, BV421-conjugated anti-CD49b, PE-conjugated anti-CD49a (all from BD BioScience, except anti-Ly6G from eBioscience), or PE-Cy7-conjugated (BD Biosciences) or FITC-conjugated (eBioscience) anti-CD27. Cells were then fixed with 1% PFA for 1 hour, washed and acquired in 0.5% BSA/PBS solution.

In some experiments, following extracellular staining, samples were stained intracellularly for Ki67, active Caspase 3 or p53. For APC-conjugated anti-Ki67 and PE-conjugated anti-active Caspase 3 (both from BD Biosciences) cells were initially fixed and permeabilized using BD Cytotfix/Cytoperm (BD Biosciences) for 30 minutes at 4° C and then stained for 1 hour. Cells were washed and acquired. For p53 staining, cells were initially fixed and permeabilized for 1 hour using the Foxp3/Transcription Factor Staining Buffer Set (eBioscience) and then stained using the PE-conjugated anti-p53 Set (BD Biosciences) was used according to the manufacturer's instructions. The provided PE-conjugated isotype was used as a control.

In experiments involving bone marrow progenitors, cells were processed, counted, stained for viability and blocked as before. Cells were then stained with biotin conjugated anti-Ly6C/G, anti-CD5, anti-B220, anti-Ter119, anti-CD4 and anti-CD8 for 20 minutes at 4° C. Cells were then washed and stained with APC-Cy7-conjugated streptavidin, APC-conjugated anti-cKit, PE-Cy7-conjugated Sca-1 for LKS cells. For CMP/GMP experiments, cells were not blocked and instead FITC-conjugated anti-CD34 and PerCP-eFluor780-conjugated anti-CD16/32 (all from BD Biosciences, except anti-CD16/32 from eBioscience) were added to the previous cocktail. For NK

cell progenitors, PE-CF594-conjugated anti-CD122 and BUV395-conjugated anti-CD244.2 were added along with anti-CD27 and anti-CD127 (BD Biosciences) as previously described.

Finally, for experiments involving intracellular cytokine staining (ICS), 2×10^6 single splenocytes or BAL cells were incubated for 4 hours at 37° C in the presence of PMA/Ionomycin and Brefeldin A (Cell Activation Cocktail; BioLegend) or GolgiPlug control (BD Biosciences). Cells were then stained extracellularly, fixed and permeabilized using BD Cytofix/Cytoperm (BD Biosciences), before being stained intracellularly for PE-conjugated anti-IL-22 and APC-conjugated anti-IFN- γ (BD Biosciences).

Flow cytometry acquisition was performed using BD LSRFortessa X-20 (BD Biosciences) with FACSDiva Software version 8.0.1 (BD Biosciences). Analysis was performed using FlowJo software version 10 (Tree Star).

Adoptive transfer model

NK cells were purified from uninfected spleens of WT and *CypD*^{-/-} mice using the EasySep Mouse NK Cell Isolation Kit (Stem Cell Technologies) according to the supplier's recommendations. Sorted cells were counted, washed (cold sterile PBS) and normalized to 1×10^5 cells/50 μ L of sterile PBS. Purity was verified by flow cytometry and purity was always over 85% NK cells prior to transfer. NK cells were then transferred into *I122*^{-/-} mice on day 5 post-infection (50 PFU) via the intratracheal route. 2 days later, BAL were harvested for lung damage assays or histology, and lungs were harvested for viral load analysis.

IL-22 or IFN- γ treatment

Recombinant murine IL-22 or IFN- γ was purchased from Peprotech. Mice were intranasally infected with 50 p.f.u. of IAV. On day 5 post-infection, mice were given either PBS, IL-22 or IFN- γ (both 100ng/25 μ L) intranasally. Mice were sacrificed on day 7 post-infection, and the lungs were harvested and processed to determine the pulmonary viral load, or the BAL collected for damage assays. In some experiments, mice were infected with 90 PFU and IL-22 was delivered as stated and survival was monitored.

Histopathological analysis

Lungs were inflated and fixed for 48 h with 10% formalin, then embedded in paraffin. Next, 5 μm sections were cut and stained with haematoxylin and eosin. Slides were scanned at a resolution of 40 \times magnification and pictures were taken using a Leica Aperio slide scanner (Leica).

Total bioactive IFN-I assay

Secretion of total active IFN-I (both IFN- α and IFN- β) in cell culture supernatants was assessed using the B16-Blue IFN- α / β reporter cell line for murine samples (InvivoGen), according to the specifications of the manufacturer. B16 cells were maintained in RPMI supplemented with 10% (v/v) FBS, 2 mM L-glutamine and 100 U ml⁻¹ penicillin/streptomycin.

Cell death analysis

Lactate dehydrogenase release in the BAL of IAV-infected mice was quantified using the CytoTox 96 Non-Radioactive Cytotoxicity Assay (Promega), per the manufacturer's recommendations. Dead cell levels *in vivo* were assessed using PE-AnnexinV (BioLegend) and NucSpot Far-Red (Biotium), according to the manufacturer's instructions and unfixed cells were acquired immediately by flow cytometry.

Wet-to-dry ratio

Lungs were harvested from naive or IAV-infected mice (50 PFU.; day 7 post-infection), and blood clots were carefully removed. Then, the lungs were weighed (wet weight) and dried in an oven (56 °C, 2 d; dry weight), and the dry weight was measured. Data are presented as the ratio of wet weight to dry weight.

RNA isolation and reverse transcription quantitative PCR (qPCR)

RNA from purified NK cells was extracted using an RNeasy Kit (Qiagen) according to the manufacturer's instructions. Some 500 ng of RNA was reverse transcribed using the ABM 5X RT MasterMix (Applied Biological Materials), as directed by the manufacturer. Complementary DNA was generated by qPCR using BrightGreen SYBR Green (Applied Biological Materials). Cq

values obtained on a CFX96 PCR System (Bio-Rad) were analysed using $2^{-\Delta C_q}$ formula normalizing target gene expression to *GAPDH*.

ELISA

IFN- β levels in infected lungs and BAL were measured using a VeriKine Mouse IFN- β ELISA kit (PBL Assay Science). IFN- γ and IL-22 (R&D Systems) levels were assessed by ELISA according to the manufacturer's instructions.

Statistical analysis

Data are presented as means \pm s.e.m. Statistical analyses were performed using GraphPad Prism version 8.0.2 software (GraphPad). Statistical differences were determined using a two-sided log-rank test (survival studies), one-way analysis of variance (ANOVA) followed by Sidak's multiple comparisons test, two-way ANOVA followed by Sidak's or Dunnett's multiple comparisons test, or two-tailed Student's T-Test, as outlined in the Figure Legends. All means are depicted \pm SEM with significance denoted by * $p < 0.05$, ** $p < 0.01$, *** $p < 0.001$, **** $p < 0.0001$.

Ethics

All experiments involving animals were approved by McGill University (permit number 2010-5860) in strict accordance with the guidelines set out by the Canadian Council on Animal Care.

3.7: Acknowledgements

The authors would like to thank members of the Small Animal Imaging Labs (SAIL) of the RI-MUHC for assistance with the experiments in Figure 1I, particularly Dr. Barry Bedell and Mathieu Simard. Additionally, the authors thank the Histopathology Core of the RI-MUHC for assistance with histology experiments. This work was supported by the Canadian Institute of Health Research (CIHR) Foundation Grant (FDN-143273) to M.D. M.D. holds a Fonds de recherche du Québec–Santé (FRQS) Award and the Strauss Chair in Respiratory Diseases. J.D. was supported by the Molson Foundation Award and RI-MUHC Studentship, E.P. was supported by a Fonds de Recherche du Québec–Santé Fellowship. The funders had no role in study design, data collection and analysis, decision to publish, or preparation of the manuscript.

3.8: Figures

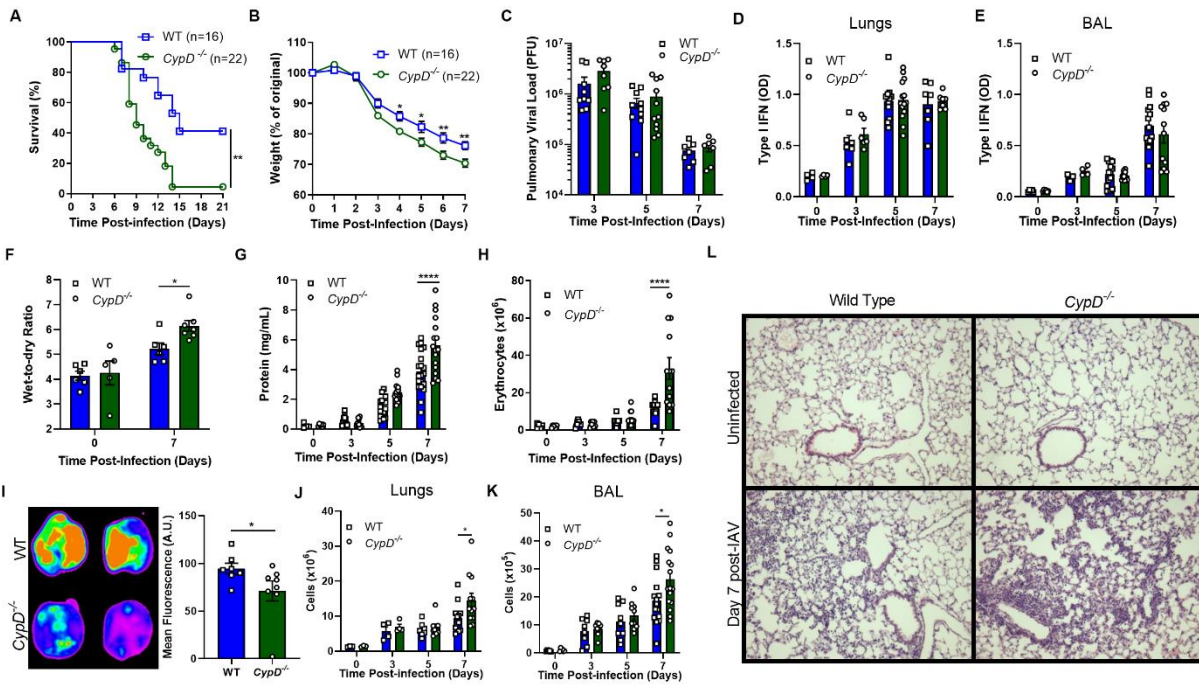


Figure 3.8.1: CypD protects against IAV infection by promoting disease tolerance. (A-B) WT and *CypD*^{-/-} mice were infected with the LD₅₀ dose of 90 PFU and survival (A) and weight loss (B) were monitored. (C-L) WT and *CypD*^{-/-} mice were infected with a sublethal dose of 50 PFU. At various time points post-infection viral load (C), total active IFN-I in the lungs (D) or BAL (E) were measured. (F) Lung wet-to-dry ratio at steady-state or at day 7 post-infection. Protein (G) or erythrocytes (H) in the BAL of mice at various timepoints post-infection. (I) Fluorescence intensity of lungs following one hour of Texas-Red Dextran administration. The left panels are representative lung images from two separate experiments and are quantified on the right. Total cell counts in the lungs (J) and BAL (K) following infection. (L) Representative micrographs of lungs stained with hematoxylin and eosin that are either uninfected or infected for 7 days. In A and B, total mice are denoted in the figures, in C-K each symbol represents a unique mice, in L micrographs are representative of at least 5 mice. All figures are a compilation of at least two experiments. Statistical analyses were performed using the Log Rank Test (A), Two-way ANOVA followed by Sidak's multiple comparison test (C-H, J-K) or Two-tailed Student's T-Test (I).

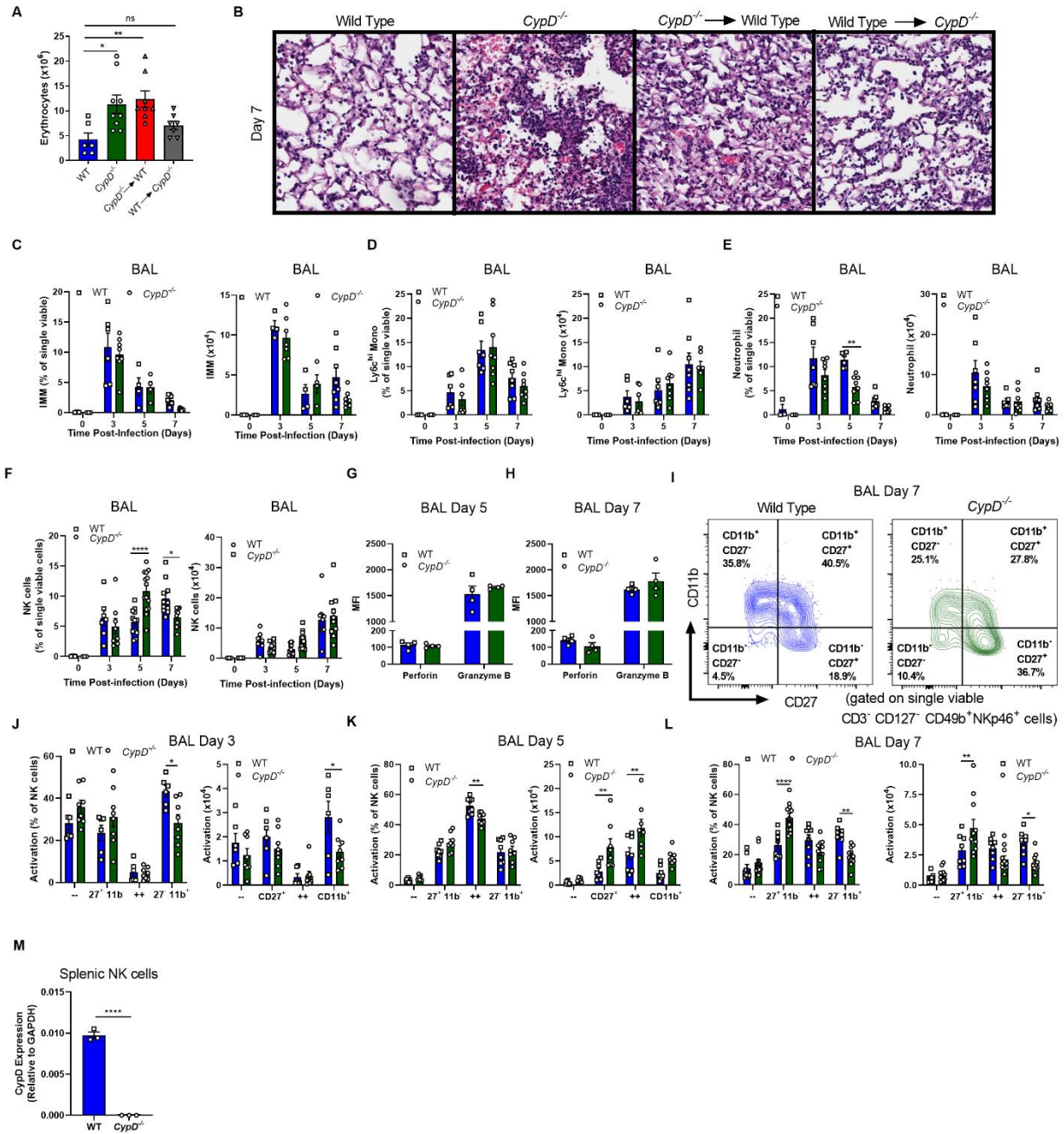


Figure 3.8.2: CypD mediates disease tolerance via hematopoietic cells and mice exhibit altered NK cell kinetics upon infection. (A-L) Mice were infected with 50 PFU of IAV. (A-B) Chimeric mice were generated by reconstituted irradiated CypD-deficient mice with CD45.1 bone marrow (WT \rightarrow CypD^{-/-}) or irradiated CD45.1 mice with CypD-deficient bone marrow (CypD^{-/-} \rightarrow WT). Chimeric mice were infected for 7 days and total erythrocytes in the BAL (A) were quantified. (B) Representative micrographs of hematoxylin and eosin stained lungs. (C-F) BAL from WT and CypD^{-/-} mice were phenotyped by flow cytometry and total frequencies (left panels) and total cell counts (right panels) of IMM (C), Ly6C^{hi} monocytes (D), neutrophils (E) and NK cells (F) quantified. Mean fluorescence intensities of perforin and granzyme B on the surface of NK cells at day 5 (G) or day 7 (H) post-IAV infection. (I) Representative FACS plot of CD27 and CD11b expression on NK cells in the BAL of WT versus CypD-deficient mice at 7 days post-infection. (J-L) Quantifications of the percentages (left panels) and total cells counts (right panels) of NK cell activation subsets in the BAL at day 3 (J), day 5 (K) and day 7 (L) post-infection. (M) Relative expression of CypD transcripts in purified splenic NK cells of naive mice. In each panel, each symbol indicates a separate mouse, except in B, which is a representative figure of 4 mice/group and I, which is a representative plot compiled in L. All figures are a compilation of at least two experiments, except G and H, which are one representative experiment of two. Statistical analyses were performed using the One-way ANOVA followed by Dunnett's multiple comparisons (A), Two-way ANOVA followed by Sidak's multiple comparison test (C-F, J-L) or Two-tailed Student's T-Test (G-H and M).

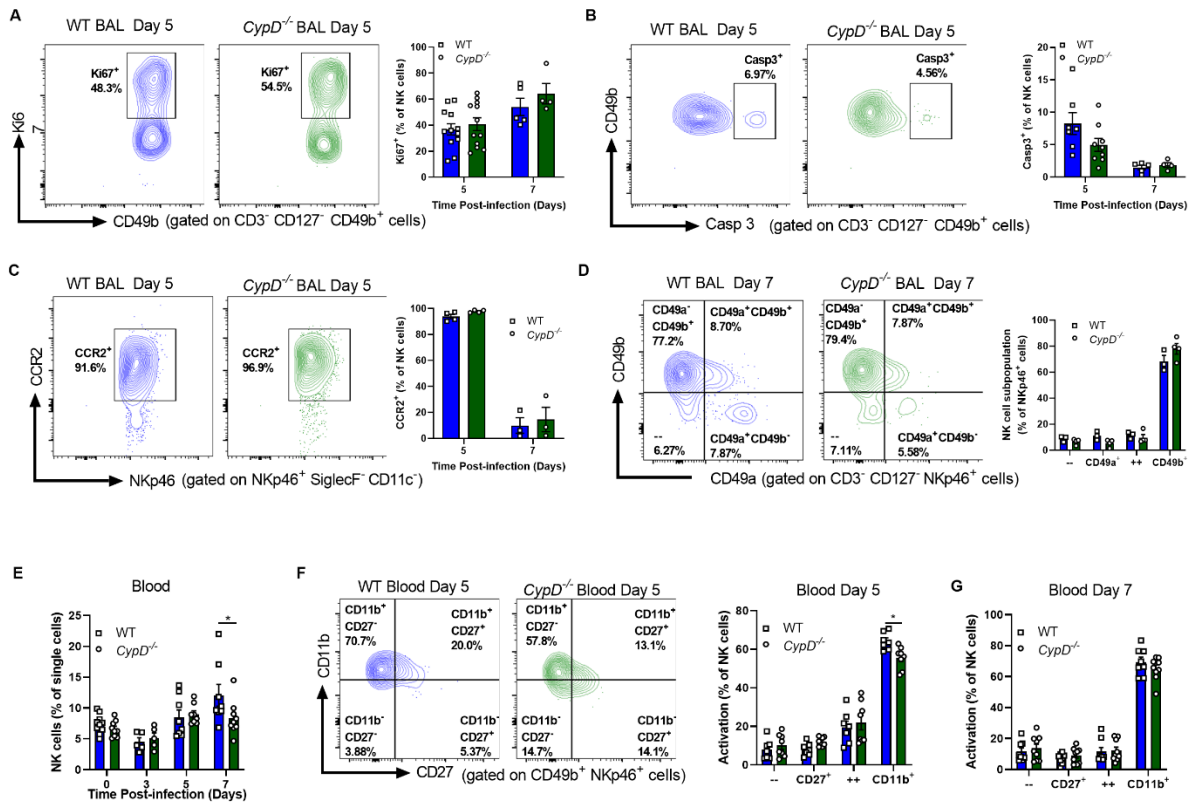


Figure 3.8.3: CypD-deficient mice have impaired recruitment of activated NK cells from the peripheral blood. (A-G) WT and *CypD*^{-/-} were infected with 50 PFU. (A) Intracellular expression of Ki67, indicative of proliferative cells, in NK cells of the BAL. Left panels show a representative FACS plot as quantified on the right at day 5 post-infection. (B) Intracellular expression of active Caspase 3 expression by flow cytometry, indicative of apoptotic NK cells in the BAL of infected mice. The panels on the left are of a representative FACS plot at day 5 post-infection, as quantified on the right. (C) CCR2 expression on NK cells of the BAL with a day 5 representative FACS plot on the left and quantified on the right. (D) Differential expression of CD49b versus CD49a on NK cells of the BAL with a representative FACS plot on the left. (E-F) At various times post-infection peripheral blood was collected and the frequency of NK cells (E) and their activation state as defined by CD27 and CD11b (F-G) were quantified. In the left panel of F is a representative FACS plot of NK cells at day 5 post-infection. Each panel represents the combination of at least two experiments, except C which is one representative of two independent experiments. Each symbol represents one unique mouse. For all panels, Two-way ANOVA followed by Sidak's multiple comparisons test was performed to determine significance.

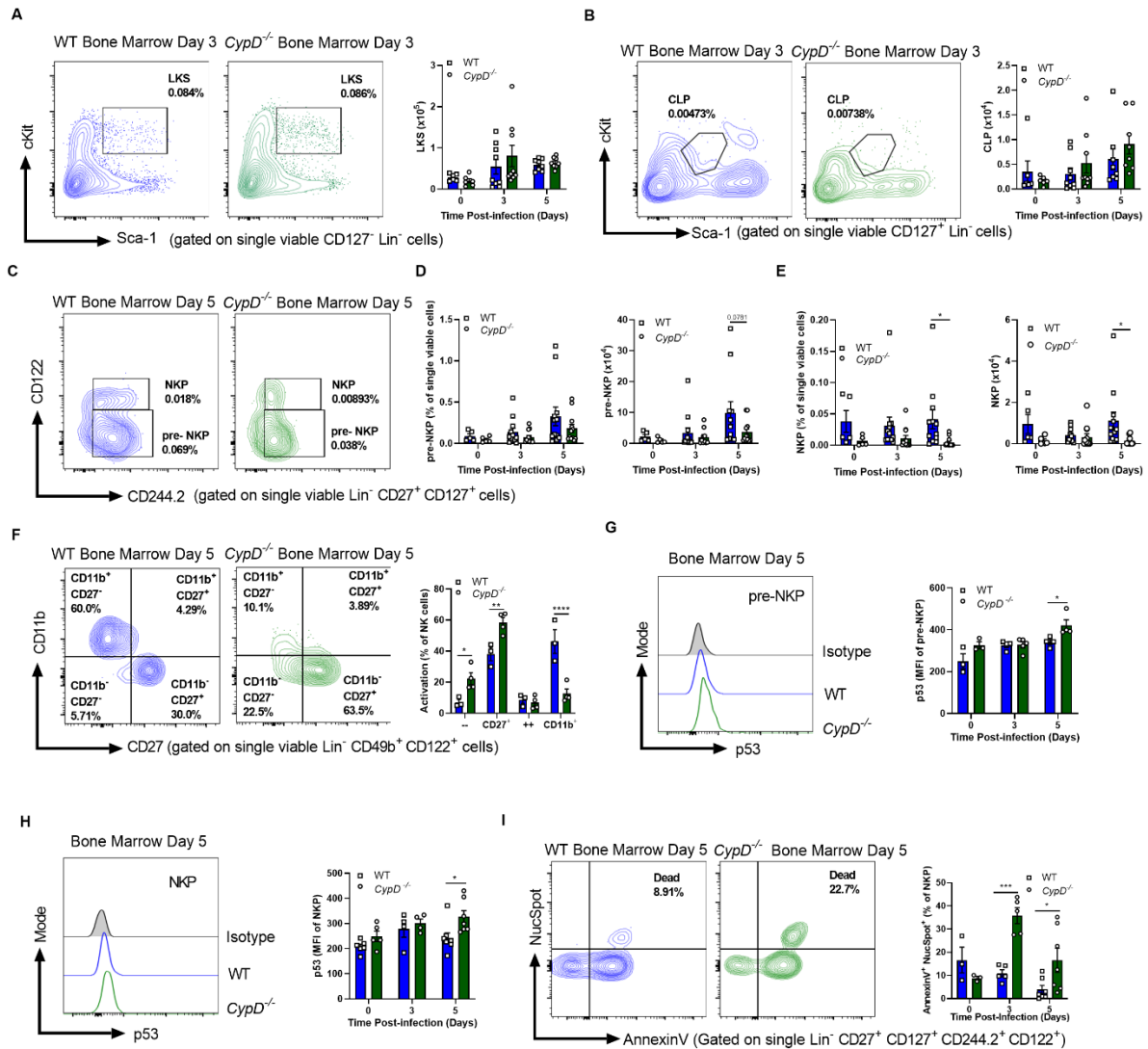


Figure 3.8.4: *CypD*^{-/-} mice have reduced NK cell hematopoiesis in the bone marrow of infected mice due to dysregulated cell death of progenitors. (A-F) Total cell counts of LKS (A), CLP (B), pre-NKP (C-D), NKP (E) and differential activation statuses of mature NK cells (F) as assessed by flow cytometry. (C) Representative FACS plots of pre-NKP and NKP populations in the bone marrow at 5 days post-infection. In A, B and F, left panels are representative FACS plots taken at day 3 (A-B) and day 5 (F) post-infection. (G-H) Expression of p53 within pre-NKP (G) and NKP (H) populations in the bone marrow. Left panels are representative histograms taken at 5 days post-infection as quantified in the right panels. (I) Differential expression of AnnexinV and NucSpot to determine the levels of dead cells within the NKP population at various times post-infection. FACS plots on the left are taken from day 5 post-infection. Panels in A-E are a compilation of at least 2 experiments, while F-I are one representative experiment of three independent experiments, with each symbol representing an individual mouse. In all panels, significance was assessed by Two-way ANOVA followed by Sidak's multiple comparisons test.

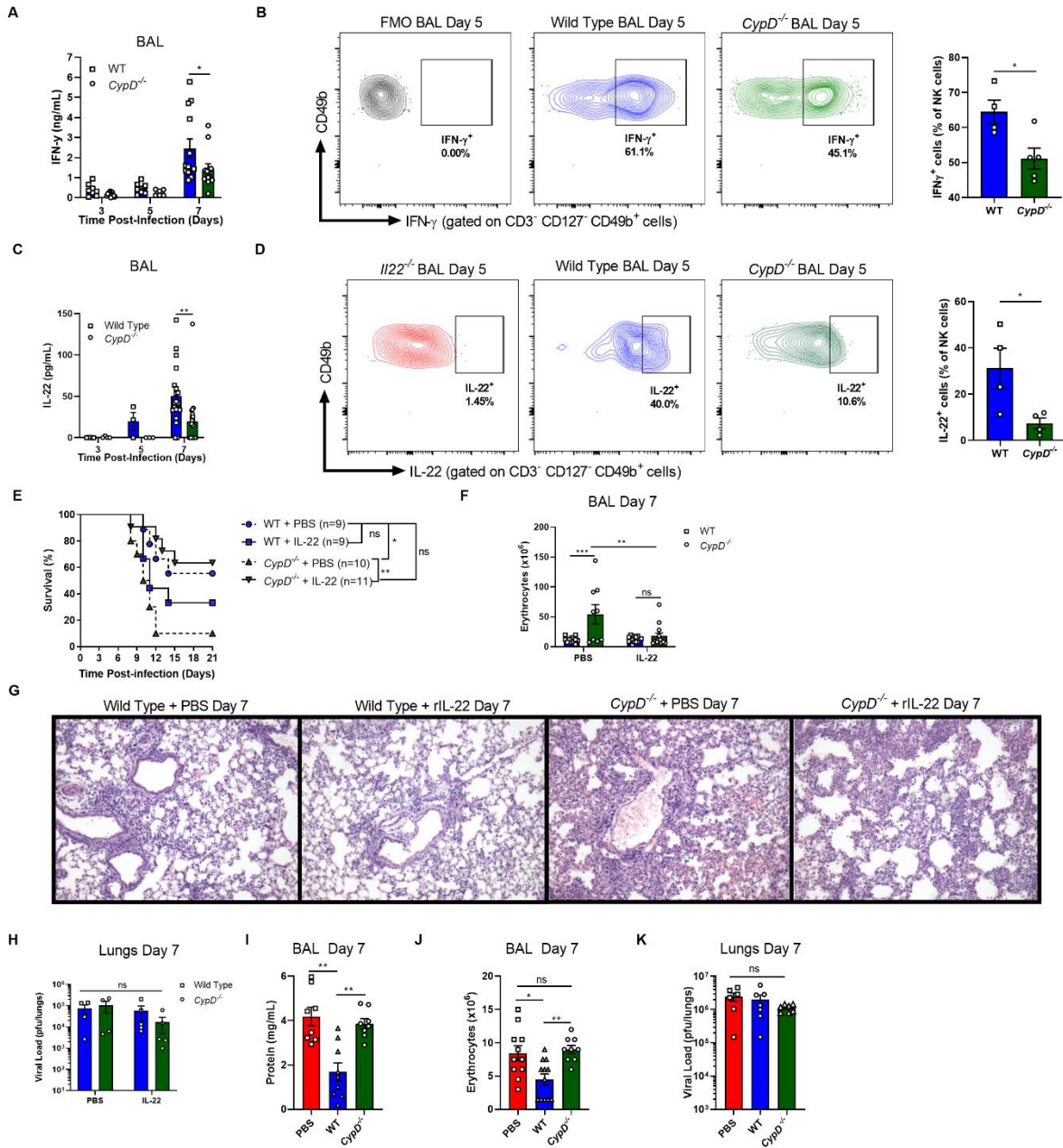


Figure 3.8.5: A lack of IL-22 production by NK cells in the airways is responsible for the susceptibility of *CypD*^{-/-} mice in a disease tolerance manner. (A) Levels of IFN- γ in the BAL of infected WT and *CypD*^{-/-} mice as determined by ELISA. (B) Intracellular cytokine staining of IFN- γ in NK cells. FACS plots are representative of the quantification on the right and are gated against the FMO. (C) Levels of IL-22 in the BAL of infected WT and *CypD*^{-/-} mice as determined by ELISA. (D) Intracellular cytokine staining for IL-22 by NK cells in the BAL of day 5 infected mice. FACS plots on the left are representative of the quantification on the right. An IL-22-deficient mouse was used as a staining control for specificity. (E) Mice were infected with LD₅₀ 90 PFU and administered recombinant IL-22 or PBS; survival was monitored. In F-H a sublethal 50 PFU dosage was used and mice were administered IL-22 or PBS. At day 7, erythrocytes in the BAL were enumerated (F), pulmonary inflammation was assessed by hematoxylin and eosin staining (G) and viral loads quantified (H). On day 7 post-infection, day 2 post-transfer, protein (I) and erythrocyte (J) levels in the BAL and lung viral loads (K) were assessed. In panels A, C, E-F, I-K data are combinations of two or three independent experiments. In B, D and H data are from one experiment that is representative of three independent experiments. Micrographs in G are representative of 3 or 4 individual mice. In A-D, F, and H-K, each symbol represents data from one individual mouse, while in E total n values are displayed in the panel legend. Statistical analyses were performed as follows: in A, C Two-way ANOVA followed by Sidak's multiple comparisons test; in B, D Two-Tailed Student's T-test; Log Rank Test; G, H Two-way ANOVA followed by Tukey's multiple comparisons test; I-K One-way ANOVA followed by Dunn's multiple comparisons test.

PREFACE TO CHAPTER 4

Initially thought to be confined exclusively to cells of the adaptive system, the realization that the mammalian innate immune system can also exhibit memory-like responses, termed trained immunity (292), led to intense study of the phenomenon and its role in disease pathogenesis and prevention. As outlined in chapter 1, trained immunity refers to how innate cells, predominantly monocyte-derived macrophages but also other cells like NK cells, in response to certain stimuli, become “trained” to respond more robustly to secondary heterologous challenges. Such known inducers of trained immunity in monocyte/macrophages are BCG, the vaccine against *Mtb*, and β -Glucan, a polysaccharide PAMP (105). Although we recently showed that HSC reprogramming and biasing of hematopoiesis towards myelopoiesis by BCG in the bone marrow were critical in conferring long-term trained macrophage responses against subsequent *Mtb* infection (304), the cellular signalling pathways involved in the imprinting and myeloid biasing were still unclear. Additionally, although much study has centred around the protective capacity of trained immunity, it can also be manifest detrimentally, depending on inflammatory context (299). Thus, we sought to better understand the underlying mechanisms of this duality of training, using evolutionarily related mycobacteria. We found that one virulence strategy of *Mtb*, compared to BCG, is the biasing of hematopoiesis towards lymphopoiesis—at the expense of myelopoiesis—that conferred impaired trained macrophage responses and promoted tuberculosis pathogenesis in the lung. We found that the observed reprogramming of the HSCs depended upon the magnitude of IFN-II (protective training; myeloid-biasing) and IFN-I (detrimental training; lymphoid biasing) signatures that were greater in BCG and *Mtb*, respectively. This reprogramming had long-lasting effects on the antimycobacterial capacity of macrophages, lasting up to at least one year, and *Mtb*-exposed HSCs were severely compromised in their reconstitution capacity when compared to BCG-exposed cells. Thus, *Mtb* has evolved virulence strategies in the bone marrow to subvert the host’s immune response and promote TB pathogenesis in the lung.

CHAPTER 4:

**M. tuberculosis reprograms HSCs to limit myelopoiesis and impair
trained immunity via a type I IFN/iron axis**

***M. tuberculosis* reprograms HSCs to limit myelopoiesis and impair trained immunity via a type I IFN/iron axis**

Nargis Khan^{1,7}, Jeffrey Downey^{1,7}, Joaquin Sanz², Eva Kaufmann¹, Birte Blankenhaus³, Alain Pacis⁴, Erwan Pernet¹, Eisha Ahmed¹, Silvia Cardoso³, Anastasia Nijnik⁵, Bruce Mazer¹, Christopher Sasseti⁶, Marcel A. Behr¹, Miguel P. Soares³, Luis B. Barreiro⁴, and Maziar Divangahi^{1,8*}

¹Meakins-Christie Laboratories, Department of Medicine, Department of Microbiology and Immunology, Department of Pathology, McGill International TB Centre, McGill University Health Centre, Montreal, Quebec, Canada

²Department of Theoretical Physics, University of Zaragoza, Institute BIFI for Bio-computation and Physics of Complex Systems, University of Zaragoza

³Instituto Gulbenkian de Ciencia, Oeiras, Portugal

⁴Department of Medicine, Genetic Section, University of Chicago, Chicago, Illinois, USA

⁵Department of Physiology, Complex Traits Group, McGill University, Montreal, Quebec, Canada

⁶Department of Microbiology and Physiological Systems, University of Massachusetts Medical School, Worcester, Massachusetts, USA

⁷These authors equally contributed to this study

⁸Lead Contact

* Corresponding author: maziar.divangahi@mcgill.ca

Cell. 2020 Oct 29;183(3):752-770.e22. doi: 10.1016/j.cell.2020.09.062.

4.1: Highlights

- BCG and *Mtb* challenges uniquely reprogram HSCs for at least one year post-exposure
- *Mtb* suppresses myelopoiesis at the level of committed progenitors and impairs HSC engraftment
- *Mtb* hijacks a host type I IFN/iron axis to induce RIPK3-dependent necroptosis specifically in myeloid progenitors
- Reprogramming of HSCs by a type I IFN/iron axis prevents the induction of trained immunity to *Mtb*

4.2: Abstract

A greater understanding of hematopoietic stem cell (HSC) regulation is required for dissecting protective versus detrimental immunity to pathogens that cause chronic infections such as *Mycobacterium tuberculosis* (*Mtb*). We have shown that systemic administration of BCG or β -glucan reprograms HSCs in the BM via a type II interferon (IFN-II) or IL1 response, respectively, that confers protective trained immunity against *Mtb*. Yet, whether BCG/ β -Glucan is unique in its ability to induce this protection remains unknown. Herein, we demonstrate that unlike BCG or β -glucan, *Mtb* reprograms HSCs via IFN-I response that suppresses myelopoiesis and impairs the development of protective trained immunity to *Mtb*. Mechanistically, IFN-I response dysregulates iron metabolism, depolarizes mitochondrial membrane potential, and induces cell death in myeloid progenitors. Additionally, the activation of IFN-I/iron axis in myeloid progenitors impairs trained immunity to *Mtb* infection. These results identify an unanticipated immune evasion strategy of *Mtb* in the bone marrow that controls the magnitude and anti-microbial capacity of innate immunity to infection.

4.3: Introduction

During infection or stress, hematopoietic stem cells (HSCs) interrupt dormancy and adapt to meet the peripheral demand for immune cells via their expansion and differentiation into more lineage-restricted progenitors, primarily within the bone marrow (BM). This process must be tightly controlled to avoid the costs of dysregulated HSC activation that may lead to exhaustion, or even complete depletion, with devastating effects on the systemic immune compartment (266, 267, 394). Infection-specific changes in hematopoiesis may restrict or promote the generation of specific lineages to centrally bias the overall systemic immune response. For instance, we have recently demonstrated that exposure of HSCs to *Bacillus Calmette-Guérin* (BCG) or β -glucan (a component of fungal cell membrane) in the BM results in their reprogramming to promote myelopoiesis and protective immunity against *Mtb* infection in type II IFN or IL1 dependent manner, respectively (304, 395). Thus, safeguard mechanisms must be engaged to ensure the maintenance and survival of the HSC pool as well as their commitment towards myelopoiesis, providing immune-driven resistance to infection.

While initially confined to cells of the lymphoid lineage, memory-like responses have now been extensively described in myeloid cells and particularly within monocyte-derived macrophages, in a process coined trained immunity (105). The relatively short lifespan of innate immune cells, however, limits the effectiveness of this protective response against chronic infections. Interestingly, enhancing myelopoiesis in the BM has been shown to have a significant impact on the generation of trained macrophages (290, 291, 396). Moreover, others (296) and we (304, 395) have also demonstrated that trained immunity is driven by epigenetic imprinting of HSCs, where it can then be transmitted to BM-derived monocyte/macrophages. Thus, imprinting of innate memory signatures by HSCs appears to overcome the limitation of the short half-life of fully differentiated BM-derived innate immune cells. Although many examples of protective trained immunity have been documented, this process may also manifest deleteriously. For example, the persistent hyperactive state of trained innate cells can trigger tissue damage or chronic inflammation upon exposure to endogenous ligands (397, 398) or pathogen-associated molecular patterns (PAMPs) (399), suggesting that the stimulus, localization and cell type are crucial in promoting the development of a protective versus detrimental epigenetic rewiring. While exposure

of HSCs to pathogens and/or PAMPs appears to be an important step in the generation of protective trained immunity, the current understanding of the mechanistic basis of this process remains largely unknown.

Type I interferon (IFN- α and β ; IFN-I) and type II interferon (IFN- γ ; IFN-II) signaling pathways are critical in regulation of HSC activation (265-267, 400) and are also involved in generation of epigenetic-mediated innate memory responses (401). Moreover, chronic exposure of HSCs to either IFN-I (266) or IFN-II (268) leads to excessive proliferation and exhaustion of HSCs. IFN-II signaling has also been shown to be required for HSC proliferation under steady state (265) and to promote myeloid cell responses in systemic BCG vaccination (304) or malaria infection (400). Although these cytokines are involved in promoting survival and expansion of progenitors, there is little evidence that their signaling directly regulates lineage commitment in HSCs. Progenitor cell death appears to be a key mechanism that drives HSC proliferation and regulates skewing of the HSC and progenitor populations towards the myeloid versus lymphoid lineage. For instance, during bacterial infection, IFN-I signaling inhibits HSC expansion via increased necroptosis (271), while overexpression of anti-apoptotic proteins Bcl-xL (402) or Bcl-2 (403) rescues erythropoiesis in erythropoietin (EPO)-deficient mice or lymphopoiesis in IL7R-deficient mice, respectively. However, the factors and molecular mechanisms involved in HSC fate decisions are incompletely understood.

Iron (Fe) is a vital micronutrient that supports fundamental cellular functions in most, if not all, living organisms and is, therefore, of particular relevance in the context of host pathogen interactions (404). While vital to sustain life, Fe can also be deleterious if allowed to exchange electrons in an unrestrained manner to generate free radicals, like hydrogen peroxide (H₂O₂). This leads to the production of intracellular hydroxyl radicals and hydroxide ions, via Haber–Weiss/Fenton reactions, triggering lipid peroxidation and driving a form of programmed cell death known as ferroptosis (405, 406). Thus, it is not surprising that the regulation of iron metabolism has emerged early in life to form an evolutionary conserved host defense strategy (407-409) to effectively instruct host resistance and disease tolerance against infections (410). During chronic *Mtb* infection, the host minimizes iron availability to inhibit bacterial growth (411, 412) and any major alteration in iron metabolism leads to severe infection and susceptibility to TB (413, 414).

Moreover, regulation of iron metabolism plays a key role in the maintenance of HSCs as iron overload promotes HSC exit from quiescence (415), which is frequently associated with myelodysplastic syndrome (MDS) caused by failure of hematopoiesis (416). However, the potential contribution of iron in HSC lineage fate decisions during infection is, to the best of our knowledge, unknown.

Given that access of the BCG vaccine to the BM reprograms HSCs towards the myeloid lineage and generates protective trained immunity against subsequent *Mtb* infection (304), we investigated whether the virulent strain of *Mtb* in the BM impacts host innate immunity to infection. Here, we demonstrate that while access of *Mtb* to the BM changes the transcriptional landscape of HSCs and MPPs similarly to BCG, the magnitude of some of these pathways, in particular IFN-I and heme metabolism, significantly differed between BCG and *Mtb*. In sharp contrast to BCG, *Mtb* infection induced RIPK3-dependent necroptosis in myeloid progenitors (CMP/GMP) downstream of HSCs via an IFN-I/iron axis, which then led to enhanced lymphopoiesis. Dysregulated iron metabolism in myeloid progenitors was associated with increased mitochondria-mediated necroptosis and subsequent suppression of myelopoiesis. Thus, *Mtb* reprogrammed HSCs via an IFN-I/iron axis failing to generate trained immunity to *Mtb* infection. Importantly, the protective signatures of BCG or the detrimental imprints of *Mtb* on HSCs were maintained for a long time (~ one year). Thus, our study indicates that *Mtb* accesses the BM to target innate immunity via imprinting HSC populations with a unique transcriptomic profile that suppresses myelopoiesis and is associated with reduced ability to control *Mtb* infection.

4.4: Results

Systemic *Mtb* Differentially Modulates Hematopoiesis Compared to BCG in an RD-1-Dependent Manner

We have recently demonstrated that following systemic (intravenous; iv), but not subcutaneous, vaccination, BCG (TICE) bacteria accessed the BM, reprogrammed HSCs to promote myelopoiesis and generated trained immunity in macrophages to confer protection against a subsequent virulent *Mtb* infection (304). Similarly, we have shown that systemic administration of β -glucan promotes HSC-myelopoiesis and protection against pulmonary *Mtb* infection (Moorlag et al., 2020). These studies collectively reveal that skewing hematopoiesis towards myelopoiesis appears to be a protective mechanism in immunity to *Mtb* infection. While it has been previously shown that *Mtb* can disseminate to the BM in diverse TB patient populations, ranging from asymptomatic individuals to those suffering from AIDS (417), the impact of *Mtb* accessing the BM in comparison to BCG on disease pathogenesis and trained immunity, as well as HSC proliferation and fate decision remains unknown. To investigate this, we began by determining the effects of the same dose (1×10^6 CFU) of intravenous BCG vaccine or *Mtb* (H37Rv) infection (**Figure 1A**) on survival, BM bacterial loads and hematopoietic cell responses in wild type (WT; C57BL/6J) mice. While all BCG-iv vaccinated and control mice survived, *Mtb*-iv infected mice succumbed to infection by approximately 120 days (**Figure 1B**). When administered systemically, *Mtb* rapidly accessed the BM and persisted until at least 28 days post-infection, coinciding with the earliest onset of mortality. At these timepoints, both BCG and *Mtb* entered and replicated to similar extents within the BM (**Figure 1C**). As was previously shown with BCG-GFP (304), *Mtb* (H37Rv-GFP) was unable to infect $\text{Lin}^- \text{c-Kit}^+ \text{Sca-1}^+$ (LKS) cells, while Lin^+ cells were readily infected by *Mtb* as evidenced by both ImageStream (**Figure 1D-E**) and flow cytometry (**Figure 1F-G**). Thus, any effect of these mycobacteria on hematopoietic cells must be indirect.

To quantify these potential effects, we directly compared the impact of *Mtb*-iv versus BCG-iv on HSC and MPP kinetics (full gating strategy **Figure S1A**). The presence of *Mtb* or BCG in the BM correlated with a significant expansion of the LKS population (**Figure 1H**, quantified in the panels on the right), which remained elevated until at least 28 days post-infection. LKS

expansion was associated with proliferation, as monitored by the frequency of Ki67⁺ LKS cells in mice infected with *Mtb*-iv versus BCG-iv and control mice at 7 days post-infection (**Figure 1I**), yet was not due to an increase in long-term HSCs (LT-HSC; LKS⁺ CD150⁺ CD48⁻), but rather short-term HSCs (ST-HSC; LKS⁺ CD150⁺ CD48⁺) and multipotent progenitors (MPPs; LKS⁺ CD150⁻ CD48⁺) (**Figure S1B-D**). Despite a more rapid hematopoietic response in *Mtb*-iv compared to BCG-iv mice at day 7 post-infection, by day 28 the number of HSCs and MPPs was similar between two groups (**Figure S1B-D**). Our previous work showed that BCG skews HSC fate towards myelopoiesis by specifically enhancing the pool of myeloid-biased MPP3s, but not lymphoid-biased MPP4s (304), which correlated with the enhanced protection afforded by BCG-iv. Unexpectedly, the dynamics of MPP3 versus MPP4 were indistinguishable between BCG-iv and *Mtb*-iv (**Figure S1B-D**). Taken together, despite the greater virulence of *Mtb* as compared to BCG, both bacteria are able to access and persist in the BM to promote HSC expansion of myeloid-biased MPPs.

The LKS population gives rise to all cells of the hematopoietic compartment including the common myeloid progenitor (CMP) and the common lymphoid progenitor (CLP), that lead to the generation of more restricted progenitors and then mature effector cells, such as monocyte/macrophages and T- and B-cells. As the plasticity between MPPs is high (418, 419), lineage restriction is more stringently completed downstream of the common progenitor level (403, 420). Thus, we next investigated how intravenous *Mtb* or BCG affected lineage-restricted progenitors. As with LKS cells (**Figure 1D**), both *Mtb* and BCG did not infect myeloid progenitors (cKit⁺ Progenitors) (**Figure S1E**). Despite this similarity, at day 7 and continuing at days 14 and 28 post-infection, *Mtb*, but not BCG, significantly suppressed myelopoiesis and promoted lymphopoiesis, as shown by loss of the CMP (Lin⁻ cKit⁺ CD34⁺ CD16/32⁻) and the granulocyte-monocyte progenitor (GMP; Lin⁻ cKit⁺ CD34⁺ CD16/32⁺), with an increased frequency and number of common lymphoid progenitors, CLPs (Lin⁻ CD127⁺ cKit^{lo} Sca1^{lo}) (**Figure 1 J-L**). We then sought to investigate how *Mtb*, in contrast to BCG, caused these changes in hematopoiesis. It is well established that the region of difference 1 (RD-1) is present in all virulent strains of *Mtb*, but absent in BCG. Deletion of the 9.5-kb RD1 region from *M. tuberculosis* (H37Rv:ΔRD1) results in an attenuation that is strikingly similar to that of BCG in cultured macrophages and mice (421, 422). Considering RD-1 is an important region required for *Mtb* virulence, we hypothesized that

RD1 may be responsible for the observed alterations in hematopoiesis. To test this hypothesis, we performed similar experiments using the Δ RD1 strain of H37Rv (*Mtb*- Δ RD1). We found that there was no difference between *Mtb*- Δ RD-1, *Mtb* and BCG in expanding LKS or HSC populations at 28 days post-infection (**Figure 1M-O** and **Figure S1F-G**). However, the skewing of hematopoiesis towards lymphopoiesis in *Mtb*-iv mice was completely dependent on RD1-expression, as BCG and *Mtb*- Δ RD1 had equal levels of myeloid/lymphoid progenitors (**Figure 1N** and **Figure S1G**; left panel), while *Mtb* significantly suppressed myelopoiesis (CMP/GMP) and promoted lymphopoiesis (CLP) compared to *Mtb*- Δ RD1 (**Figure 1O** and **Figure S1G**; right panel).

Downstream of the CMP/GMP, the granulocyte progenitor (GP; Lin⁻ Sca-1⁻ cKit⁺ CD16/32⁺ CD34⁺ Flt3⁻ Ly6C⁺ CD115⁻) gives rise to mainly neutrophils, while the macrophage/dendritic cell progenitor (MDP; Lin⁻ Sca-1⁻ cKit⁺ CD16/32⁻ CD34⁺ Flt3⁺ Ly6C⁻ CD115⁺) and the common monocyte progenitor (cMoP; Lin⁻ Sca-1⁻ cKit⁺ CD16/32⁺ CD34⁺ Flt3⁻ Ly6C⁺ CD115⁺) can differentiate into all cells of the mononuclear phagocyte lineage and Ly6C^{hi} monocytes, respectively. Correlating to the reduction in CMP/GMP, at day 28 post-*Mtb* infection, we observed a significant reduction in the frequency and number of the MDP, cMoP and GP, and the number, but not frequency, of mature Ly6C^{hi} monocytes and neutrophils (**Figure 1P-S** and **Figure S1 H-L**). Therefore, the loss of myeloid progenitors leads to a loss of mature myeloid cells.

Finally, while the role of the spleen in hematopoiesis at steady-state is mostly considered negligible, under stress it is the major contributor to extramedullary leukocyte hematopoiesis (423). To investigate whether the spleen may compensate for the suppressed BM myelopoiesis during systemic *Mtb* infection, we phenotyped splenic progenitors at day 28 post BCG-iv or *Mtb*-iv infection. As expected, we observed a smaller proportion of LKS cells in the spleen than the BM that was nevertheless equal between groups (**Figure S1M**). Moreover, we noted an identical phenotype in the spleen as in the BM in terms of HSCs and the CMP/GMP versus CLP (**Figure S1N**), albeit at lower frequencies. Thus, although the contribution of the spleen to the leukocyte pool is likely smaller than the BM, *Mtb* universally regulates hematopoiesis to restrict myelopoiesis.

***Mtb* Uniquely Reprograms HSCs and Impairs Trained Macrophage Immunity**

Because of the similar responses at the cellular level in HSCs, but divergence at the progenitor level, we postulated that *Mtb* transcriptionally reprogrammed HSCs to modulate downstream progenitors. To test this, we performed bulk RNA sequencing (RNA-seq) on HSCs (LKS⁺CD150⁺) and MPPs (LKS⁺CD150⁻) isolated from the BM of C57BL/6J mice at day 28 post-injection with BCG-iv, *Mtb*-iv or PBS-iv (control). For both MPPs and HSCs, the first principal component (PC1) of gene expression data explained over 40% of the total variance and segregated *Mtb*-iv versus BCG-iv or PBS-treated control mice (**Figure 2A**; one tailed t-test, $p=0.023$ and 5.1×10^{-7} for HSCs and MPPS, respectively). Accordingly, we found extensive differences in the gene expression levels between *Mtb*-iv and BCG-iv as compared to PBS-treated control mice (**Figure 2B**; *Mtb*-iv versus control: 1282 (10.6%) and 2952 (24.3%) differentially expressed genes in HSCs and MPPs, respectively; BCG-iv versus control: 1793 (14.8%) and 2646 (21.8%) differentially expressed genes in HSCs and MPPs, respectively; false discovery rate [FDR] < 0.01). Regulation of gene expression induced by *Mtb* and BCG were highly concordant in both MPPs and HSCs (**Figure 2C**; Pearson correlation of *Mtb*-iv vs BCG-iv effects: 0.751 and 0.837 in HSCs and MPPs, respectively, $p < 1 \times 10^{-10}$ in both), as well as the gene ontology terms enriched among genes that significantly changed expression levels in response to *Mtb* or BCG (**Figure S2A**: Pearson correlation of significance levels: $r=0.68$ (HSCs), $r=0.77$ (MPPs), $p < 1 \times 10^{-10}$). Globally, differentially expressed genes in BCG-iv or *Mtb*-iv infection were strongly enriched for gene sets involved in IFN-I and IFN-II responses, T cell activation and proliferation as well as glycolysis (**Figure S2B**), suggesting that the presence of mycobacterium in the BM alters the activity of the interferon-related pathways and rewires HSCs and MPPs, consistent with our previous report (304).

Despite the overall similarities in the gene expression response of HSCs and MPPs to BCG and *Mtb*, we found significant differences between infections in genes that respond to either *Mtb*-iv or BCG-iv. 689 of these infection-responsive genes in HSCs and 402 in MPPs showed significant differences in expression across mycobacteria (FDR<10%). Gene Set Enrichment Analyses showed that genes involved in IFN-I signaling, glycolysis, and inflammation were significantly enriched in *Mtb*-iv versus BCG-iv (**Figure 2D**). In contrast, genes more differentially

expressed following BCG-iv versus *Mtb*-iv were enriched for those involved in heme metabolism (**Figure 2D**). As the cellular response between BCG and *Mtb* at the HSC/MPP level was similar (**Figure S1B-D**), but highly discordant at the committed progenitor level (**Figure 1J-L** and **Figure 1P-R**), these data suggested that intrinsic differences in the transcriptional magnitude of pathways involved in IFN-I signaling and heme in HSC/MPP populations might be transmitted to the more committed progenitors and effector cells, modulating their numbers and/or function.

Intriguingly, in line with our RNA-seq data, a loss of heme oxygenase (424) or iron sequestration (425) in BM-derived macrophages (BMDM) greatly enhances susceptibility to *Mtb*, while enhanced IFN-I signaling impairs the mycobactericidal capacity of macrophages (426), suggesting our observed imprinting of these pathways by *Mtb* may contribute to a loss of *in vitro* control of *Mtb* in macrophages. Given the importance of BMDM in immunity to *Mtb* (427, 428), we investigated whether suppression of myelopoiesis impacted either BM progenitor differentiation into macrophages *in vitro* and/or the antimycobacterial capacity of macrophages. We generated BMDM from BCG-iv, *Mtb*- Δ RD1, *Mtb*-iv and control PBS mice and infected them with *Mtb* (**Figure 2E**). To ensure there was no contamination with *Mtb* from the *in vivo* infection, we cultured cells with anti-TB drugs and all BMDM cultures were *Mtb* and BCG free at the time of *in vitro* infection with *Mtb*. Similar to the results of *in vivo* myelopoiesis (**Figure 1J-K** and **Figure 1P-S**), *Mtb*-infected mice generated fewer BMDM than BCG-vaccinated or *Mtb*- Δ RD1-infected mice, relative to PBS control mice (**Figure 2F**). Moreover, despite culturing the same number of macrophages in each group prior to *in vitro* *Mtb* infection, BMDM from *Mtb*-infected mice, in contrast to BCG-iv vaccinated mice, failed to control *Mtb* growth at day 5 post-infection (**Figure 2G**), suggesting that access of *Mtb* to the BM suppresses myelopoiesis and impairs the intrinsic protective capacity of macrophage immunity to *Mtb*. This finding was again contingent upon presence of RD1 (**Figure 2G**). Although we observed a decrease in the number of macrophages generated in the *Mtb*-iv group (**Figure 2F**), the purity and activation levels (CD80, CD40 and MHC-II) were similar to the BCG-iv and PBS group (**Figure S2C-F**). Therefore, the impaired training of BMDM in the *Mtb*-iv group is not due to the presence of immature macrophages or contamination by other cell types. To investigate whether the detrimental impact of *Mtb* infection on BMDMs was independent of a constant presence of the bacteria *in vivo*, we treated BCG-iv, *Mtb*-iv and control PBS mice with anti-TB drugs for 28 days followed by two weeks rest. We then generated BMDM from these mice and subsequently infected them with *Mtb in vitro* (**Figure S2G**). BM and BMDM cultures were free of mycobacteria (*Mtb* or BCG) prior to *in vitro* infection with *Mtb*. Yet again, BMDM from *Mtb*-iv mice showed impaired capacity to control *Mtb* growth, as compared to BMDM from BCG-iv or control

PBS-iv mice (**Figure S2H**). Thus, the trained immunity is independent of constant exposure of HSCs to mycobacteria.

Finally, to directly assess the functional anti-*Mtb* capacity of BMDM *in vivo*, we performed adoptive transfer experiments. We generated BMDM in the presence of anti-TB drugs from PBS control, BCG-iv and *Mtb*-iv groups at day 28, then infected these macrophages *in vitro* with *Mtb* and adoptively transferred them (intratracheally) into RAG1-deficient mice (lacking B and T cells) (**Figure 2H**). Consistent with our previous observations (304), BMDM from the BCG-iv group provided enhanced protection when transferred into *Rag1*^{-/-} mice (**Figure 2I**). However, *Rag1*^{-/-} mice that received macrophages from the *Mtb*-iv group had significantly higher bacterial burdens in the lung than the PBS control and BCG-iv mice. This difference was observed despite the fact that the number of *Mtb* in macrophages from the BCG-iv group was slightly higher than the PBS or *Mtb*-iv group prior to the transfer into the RAG1-deficient mice (**Figure S2I**). Thus, *Mtb*, in contrast to BCG, suppresses HSC-myelopoiesis to impair BMDM generation and their intrinsic antimycobacterial capacity *in vitro*, and *in vivo*, uncovering an important strategy of *Mtb* pathogenesis in the BM.

***Mtb* Suppresses Myelopoiesis Preventing the Induction of Trained Immunity after Pulmonary Infection**

The systemic model of *Mtb* infection does not represent the natural route of infection in humans. Thus, to extend our findings to a physiological model of pulmonary tuberculosis, we infected mice with a low dose of *Mtb* (~75 CFU) via the aerosol route (**Figure 3A** and **Figure S3A**). It is well established that following aerosolized *Mtb* infection, within 10-14 days, the bacteria disseminate to the pulmonary draining lymph nodes via infected dendritic cells and/or monocytes that leads to T cell priming (429-431). Interestingly, we found that *Mtb* also reached the BM at 10 days post-infection and continued to grow over the course of infection until the last time point analyzed at 120 days, when the number of *Mtb* in the BM was close to the intravenous model (**Figure 3B**). Similar to the *Mtb*-iv model, this was associated with the expansion of LKS population (**Figure 3C-D**) via expansion of ST-HSCs and MPPs, but not LT-HSCs (**Figure 3E-H** and **Figure S3B-D**). Moreover, aerosolized *Mtb* equally skewed hematopoiesis towards the myeloid-biased multipotent progenitor MPP3 (~5-fold increase compared to uninfected) versus

the lymphoid-biased MPP4 (~2-fold increase compared to uninfected) (**Figure 3I** and **Figure S3E**). In the lineage-restricted progenitors, we again observed a reduction in the CMP/GMP and an expansion of the CLP (**Figure 3J-L** and **Figure S3F-H**), as well as a significant reduction in the numbers, of the MDP and GP (**Figure 3M-N**) and a minor decrease in cMoP numbers (**Figure S3I**). This reduction of myelopoiesis led to a decreased number of mature neutrophils and Ly6C^{hi} monocytes in the BM by day 120 compared to steady-state (**Figure S3J-K**), as well as a gradual loss of Ly6C^{hi} monocytes from peak levels (day 14 versus 120) but an increase in T-cells (**Figure S3L-O**) in the lung. Thus, these data indicate that BM hematopoiesis biasing may contribute to driving the shift in the pulmonary immune response from innate to adaptive immunity. Thus following pulmonary *Mtb* infection, *Mtb* access to the BM and manipulation of the HSC and progenitor responses to *Mtb* are conserved regardless of the route of infection.

Next, we sought to characterize at single cell resolution the transcriptional response of HSCs and progenitor cells to *Mtb* aerosol infection. To do so, we performed droplet-based single-cell RNA sequencing (scRNA-seq) (432) on sorted LKS and cKit⁺ progenitors from the BM at 120 days post-aerosol *Mtb* infection (see STAR Methods). Following quality control, we kept a total of 5,698 high quality LKS cell transcriptomes (LKS dataset: 2,388 derived from PBS control mice and 3,310 derived from the aerosolized *Mtb* group), and 5,745 transcriptomes from myeloid progenitor cells (Progenitors dataset: 2,241 PBS, 3,504 aerosolized *Mtb*). LKS cells were classified into six clusters based on known canonical markers, as well as genes that were differentially expressed between subsets of LKS cells (433) (see STAR Methods, **Figure S3P**): a cluster of long-term HSCs (HSC_LT), three clusters of short-term HSCs (HSC_ST_A, B and C), one cluster of lymphoid-biased progenitors (MPP4), and one last cluster of myeloid-biased progenitors (MPP3) (**Figure 3O** and **3Q**). Among cKit⁺ progenitor cells we identified two clusters of common myeloid progenitors (CMPs), four clusters of granulocyte-monocyte progenitors (GMPs) and three clusters of megakaryocyte-erythrocyte progenitors (MEPs) (**Figure 3P-Q** and **Figure S3Q-R**). In accordance with the flow-cytometry data, we observed an expansion of ST-HSCs (up to $\log_2(\text{OR})=3.3$ in HSC_ST_C, $p<2.2\text{E-}16$) and depletion of monocyte precursors (GMP_MonP, $\log_2(\text{OR})=-1.2$, $p<1\text{E-}7$) in the *Mtb* group as compared to PBS controls (**Figure S3S-T**).

We found many differences in gene expression across all clusters when comparing cells derived from *Mtb* challenged mice and controls. LKS cells were the most responsive to *Mtb* infection (**Figure 3R**; top panel), showing between 506 (HSC_ST_A) and 2,269 differentially expressed (DE) genes (HSC_ST_B) (FDR<5% and an absolute fold-change ≥ 0.1). Although by comparison less frequently, aerosolized *Mtb* also had a large impact on the transcriptional profile of progenitor cells, ranging from 203 DE genes among monocyte precursors (cluster GMP_MonP) and 851 DE genes among CMP_MegP (**Figure 3R**; bottom panel).

Despite differences in the number of DE genes identified within each cell type—which in part reflects differences in statistical power due to differences in cell numbers (**Figure S3U**)—the response to aerosolized *Mtb* was concordant across all cell types, with stronger correlations among cell types that are functionally more related. For example, the correlation in the transcriptional response to *Mtb* between MPP3 and MPP4 cells was 0.76, ($p < 2.2E-16$), as compared to only 0.48 ($p < 2.2E-16$) between MPP3 and LT-HSCs (**Figure S3V**). Gene Set Enrichment analyses (GSEA) revealed that the two pathways most enriched among genes up-regulated in response to aerosolized *Mtb* infection were the interferon gamma (IFN-II) and interferon alpha (IFN-I) pathways (enriched in all clusters: normalized enrichment score (NES) across clusters ranges from 1.51 to 3.23, FDR<0.05), further highlighting the key importance of interferon signaling in the reprogramming of HSCs and progenitor cells in the BM (**Figure 3S**). For example, *Stat1*, a key TF involved in the response to IFN-II and IFN-I, was significantly up-regulated in response to *Mtb* in virtually all clusters (**Figure 3T**). As with *Mtb*-iv infection, this imprinting in the BM correlated with a loss of *in vitro* control of *Mtb* by BMDM from aerosol *Mtb*-infected mice (**Figure 3U**).

Taken together, our results indicate that during infection, in contrast to BCG, *Mtb* imprints HSCs and progenitors to blunt myelopoiesis and generate macrophages that lack the ability to control *Mtb* growth.

IFN-I Signaling Restricts Myelopoiesis and Impairs Macrophage Responses to Confer Susceptibility to *Mtb* Infection.

The RNA-seq analyses of HSCs/MPPs and cKit⁺ progenitors indicated that IFN signaling pathways were significantly modulated by *Mtb* in comparison to BCG. We and others have shown that IFN-II signaling is critical for HSC expansion and myelopoiesis (265, 304, 400), while IFN-I signaling induces loss of stem cell numbers and function (271, 419). Interestingly, during *Mtb* infection, IFN-II signaling is essential for host survival (434), while IFN-I signaling is detrimental (435). Thus, we sought to determine how *Mtb*-induced IFN-I signaling may specifically affect lineage commitment and subsequent macrophage anti-microbial responses. We infected WT and *Ifnar1*^{-/-} (lacking IFN-I signaling) mice with either aerosol or iv *Mtb* and observed that survival was significantly enhanced in *Ifnar1*^{-/-} mice (**Figure 4A-B**) and was associated with a significant increase of CMPs and GMPs, post-*Mtb*-iv (**Figure 4C-D** and **Figure S4A-B**). Interestingly, no differences were discerned in CLP expansion in both *Mtb*-iv or aerosol *Mtb* infection model (**Figure 4E** and **Figure S4C**), indicating that additional factors other than IFN-I promote lymphopoiesis during *Mtb* infection. Similar effects of IFN-I signaling on progenitor populations were observed following aerosol infection (**Figure S4D-F**).

It has been shown that IFN-I impairs macrophage anti-*Mtb* immunity (426) and that IFN-I receptor signaling enhances susceptibility to *Mtb* infection via the recruitment of permissive BM-derived CCR2⁺ monocytes into the lungs (435). Thus, we investigated what role IFN-I responses had, if any, on the generation of BM derived macrophages and trained immunity. In line with a detrimental role for IFN-I signaling on myeloid cells, *Ifnar1*^{-/-} mice showed enhanced macrophage yield following *in vitro* BMDM culture (**Figure 4F**). Moreover, using our *ex vivo* model (**Figure 2E**) and *in vivo* model (**Figure S2G**), we showed that the lack of protection by BMDM from *Mtb*-infected mice was entirely dependent on IFN-I signaling (**Figure 4G-H**, respectively).

To determine the specific role of IFN-I in hematopoiesis, we used a model of systemic IFN-I production through the intraperitoneal administration of the TLR3 synthetic viral ligand Polyinosinic:polycytidylic acid (Poly (I:C)). Mice received Poly(I:C) (200µg/mouse) on days 0, 2, 4 and 6 (271). The effects on BM progenitors were then assessed at days 3 and 7 post-initial Poly (I:C) treatment (**Figure 4I**), which correlates with the early changes in hematopoiesis observed upon *Mtb* infection (**Figure 1H**). In line with previous reports (419), an increase in BM IFN-I was observed in mice shortly following Poly (I:C) administration (**Figure S4G**). Similar to *Mtb*, Poly (I:C) increased

the numbers of LKS/ST-HSCs/MPPs but not LT-HSCs (**Figure 4J-N** and **Figure S4H-J**) and decreased the CMP, while increasing CLP frequencies and cell numbers (**Figure 4O-P**; **Figure S4K-L**). Poly(I:C)-treated WT mice also displayed reduced MDPs, cMoPs and GPs downstream of the CMP, as well as Ly6C^{hi} monocytes and neutrophils, at day 3 post-administration (**Figure S4M-Q**). As expected, the effects of Poly (I:C) on BM hematopoiesis were entirely IFN-I-dependent, as revealed in *Ifnar1*^{-/-} mice (**Figure 4J-P** and **Figure S4H-Q**). Like BMDM from *Mtb*-infected mice, BMDM from Poly (I:C)-treated WT mice showed impaired resistance to *Mtb*, which required IFN-I signaling (**Figure 4Q**). Thus IFN-I signaling is required to inhibit myelopoiesis in the BM and to prevent the generation of protective trained immunity in macrophages.

To contrast the impact of Poly(I:C) on suppression of myeloid lineage and trained immunity, we next used β -Glucan (**Figure 4R**), which has been shown to promote myelopoiesis (296, 395). β -Glucan-treated mice showed enhanced LKS/LT-HSC/ST-HSC/MPPs at 7 days post-treatment (**Figure S4R-U**) with expansion of myeloid CMP/GMP progenitors (**Figure S4V-W**) with no changes in CLP (**Figure S4X**). To determine the protective imprinting of β -Glucan on myelopoiesis, we generated BMDM from β -Glucan or PBS-control treated mice, which were subsequently infected with *Mtb*, *in vitro* (**Figure 4R**). BMDM from β -Glucan treated mice provided protection against *Mtb* infection, via an IFN-I-independent mechanism (**Figure 4S**). Importantly, while BCG protection was afforded by IFN-II signaling (304), β -Glucan protection was dependent on IL1 signaling (395). Remarkably, the protective capacity of β -Glucan was long-lived *in vivo*, as 100% of control PBS-treated mice succumbed to aerogenic *Mtb* infection within ~400 days, while 60% of β -Glucan-treated mice survived up to ~500 days post-infection (**Figure 4T**) and similar results were observed in Balb/c mice (395). Together these data indicate that there are multiple signaling pathways involved in hematopoietic stem and progenitor cells imprinting to promote myelopoiesis and generate protective trained immunity (e.g. IFN-II or IL1) or to suppress myelopoiesis and generate failed trained immunity (e.g. IFN-I) against *Mtb*.

IFN-I Signaling Modulates Iron Metabolism in Myeloid Progenitors to Limit Myelopoiesis and Enhance Susceptibility to *Mtb*

Considering the important role of IFN-I signaling in regulating hematopoietic progenitor cells via the induction of cell death during bacterial infection (271) as well as the critical role of cell death programs in HSC lineage decisions (270), we next investigated whether cell death pathways limit myeloid lineage expansion. We found that the level of necrotic cell death was significantly increased in the CMP/GMP of *Mtb*-iv infected mice compared to BCG-iv vaccinated mice (**Figure 5A**), while there were no differences in CLP death programs (**Figure S5A**). Interestingly, the expression levels of *Ripk3*, a key mediator of necroptosis (436), were significantly increased in HSCs from *Mtb*-iv infected mice, but not BCG-iv vaccinated mice (**Figure 5B**). Given our observation that *Mtb* induced necrosis of myeloid progenitors and the reported role of RIPK-dependent necroptosis in HSC death (271), regulation of myelopoiesis (263) and susceptibility to *Mtb* (212, 314, 437), we hypothesized that RIPK3 mediates cell death in myeloid progenitors during infection with *Mtb*. Prior to *Mtb* infection, the numbers of CMPs/GMPs/CLPs in naïve WT and *Ripk3*^{-/-} mice were similar (**Figure S5B-D**). However, at 7 days post-*Mtb* infection RIPK3-deficient mice had significantly increased frequencies and numbers of CMPs and GMPs when compared to WT mice, with no effect on CLPs (**Figure 5C-E** and **Figure S5E**). These data collectively indicate that *Mtb* induces RIPK3-mediated necroptosis in myeloid progenitors to suppress myelopoiesis.

The results from HSC-RNA-seq indicated an enrichment for heme metabolism in BCG-iv vaccinated compared to *Mtb*-iv-infected mice (**Figure 2D**). Interestingly, dysregulation of iron/heme metabolism in HSCs leads to oxidative stress and HSC ablation (415). Additionally, a reduction in the cellular iron pool through chelation or cellular stress is associated with cell death via mitochondrial dysfunction (438) and a loss of myeloid cells (439). Thus, we postulated that dysregulation of iron metabolism is in part responsible for the contraction of BM myeloid progenitors during *Mtb*-infection or in response to Poly (I:C) administration, while appropriate regulation of iron metabolism is maintained in BCG-vaccinated mice. We first found that the increase in necroptosis was accompanied by mitochondrial dysregulation in CMPs (**Figure 5F**), but not in CLPs (**Figure S5F**). This correlated with a reduction in the mitochondrial iron content in the CMPs of *Mtb*-infected versus BCG-vaccinated mice (**Figure 5G**), but not in the CLPs (**Figure S5G**). In line with the reduction of mitochondrial iron content, there was upregulation of the transferrin receptor (CD71) on CMPs, which plays a critical role in iron import and regulation of intracellular iron levels (440) (**Figure 5H**). This was at least partly IFN-I-dependent, as the levels of CD71 expression in CMPs and CLPs (**Figure 5I** and **Figure S5H**), as well as the frequency of necrotic CMPs, was also significantly reduced in *Mtb*-infected *Ifnar1*^{-/-} mice (**Figure 5J**). Additionally, the mitochondrial

iron level (**Figure 5K**) and mitochondrial membrane potential (**Figure 5L**) remained at the same level as uninfected controls in *Ifnar1*^{-/-} mice, confirming the importance of IFN-I signaling in modulating CMP iron metabolism. Similar to *Mtb* infection, the expression levels of CD71 were also significantly increased in CMPs, but not CLPs, after Poly(I:C) treatment in WT mice (**Figure 5M** and **Figure S5I**). This was associated with iron accumulation within the BM (**Figure 5N**) along with a reduction mitochondrial iron content (**Figure 5O** and **Figure S5J**) and membrane potential loss (**Figure 5P** and **Figure S5K**) in CMPs, but not CLPs, in an IFN-I-dependent fashion. The loss of mitochondrial potential was furthermore linked to an accumulation of mitochondrial reactive oxygen species (ROS) and necrosis in myeloid (CMP) but not lymphoid progenitors (CLP) (**Figure 5Q-R** and **Figure S5L-M**). Similar results were obtained using the aerosol model of *Mtb* infection (**Figure 5S-V**).

Having established that IFN-I signaling modulated iron metabolism specifically within myeloid progenitors to induce necrosis and impair macrophage trained immunity, we next investigated whether altered iron metabolism, using an inducible mouse model of ferritin H chain (FTH)—the key iron sequester in cells (441)—dysregulated hematopoiesis and/or trained immunity to *Mtb* infection. Whole-body tamoxifen-inducible *Fth* deletion via Cre-recombinase activity under the ROSA26 promoter in adult mice (referred to as *Fth*^{Δ/Δ} mice) (**Figure 6A**) is lethal shortly after tamoxifen administration (441). While the cause of death in *Fth*^{Δ/Δ} mice has been suggested to be due to altered thermogenesis (441), we also found that the hematopoietic system was severely suppressed, as the frequency and numbers of CMP/GMPs and CLPs in *Fth*^{Δ/Δ} mice were significantly reduced in comparison to control *R26*^{Cre} or *Fth*^{fl/fl} control mice (**Figure 6B-C** and **Figure S6A**). This suggests that FTH is essential to sustain hematopoiesis. To overcome the short life expectancy of *Fth*^{Δ/Δ} mice, we next generated BM chimeric mice in which FTH is deleted specifically in the hematopoietic compartment, allowing us to investigate the role of FTH in hematopoietic cells. Lethally irradiated WT (CD45.1⁺) mice reconstituted with ROSA26^{Cre}ER^{T2}Fth^{lox/lox} BM (CD45.2⁺) (hereafter referred to as BM-*Fth*^{-/-} mice) or vehicle (BM-*Fth*^{+/+} mice) received tamoxifen for 5 days to induce *Fth* deletion specifically in the BM hematopoietic compartment (**Figure 6D-E**). Similar to *Mtb*-infected or Poly (I:C)-treated mice, in BM-*Fth*^{-/-} mice, the frequency and total cell numbers of CMPs (**Figure 6F**) were significantly decreased, which correlated with reduced mitochondrial Fe²⁺ (**Figure 6G**) and elevated mitochondrial depolarization (**Figure 6H**) in CMPs. In BM-*Fth*^{-/-}, the frequency but not total cell numbers of CLP (**Figure S6B**) was significantly increased and no alterations in mitochondrial iron were observed in CLPs (**Figure S6C**). Strikingly, this dysregulation of myelopoiesis in BM-*Fth*^{-/-} mice had substantial impact on macrophage anti-mycobacterial responses, as BMDM from BM-*Fth*^{-/-} mice failed to control the growth of the virulent *Mtb*, but not the avirulent strain BCG (**Figure 6I** and **Figure S6D**). These impaired macrophage responses were relevant *in vivo* as, similar to mice lacking FTH specifically in

myeloid cells (442), mice deficient for FTH in the entire hematopoietic compartment were severely susceptible to low-dose aerosol *Mtb* infection, despite largely normal myeloid cell frequencies in the lung, BM and spleen, prior to infection (**Figure S6E-G**). The growth of *Mtb* was significantly increased in the BM, liver, spleen and lung of *Mtb*-infected BM-*Fth*^{-/-} (**Figure 6J-M**), which succumbed to death within 50 days of infection (**Figure 6N**). These results collectively indicate that dysregulation in IFN-I/iron axis severely impairs myelopoiesis and trained immunity causing susceptibility to *Mtb* infection.

The longevity of mycobacteria mediated trained immunity in BM-HSCs and progenitors is maintained up to at least one year

Our results indicate that BCG reprogram HSCs, ultimately leading to the induction of trained immunity and increased protection against TB. In sharp contrast, *Mtb* induces regulatory changes in HSCs that fail to induce trained immunity and instead lead to generation of macrophages with impaired capacity to control *Mtb* infection. HSC exhaustion in the BM has been reported in human TB cases since the 1980s (443), but how *Mtb*/BCG may modulate the long-term functional capacity of HSCs is unknown. To directly compare the reconstitution capacity of mycobacterial-exposed BM cells, we performed a competitive mixed chimera experiment. Lethally irradiated mice were reconstituted intravenously with mixed bone marrow cells (50:50) of *Mtb* (CD45.1⁺), BCG (CD45.2⁺) or PBS (either CD45.1⁺ or CD45.2⁺) and treated with antibiotics for 4 weeks to eliminate mycobacteria and then rested for 2 weeks (**Figure 7A**). Beginning at 4 weeks post-reconstitution and continuing every 4 weeks until 16 weeks post-reconstitution, when HSCs are completely engrafted, we sampled peripheral blood and analyzed the percentage of CD45.1⁺ versus CD45.2⁺ leukocytes. Importantly, by 16 weeks, in the PBS:PBS group, frequencies of CD45.1⁺ compared to CD45.2⁺ donor cells in all leukocyte populations tested were equal (**Figure S7A-D**, top left panel), excluding any potential bias in engraftment of CD45.1⁺ cells compared to CD45.2⁺ cells in control groups. However, while the proportion of circulating leukocytes was comparable between *Mtb*:PBS group (**Figure 7B-C**, left panel and **Figure S7C-D**, top right panel), strikingly, in both the BCG:PBS and BCG:*Mtb* groups, peripheral blood leukocytes in the recipient mice showed a significant bias to be driven from BCG-vaccinated mice rather than PBS-control or *Mtb*-infected groups (**Figure 7B-C**, right panel and **Figure S7C-D**, bottom panels). This propensity was due to a greater engraftment of BCG-derived HSCs, as at 16 weeks post-reconstitution, the chimerism of the BCG:*Mtb* recipients was dominated by BCG-derived HSCs and progenitors, as well as effector leukocytes in the BM and lung (**Figure 7D-L** and **Figure S7E-I**). Thus,

BCG-exposed HSCs exhibit superior engraftment when compared to control or *Mtb*-exposed HSCs, indicating that BCG reprograms HSCs to enhance their functional capacity, in addition to trained immunity.

To further explore the durability and length of HSC imprinting following exposure to mycobacteria, we next employed an *in vivo* serial engraftment model. CD45.2⁺ mice were infected with *Mtb*, BCG or PBS-control for 4 weeks, then treated with anti-mycobacterial drugs for 4 weeks and rested for 2 weeks. BM was harvested from each group and transplanted into lethally irradiated CD45.1⁺ mice (primary engraftment). After 16 weeks, BM was re-harvested and transplanted into a second group of lethally irradiated CD45.1⁺ mice (secondary engraftment) (**Figure 7M**). After 20 weeks of secondary engraftment, when no mycobacteria could be found in the BM (**Figure S7J**), we analyzed the peripheral blood and there was a significant reduction in total myeloid cells, as well as Ly6C^{hi} monocytes and neutrophils in the recipients of *Mtb*-iv BM (**Figure S7K-M**). In line with the reduced leukocytes in the circulation, the HSC compartment of the recipients of *Mtb*-iv BM had fewer LKS and LT-HSCs, as well as CMPs (**Figure 7N-P** and **Figure S7N-P**). Additionally, we incubated BM cells from each group in MethoCult medium (StemCell Technologies) to assess hematopoietic output potential. BM cells from the mice that were reconstituted by the BM of BCG-iv-vaccinated mice produced a greater number of colonies and mature CD11b-expressing myeloid cells (as determined by flow cytometry) than the mice that received BM from *Mtb*-iv infected mice (**Figure 7Q-R**). Having determined the impaired engraftment and reconstitution ability of *Mtb*-exposed HSCs, we then sought to elucidate the longevity of the training signatures in HSCs that can still be observed in macrophages. Thus, we derived BMDM from the secondary engraftment mice and infected them with *Mtb in vitro*. Remarkably, after two rounds of reconstitution and almost a year after the initial mycobacterial exposure, BMDM from BCG-iv vaccinated mice were still able to significantly control the growth of *Mtb*, while macrophages from the *Mtb*-iv infected mice continued to exhibit impaired control (**Figure 7S**).

To examine the training program of BM-HSCs and progenitors after secondary engraftment, we performed scRNA-seq on HSCs and progenitor cells derived from animals that had originally been exposed to BCG, *Mtb* or PBS to evaluate if there were any transcriptional differences still present after about year post the original challenge. After QC, we kept a total of 7,959 LKS cell transcriptomes (3,872 PBS, 2,524 BCG and 1,563 *Mtb*), and 9,859 transcriptomes from cKit⁺ myeloid progenitor cells (3,353 PBS, 5,020 BCG and 1,486 *Mtb*). These cells were clustered in 7 and 8 groups, in the LKS and progenitor populations, respectively (**Figure S7Q-S**; STAR Methods and **Figure S7T-V** for details on LKS and progenitor clustering inference and validation). In the LKS population we

observed 2,684 and 2,230 genes that are DE between PBS and either *Mtb* or BCG, in at least one of the cell clusters (**Figure 7T**). In progenitor cells, the effects of *Mtb* appeared to be much more pronounced than those of BCG with 5,574 identified as DE when contrasting *Mtb* to PBS versus only 1,392 between BCG and PBS (**Figure 7U**). Genes that respond significantly to either treatment ($FDR < 0.05$ & $abs(logFC) > 0.1$ for BCG-PBS or *Mtb*-PBS) show highly correlated treatment effects (Pearson correlation averaged across clusters $r = 0.53$ and 0.47 for LKS and progenitor populations, respectively, $p < 1E-18$ in all clusters, **Figure S7W**). Interestingly, among all cell clusters identified, the most committed monocytic precursors (GMP_MonP) are the ones showing the most divergent response between BCG and *Mtb*, which possibly explains the remarkable differences in the ability of BMDM derived from *Mtb*-iv vs BCG-iv groups to control *Mtb* growth (**Figure 7S**). To further explore the pathways differently regulated in monocytic precursors between the two groups we performed Gene Set enrichment analyses on the *Mtb* and BCG effects in this cluster. Focusing on the hallmark list of gene sets (444), we detected 27 gene-sets significantly enriched among genes differentially expressed between BCG-iv or *Mtb*-iv and PBS control conditions (**Figure 7V**, $FDR < 0.01$, see STAR Methods), with most pathways enriched uniquely in either BCG-iv or *Mtb*-iv conditions. To explicitly dissect the divergence in the regulatory pathways altered by BCG-iv and *Mtb*-iv, for every monocytic precursor cell, we calculated the average gene expression of all genes annotated in each of the gene sets analyzed. We then compared differences in the overall activity of each of the pathways between monocytic precursor cells derived from the different groups of animals (**Figure 7W**). These analyses revealed that monocyte progenitors from *Mtb*-iv animals present a phenotype that is characterized by an impaired inflammatory activity, as shown by the coordinated decrease in the expression levels of genes associated with the regulation of inflammatory responses, as well as IFN-I and II. In contrast, genes involved in the E2F pathway, which is a critical regulator of cell proliferation versus cell death via apoptosis (445), showed increased activity in monocyte progenitors from *Mtb*-iv animals as compared to BCG-iv. Consistent with these findings, gene-ontology enrichment analyses for the set of genes differentially expressed between monocyte progenitors from BCG-iv and *Mtb*-iv (1,707 under a more stringent cutoff: $abs(logFC) > 0.2$ & $FDR < 0.01$) revealed that genes up-regulated in BCG-iv as compared to *Mtb*-iv were significantly enriched among terms related to the regulation of cytokines production, such as IFN-I ($FDR = 1.5E-4$) or IL6 ($FDR = 2.6E-5$). In turn, genes more highly expressed in *Mtb*-iv than BCG-iv were enriched in functions related to regulation of cell proliferation

such as mitotic nuclear division (FDR=2.1E-23) as well as terms related to mitochondrial respiration, such as oxidative phosphorylation (FDR=8.1E-17), ATP biosynthetic process (FDR=2.9E-8) and respiratory electron transport chain (FDR=6.5E-10). Key genes for the regulation of hematopoiesis (Flt3) and the deployment of inflammatory responses (Il6ra) appear to be divergently regulated between *Mtb* vs BCG (**Figure 7X**). Collectively, these results demonstrate that the impact of BCG and *Mtb* on the transcriptional profile of HSCs and progenitor cells lasts for at least one year and generates protective or failed trained immunity in macrophages after BCG-iv vaccination or *Mtb*-iv infection, respectively.

4.5 Discussion

One of the hallmarks of chronic infection is impaired immune-driven resistance, allowing pathogen persistence (164, 446). Given that HSCs are responsible for generating all non-embryonically seeded immune cells, any manipulation of HSC responses by a pathogen will impact resistance to infection. While some of the cellular and molecular mechanisms of rapid HSC adaptation, such as emergency granulopoiesis, to acute systemic infections (e.g. *E. coli*) have been studied, understanding of the HSC response program to chronic infectious diseases, including *Mtb* is extremely limited. Interestingly, BM suppression in TB was documented in the late 1980s (443), although the pathophysiology of such a syndrome was not understood. Notably, it has been recently shown that *Mtb* accesses the BM by exploiting the mesenchymal stem cells as a potential niche for its survival (417). However, its persistence in the BM and impact on HSCs and progenitor cells remains incompletely understood. In the current study, we demonstrate that *Mtb* accesses the BM as early as 10 days after pulmonary infection and reprograms HSCs at two critical levels: 1) depleting myeloid progenitors and 2) generating failed trained immunity, both of which compromise host resistance to infection. Thus, *Mtb* may have evolved to access the BM and imprint the hematopoietic system to generate inadequate host immunity.

We have recently shown how BCG or adjuvants like β -Glucan reprogram HSCs towards myelopoiesis via imprinting protective trained immunity against *Mtb* (304, 395). Although there is a striking difference in pathogenesis of BCG versus *Mtb* (**Figure 1B**), with the exception of a very early timepoint (day 7), the absolute numbers of HSC and MPP populations remained remarkably similar between BCG and *Mtb* time courses. However, BCG and *Mtb* were highly dichotomous in their modulations of lineage restricted progenitors, whereby *Mtb*, unlike BCG, specifically skewed immune cell development toward lymphopoiesis at the expense of myelopoiesis. As the hematopoietic system is hierarchical with HSCs/MPPs giving rise to all of the blood cell lineages (e.g. CMP/GMP or CLP) at the apex, it was initially thought that specific transcriptional networks of individual HSCs are the major determinants for driving specific hematopoietic lineages (447, 448). However, similar to a recent study (449), we found that the specific lineage transcriptional networks for myelopoiesis or lymphopoiesis were similar in HSCs/MPPs after BCG vaccination or *Mtb* infection. Despite this similarity, transcriptomic profile of HSCs and MPPs from BCG vaccinated and *Mtb* infected mice showed considerable differences in the magnitude of several key pathways, including IFN-I and heme/iron metabolism, which were both implicated in lineage commitment downstream of HSCs/MPPs.

Our results highlight the importance of IFN-I/iron axis in lineage commitment, considering the susceptibility of myeloid progenitors (CMP) compared to lymphoid progenitors (CLP) in undergoing programmed cell death, following *Mtb* infection. It has been shown that during shock-like ehrlichial infection, IFN-I severely limits HSC and progenitor cell proliferation and induces necroptosis in progenitor cells (271). Our findings additionally establish that IFN-I alters intracellular iron levels specifically in myeloid progenitors, resulting in the disruption of mitochondrial function, as illustrated by the loss of mitochondrial membrane potential, and presumably driving programmed cell death. Interestingly, Poly (I:C)—a potent inducer of IFN-I response—also induced necrosis of myeloid progenitors via a mechanism associated with profound alteration of intracellular iron metabolism. Poly (I:C) equally induces lymphopoiesis, but, unlike *Mtb*, this was fully dependent on the IFN-I pathway, this difference is likely due to the fact that, Poly (I:C) triggers only the IFN-I pathway acutely, while *Mtb* chronically activates a multitude of pathways, which can either inhibit or promote lymphopoiesis. Thus, closer examination of the kinetics of the IFN-I response to *Mtb* infection may resolve this dichotomy.

The overwhelming majority (>80%) of the iron available in mammals exists in the form of heme, a hydrophobic tetrapyrrole ring that binds iron through nitrogen atoms, and presumably therefore pathogenic microorganisms evolved to re-direct not only iron but also heme from their hosts (409). In keeping with this notion, mice lacking the heme catabolizing enzyme heme oxygenase 1 (HO-1) are highly susceptible to *Mtb* infection (424, 450). The iron generated via heme catabolism by HO-1 must be stored by ferritin in its inert ferric form. Interestingly, we also found that the heme metabolic pathway significantly differed in HSCs/MPPs of BCG-vaccinated mice versus *Mtb*-infected mice.

Iron plays an important role in TB pathogenesis as it is required for the growth of *Mtb* (451, 452). Thus, iron needs to be tightly regulated in host cells because alteration of iron levels affects numerous processes, including mitochondrial function, and a deficiency or excess of iron promotes the generation of the hydroxyl radical-mediated cell death. Similar to *Mtb* infection, mice harboring ferritin-deficient BM cells showed a reduction of myelopoiesis at the steady state and were highly susceptible to subsequent *Mtb* infection. Although we have not directly linked the alteration of iron metabolism to specific cell death programs, including ferroptosis or RIPK1/3-mediated necroptosis, the increased expression of RIPK3 in HSCs (**Figure 5B**), the involvement of necroptosis pathway in BM failure (271, 453, 454), and the unique evolutionary link between *Mtb* and necroptosis (212, 314, 437, 455) all suggest that the IFN-I/iron axis limits myelopoiesis via necroptosis during *Mtb* infection. Furthermore, our results provide direct evidence

that myeloid progenitor viability can be preserved in *Mtb*-infected *Ripk3*^{-/-} mice supporting the notion that RIPK3-dependent necroptosis is a major determinant of lineage bias during hematopoietic stress.

It remains to be determined how HSC/MPP populations resist cell death despite significant imprinting of genes involved in cell death programs (e.g. RIPK3, **Figure 5B**) during infection. However, our results are compatible with an elegant and very recent study from Passegué's group demonstrating that while TNF promotes cell death in myeloid progenitors, it prevents necroptosis in HSCs (263). These findings collectively suggest that there are safeguard mechanisms engaged in HSCs to prevent HSC depletion/exhaustion and BM failure syndrome. Adding additional complexity is the requirement for host-derived iron by *Mtb* for its cellular functions. Induction of cell death through modulation of iron metabolism could potentially link the acquisition of iron by *Mtb* with its dissemination and persistence in the BM, as has been suggested recently in the lung (425). How exactly *Mtb* benefits specifically from modulating these pathways is an intriguing area for future work. Moreover, other metals like zinc are required by *Mtb* (456) and modulate the balance of lymphopoiesis versus myelopoiesis (457). Therefore, metal acquisition in hematopoietic compartments appears to have substantial impact on an evolutionarily conserved host defense strategy coined originally as nutritional immunity (458) and further studies are required to identify mechanisms involved in innate nutritional immunity (404).

While *Mtb* specifically targets progenitors of myeloid lineages to restrict the generation of the innate compartment, it also alters the quality of the innate immune cells, as BMDM from *Mtb*-infected mice are extremely permissive to subsequent *Mtb* infection in an IFN-I-dependent manner. This observation provides more supportive evidence that ligands, such as β -Glucan via IL-1 signaling (395), or live vaccines like BCG via IFN-II (304), sustain myelopoiesis with protective imprinting to generate trained macrophages which are then able to prevent the growth of *Mtb* (296, 304). Thus, although the hematopoietic system is able to rapidly adapt to stress to meet the higher demand of the host immune responses, this demand-adapted hematopoiesis is context-specific and depends on unique imprinting and lineage fate decisions. It is also important to note that perhaps the collective magnitudes of these reprogramming signals in HSCs determines a protective or detrimental immunity to a given infection. For instance, IFN-I therapies have been rarely associated with BM suppression (459, 460), indicating that IFN-I signaling alone is not the cause of BM failure and it requires a secondary stimuli. During LCMV infection the suppressive effects of IFN-I on hematopoiesis requires IFN-II (461). As the levels of IFN-II gene expression in HSCs and progenitor cells are very similar between BCG and *Mtb* infection, it is tempting to speculate that during *Mtb* infection, IFN-I may override the protective effects of IFN-II that we observed in BCG-vaccinated mice. There are recent studies suggesting that the induced epigenetic signature can be erased by other

signaling pathways (462). Thus, further investigation at the levels of chromatin and gene interactions will provide more mechanistic understanding of the interaction of these signaling pathways during infectious diseases.

One of the outstanding questions in the field of trained immunity is the longevity of imprinting in trained immune cells. In the current study, by using competitive mixed BM chimeric experiments we have demonstrated that HSCs from BCG-vaccinated donors have superior engraftment capacity compared to the HSCs from *Mtb*-infected donors. This indicates that BCG reprograms HSCs with a remarkable repopulation capacity. Furthermore, via our serial engraftment study, we have demonstrated that the BCG or *Mtb* reprogramming of HSCs lasts for at least a year. Remarkably, the protective or detrimental signatures of HSCs were also transmitted to macrophages after one year. The mechanisms of how HSCs were able to maintain these epigenetic signatures in the complete absence of mycobacteria for this lengthy period of time are unknown, but the basal levels of PAMPS in the circulation may at least partially contribute to this maintenance (463, 464). Equally, the observation that the epigenetic/transcriptional signatures of mycobacteria-exposed HSCs are sustained over successive engraftments intimates potentially important effects on bone marrow transplantation and subsequent protection/susceptibility to infections in patients, as has been previously suggested (465). However, more studies need to be directed at identifying the cellular and molecular mechanisms involved in this phenomenon.

Our understanding of the immune response to *Mtb* infection in the BM as well as the dynamic between innate and adaptive immune cells/mediators and stromal/HSCs is extremely limited, which is necessary to understand the mechanism of direct or indirect effects of *Mtb* infection on hematopoietic system. It is tempting to speculate that the observed effect of IFN-I on iron metabolism is related to an antimicrobial response that limits the availability of this essential nutrient to potential pathogens. In this context, the ability of this response to bias hematopoiesis to the benefit of *Mtb* would reflect the subversion of host immunity by this highly-adapted pathogen. This type of immune subversion is conceptually similar to the observations that human T cell epitopes of *Mtb* are evolutionary hyperconserved (466) and T cells have been in fact proposed to contribute to TB transmission by participating in the induction of cavitary lung disease (467, 468). Moreover, it is plausible that while *Mtb* bias HSCs toward lymphopoiesis, they may also intrinsically reprogram lymphoid lineages generating ineffective lymphocytes against TB. Certainly, future studies investigating the potential impact of *Mtb* on lymphopoiesis are required to carefully test this hypothesis. While our findings identified RD1 of the *Mtb* genome to be critical in detrimentally manipulating hematopoiesis in response to *Mtb*, how exactly RD1 does this, as well as which

components of the BCG genome are conversely protective remain to be investigated but are essential to further develop therapeutic interventions or novel vaccine.

4.6: Materials & Methods

Experimental Model and Subject Details

Mice. Six- to ten-week old CD45.1 and CD45.2 C57BL/6J, *Ifnar1*^{-/-}, and *Ripk3*^{-/-} (kindly provided by Dr. Vishva Dixit, Genentech) mice were housed and bred at the RI-MUHC, Montreal, QC, Canada. *Rosa26*^{Cre}*ER*^{T2}*Fth*^{lox/lox} mice were provided by MP Soares (Portugal) and tamoxifen treatment was performed as previously described (441). All animal studies were conducted in accordance with the guidelines of, and approved by, the Animal Research Ethics Board of McGill University (project ID: 5860). Mice were housed under SPF conditions with *ad libitum* access to food and water. Experiments were conducted using male and female sex- and age-matched mice that were randomly assigned to experimental groups.

Bacterial culture. *Mtb* H37Rv, *Mtb* H37Rv Δ RD1 (421) and BCG-TICE were grown in 7H9 broth (BD) supplemented with 0.2% glycerol (Wisent), 0.05% Tween80 (Fisher), and 10% albumin-dextrose-catalase (ADC) under constant shaking at 37° C. For experiments involving *Mtb*-GFP and BCG-GFP bacteria were grown as above with the addition of kanamycin (25 μ g/mL; Pfizer) for selection of resistant bacteria. For *in vitro* and *in vivo* experiments, *Mtb* (H37Rv) bacteria in log growing phase (OD 0.4 – 0.9) were centrifuged (4000 RPM, 15 minutes) and resuspended in RPMI without penicillin/streptomycin or sterile PBS. Single cell suspensions were obtained by passing the bacteria 10-15 times through a 22G needle (Terumo).

In vivo experiments

Mtb infection or BCG vaccination of mice

Throughout the study, mice were intravenously (iv) infected with *Mtb* H37Rv, *Mtb* H37Rv- Δ RD-1 or vaccinated with BCG-TICE with a dose of 1x10⁶ single-suspended bacteria in 100 μ l PBS, unless otherwise indicated. For aerosol infection, mice were infected with approx.50-100 CFU of *Mtb* H37Rv in a nose-only aerosol exposure unit (Intox). Infection dose was confirmed by enumerating the lung CFU one-day after infection.

Antibiotic treatment of mice

For antibiotic treatment with antimycobacterial drugs, the drinking water of the mice was supplied with 100mg/L Isoniazid (INH; Sigma-Aldrich) and 100mg/L Rifampicin (RIF; Fisher) for four weeks. The antibiotic treatment was followed by a two-week wash-out period on regular water.

Poly (I:C) and β -Glucan treatment

C57BL/6J and *Ifnar1*^{-/-} mice were treated with Poly (I:C) (Invivogen) (200 μ g/mouse) intraperitoneally (i.p.) at day 0, 2, 4, 6. Mice were sacrificed at day 3 and day 7 depending on the experiment. For β -glucan (Sigma, catalogue #G5011), mice were treated with 1mg/mouse i.p. at day 0 and day 3. Mice were sacrificed at day 7.

Adoptive transfer experiment: C57BL/6J mice were vaccinated with BCG-iv or infected with *Mtb*-iv (1x10⁶ CFU) or PBS injected (PBS-iv). After 4 weeks, BM cells were harvested and differentiated into BMDMs in the presence of anti-TB drugs to kill any residual *Mtb*. BMDMs were infected with H37Rv (MOI of 0.2) for 30 minutes at 37 °C and 5% CO₂ with frequent agitation. Free bacteria were then removed by washing 5x with cold RPMI, each followed by centrifugation (1500 RPMI) for 10 min at 4 °C. BMDMs (0.5x10⁶ cells) were resuspended in 40 μ l PBS and then intratracheally transferred into naive *Rag1*^{-/-} mice (Divangahi et al., 2009; 2010). The initial number of bacteria prior to transfer was assessed by plating *Mtb*-infected macrophages on 7H10 agar plates.

Competitive Mixed chimeric mouse model

C57BL/6J mice were either PBS-injected or BCG iv-vaccinated or *Mtb* iv-infected (1x10⁶ bacteria). After four weeks, mice were treated with anti-TB drugs for four weeks. The antibiotic treatment was followed by a two-week wash-out period on regular water. BM cells (2x10⁵) from either BCG iv-vaccinated or *Mtb*-iv infected were admixed with 2x10⁵ rescue BM cells and were intravenously injected into CD45.1⁺ recipient C57BL/6J mice 16 hours post lethal irradiation with 9 Gy. Mice were kept under antibiotic treatment (0.5g Enrofloxacin (Bayer) per litre of drinking

water) for three days before and two weeks after irradiation and reconstitution. Engraftment was measured after 4, 8, 12 and 16 weeks of reconstitution by staining peripheral blood cells.

Secondary engraftment mouse model

C57BL/6J mice were either PBS-injected or BCG iv-vaccinated or *Mtb* iv-infected (1×10^6 bacteria). After four weeks, mice were treated with anti-TB drugs for four weeks. The antibiotic treatment was followed by a two-week wash-out period on regular water. CD45.2⁺ BM cells (4×10^6) either from BCG iv-vaccinated or *Mtb* iv-infected mice were intravenously injected into congenic CD45.1⁺ C57BL/6J mice 16 hours post lethal irradiation with 9 Gy. CD3⁺ T cells were depleted from the BM by MACS sorting prior to transplantation. Mice were kept under antibiotic treatment (0.5g Enrofloxacin (Bayer) per litre of drinking water) for three days before and two weeks after irradiation and reconstitution. The chimerism was validated after 16 weeks of reconstitution by flow cytometry and was >96%. For the second engraftment, CD45.2⁺ BM cells (4×10^6) from the 16 week-reconstituted mice were intravenously injected into CD45.1⁺ C57BL/6J mice 16 hours post irradiation with 9 Gy. The chimerism was validated after 20 weeks of reconstitution by flow cytometry and was >96% and subsequent experimentation was performed.

Generation of chimeric mice using inducible Tamoxifen model

CD45.1⁺ B6 mice were lethally irradiated with 9 Gy following 3 days of antibiotic treatment (0.5g Enrofloxacin (Bayer) per litre of drinking water). 16 hours later, the BM compartment was reconstituted with 4×10^6 nucleated cells from Rosa26^{Cre}ER^{T2}Fth^{lox/lox} mice (CD45.2⁺) and antibiotic treatment was maintained for 2 additional weeks. Between 8-12 weeks post-injection, reconstitution was validated by flow cytometry and was >90%. Tamoxifen was administered at 50mg/kg (10% ethanol in corn oil v/v) i.p. for 5 consecutive days and the mice were then rested for 1 week.

***In vitro* experiments**

Generation of BMDM

BM from both femurs and tibiae was harvested in RPMI (Wisent) supplemented with 10% heat-inactivated FBS (Wisent). Cells were subsequently seeded in 7ml RPMI supplemented with 2mM L-glutamine, 10% FBS, 2% HEPES, 1% non-essential amino acids, 1% essential amino acids, 0.14% 5N NaOH, 1mM sodium pyruvate, 100U/ml penicillin, 100mg/ml streptomycin (all Wisent), 30% of L929-conditioned media (LCM) and isoniazid (INH 5µg/ml) in petri dishes. After 3 days of incubation at 37°C with 5% CO₂, fresh medium containing LCM and INH (5µg/ml) was added. Cells were allowed to differentiate into macrophages for a total of 6 days and then were harvested by removing the supernatant and addition of 4ml cell stripper (Corning) for 20 minutes at 37°C. As evaluated by flow cytometry, the purity was >95%. INH was added only during the differentiation of the BMDM derived from BM cells of non-treated BCG-iv or *Mtb*-iv infected mice. Yield was determined by trypan blue dead cell exclusion counts and normalized to PBS control mice yields. For all experiments equal number of macrophages were seeded.

***In vitro* Macrophage Infection**

BMDMs (1x10⁶ cells) were seeded in 6-well plates supplemented with RPMI without penicillin/streptomycin (1 ml) and incubated overnight at 37°C with 5% CO₂. The next day, cells were infected with *Mtb* H37Rv (MOI 1), or BCG (MOI 10) unless otherwise indicated. Cells were incubated for 4 hours at 37°C with 5% CO₂. Subsequently, cells were washed 3x with sterile PBS and were then incubated in supplemented RPMI without penicillin/streptomycin. CFUs were enumerated at 4 hours, day 3 and day 5 post-infection.

Mycobacterial CFU Enumeration

For CFU enumeration in *in vitro* infected cells, cells were lysed with 500µl sterile H₂O for five minutes, followed by addition of 500µl PBS supplemented with 0.05% Tween80. For CFU enumeration in tissues, organs were homogenized in 1ml 7H9 broth (BD) supplemented with 0.2% glycerol (Wisent), 0.05% Tween80 (Fisher), and 10% ADC using OmniTip Plastic Homogenizer Probes (Omni International). Serial dilutions in PBS+0.05% Tween80 were plated on 7H10 agar

plates with 10% OADC enrichment and PANTA (BD). Plates were then incubated at 37°C and counted after 21 days.

Flow Cytometry

BM/Spleen cells (3×10^6 cells) after RBC lysis were stained with fixable viability dye eFluor501 (eBioscience) at the concentration of 1:1000 for 30 minutes (4°C). Subsequently, the cells were washed with PBS supplemented with 0.5% BSA (Wisent) and incubated with anti-CD16/32 (clone 93, eBioscience) at a concentration of 1:100 in PBS/0.5% BSA at 4°C for 10 minutes except for myeloid progenitor and downstream progenitors staining. The following antibodies were then used for staining: anti-Ter-119, anti-CD11b (clone M1/70), anti-CD5 (clone 53-7.3), anti-CD4 (clone RM4-5), anti-CD8a (clone 53-6.7), anti-CD45R (clone RA3-6B2), and anti-Ly6G/C (clone RB6-8C5) all were biotin-conjugated (all BD Bioscience) and added at a concentration of 1:100 for 30 minutes at 4°C. Cells were subsequently washed with PBS/0.5% BSA. For staining of LKS, HSCs, and MPPs: Streptavidin-APC-Cy7 (eBioscience), anti-c-Kit-APC (clone 2B8, eBioscience), anti-Sca-1-PE-Cy7 (clone D7, eBioscience), anti-CD150-eFluor450 (clone mShad150, eBioscience), anti-CD48-PerCP-eFluor710 (clone HM48-1, BD Bioscience), anti-Flt3-PE (clone A2F10.1, BD Bioscience), and anti-CD34-FITC (clone RAM34, eBioscience) (all 1:100) were added and incubated at 4°C for 30 minutes. For staining of myeloid and lymphoid progenitors: Streptavidin-APC-Cy7 (eBioscience), anti-c-Kit-APC (clone 2B8, eBioscience), anti-Sca-1-PE-Cy7 (clone D7, eBioscience), anti-CD34-FITC (clone RAM34, eBioscience), anti-CD16/32 PerCP-eFluor710 (clone 93, eBioscience) and anti-CD127 BV786 (clone A7R34, BD bioscience) (all 1:100) were added and incubated at 4°C for 30 minutes. For cMoPs and downstream progenitors: BM cells were incubated with biotin antibodies against lineage markers as mentioned above, except without anti-Ly6C/6G, at 4°C for 30 minutes. Cells were subsequently washed with PBS/0.5% BSA. Following antibodies were added: Streptavidin-BUV-395(BD Bioscience), anti-c-Kit – Pacific Blue (clone 2B8, BD Bioscience), anti-Sca-1-PE-Cy7 (clone D7, eBioscience), anti-CD34-FITC, anti-CD16/32-PerCP-efluor710 (clone 93, eBioscience), anti-CD115 BV711 (clone AFS98, BioLegend), anti-Flt3-PE (clone A2F10.1, BD Bioscience), anti-Ly6C-APC (clone HK1.4, eBioscience) and anti-Ly6G AF700 (clone 1A8-Ly6G, eBioscience) all (1:100 except Streptavidin BUV395 at 1:50) were added and incubated at 4°C for 30 minutes. In some

experiments cells were further stained with AnnexinV-PE and 7AAD (Biolegend) or NucSpot Far-Red (Biotium), according to the manufacturer's instructions and unfixed cells were acquired immediately. In another set of experiments, cells were fixed and permeabilized using the FOXP3 Transcription Factor Staining Kit (eBioscience) for 1 hour at 4°C. Then, cells were stained with anti-Ki67-PE (clone 16A8, BioLegend) (1:400) for 1 hour at 4°C and acquired.

Staining for innate and adaptive immune cells: Red blood cells were lysed in bone marrow and collagenase IV (Sigma)-treated lung samples. Lung, spleen or BM cells (3×10^6) were then stained with fixable viability dye eFluor501 (eBioscience) at the concentration of 1:1 000 for 30 minutes (4°C). Subsequently, the cells were washed with PBS supplemented with 0.5% BSA (Wisent) and incubated with anti-CD16/32 (clone 93, eBioscience) at a concentration of 1:100 in PBS/0.5% BSA at 4°C for 10. After washing, cells were incubated with fluorochrome tagged antibodies at 4°C for 30 minutes. Antibodies for the innate panel: anti-CD11b-Pacific Blue (clone M1/70, eBioscience), anti-CD11c-PE-Cy7 (clone N418, BD Bioscience), Siglec-F-PE-CF594 (clone E50-2440, BD Bioscience), F4/80-APC (clone BM8, eBioscience), Ly6C-FITC (clone HK1.4, BD Bioscience), Ly6G-PerCP-eFluor710 (clone 1A8, eBioscience). Antibodies for the adaptive panel: anti-CD3-PE (clone 145-2C11, eBioscience), anti-CD19-PE-Cy7 (clone eBio1D3 (1D3), eBioscience), anti-CD4-eFluor450 (clone GK1.5, eBioscience), anti-CD8-AF700 (clone 53-6.7, BD Bioscience). All cells were subsequently washed with PBS/0.5% BSA and resuspended in 1% paraformaldehyde.

Blood Leukocytes: 50 μ L of whole blood collected in heparin tubes (BD) was incubated with fluorochrome tagged antibodies at 4°C for 30 minutes. Antibodies for the innate panel: anti-CD11b-Pacific Blue (clone M1/70, eBioscience), anti-CD11c-PE-Cy7 (clone N418, BD Bioscience), Siglec-F-PE-CF594 (clone E50-2440, BD Biosciences), F4/80-APC (clone BM8, eBioscience), Ly6C-FITC (clone HK1.4, BD Bioscience), Ly6G-PerCP-eFluor710 (clone 1A8, eBioscience). Antibodies for the adaptive panel: anti-CD3-PE (clone 145-2C11, eBioscience), anti-CD19-PE-Cy7 (clone eBio1D3 (1D3), eBioscience), anti-CD4-eFluor450 (clone GK1.5, eBioscience), anti-CD8 AF700 (clone 53-6.7, BD Bioscience). After RBC lysis, cells were subsequently washed with PBS/0.5% BSA and resuspended in 1% paraformaldehyde.

If required, panels were modified to contain anti-CD45.1–APC (clone A20, BD Bioscience, 1:100) and anti-CD45.2–BUV395 (clone 104, BD Bioscience, 1:100).

Cells were acquired on the Fortessa-X20 (BD) and analyzed using FlowJo software (version 10.6.1).

Evaluation of Mitochondrial Fe²⁺, Mitotracker Green/Orange and MitoSox Red. BM mononuclear cells were stained with rhodamine B 4-[(1,10-phenanthrolin-5-yl)aminocarbonyl]benzyl ester (RPA) (Squarix) at 0.2 μM, or Mitotracker Green and Orange 1 μM, or MitoSox Red 1 μM (all from Invitrogen technologies) in PBS for 30 min at 37 °C and then washed with PBS. The dye-loaded cells were further stained with antibodies for progenitors as mentioned above. RPA MFI fluorescence was normalized to PBS groups, inversed and multiplied by 100 to give a percentage of iron pools compared to PBS, as fluorescence is quenched by higher levels of iron. For experiments involving mitochondrial potential, dysregulated mitochondria were considered as Mitotracker Green^{hi} and Mitotracker Orange^{lo} as previously described (469).

Perls' Prussian blue iron staining. Bone epiphyses were removed and femurs were fixed in 4% PFA for 24-48h followed by washing with PBS. Perls' staining was performed by Histopathology Core of RI-MUHC, Montreal, QC, Canada.

ImageStream. Freshly isolated BM cells from naïve C57BL/6J mice were infected with *Mtb*-GFP (MOI 3) for 4 hours. BM cells were then stained with antibodies for LKS and Lineage⁺ cells. Images were captured on an Amnis ImageStream Mark II Imaging Flow Cytometer with 40X magnification (EMD Millipore). Data were acquired and analyzed using Amnis INSPIRE software and Amnis IDEAS software, respectively. ImageStream samples were also acquired using Fortessa-X20 (BD) and then analyzed using FlowJo software.

Methylcellulose assay.

5x10³ BM cells were suspended in methocult medium (MethoCult GF M3534; Stem Cell Technologies) with specific cytokines to promote the growth of myeloid progenitors. Colonies were counted after 10-12 days. Cells were collected by washing with PBS and stained for anti-CD11b and cKit⁺ cells.

Cell Sorting

For stem cell sorting, BM cells were harvested from femurs, tibiae, humeri and ilia, and incubated with the described biotin-conjugated antibodies against lineage-committed cells. Subsequently, the cells were incubated with MACS streptavidin conjugated microbeads (Miltenyi) for 30 minutes at 4°C. A depletion of the lineage-committed cells was performed using MACS magnets with LS Columns (Miltenyi, #130-042-401). The remaining cells were incubated with the above described antibodies for LKS/HSCs/MPPs. DAPI (0.005µg) was added for viability staining to 10x10⁶ cells right before sorting on a BD FACSAria Fusion sorter. Cells were sorted in 200µl lysis buffer of Magmax-96 Total RNA Isolation Kit (life technologies, Ambion 1830) at room temperature or in PBS containing 0.04% BSA for single cell sequencing. RNA samples were vortexed for 30 seconds, and subsequently stored at -80°C until RNA extraction.

RNA Extraction. Total RNA was extracted from the sorted HSCs and MPPs using Magmax-96 Total RNA isolation kit (life technologies, Ambion 1830M). RNA quality was evaluated spectrophotometrically, and quality was assessed with the Agilent 2100 Bioanalyzer (Agilent Technologies). All samples showed RNA integrity number >8.

RNA-seq Analyses: Pre-processing Steps.

Experimental mice were split into three treatment groups, (either BCG-iv, *Mtb*-iv or the control: PBS-iv) with 4 animals each. 28 days after treatment, animals were sacrificed, and their BM extracted. Hematopoietic stem cells (HSCs; Lin⁻cKit⁺Sca-1⁺CD150⁺) and multipotent progenitors (MPPs; Lin⁻cKit⁺Sca-1⁺CD150⁻) were sorted as described above. RNA was then extracted and sequenced, generating a dataset of 23 samples (two cell types multiplied by three treatments and by four animals per group, minus one HSC-PBS sample that did not produce a valid RNA library).

As for RNA-seq data pre-processing, low-quality score bases (Phred score < 20) and adaptor sequences were trimmed using Trim Galore (version 0.2.7) (http://www.bioinformatics.babraham.ac.uk/projects/trim_galore/). Mapping of the resulting reads to the mouse genome reference sequence (Ensembl GRCm38 release 81) was done with kallisto (v0.43.0) (470). Then, protein coding genes were selected, and samples were normalized using the weighted trimmed mean of M-values algorithm (TMM), implemented in edgeR (471).

Data were log-transformed using voom, within the limma package (472) and lowly-expressed genes were filtered out, defined as those with a median log₂-transformed expression lower than 2 within all experimental groups (i.e. treatment-cell-type combinations). This produced a reads matrix of 12132 genes.

Bulk RNA-seq: differential expression analyses

The filtered matrix was then re-normalized, using EdgeR and voom, and modelled according to the following design, using limma (472):

Expression~ Cell_type+Treatment:cell_type

From the mentioned model design run over all 12132 genes in the dataset, BCG and *Mtb* effects were retrieved within each cell type. Focus was then put on genes showing treatment responses in any cell-type (2214 genes responding at 1% FDR to either BCG or *Mtb* at HSCs; 3542 for MPPs) and these genes were then tested for differences in expression between the two treatments. Differences in expression between HSCs and MPPs were also characterized. We found 581, 608 and 600 differentially expressed genes between the HSCs and MPPs, at 1% FDR, in cells coming from PBS, BCG and *Mtb* treated mice, respectively.

Single cell RNA-seq library preparation and sequencing.

Single cell transcriptomic data was collected for LKS (Lin⁻ Sca-1⁺ cKit⁺) and myeloid progenitor (Lin⁻ Sca-1⁻ cKit⁺) populations in the context of the *Mtb* aerosol challenge and the second engraftment experiments. Cells were sorted as described above into PBS containing 0.04% BSA.

Single-cell GEMs were generated using a Chromium Controller instrument (10x Genomics). Sequencing libraries were prepared using Chromium Single Cell 3' Reagent Kits (10x Genomics), according to the manufacturer's instructions. Briefly, GEM-RT was performed in a thermal cycler: 53°C for 45 min, 85°C for 5 min. cDNA was cleaned up with DynaBeads MyOne Silane Beads (ThermoFisher Scientific) and amplified with a thermal cycler: 98°C for 3 min, cycled 12 x 98°C for 15 s, 67°C for 20s, 72°C for 1 min, and 72°C 1 min. After a cleanup with SPRIselect Reagent

Kit, the libraries were constructed by performing the following steps: fragmentation, end-repair, A-tailing, SPRIselect cleanup, adaptor ligation, SPRIselect cleanup, sample index PCR, and SPRIselect size selection. Libraries were sequenced on a NovaSeq S2 flowcell with 100 bp paired-end reads.

scRNA-seq data pre-processing and quality control: Sample preprocessing was done using the count command of CellRanger (432) against the mm10 1.2.0 reference genome, yielding numbers of cells between 3,305 and 11,994 depending on experiment, cell population and condition (**Table 1, row 1**). Initially, we measured the expression of 31053 genes in each cell (**Table 1, row 2**). In each of the four datasets analyzed, we excluded lowly expressed genes, detected in less than 5 cells in all conditions, in order to select a relevant gene set in each experiment to conduct quality control on (**Table 1, row 3**). Using this reference gene set in each experiment, we determined the percentage of protein coding genes detected, as well as the percentage of mitochondrial RNA in each cell. We then excluded cells that featured: (i) a high fraction of mitochondrial RNA reads ($f_{mito} > 5\%$), (ii) a low percentage of protein-coding genes ($f_{pc} < 95\%$) or (iii) a number of UMIs that was either too low ($n_{UMI} < 5000$) or too high ($n_{UMI} > 40,000$). After the filtering, we kept variable numbers of cells per experiment and condition, comprised between 578 and 4733 (**Table 1, row 4**). Using this final set of cells, we filtered out genes detected in less than five cells in all conditions and re-normalized the percentages of protein coding genes and mitochondrial transcripts per cell on the final dataset. At the end, the number of genes included for clustering and differential expression analyses varied between 14568 and 16480, depending on the experiment and cell population (**Table 1, row 5**).

	<i>Mtb.</i> aerosol challenge				Serial engraftment					
	LKS		Progenitors		LKS			Progenitors		
	PBS	<i>Mtb</i>	PBS	<i>Mtb</i>	PBS	BCG	<i>Mtb</i>	PBS	BCG	<i>Mtb</i>
1.Cells	3305	6580	3741	8259	5391	4673	2786	5094	8987	11994
2.Genes	31053		31053		31053			31053		
3.Genes >5 cells	16071		15103		17019			16268		
4. Filtered Cells	2388	3310	2241	3504	3872	2524	1563	3353	5020	1486
5. Filtered Genes	15550		14568		16480			15676		

Table 1. Recapitulation of number of cells and genes at the different stages of the quality control process of the single-cell RNA-seq data analyses.

scRNA-seq data normalization: We used the function `computeSumFactors`, from the R package `scran` (473) to normalize the data. This method works by declaring a series of cell pools whose expressions are added and normalized against a common reference. Each of these pools is then interpreted as a linear system from which the contribution of each single cell can be deconvolved, allowing the inference of cellwise normalization factors in a way that is robust against noise and low expression levels. To ensure that a majority of genes are not DE between any of the pools and the common reference that they are normalized against, clusters of homogeneous gene expression

are first built using the function quickCluster. Thus, cell specific normalization factors n_i are inferred within each cluster, and then rescaled by normalization between clusters. Normalization used was:

$$E_{norm}(i, j) = \log_2(1 + E_{count}(i, j)/n_i) \quad (1)$$

For the j -th gene in the i -th cell, where n_i represent the normalization factor estimated for the i -th cell.

Correcting for variation in cell cycle in single cell data: Cell cycle numeric scores were inferred for each cell using the function cyclone implemented in package scran (473). The method is based on a pre-defined classifier constituted by gene pairs whose relative difference in expression depends on the cell cycle stage. By comparing the coherence of the sign of the differences observed in the data to the classifier's expectation, per-cell scores were obtained for phases G1 and G2M. These values were summarized as a single numeric score $C=(G1-G2M)/(G1+G2M)$, which we mean centered and scaled across cells. These scores were corrected for at the steps of expression data scaling and cell clustering.

Single cell data scaling: Once the data was normalized in each of the four datasets, we fitted for each gene the following linear model:

$$E \sim f_{pc} + f_{mito} + n_{UMI} + C + \varepsilon \quad (2)$$

The variance associated to the residuals ε derived from this model s_ε^2 was then fitted against mean expression of the corresponding genes using scran's smoothing function trendVar (parameters: method=loess, span=0.1, degree=2). The deviations from the inferred trend were computed per gene using scran's function decomposeVar. Then, the first decile corresponding to the genes showing the largest, negative deviations from the fitted trend were selected, and the procedure was

repeated. By doing so, we obtained an unbiased basal trend for the technical component of the residual variance that is not affected by the outliers with variance much larger than the technical variance. Finally, we calculated the biological component of the variance as the difference between the residual variance and the basal technical component:

$$s_{\varepsilon}^2 = s_{tech}^2 + s_{bio}^2 \quad (3)$$

Once the variance decomposition is ready, the scaled expression \tilde{E} was defined by rescaling the residuals ε of Equation (2) by the square-root of the technical component of the residual variance, from eq. (3)

$$\tilde{E} = \varepsilon/s_{tech} \quad (4)$$

By doing this, the mean-variance relationship was successfully removed from the data.

Selection of highly informative genes: Next, we integrated the data corresponding to the different conditions. To do so, we first selected in each case a set of highly informative genes (HIGs) whose expression is to be interrogated to complete data integration. In both LKS⁺ and progenitor datasets, we selected HIGs as those that showed both high levels of (biological) expression variance across cells and had been reported in the literature as markers of the different cell sub-populations present among LKS⁺ and progenitor cells (derived from (433) for LKS⁺ data and (474) for progenitor cells). Specifically, for LKS⁺ cells, HIGs were defined as the intersection between the following four sets of genes: (set i) the 1000 genes with mean expression higher than 0.1 that showed the largest positive biological variance s_{bio}^2 across cells in our data (“highly variable genes”. HVGs); (set ii) genes differently expressed (10% FDR) between MPPs and HSCs based on the bulk RNA-seq, in all conditions present in each experiment, (set iii) genes differently expressed between

myeloid progenitors (MPP3) and lymphoid progenitors (MPP4) (219 genes) based on the bulk RNA-seq data reported in (433) and (set iv) Genes differentially expressed between short and long term hematopoietic stem cells (105 genes) based on the bulk RNA-seq data also reported in (433). Regarding set (iv), it is important to note that the gating strategy followed in (433) is slightly different from ours. While we do not distinguish among sub-types of long-term HSCs (according to our gating strategy, LT-HSCs are just Flt3⁻, CD48⁻ and CD150⁺), Cabezas-Wallscheid et al. subdivide this population according to CD34 levels, distinguishing between cells that are Flt3⁻, Cd48⁻, CD150⁺, CD34⁻ (that they denote as *HSCs*), and cells that are Flt3⁻, CD48⁻, CD150⁺, CD34⁺ (that they denote as *MPP1s*). In what regards short term HSCs, the cell population that they denote MPP2s (Flt3⁻, CD48⁺ and CD150⁺ and CD34⁺) would be included within the population described as short-term HSCs in this work (Flt3⁻, CD48⁺ and CD150⁺). Consequently, in order to obtain genes that would mark the difference between LT- and ST-HSCs according to our gating schematics (set iv), we selected the genes that, at the same time, showed differential expression between HSCs and MPP1 vs MPP2 in the dataset from (433) according to their notation.

In what regards the identification of highly informative genes to identify sub-populations in the progenitor cells data, we used the single cell data published in (474) where an analogous population of hematopoietic progenitors (c-Kit⁺ Sca1⁻ Lin⁻) was sorted and analyzed using sc-RNAseq. From the dataset reported in this work, we extracted cluster specific fold changes for the genes showing statistically significant associations to any of the cell clusters reported in the study, and kept those that present, for some of the clusters, a fold change larger than 1.5 with respect to the average expression levels across the rest of cells in the dataset. In this case, HIGs were defined as the intersection of these genes and HVGs in our data. Following these procedures, we selected 349, 115 HIG in the aerosol LKS and progenitor cells, respectively, and 346 and 112 HIGs in LKS and progenitor cells, respectively, in the secondary engraftment dataset.

Data integration across conditions: Data were integrated across conditions using the anchoring routine proposed in Seurat (FindIntegrationAnchors) (475, 476), applied to the sub-matrix constituted by the highly informative genes previously identified. This technique works by identifying pairs of cells across conditions that represent common cell states (anchors), despite batch/condition effects, that are then used to provide a transformed (integrated) expression matrix

E_{int} where anchors will ultimately be assigned to common cell clusters. The procedure has the advantage of allowing integration over multiple samples at the same time (useful in the engraftment experiment, where we had to integrate the data across three conditions (PBS, BCG-iv and *Mtb*-iv), and features flexibility in the assignment of anchors, allowing for the possibility that some cell types are unique to one of the conditions. After data integration, the steps of variance modeling, scaling and identification of highly informative genes were repeated on the transformed data, with a procedure entirely analogous to what was previously described.

Cell clustering: The scaled version of the integrated data was used to identify different cell sub-populations in each of the datasets available. First, we performed a principal component analysis of the matrix of scaled & integrated expression levels of the HIGs identified from the integrated data. After visual inspection of elbow plots, we select the first $n=20$ PCs (with the exception of LKS cells in the engraftment experiment for which we selected $n=15$) to identify cell clusters using Seurat's functions FindNeighbors plus FindClusters. We used the default parameters except for the resolution, which was set at 0.4 for the engraftment experiment and aerosol LKS⁺ cells, 0.7 for the aerosol progenitors. In parallel, we run Uniform Manifold Approximation and Projection (UMAP) to visualize the clustering using RunUMAP, also from Seurat.

Cluster classification and validation of sub-populations (LKS): To distinguish hematopoietic stem cells (HSC), from multipotent progenitors (MPP), we used the genes differentially expressed between sorted HSCs and MPPs in the bulk RNA-seq experiments reported.. We stratified this gene-set according to the direction of the effects and computed in each cell the average integrated scaled expression of all genes that were respectively up or down regulated in HSCs vs. MPPs. By comparing the expression levels of these averaged cell-type markers across clusters we could classify HSCs and MPPs in each experiment. This allowed the identification of 4 clusters of HSCs and 2 clusters of MPPs in the aerosol experiment, and 4 HSC and 3 MPP clusters in the second engraftment experiment. (**Figure S3P** and **Figure S7S**, upper panels). Next, to distinguish between myeloid-biased (MPP3) and lymphoid-biased (MPP4) progenitors, we used the set of 219 genes (set iii) that were reported in (433) to be differentially expressed between these two populations according to the direction of effects, and computed the average expression values of these genes (integrated and scaled) in each cell. Focusing on the clusters previously defined as MPPs, we

visualized the expression of these average markers of lymphoid vs myeloid up or down-regulation to distinguish in each experiment, clusters of MPP3 vs MPP4 cells (**Figure S3P** and **Figure S7S**, center). Whilst in the aerosol experiment, we observed one cluster associated to each phenotype, in the second engraftment we identified two clusters of MPP3s and one cluster of MPP4s. Finally, in order to distinguish short versus long term HSCs, we built analogous average markers from the set of genes differentially expressed between these two cell sub-types as defined by Cabezas-Wallscheid et al. Exploring the distribution of these average markers across HSC clusters led to the identification of a marked distinction between one LT- vs three ST-HSCs in the aerosol experiment, and a more gradual distribution of transcriptional profiles, which can be associated to the existence of two vs two clusters of LT- versus ST-HSCs in the second engraftment dataset (**Figure S3P** and **Figure S7S**, bottom)

Cluster classification and validation of sub-populations (progenitor populations): In order to identify subpopulations of myeloid progenitors associated to the different developmental stages and lineage biases present in the cell population initially sorted ($c\text{-Kit}^+ \text{Sca1}^- \text{Lin}^-$), we capitalized in the data published in (474), where the same cell population was analyzed through scRNA-seq. In that work, the authors identified 19 clusters that they associate to either Common myeloid progenitors (CMPs), Granulocyte-Monocyte progenitors (GMPs) or Megakaryocyte-erythrocyte progenitors (MEPs). Within each of these broader groups, they further identified subpopulations that were polarized towards specific cell fates: CMPs biased towards a megakaryocytic cell fate, groups of MEPs distributed in a continuous gradient of bias towards erythrocyte differentiation, as well as CMPs and GMPs showing bias towards different myeloid cells: monocytes, neutrophils, eosinophils and basophils. As part of their analyses, they report a set of 3,461 genes that are specific markers of each of these clusters, providing an expression estimate of the gene in each cluster, measured as the fold change of the observed expression of a given gene, in a given cluster, compared to its average expression across all clusters.

In order to compare these data to our clustering results, we selected the subset of their cluster markers that were among the set of HIGs in the integrated data. Then, we retrieved, for each of these genes, cluster-specific expression estimates by fitting a linear model

$$\tilde{E}_{int} \sim 0 + Cluster \quad (5)$$

Which produced a cluster specific intercept $\beta_o(i, j)$, for the i th gene under scrutiny, in the j th cluster. From these cluster-specific intercepts, (which operate in log-scale) we reversed the log-transformation to retrieve a natural scale expression estimate for the expression of gene I in cluster j as $2^{\beta_o(i, j)}$, which we averaged across clusters for each gene: $\langle 2^{\beta_o(i, j)} \rangle_j$. Finally, by obtaining the ratio between those two quantities, we retrieved an estimate of the expression fold change of any given cluster with respect to the average of all clusters.

$$FC(i, j) = 2^{\beta_o(i, j)} / \langle 2^{\beta_o(i, j)} \rangle_j \quad (6)$$

These values are equivalent to the fold changes reported in (474) and were used to identify matches between our cell clusters and those reported by Paul et al. based on the correlation structure of the two datasets (**Figure S3Q** and **Figure S7T**). Cell clustering assignment was further validated by inspecting the expression levels of canonical lineage markers (**Figure S3R** and **Figure S7U**). MEP expressed Car1, Car2, Klf1 high; CD34, Cebpa, and Spi1 low; GMPs expressed Car1, Car2, Klf1 low, CD34, Cebpa, Spi1 high; and CMPs expressed Meis1 high while GMP and MEP markers were lowly expressed.

Within MEP cells, we further analyzed a series of markers that were reported to either increase or decrease continuously in earlier or more mature erythrocyte progenitors (Car1, Car2, Cited4, Epor, Gfi1b, Klf1, and Phf10; whose expression increases in more mature cells, and Gata2 and Meis1, which decreases). As it was observed in (474) our clusters of erythroid progenitors can be mapped to different developmental stages, from MEP_EP1 (earlier) to MEP_EP3 (more mature).

Within GMPs, neutrophil progenitors (GMP_NPs) were characterized by high expression levels of neutrophilic markers *Cebpe* and *Gfi1*; basophil progenitors (GMP_BPs) by high expression of basophile marker *Lmo4*; and Monocyte progenitors (GMP_MonP) by high amounts of *Irf8*.

Within-cluster differential gene expression induced by BCG and *Mtb*: Finally, we interrogated for differences in expression of genes in response to BCG or *Mtb* challenges. Since one of the putative effects of BCG and/or *Mtb* on cell phenotypes might be the promotion or arrest of cell quiescence, we used a linear model where cell cycle is not corrected for, in order to avoid masking the putative effects of treatment on the expression patterns of cell cycle-dependent genes. It is also important to note, that to avoid the distortion induced in the data by the procedures of data scaling and integration, to conduct differential expression analyses, we used the normalized, original data prior to these procedures used in cell clustering. To do these analyses, we fitted the following experimental design:

$$E \sim f_{pc} + f_{mito} + n_{UMI} + Cluster + Condition: Cluster + \varepsilon \quad (7)$$

The results of these analyses, for each cluster, are summarized in **Figure 3** and **Figure 7**, evidencing the existence of relevant effects within each of the cell clusters identified, in the four datasets here analyzed.

GO enrichments and visualization.

Gene ontology (GO) enrichment analyses were performed using the Cytoscape module ClueGO (477, 478). We conducted one-sided tests for enrichment and corrected for multiple tests using the Benjamini-Hochberg (B-H) method (479). For visualization, in **Figure S2B** analyses were focused only on terms that fell between levels 4 and 7 of the GO tree in the (Biological Process). In all analyses, we included terms that had at least 10 genes in the test gene-set and for which at least 20% of the total number of genes belonging to the GO term were present in the test gene set, except in the case of bulk-RNA-seq MPPs, where thresholds were raised to a minimum of 15, and

35%. Finally, to compile **Figure S2A**, which shows the existing correlation between GO-enrichment results after BCG vs *Mtb* treatments in each cell type, analyses were repeated removing the thresholds on gene-set size or percentage in order to avoid any selection bias. In this analysis we included all terms between levels 4 and 7 of the GO tree, regardless of enrichment significance or gene-set size. Importantly, when done, a much larger number of GO terms passed the enrichment significance threshold (between 1.4 and 7.1 times more terms enriched at 5% FDR, depending on the combination of cell-type and treatment), despite the much larger set of terms tested.

Finally, GSEA (<http://software.broadinstitute.org/gsea/>) was used to interrogate functional enrichments among genes showing differences in expression between BCG and *Mtb* treated mice, in each cell type (**Figure 2D**). It was again used to interrogate for functional enrichments among genes differentially expressed upon treatment, either *Mtb* alone in the aerosol challenge experiment (**Figure 3S**), or both BCG and *Mtb* in the serial engraftment section (**Figures 7V-W**). In all cases, we used the hallmark list of genesets, and conducted GSEA on ranks of standardized differences in expression, (mode GSEA pre-ranked, version 6.2).

Western Blot

BM cells from BM *Fth*^{-/-} or BM *Fth*^{+/+} were isolated. Briefly, cells were lysed in lysis buffer (1% Triton X-100, 150mM NaCl, 20mM Hepes pH7.5, 10% glycerol, 1mM EDTA, supplemented with anti-protease and anti-phosphatase cocktails, Roche) and protein concentration was determined using BCA assay (Pierce). 20 µg of protein was resolved by SDS-PAGE and transferred onto PVDF membranes (Biorad). Membranes were blocked and incubated overnight at 4°C with gentle agitation with anti-Fth (1:1000, Cell Signalling Technologies) or actin (1:10 000, Sigma-Adrich). Then primary antibodies were conjugated to secondary HRP-conjugated antibodies and the signal was detected using Clarity ECL kit (Biorad) and acquired on Chemidoc MP System (Biorad).

Quantification of IFN-I

Secretion of total active IFN-I (both IFN- α and IFN- β) in BM supernatants was assessed using B16-blue IFN α/β reporter cell line (InvivoGen), according to the specifications of the manufacturer.

Statistics

Statistical analyses were performed using Graph Pad Prism, version 8. Data are displayed as mean \pm SEM and n define number of animals analyzed per group. Statistical significance was determined by t test, one-way ANOVA, or two-way ANOVA as indicated in the figure legends, and is represented by the following scheme: * $p < 0.05$, ** $p < 0.01$, *** $p < 0.001$, **** $p < 0.0001$.

4.7: Acknowledgements

The authors thank Fiona McIntosh for her assistance in the experiments involving *Mtb*- Δ RD-1 as well as Marianna Orlova and Pauline Cassart for their support during the 10X Genomics experiments and Maitane Gutierrez for assistance with some of the figures. This work was supported by the Canadian Institute of Health Research (CIHR) Foundation Grant (FDN-143273), the CIHR operating grant (168884) to M.D. and the CIHR operating grants (301538 and 232519) to L.B.B. M.D. holds a Fonds de Recherche du Québec-Santé (FRQS) Award and the Strauss Chair in Respiratory Medicine. J.S. acknowledges partial support from Government of Aragón and FEDER funds through the RIS3 project LMP117-18, and from the Spanish Ministry of Science and Innovation MICINN through grants PID2019-106859GA-I00 and Ramón y Cajal research grant RYC-2017-23560. N.K. was supported by FRQS and CIHR postdoctoral fellowship. J.D was supported by the Molson Foundation Award and RI-MUHC Studentship. E.K. was supported by postdoctoral fellowships of the German Research Foundation (DFG) and FRQS. M.P.S. is supported by Fundação Calouste Gulbenkian and by Fundação para a Ciência e a Tecnologia, Portugal (PTDC/IMI-IMU/5723/2014 and 02/SAICT/2017). BB and SC were supported in part by European Community 7th Framework 294709-DAMAGECONTROL ERC-2011-AdG to MPS and FB by Marie Skłodowska-Curie Research Fellowship (REGDAM 707998).

4.8: Figures

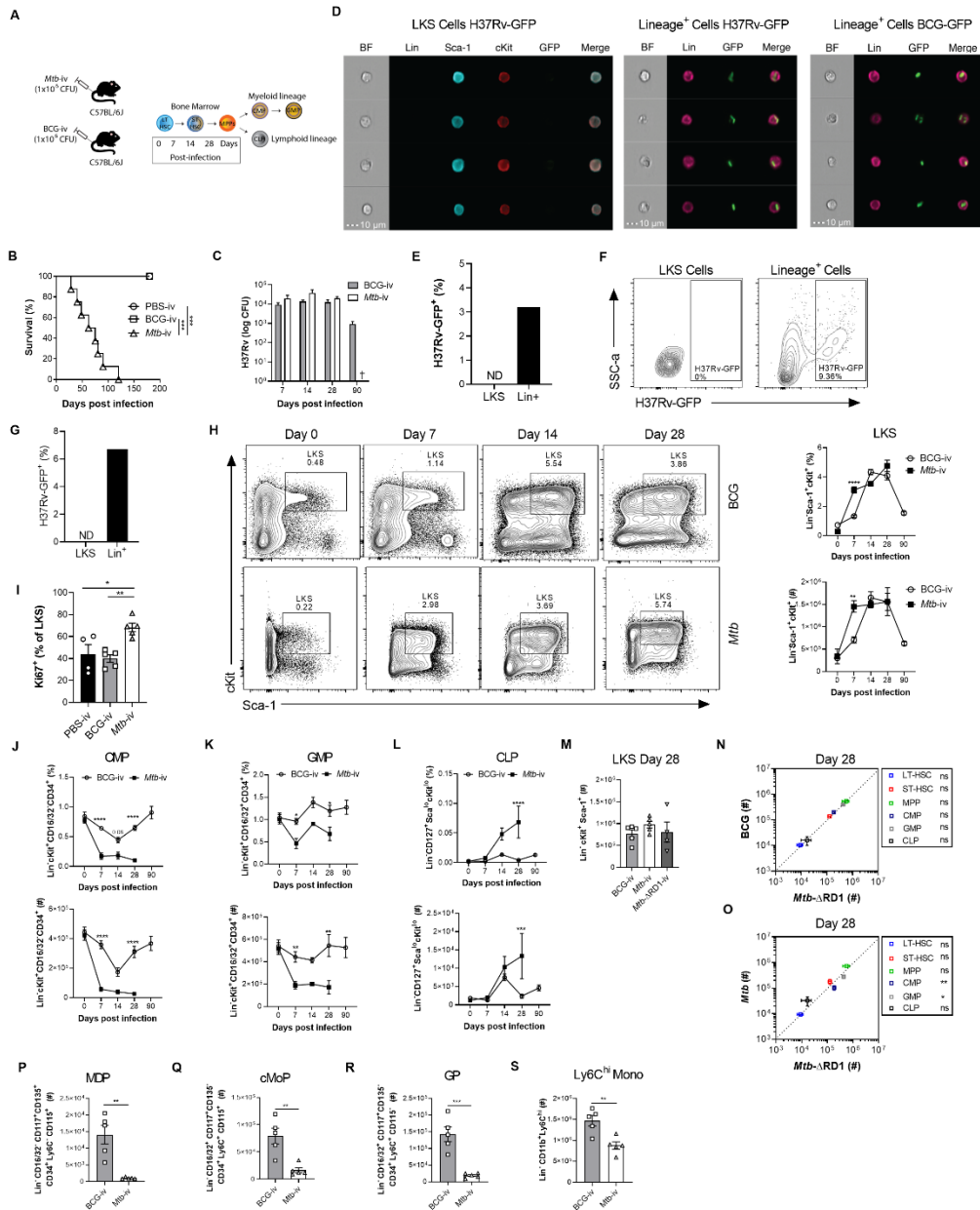


Figure 4.8.1. Systemic *Mtb* infection induces HSC expansion and suppress myelopoiesis. (A) Schematic of BCG-iv vaccination and *Mtb*-iv infection. (B-C; H-S) Mice were infected with *Mtb*, *Mtb*- Δ RD1, or vaccinated with BCG (1×10^6), intravenously. (B) Survival of WT mice after BCG vaccination or infection with *Mtb* ($n=6-8$ mice per group). (C) Kinetics of BCG and *Mtb* bacterial loads in the BM ($n=4-10$ mice/group). (D-G) BM cells were infected with H37Rv-GFP or BCG-GFP for 4 hours *in vitro* (MOI 3). (D) ImageStream analysis of H37Rv-GFP or BCG-GFP infected cells (BF=bright field) as quantified in (E). (F) Flow cytometry analysis of *in vitro* H37Rv-GFP infected BM cells (MOI 3) and quantified in (G), numbers in proximity to gates represent frequency of parent population. (H) Representative FACS plots and quantifications of LKS populations in the BM of BCG-iv vaccinated or *Mtb*-iv infected mice. Percentages listed are of single viable cells ($n=4-8$ mice/group). (I) Frequency of Ki67⁺ LKS cells in the BM of BCG-iv vaccinated or *Mtb*-iv infected mice at d7 post-injection. (J-L) Kinetics of the frequency among single viable BM cells (top panels) and total cell counts (bottom panels) of the CMP, GMP and CLP in the BM of BCG-iv vaccinated or *Mtb*-iv infected mice ($n=4-13$ mice/group). (M) Total cell counts of LKS population; (N-O) LT-HSC, ST-HSC, MPP, CMP, GMP and CLP in the BM of BCG-iv vaccinated and *Mtb*- Δ RD1 (N) or *Mtb* and *Mtb*- Δ RD1 infected mice (O) at d28 post-infection. (P-S) Total cell counts of downstream progenitors MDP (P); cMoP (Q); GP (R) and Ly6C^{hi} monocytes (S) in the BM at day 28 post BCG-iv vaccination or *Mtb*-iv infection. Means are represented as \pm SEM. * $p < 0.05$, ** $p < 0.01$, *** $p < 0.001$, **** $p < 0.0001$ via log-rank test (B), Two-way ANOVA followed by Sidak's Multiple Comparisons Test (C, H, J-L), or One-way ANOVA followed by Tukey's Multiple Comparison Test (I, M), Two-tailed Student's T-Test (N-S). In I, M and P-S, each symbol represents an individual animal.

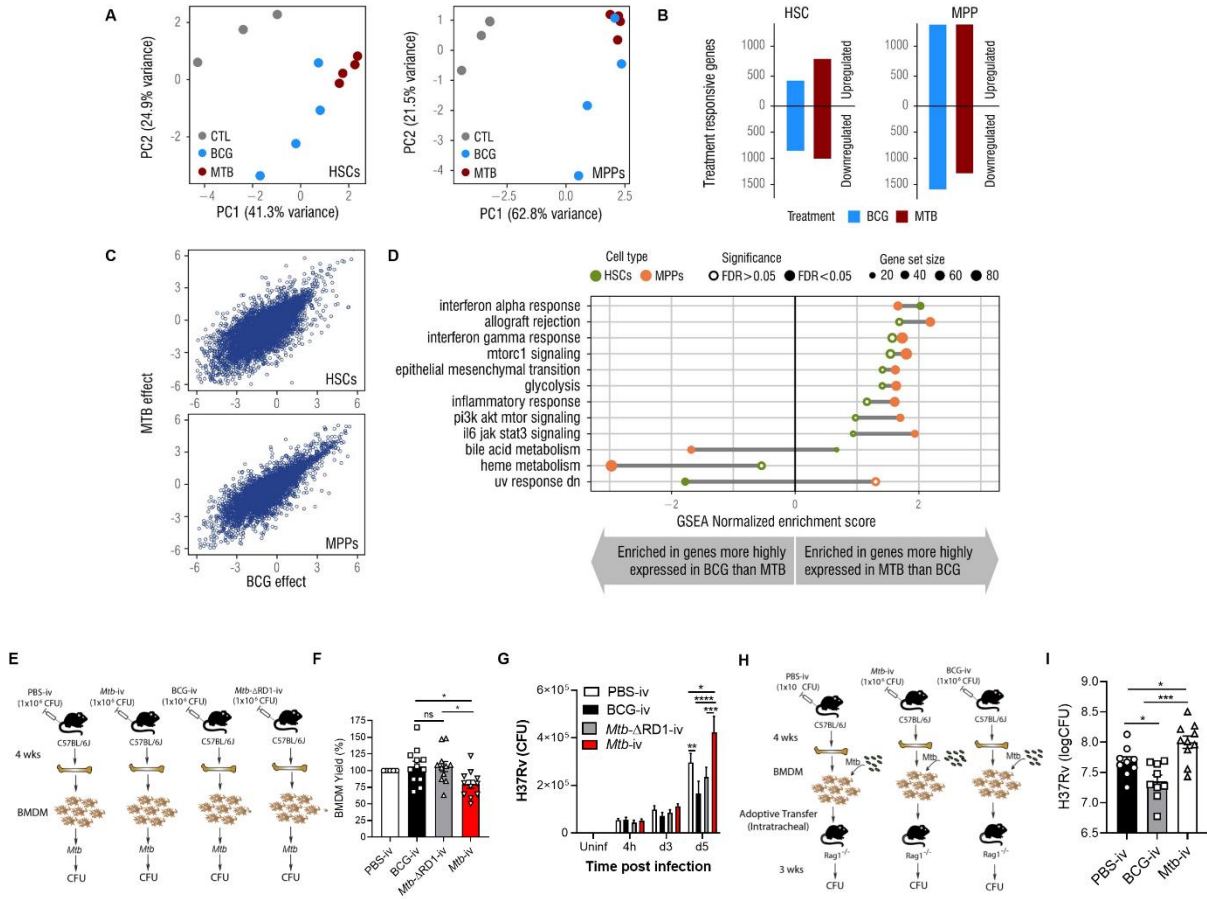


Figure 4.8.2: *Mtb-iv* imprints a unique transcriptional signature in HSCs and detrimentally trains BMDM (A) Principal component analysis of gene expression data collected from HSCs and MPPs isolated from the BM of PBS, BCG-iv (1×10^6) or *Mtb-iv* (1×10^6) infected mice, after 4 weeks infection. (B) Number of genes differentially up or down-regulated in response to BCG-iv or *Mtb-iv* infection, in HSC and MPP (FDR < 0.01). (C) Scatter plots of genome-wide effect sizes of BCG vs *Mtb* infection in HSC (up) and MPP (down). (D) Gene set enrichment analyses of genes differentially expressed between *Mtb* and BCG (FDR < 0.1). (E) Schematic representation of the experimental design of *in vitro* infection of BMDM. BM cells from 4 weeks-post BCG-iv, *Mtb-iv*, *Mtb-ΔRD1-iv* or PBS-injected mice were differentiated into macrophages in the presence of anti-TB drugs to kill any residual bacteria. (F) Relative yield of BMDM from BCG-iv vaccinated, *Mtb-iv* and *Mtb-ΔRD1-iv* infected mice. (G) CFU from *in vitro-Mtb* infected BMDM (H37Rv; MOI 1), determined at different time points after infection ($n=7-10$ mice/group). (H) Schematic representation of adoptive transfer model of macrophages. BMDM were differentiated from 4-week BCG-iv vaccinated, *Mtb-iv* infected or PBS-iv injected mice in presence of anti-TB drugs to kill any residual bacteria. BMDMs were then infected with *Mtb* (H37Rv; MOI 0.2) and subsequently 0.5×10^6 BMDMs were adoptively transferred (intratracheally) into *Rag1*^{-/-} mice (I) Bacterial burden in the lungs of *Rag1*^{-/-} mice after 3 weeks of adoptive transfer of *Mtb*-infected BMDM ($n=8-10$ mice/group). Means are represented as \pm SEM. * $p < 0.05$, ** $p < 0.001$, *** $p < 0.0001$. (F, I) one-way ANOVA followed by Tukey's Multiple Comparison Test. (G) Two-way ANOVA followed by Sidak's Multiple Comparisons Test. Data shown are pooled from 2-3 independent experiment. In F and I each symbol represents an individual animal.

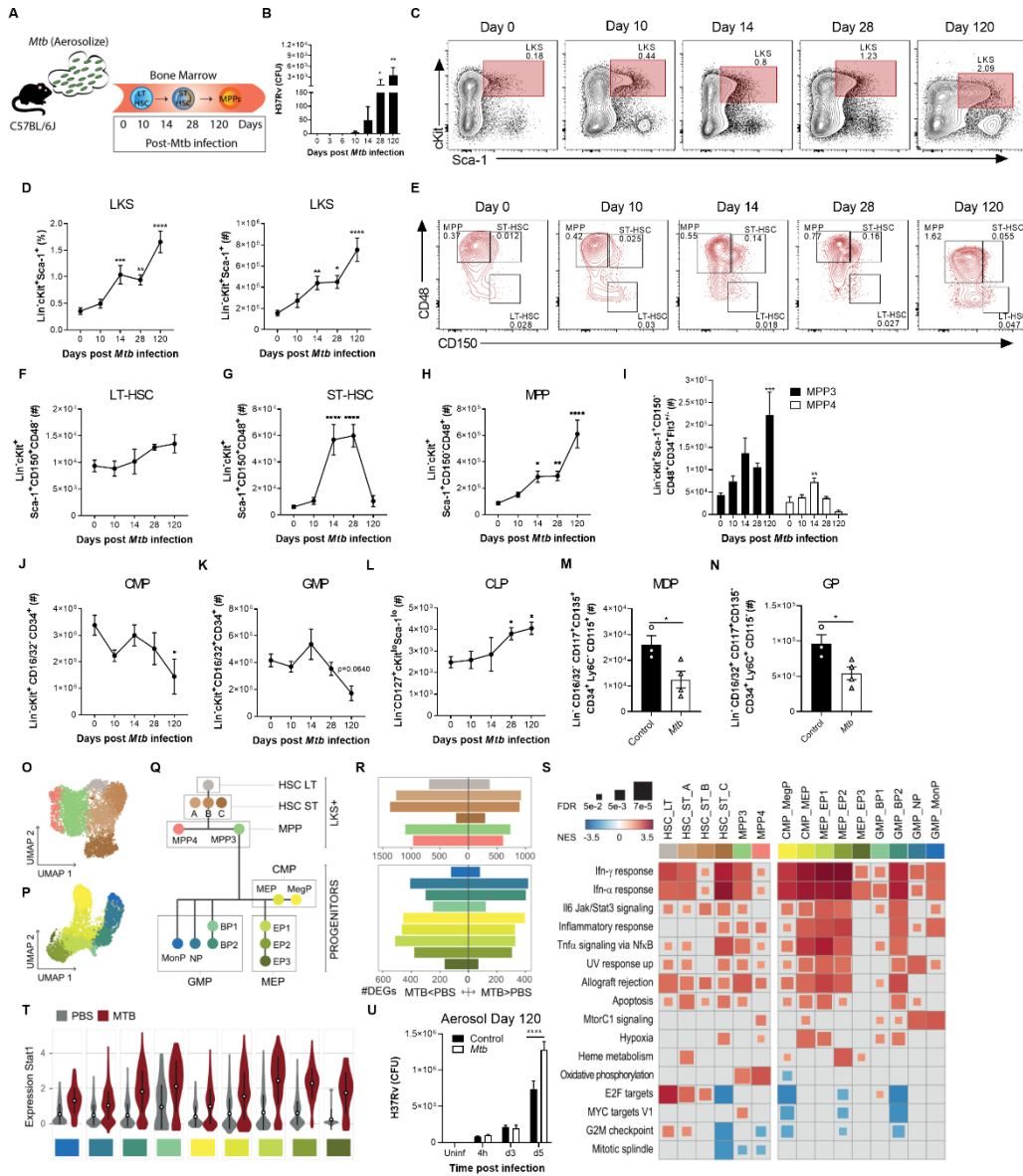


Figure 4.8.3. *Mtb* disseminates to the BM and induces LKS expansion following aerosolized infection. (A) Schematic of aerosol *Mtb* infection. (B-N, U) Mice were infected with *Mtb* through the aerosol route with the deposition of 50-100 CFU per mouse. (B) CFU of *Mtb* growth in the BM. (C) Representative FACS plots of the LKS population in the BM of *Mtb* infected mice as quantified in (D) as frequency of single viable cells (left panel) and total number of LKS population (right panel). (E) Representative FACS plots of frequencies LT-HSC, ST-HSC and MPP in the BM of *Mtb* infected mice. Kinetics of the total number of LT-HSC (F); ST-HSC (G); MPP (H); MPP3/MPP4 (I) in the BM of *Mtb* infected mice (n=4-10 mice/group). (J-L) Kinetics of the total cell counts of the CMP (J), GMP (K) and CLP (L) in the BM of *Mtb* infected WT mice (n=4-8 mice/group). Total cell counts of downstream myeloid progenitors MDP (M); GP (N) in the BM of *Mtb* infected mice at day 120 post-infection (n=3-4 mice/group). (O-P) UMAP dimensionality reduction plots for LKS+ and myeloid progenitor cells, respectively. (Q) Schematic hematopoietic tree diagram showing the approximated position of the different clusters identified (cluster specific color code common to panels O-T). (R) Number of genes up- and down-regulated by *Mtb* in each cluster (abs(logFC)>0.1 & FDR<0.05) (S) Gene Set Enrichment Analyses in genes ranked according to *Mtb* effects in each cluster (from most significant up-regulation -red- to most significant down regulation -blue-). (T) Stata1 expression across clusters and treatments. (U) BM cells were differentiated into macrophages from 120 days post-*Mtb* infected mice. CFU from *in vitro*-*Mtb* infected BMDM (H37Rv; MOI 1), determined at different time points after infection (n=3 mice/group). In C the LKS population is highlighted in red and sub-gated in E. For C and E, the frequency in proximity to the gate represent that population's percentage of single viable cells. Means are represented as \pm SEM. *p<0.05, ***p<0.001, ****p<0.0001. (B, D, F-L) via One-way ANOVA followed by Tukey's Multiple Comparisons Test and (U) Two-way ANOVA followed by Sidak's Multiple Comparisons Test. (M-N) Two-tailed Student's T-Test. In M-N each symbol in bar graph represents an individual animal.

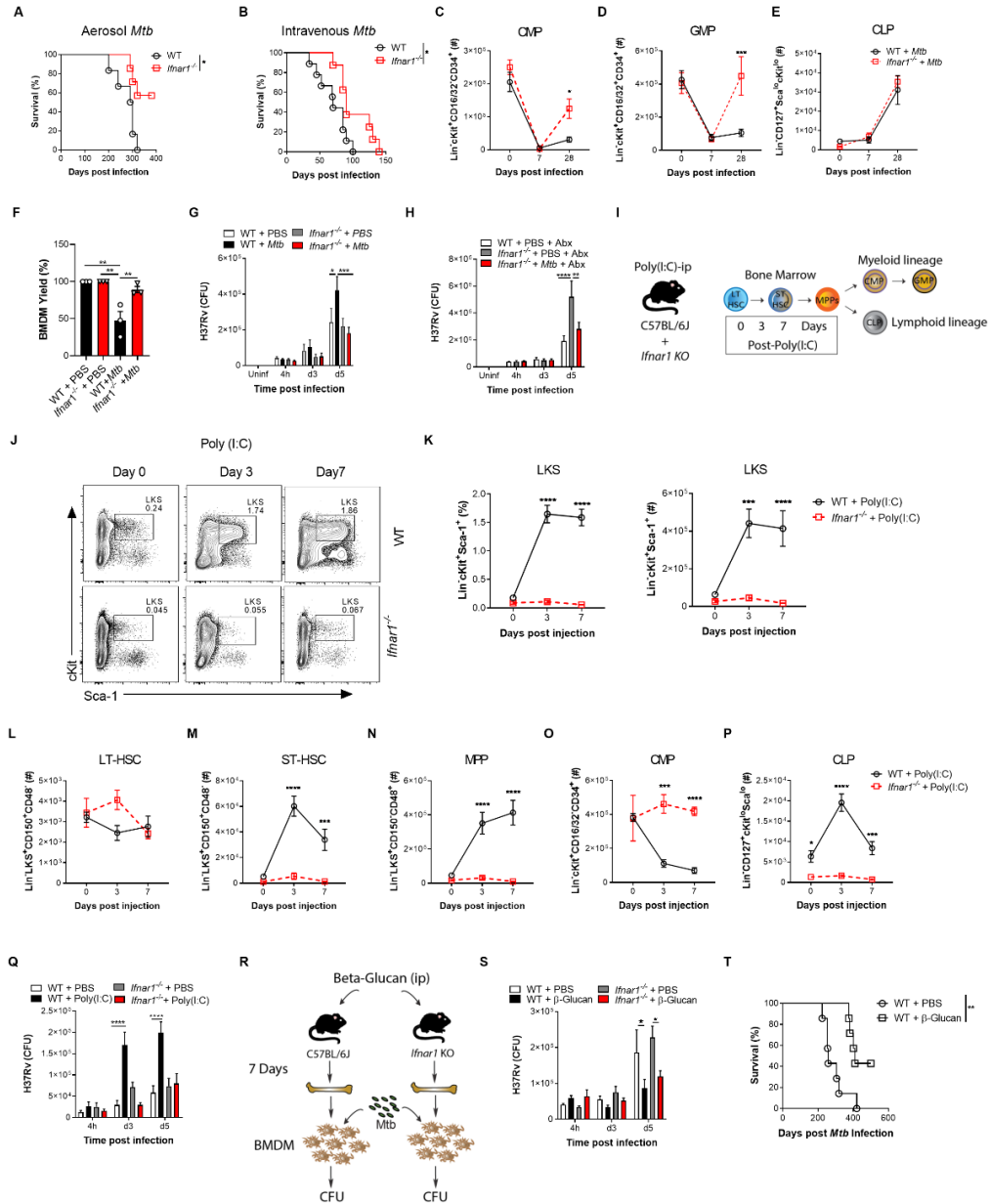


Figure 4.8.4: *Mtb* suppresses myelopoiesis and impairs innate training in an IFN-I-dependent manner. (A-B) Survival of C57BL/6J WT and *Ifnar1*^{-/-} mice after H37Rv infection via the aerosol (deposition of 50-100 CFU in lungs) (A) or intravenous (1×10^6) (B) route. Kinetics of the total cell counts of CMPs (C), GMPs (D) and CLPs (E) in BM of *Mtb*-iv infected WT or *Ifnar1*^{-/-} mice. (F) Relative yield of BMDM differentiated from the BM cells of *Mtb*-iv infected WT and *Ifnar1*^{-/-} mice after 28 days of *in vivo* infection. (G) BMDM were infected (MOI 1) and CFU were determined at different time points after infection. (H) 4-week *Mtb*-iv or control PBS mice were treated with anti-mycobacterial drugs (INH and RIF, labelled "+Abx") for 4 weeks. BMDM derived from the BM cells of these mice were infected with *Mtb* (H37Rv; MOI 1) and the number of CFU was determined at different time points after infection. (I) Schematic representation of Poly (I:C)-treatment model. WT and *Ifnar1*^{-/-} mice were treated with Poly (I:C) i.p. at day 0, 2, 4, 6. (J) Representative FACS plots of the frequencies of the LKS in the BM of PBS or Poly (I:C) treated WT and *Ifnar1*^{-/-} mice with frequencies in proximity to the gate representing the percentage of cells in that gate as a percentage of single viable cells. (K) Frequencies among single viable BM cells (left panel) and total cell counts (right panel) of LKS in PBS or Poly (I:C) i.p. treated mice. (L-P) Total cell counts of LT-HSCs (L), ST-HSCs (M), MPPs (N), CMPs (O) and CLPs (P) in PBS or Poly (I:C) i.p. treated WT and *Ifnar1*^{-/-} mice. (Q) CFU was determined at different time points following H37Rv infection (MOI 1) of WT and *Ifnar1*^{-/-} mice following Poly (I:C) or PBS injection. (R) Schematic representation of β-Glucan treated model. WT mice were treated with the β-glucan at day 0 and day 3. (S) CFU from H37Rv-infected (MOI 1) BMDM of WT and *Ifnar1*^{-/-} mice following PBS or β-Glucan injection. (T) Survival of β-glucan treated mice with aerosol *Mtb* infection. Means are represented ± SEM. * $p < 0.05$, ** $p < 0.01$, *** $p < 0.001$, **** $p < 0.0001$. (A-B, T) Log-rank test. (C-E, G-H, K-Q, S) Two-way ANOVA followed by Sidak's Multiple Comparisons Test. (F) One-way ANOVA followed by Tukey's Multiple Comparisons Test. In F each symbol in bar graph represents an individual animal.

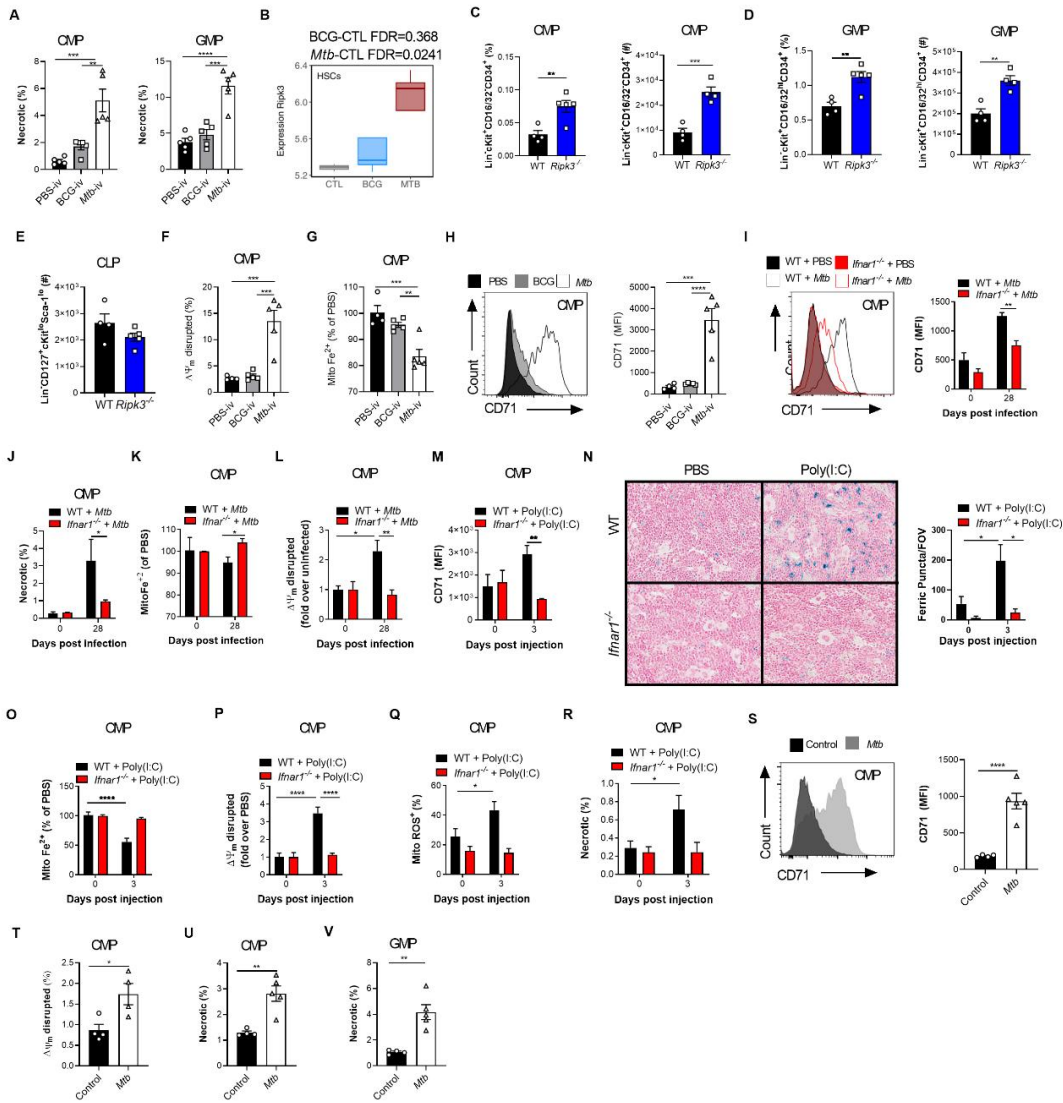


Figure 4.8.5: IFN-I regulates the iron metabolism of myeloid progenitors and triggers the cell death. (A) Frequencies of necrotic (NucSpot⁺ AnnexinV)⁺ CMP (left panel) and GMP (right panel) in the BM of BCG-iv vaccinated and *Mtb*-iv infected mice at day 7. (B) Boxplot panel: Log₂(cpm) expression levels of *Ripk3* in HSC isolated from the BM of PBS-iv, BCG-iv or *Mtb*-iv infected mice. (C-E) Frequency among single viable BM cells and total cell counts of CMP and GMP (C-D); total cell counts of CLP (E) in the BM of *Mtb*-iv infected *Ripk3*^{-/-} mice at day 7. (F) Frequency of CMP with disrupted mitochondrial membrane potentials in the BM of BCG-iv vaccinated and *Mtb*-iv infected mice at day 7. (G) Relative accumulation of Fe²⁺ iron dye in the mitochondria of CMP in the BM of BCG-iv vaccinated and *Mtb*-iv infected mice at day 7. (H) Representative histograms (left panel) of the expression of CD71 on CMP of BCG-iv or *Mtb*-iv infected mice and quantified in the right panel at day 7. (I) Representative histograms (left panel) of CD71 expression on CMP in the BM of *Mtb*-iv infected WT and *Ifnar1*^{-/-} mice following 28 days of infection as quantified on the right. (J) Frequencies of necrotic (NucSpot⁺ AnnexinV)⁺ CMP in the BM of *Mtb*-iv infected WT and *Ifnar1*^{-/-} mice following 28 days of infection. (K) Relative accumulation of Fe²⁺ iron dye in the mitochondria of CMP in the BM of *Mtb*-iv infected WT and *Ifnar1*^{-/-} mice following 28 days of infection. (L) Frequency of CMP with disrupted mitochondrial membrane potentials in the BM of *Mtb*-iv infected WT and *Ifnar1*^{-/-} mice following 28 days of infection. (M) Expression of CD71 on CMP in the BM of Poly (I:C) or PBS treated WT and *Ifnar1*^{-/-} mice. (N) Perls' Prussian Blue staining to show ferric deposition in the BM. Quantification of ferric puncta from the BM of WT and *Ifnar1*^{-/-} mice treated with Poly (I:C) at day 3. (O) Relative accumulation of iron dye (Fe²⁺) in the mitochondria of CMP in the BM of WT and *Ifnar1*^{-/-} mice treated with Poly (I:C). (P) Frequency of CMP with disrupted mitochondrial membrane potential (P), or positive for mitochondrial ROS (Q) or necrotic (NucSpot⁺ AnnexinV)⁺ in the BM of WT and *Ifnar1*^{-/-} mice treated with Poly (I:C). (S) Representative histograms (left panel) of CD71 expression on CMP in the BM of *Mtb* infected mice following 120 days of aerosol infection as quantified on the right. (T) Frequency of CMP with disrupted mitochondrial membrane potentials in the BM of *Mtb* infected mice following 120 days of aerosol infection. Frequencies of necrotic (NucSpot⁺ AnnexinV)⁺ CMP (U) and GMP (V) in the BM of *Mtb* infected mice following 120 days of infection. Means are displayed ± SEM. *p<0.05, **p<0.01, ***p<0.001, ****p<0.0001. (A, F-H) One-Way ANOVA followed by Tukey's Comparison Test, (C-E; S-V) Two-tailed Student's T-Test or (I-R) Two-Way ANOVA followed by Sidak's, Tukey's or Dunnett's Multiple Comparisons Test. In A, C-H and S-V each symbol in bar graph represents an individual animal.

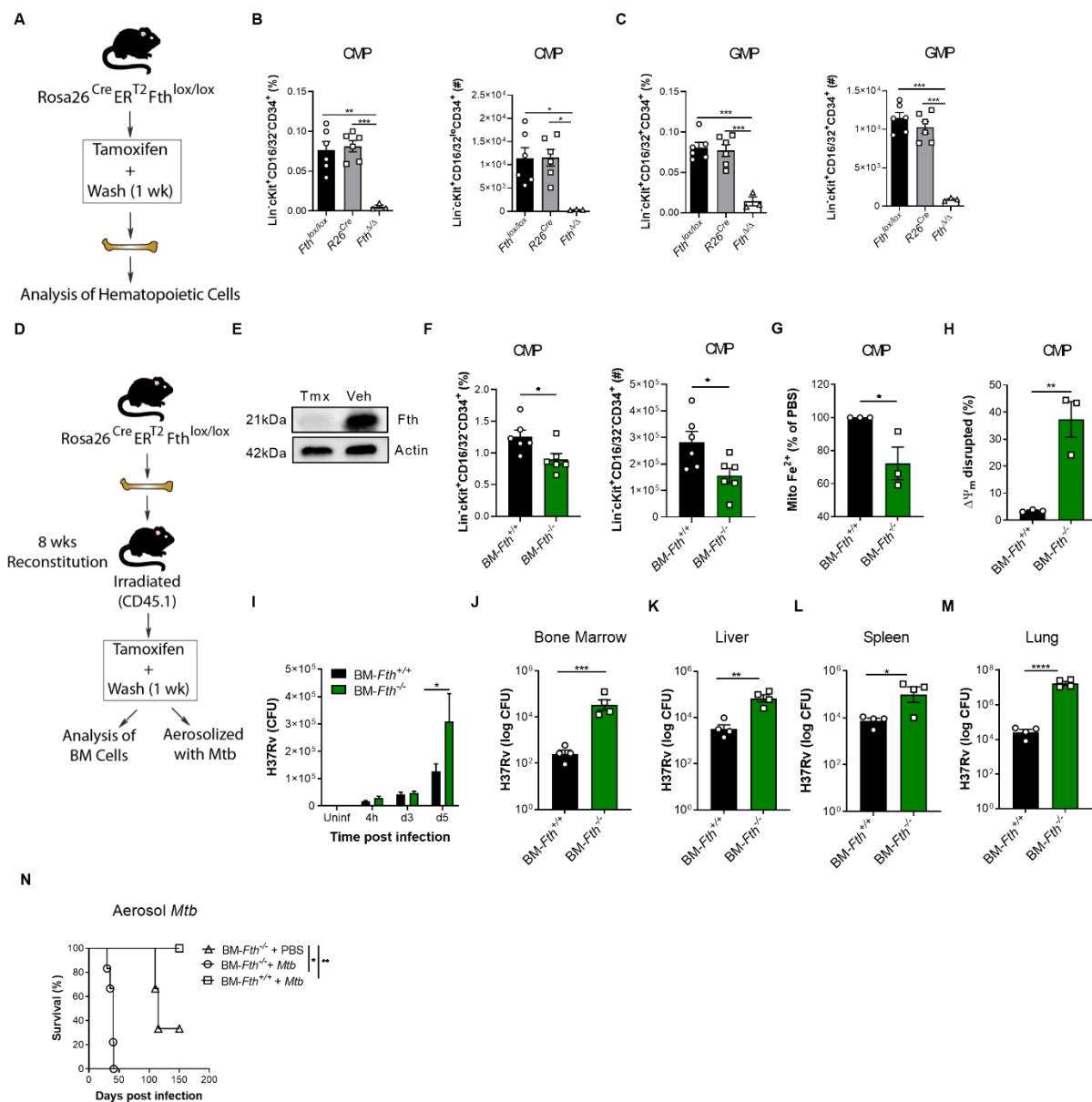


Figure 4.8.6: Iron dysregulation in the BM promotes the susceptibility to TB. (A) Schematic of the generation of *Fth*^{Δ/Δ} mice. (B-C) Frequency and number of CMPs (B) and GMPs (C) in the BM of *Fth*^{Δ/Δ} mice. (D) Schematic of the generation of BM-*Fth*^{-/-} chimeric mice. 8 weeks after reconstitution, mice were treated with tamoxifen for 5 days. (E) Immunoblot of ferritin expression in the BM cells of chimeric mice post-tamoxifen or vehicle control treatment. Actin was used as a loading control. (F) Frequency (left panel) among BM cells and total cell counts (right panel) of CMPs in the BM-*Fth*^{+/+} or BM-*Fth*^{-/-} chimeric mice. Relative accumulation of iron (Fe²⁺) in mitochondria (G) or disrupted mitochondria (H) in the CMPs of BM-*Fth*^{+/+} or BM-*Fth*^{-/-} mice. (I) BMDM derived from the BM cells of BM-*Fth*^{+/+} or BM-*Fth*^{-/-} mice were infected with *Mtb* (H37Rv; MOI 1) and the number of CFU was determined at different time points after infection. (J-N) BM-*Fth*^{+/+} or BM-*Fth*^{-/-} chimeric mice were infected with *Mtb* through aerosol route. Bacterial burden in the BM (J), liver (K), spleen (L) and lung (M) of BM-*Fth*^{+/+} or BM-*Fth*^{-/-} chimeric mice day 28 post aerosol *Mtb* infection. (N) Survival of aerosol-infected BM-*Fth*^{+/+} or BM-*Fth*^{-/-}. Means are represented ± SEM. *p<0.05, **p<0.01, ***p<0.001, ****p<0.0001 determined by One-way ANOVA followed by Tukey's Multiple Comparison Test (B-C), Two-tailed Student's T-Test (F-H; J-M), Two-way ANOVA followed by Sidak's Multiple Comparison Test (I) or log-rank test (N). In figures B-C, F-H and J-M each symbol represents an individual mouse.

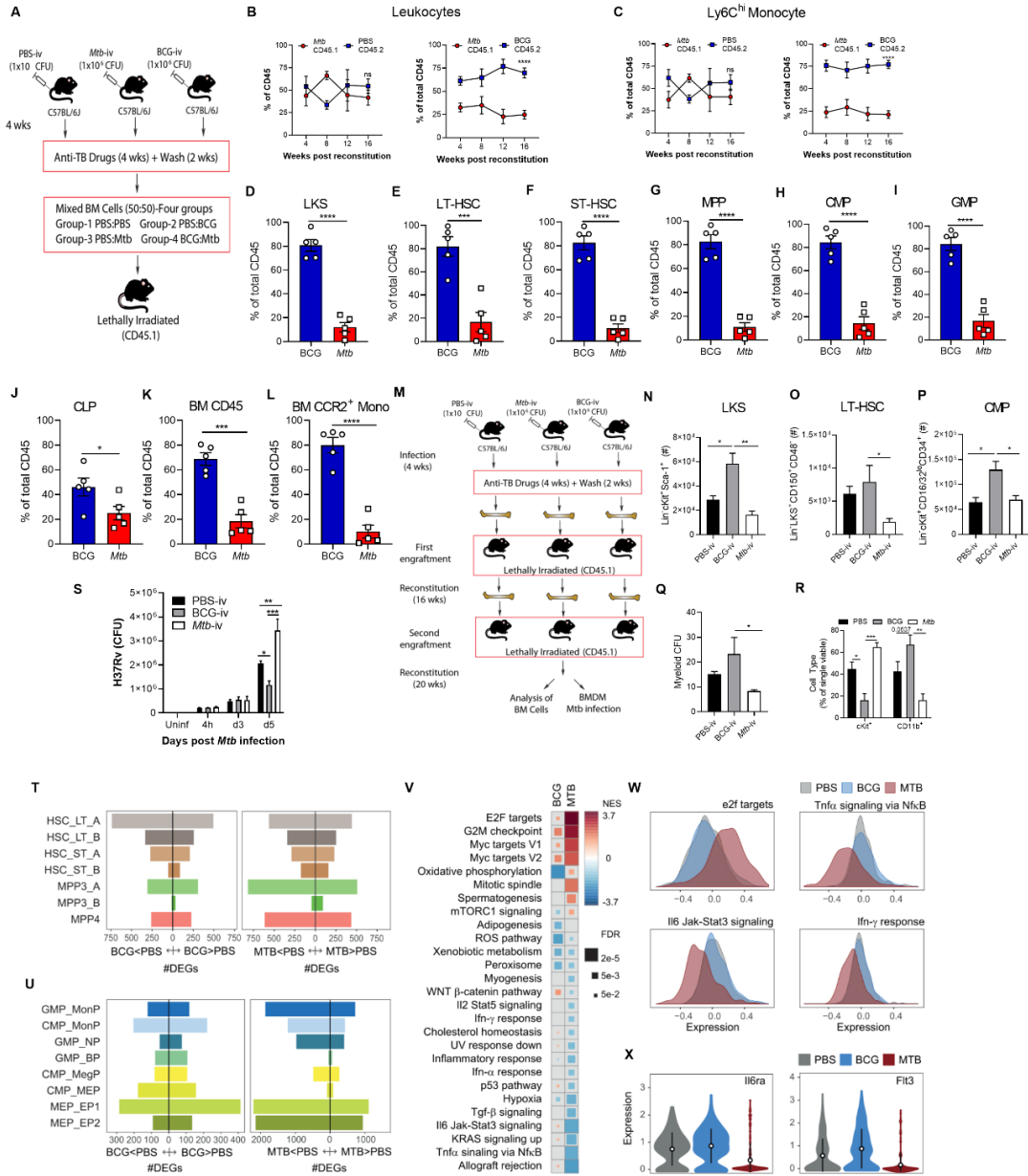


Figure 4.8.7: *Mtb-iv* infection causes BM exhaustion and has long-term negative effects on BMDM training. (A) Model of the mixed chimera experimental plan. (B-C) At 4-week intervals post-reconstitution, leukocytes from the peripheral blood were phenotyped by flow cytometry and expressed as percentage of total blood leukocytes (CD45.1⁺ versus CD45.2⁺ as a frequency of total CD45⁺ cells). (D-L) After 16 weeks of reconstitution, mice were sacrificed and their BM phenotyped to compare frequencies of donor HSC, progenitor and effector cells. Percentages are expressed as a frequency of total CD45⁺ cells. (M) Schematic of secondary engraftment experiment. Following 20 weeks of secondary reconstitution, BM were harvested and the total LKS (N), LT-HSC (O) and CMP quantified (P). (Q-R) 5000 BM cells were cultured in MethoCult media. After 10-12 days, total CFU were counted (Q) and CFU were harvested and phenotyped by flow cytometry ®. (S) BMDM from each group were differentiated from BM cells and infected *in vitro* with *Mtb* (H37Rv; MOI 1) and CFU were quantified at the indicated time points. (T-U) Number of genes up and down-regulated by *Mtb* and BCG in each cluster (abs(logFC)>0.1 & FDR<0.05) of LKS (T) and myeloid progenitor cells (U) Gene Set Enrichment Analyses in genes ranked according to BCG (left column) or *Mtb* effects (right column) in the monocytes precursors cluster (GMP_MonP), from most significant up-regulation -red- to most significant down regulation -blue-. (W). Distribution of expression levels in the monocyte precursor cluster (GMP_MonP) for gene set average markers in four different Hallmark gene sets that show differences between treatments. (X) Expression of Il6ra and Flt3 in the GMP_MonP cluster. Means are represented ± SEM. *p<0.05, **p<0.01, ***p<0.001, ****p<0.0001. Two-way ANOVA followed by Sidak's Multiple Comparison Test (B and C; R and S), One-way ANOVA followed by Tukey's Multiple Comparison Test (N-Q), Two-tailed Student's T-Test (D-L). In B and C, only significant differences occurring at 16 weeks were labelled. In D-L and N-P each symbol represents a unique mouse and in Q each symbol is a replicate of 5000 cells/mouse.

PREFACE TO CHAPTER 5

As introduced in chapter 1, the influenza vaccine fails to provide reliable protection through the conventional strategy of generating long-lived homologous memory responses, due in part to the highly mutative nature of influenza viruses. Despite some recent advances in universal vaccine design by targeting different, more conserved components of the virus, as of yet no approved alternative exists. Therefore, novel vaccination strategies that afford better and longer-lived protection are urgently needed. In chapter 4, we investigated the induction of trained immunity and uncovered how BCG and β -Glucan protect against virulent *Mtb* infection through reprogramming of HSCs to promote myelopoiesis and trained immunity. Interestingly, BCG vaccination is known to non-specifically protect against other infectious diseases in humans and experimental models (480). We hypothesized that inducers of trained immunity could, therefore, act as vaccines against IAV. Using our established BCG and β -Glucan immunization models, we found that both protected against lethal IAV infection, via host resistance and disease tolerance, respectively. Although the mechanisms of this protection are future directions of study, BCG vaccination generated a unique subset of CX₃CR1 effector memory T-cells that homed to lung and responded to infection. Alternatively, BMDM from BCG-vaccinated mice exhibited trained immune responses against *in vitro* IAV infection. Taken together, inducers of trained immunity are intriguing novel vaccine candidates against IAV, perhaps through a combination of trained innate and adaptive responses.

CHAPTER 5:

**Trained immunity as a vaccination strategy against influenza A
virus infection**

Trained immunity as a vaccination strategy against influenza A virus infection

Jeffrey Downey¹ and Maziar Divangahi¹

1. Department of Medicine, Department of Pathology, Department of Microbiology & Immunology, McGill University Health Centre, McGill International TB Centre, Meakins-Christie Laboratories, McGill University, 1001 Decarie Boulevard, Montreal, Quebec, H4A 3J1, Canada.

Corresponding Author:

Maziar Divangahi, Ph.D.

Associate Professor of Medicine

RI-MUHC, Centre for Translational Biology

Meakins-Christie Laboratories

1001 Decarie Blvd,

Block E (EM3.2248)

Montreal, Quebec H4A 3J1

Tel: (514) 934-1934 Ext. 76431

e-mail: maziar.divangahi@mcgill.ca

Manuscript in preparation for submission

5.1: Summary

Vaccination is essential in disease prevention. Currently commercialized influenza vaccines that target the adaptive system fail to provide consistent and robust protection. Here, we explore the possibility of harnessing the power of trained immunity in vaccine against IAV.

5.2: Abstract

Effective vaccines provide the greatest hope for disease control and eradication. Currently licensed vaccines aim to generate long-term protective memory responses by priming the adaptive response and are responsible for saving millions of lives per year. However, conventional strategies targeting highly specific adaptive immune responses have failed to consistently provide an effective vaccine against influenza viruses, due in large part to yearly strain variation of the viruses, and attempts to generate a more universal vaccine have yet to fully materialize. This suggests that new strategies are warranted. Here, we show that prophylactic administration of inducers of trained immunity Bacillus Calmette–Guérin (BCG) and β -Glucan are protective against H1N1 influenza A virus (IAV) infection. BCG generated a subset of CX₃CR1-expressing T-cells that responded to IAV, as well as promoted trained macrophage responses. Further study is required to understand the exact nature of this protection, but our results provide evidence into the potential for trained immune in vaccine design.

Keywords: Influenza, vaccination, trained immunity, BCG, β -Glucan

5.3: Introduction

Seasonal influenza epidemics are responsible for substantial global health and economic burden, resulting in approximately 1 billion infections, 3-5 million cases of severe illness and between 300 000 and 500 000 deaths, primarily concentrated in those over 65 or under 2 (27). The major disease-causing influenza viruses are two influenza A viruses (IAV), an H3N2 and an H1N1, descendants of the 1968 and 1991 pandemics, respectively; and two influenza B viruses (IBV): Yamagata and Victoria (481). Because of the ability to undergo antigenic shift and cause pandemics, IAV remains the greatest threat to human health. To combat influenza infections, global vaccination campaigns exist and each year coverage reaches between 50 to 60% of recommended individuals in the United States, totaling between 162 and 169 million doses (482). Several vaccination types are routinely used, including inactivated influenza vaccine (IIV) and live attenuated influenza vaccines (LAIIV) with recommendations for different age groups varying per region. These vaccines can either target both IAVs and a single IBV (trivalent), or both IAVs and IBVs (quadrivalent) (483). Yet, despite the substantial coverage and various options, effectiveness of the vaccine is usually low and variable, having been only 36% effective during the 2017-2018 season (482). This low effectiveness is likely due to a combination of factors, including strain mismatch and poor immunogenicity, especially in older populations where the disease is most severe (484, 485). Thus, improved vaccines are needed against influenza viruses.

Traditional influenza vaccine efficacy is measured primarily by its ability to generate neutralizing IgG against the hemagglutinin (HA) protein. However, this is a highly mutative region that is also poorly conserved between IAV subtypes (i.e. H3 versus H1) and, thus, necessitates yearly vaccination and multivalent formulas. Longer-lived and more universal vaccines better targeting the conserved stalk region of the HA protein, the neuraminidase (NA) protein, or cytotoxic T-cell responses against the well-conserved nucleoprotein (NP) have been explored (486). Today, clinical trials are ongoing with a stalk-targeting nanoparticle vaccine (487). Yet, to date no alternative vaccine has been approved for human use nor shown to be broadly protective. Ideal vaccine candidates would, therefore, already be approved for human use and universal in their protection to influenza and potentially other infections.

The innate immune system historically has been precluded from vaccine design due to its perceived lack of memory. Observation that innate immune cells can exhibit enhanced secondary memory responses through epigenetic and metabolic reprogramming, however, opened the door for their potential use in new vaccines (300). This process of innate immune memory is referred to as trained immunity, whereby innate immune cells are epigenetically reprogrammed by an initial stimulus to respond to a secondary and unrelated stimulus more robustly and heighten protection (105). The live vaccine against *Mycobacterium tuberculosis* BCG and the fungal pathogen-associated molecular pattern (PAMP) β -Glucan are prototypical inducers of trained immunity (296, 302, 304, 395). BCG is the most widely deployed vaccine globally and has been shown to lower all-cause mortality in children compared to unvaccinated controls (480, 488). Experimentally, both BCG and β -Glucan have been shown to cross-protect against a variety of pathogens, including influenza (489, 490). However, the mechanism of this protection remains completely unknown.

Early studies on BCG and trained immunity centred upon monocyte/macrophages and their enhanced production of cytokines (e.g. IL-1 β) following the second stimulus (302). Effector leukocytes, like monocyte/macrophages, have a short lifespan, such that the relevancy of this training in vaccine design remained refractory. We recently showed, however, that if BCG accesses the bone marrow via intravenous administration rather than intradermal or subcutaneous, then it can “train” hematopoietic stem cells (HSC). This training is then passed on to further refined progenitor cells in the bone marrow all the way to mature macrophages, making them more protective against subsequent *Mtb* infection (304) and a similar mechanism has been shown for β -Glucan (296, 395). Thus, inducers of trained immunity rewire hematopoiesis and seem to promote myelopoiesis and trained macrophage responses. However, it has also been proposed that heterologous T-cell responses may play a role in the cross-protection of BCG to viral infections (491). As a result, we speculated that the ability of BCG and β -Glucan to cross-protect is due their ability to induce trained innate and/or adaptive responses that protect against subsequent infection. In line with our hypothesis, we observed that both BCG and β -Glucan protected against lethal IAV infection. Finally, we propose that BCG induces trained immunity in macrophages and T-cells that may be responsible for the protection.

5.4: Results & Discussion

BCG and β -Glucan cross-protect against lethal influenza infection via host resistance and disease tolerance, respectively

BCG and β -Glucan have been shown to be protective against a variety of unrelated pathogens through trained immunity; including *Candida albicans*, *Mtb* and an attenuated yellow fever virus (302, 304, 395, 492) in both mice and humans (493). They have equally been suggested to be protective against IAV, although the mechanism for this protection was entirely unexplained (489, 490). Thus, we sought to investigate the role of trained immunity in this protection. To begin, we infected WT mice intravenously vaccinated with BCG for 28 days with a lethal dose (90 PFU) of IAV and monitored morbidity and mortality. Although similar weight loss was observed in both groups (**Fig. 1A**), we observed a significant increase in survival in vaccinated mice (**Fig. 1B**). We found that the protection afforded by BCG against IAV was dependent upon host resistance mechanisms, as we observed a decrease in viral titres in the lung at day 3 post-infection (**Fig. 1C**), as well as a correlative increase in total active IFN-I (**Fig. 1D**) and IFN- β and IFN- α (**Fig. S1A-B**). We also observed that β -Glucan was protective against IAV infection with mice receiving β -Glucan exhibiting less weight loss and enhanced survival (**Fig. 1E-F**). This decreased susceptibility of β -Glucan-treated mice was, in contrast to BCG, not related to a reduction in viral load or enhanced resistance responses, as PBS control mice and β -Glucan-treated mice had similar viral loads and active IFN-I responses (**Fig. 1G-H**).

Interestingly, both BCG and β -Glucan offer significant protection to a subsequent lethal IAV infection. However, they exhibit different mechanisms of protection (i.e. host resistance versus disease tolerance). Our results with β -Glucan offer novel insight into potential protection by vaccines that promote cross-protection via disease tolerance rather than host resistance. Similarly, these results offer potential for β -Glucan to be used independently or as an adjuvant in a conventional vaccine that enhances antiviral memory responses.

BCG vaccination generates a unique subset of CX₃CR1-expressing T-cells that migrate into the lung parenchyma and other tissues

Having established the protective capacity of BCG-iv against IAV infection, we next sought to elucidate cell type(s) responsible for this protection. Previous work has shown that BCG generates a subset of CX₃CR1-expressing T-cells (494). Although these cells are ineffective against *Mtb*, they have been shown to be protective against viral infection (495, 496). Beginning at 2 weeks post-vaccination and continuing until at least 4 weeks, we observed a significant enrichment of CX₃CR1⁺ T-cells in the blood of vaccinated compared to unvaccinated mice (**Fig. 2A-B**). Although both CD8⁺ and CD4⁺ CX₃CR1⁺ were detected in the blood, there was a strong bias switch from CD8⁺ T cells at homeostasis towards CD4⁺ T cells, beginning at 3 weeks post-vaccination (**Fig. 2C**). During *Mtb* infection, these T-cells remain in the vasculature, rather than migrate into the lung parenchyma and, as a result, fail to protect against *Mtb* (494). To see if these cells in the absence of *Mtb* infection home into the lung parenchyma, we performed intravascular CD45.2 staining (497), which allows for the differentiation between leukocytes in the vasculature and those in the parenchyma by *in vivo* and *ex vivo* staining of CD45.2. Double positive leukocytes are present in the vasculature, while those singularly positive are parenchymal (**Fig. 2D**). Using this technique, we found that following vaccination CX₃CR1 T-cells did in fact penetrate the parenchyma and remained there until at least 4 weeks post-vaccination (**Fig. 2E-F**) and they exhibited similar proportions of CD4⁺ and CD8⁺ cells at 4 weeks (**Fig. 2G**). As previously reported (496), at 4 weeks post-vaccination, the vast majority of CX₃CR1⁺ T-cells (both CD8⁺ and CD4⁺) in both the peripheral blood and the lung tissue were T effector memory (T_{EM}) cells, as assessed by CD44^{hi} and CD62L⁻ staining (**Fig. 2H-I**). T_{EM} cells are known for their production of effector cytokines and as such to determine if these CX₃CR1⁺ T-cells were active against heterologous IAV infection, we infected 4-week vaccinated mice and evaluated IFN- γ production by intracellular cytokine staining. At day 3 post-IAV infection, a higher frequency of CX₃CR1⁺ T-cells were positive for IFN- γ in the BCG-vaccinated than control mice, in the presence of PMA and ionomycin (**Fig. 2J**). Finally, we also observed an accumulation of CD8⁺ CX₃CR1⁺ T_{EM} in the bone marrow of vaccinated mice, albeit to a lesser extent than the blood and lung (**Fig. 2K-M**). Interestingly, these cells are known to support the number and differentiation capacity of HSCs in the bone marrow (498). Additionally, as a source of IFN- γ , they may provide the pro-myeloopoiesis

signal that BCG elicits to imprint HSCs to promote trained immunity in other models (304, 498, 499). Certainly, further investigation of this T-cell subset in the bone marrow is warranted.

Taken together these results show that BCG vaccination generates a unique subset of T-cells that express CX₃CR1 and are active against heterologous IAV infection, suggesting they may contribute to control of IAV early upon infection, already being primed in the lung. On the other hand, the polysaccharide PAMP β -Glucan does not generate this population of conventional T-cells (**Fig. S1C**), arguing for alternate methods of protection via disease tolerance in these mice. Although T-cells are usually regarded for antigen-specific responses, the observation that unconventional T-cell responses elicited by BCG may contribute to heterologous protection to pathogens has been proposed (491, 500). In this vein, our findings support the notion that BCG vaccination may cross-protect by promoting unconventional heterologous T-cell responses.

Bone marrow-derived macrophages from BCG-vaccinated mice are trained and exhibit heightened cytokine production against *in vitro* IAV infection

Innate immunity is investigated as the primary mechanism behind trained immunity and heterologous protection, given its non-specific responses to pathogens. To examine any early differences in the innate cellular response to vaccination/infection in the lung, we began by phenotyping the innate compartment of 3-day infected mice that had been vaccinated for 28 days, as well as PBS controls. We observed no differences in the recruited innate cellular response to infection in vaccinated and unvaccinated mice (**Fig. 3A**). However, despite no differences in the quantity of innate immune cells in the lung, trained immunity is demarcated by an enhanced quality of responses to a secondary stimulus rather than quantity. Therefore, given the importance of macrophages in response to IAV (66, 154, 174) and in line with findings by us and others that BCG trains BMDM (302, 304), we wondered if BCG trained macrophages to potentially contribute to immunity against IAV. To assess this, BMDM from 28 day-vaccinated mice were infected with IAV *in vitro* and their cytokine profile investigated. In the absence of infection, vaccinated and unvaccinated macrophages behaved the same; however, upon infection, macrophages from BCG-vaccinated mice elicited a stronger response, producing more TNF- α (**Fig. 3B**) and active IFN-I

(Fig. 3C). Thus, heightened inflammatory and antiviral cytokine responses by trained macrophages may contribute to the protection afforded by BCG against IAV and that the contributory cellular mechanisms to this phenomenon may be multifaceted, requiring both trained innate and adaptive responses.

The recent realization that memory responses are not restricted to the adaptive arm of immunity, but are also conveyed by innate immune cells, has led to a flurry of activity in understanding trained immunity and potentially harnessing its value in a clinical setting. Since then, both BCG (the live attenuated vaccine against *Mtb*) and β -Glucan (a polysaccharide-based PAMP) have emerged as major inducers of trained immunity, with study primarily focussed on *in vitro* stimulation of monocyte/macrophage populations in the heightened response against secondary infection (302, 501). Yet, the ability to exploit trained immunity in long-lasting protection against infection and incorporation into vaccine design seems to be dependent upon the reprogramming of hematopoietic stem cells (HSC), which then transmit this protective signature to effector cells over the course of the host's lifetime (304, 502) through alterations in hematopoiesis (296, 304). In addition to innate responses, non-specific T-cell responses have equally been thought to play a role (491, 500).

Although cross-protection against viruses, including IAV, has been appreciated by BCG and β -Glucan before (489, 490), how this protection occurs is unknown. In this study we sought to determine the potential ability of BCG and β -Glucan to protect against H1N1 IAV infection and if this protection was due to heterologous trained responses of the innate and/or adaptive immune systems. Our results confirm that both BCG and β -Glucan do protect against lethal H1N1 IAV infection. While BCG enhances host resistance responses, β -Glucan protects against IAV by promoting disease tolerance, adding further evidence to the importance of disease tolerance in immunity to infectious diseases (106), as well as novel considerations for vaccine design that canonically focus on enhancing disease tolerance.

Despite the fact our study did not fully ascertain the cell type required for the observed protection of BCG vaccination or β -Glucan administration against IAV, it does suggest that multiple immune cells may be involved from both the innate and adaptive arms. In **Figure 2**, we describe a unique subset of α/β T-cells that are generated in response to BCG vaccination within

the first 2 weeks, which express CX₃CR1 and have a majority T_{EM} profile. These cells exhibited effector function (i.e. IFN- γ production) in the lung during IAV infection, which may contribute directly to viral killing, and also homed to the bone marrow. Interestingly, CD8⁺ T_{EM} cells are known to support HSC function and hematopoiesis (498). Moreover, we have shown the importance of IFN- γ signalling in the bone marrow in promoting HSC expansion and the protective imprinting of HSCs to promote trained macrophage responses (304). It is intriguing to speculate that the generation of this T-cell subset following systemic BCG administration may then provide IFN- γ to imprint HSCs to promote the trained macrophage responses observed in **Fig. 3B-C** that restrict viral replication and/or contribute to wound healing. Certainly, further validation of this concept is required using adoptive transfer models and *Ifngr*^{-/-} or TCR α/β -deficient mice. Additionally, transfer of BCG-trained macrophages into the airways of IAV-infected mice would provide confirmation of their importance in the protective signature of BCG against IAV. Finally, although this study and one by Spencer et al. (489) support cross-protection of BCG against H1N1 IAV, recent work using a highly pathogenic avian influenza (H7N9) virus showed no protection following intravenous BCG administration in mice (503). Thus, it is possible that the ability of BCG to cross-protect against IAV is strain-specific. However, in that study BCG was administered 7 days prior to infection, which precedes the enrichment of the CX₃CR1⁺ T-cells that we observed. More investigation into the strain-specificity of BCG against IAV, as well as longer vaccination periods prior to infection are required to resolve this dichotomy.

Taken together, our results suggest that both live BCG vaccine and the polysaccharide PAMP β -Glucan protect against H1N1 IAV infection, by promoting host resistance and disease tolerance, respectively, as well as providing a potential cellular mechanism for the protection elicited by BCG. Continued study into the nature of both trained innate and adaptive immune responses in response to BCG and β -Glucan will likely contribute to future vaccine design.

5.5: Materials & Methods

Mice. Six- to ten-week old CD45.2 C57BL/6J mice were housed and bred at the RI-MUHC, Montreal, QC, Canada. All animal studies were conducted in accordance with the guidelines of, and approved by, the Animal Research Ethics Board of McGill University (project ID: 5860). Mice were housed under SPF conditions with *ad libitum* access to food and water. Experiments were conducted using male and female sex- and age-matched mice that were randomly assigned to experimental groups.

Bacterial culture. BCG-TICE was grown in 7H9 broth (BD) supplemented with 0.2% glycerol (Wisent), 0.05% Tween80 (Fisher), and 10% albumin-dextrose-catalase (ADC) under constant shaking at 37° C. For experiments, BCG bacteria in log growing phase (OD 0.4 – 0.9) were centrifuged (4000 RPM, 15 minutes) and resuspended in sterile PBS. Single cell suspensions were obtained by passing the bacteria 10-15 times through a 22G needle (Terumo).

Viruses & Infection. All *in vivo* infections were performed using mouse adapted influenza A/Puerto Rico/8/34 (H1N1) virus (IAV), kindly provided by Dr. Jonathan A. McCullers (St. Jude Children Research Hospital). Mice were challenged intranasally (in 25µL PBS) with IAV at a sublethal dose of 50 PFU or a lethal dose (LD₅₀) of 90 PFU. 90 PFU was used for the survival experiments in **Fig. 1B** and **Fig. 1F**. For all other experiments, 50 PFU was used. During survival experiments mice were monitored twice daily for signs of duress and weighed daily. Mice reaching 75% of original body weight were considered moribund and sacrificed. Viruses were propagated and isolated from Madin-Darby Canine Kidney (MDCK) cells and titrated using standard MDCK plaque assays. MDCK cells were obtained from the American Type Culture Collection and maintained in Dulbecco's modified Eagle medium enriched with 10% (*v/v*) FBS, 2 mM L-glutamine and 100 U ml⁻¹ penicillin/streptomycin.

BCG vaccination of mice. Throughout the study, mice were intravenously (iv) vaccinated with BCG-TICE with a dose of 1x10⁶ single-suspended bacteria in 100µl PBS, unless otherwise indicated.

β-Glucan treatment. C57BL/6J mice were treated with 1mg/mouse i.p. of β-glucan (Sigma, catalogue #G5011) at day 0 and day 3. Mice were infected at day 7.

Flow Cytometry. Lung tissues were perfused with 10 mL of PBS, harvested and minced before collagenase digestion (150 U mL^{-1}) for 1 h at 37°C . Lungs were passed on a $40 \mu\text{m}$ nylon mesh, and red blood cells were lysed. Then total cell counts were determined with a haemocytometer, and two to three million cells were used for staining. For peripheral blood staining, the blood was collected by cardiac puncture in a BD Microtainer tube and stained extracellularly; red blood cells were then lysed. For innate and adaptive cells, cells were initially stained with eFluor-506 viability dye in PBS (eBioscience; 20 min; 4°C), washed and surface stained with anti-CD16/32 (BD Biosciences) in 0.5% BSA/PBS solution to block non-specific antibody interactions with Fc receptors (10 min; 4°C). Cells were then surface stained with combinations of PE-CF594-conjugated anti-SiglecF, BUV395-conjugated anti-CD11b, PerCP-eFluor780-conjugated anti-Ly6G, fluorescein isothiocyanate (FITC)- or allophycocyanin (APC)-conjugated anti-Ly6C, APC-eFluor780-conjugated anti-F4/80, BV421-conjugated anti-CD11c, FITC- or BUV395-conjugated anti-CD45.2 or APC-conjugated anti-CD45.1, Pe-Cy7-conjugated anti-CD3, BV786-conjugated anti-CD127, APC- or BUV737-conjugated anti-NKp46, BV421-conjugated anti-CD49b, PE-conjugated anti-CD49a (all from BD BioScience, except anti-Ly6G from eBioscience), or BV-786 conjugated anti-CX3CR1 (BD Bioscience). For experiments involving intracellular cytokine staining (ICS), 2×10^6 lung cells were incubated for 4 hours at 37°C in the presence of PMA/Ionomycin and Brefeldin A (Cell Activation Cocktail; BioLegend) or GolgiPlug control (BD Biosciences). Cells were then stained extracellularly, fixed and permeabilized using BD Cytotfix/Cytoperm (BD Biosciences), before being stained intracellularly for PE-CF594-conjugated anti-IFN- γ (BD Biosciences).

In all experiments, cells were then fixed with 1% PFA for 1 hour, washed and acquired in 0.5% BSA/PBS solution. Flow cytometry acquisition was performed using BD LSRFortessa X-20 (BD Biosciences) with FACSDiva Software version 8.0.1 (BD Biosciences). Analysis was performed using FlowJo software version 10 (Tree Star).

Generation of BMDM. Murine Bone Marrow-Derived Macrophages (BMDM) were isolated following aseptic flushing of tibiae and femurs of eight- to ten-week-old mice. Macrophages were differentiated from bone marrow precursors for 7 days in RPMI-1640 supplemented with 30%

(vol/vol) L929 cell- [American Type Culture Collection (ATCC)] conditioned medium, 10% (vol/vol) FBS, 2 mM L-glutamine, 1 mM sodium pyruvate, 1% essential and nonessential amino acids, 10mM HEPES and 100 U/mL penicillin/streptomycin. *In vitro*, BMDM were seeded in tissue culture plates the day before infection and infections were performed in fresh medium lacking L929 cell-conditioned medium with a multiplicity of infection (MOI) of 0.25.

Total bioactive IFN-I assay. Secretion of total active IFN-I (both IFN- α and IFN- β) in cell culture supernatants was assessed using the B16-Blue IFN- α / β reporter cell line for murine samples or HEK-Blue IFN- α / β reporter for human samples (both from InvivoGen), according to the specifications of the manufacturer. B16 cells were maintained in RPMI supplemented with 10% (v/v) FBS, 2 mM L-glutamine and 100 U ml⁻¹ penicillin/streptomycin.

ELISA. IFN- β / α levels in infected lungs were measured using a VeriKine Mouse IFN- β or IFN- α ELISA kit (PBL Assay Science). TNF- α was measured in tissue culture supernatants (R&D Systems). All measured according to the manufacturer's instructions.

Statistical analysis. Data are presented as means \pm s.e.m. Statistical analyses were performed using GraphPad Prism version 8.0.2 software (GraphPad). Statistical differences were determined using a two-sided log-rank test (survival studies), one-way analysis of variance (ANOVA) followed by Sidak's multiple comparisons test, two-way ANOVA followed by Sidak's or Dunnett's multiple comparisons test, or two-tailed Student's T-Test, as outlined in the Figure Legends. All means are depicted \pm SEM with significance denoted by * p<0.05, ** p<0.01, ***p<0.001, ****p<0.0001.

5.6: Acknowledgements

This work was supported by the Canadian Institute of Health Research (CIHR) Foundation Grant (FDN-143273), the CIHR operating grant (168884) to M.D. M.D. holds a Fonds de Recherche du Québec-Santé (FRQS) Award and the Strauss Chair in Respiratory Medicine. J.D was supported by the Molson Foundation Award and RI-MUHC Studentship.

5.7: Figures

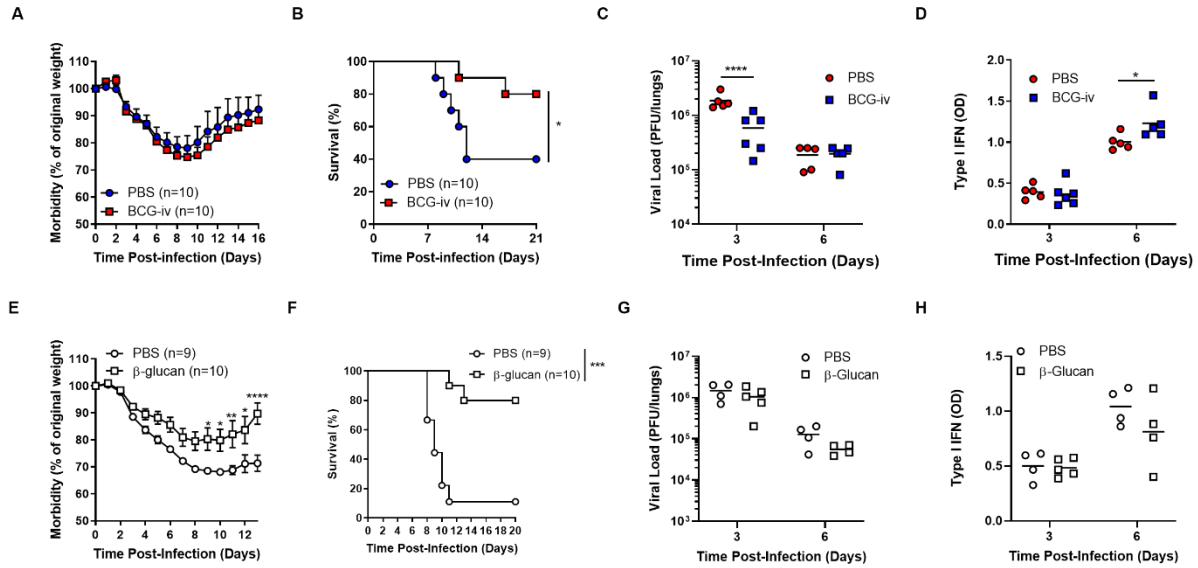


Figure 5.7.1: Inducers of trained immunity provide protection against H1N1 IAV infection. (A-D) Mice were vaccinated for 28 days with BCG and then infected with 90 PFU (A-B) or 50 PFU (C-D) of IAV. Morbidity (A) and mortality (B) of mice following infection. Pulmonary viral loads (C) and active type I IFN (D) at various timepoints post-infection. (E-H) Mice were administered β -Glucan for 7 days and infected with 90 PFU (E-F) or 50 PFU (G-H) and morbidity (E), mortality (F), pulmonary viral loads (G) or active type I IFN (H) were assessed. Means are represented \pm SEM. For survival experiments in A and F differences were determined by Log-rank Test and Two-way ANOVA followed by Sidek's Multiple Comparisons test in all other panels.

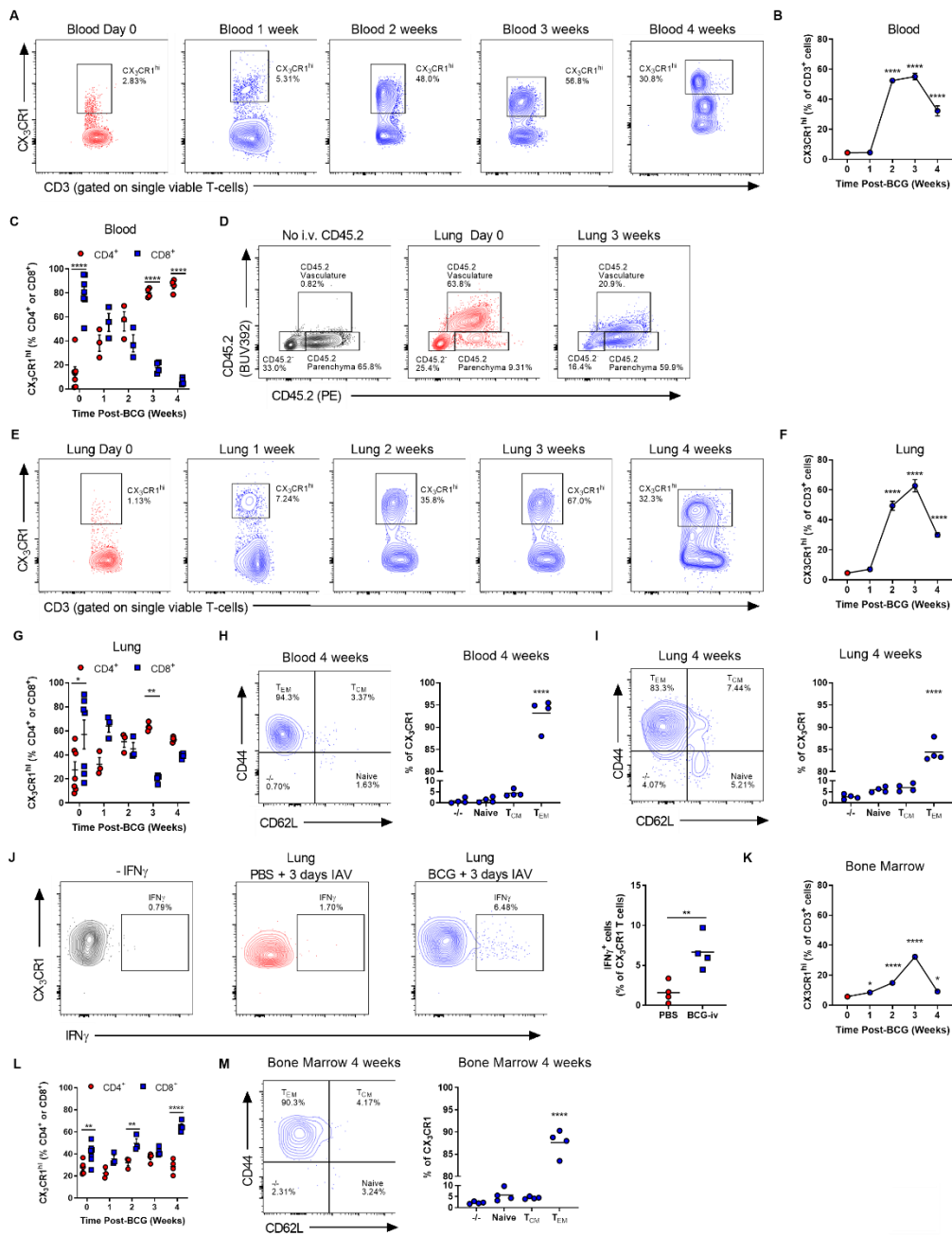


Figure 5.7.2: BCG vaccination generates CX₃CR1-expressing T-cells (A-L) Mice were vaccinated with BCG. (A) Representative FACS plots of CX₃CR1 expression on T-cells at various times in the blood post-vaccination as quantified in (B). (C) Expression of CD4 or CD8 on CX₃CR1 T-cells. (D) Representative FACS plot illustrating differential vasculature/parenchymal staining. (E) Representative FACS plots of CX₃CR1 expression on T-cells at various times post-vaccination in the lung as quantified in (F). (G) Expression of CD4 or CD8 on CX₃CR1 T-cells. Effector profile of CX₃CR1 T-cells in the blood (H) or lung (I). Left panels are representative FACS plots as quantified in the right panels. (J) Production of IFN-γ by CX₃CR1 T-cells in the lung with the left panel representing the FACS enumerated in the right panel. (K) Levels of CX₃CR1 T-cells in the bone marrow and broken down by CD4 and CD8 expression (L) and effector profile (M). Means are represented ± SEM. Differences were determined by One-way ANOVA followed by Tukey's multiple comparisons test in (B, F, K and H, I, M), two-way ANOVA followed by Sidak's multiple comparisons test in C, G and L or two-tailed Student's t-test in J.

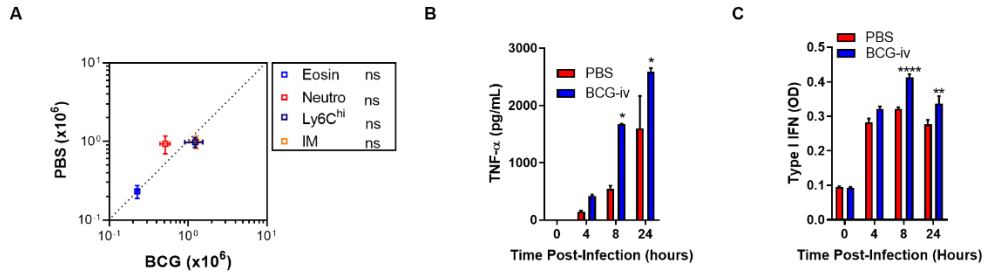


Figure 5.7.3: BCG vaccination promotes trained immunity to IAV. (A) Mice were vaccinated for 28 days with BCG, or not and infected for 3 days with IAV. Total cell counts of recruited innate immune cells in the lung post-infection were determined by flow cytometry. (B-C) BMDM from vaccinated or control mice were generated and infected *in vitro* with IAV and levels of TNF- α (B) or active type I IFN were evaluated in the tissue culture supernatants at various timepoints post-infection. Means are represented \pm SEM. Differences were assessed by two-tailed Student's T-test in (A) or two-way ANOVA followed by Sidak's multiple comparisons test in B and C.

CHAPTER 6:
DISCUSSION, MAIN CONCLUSIONS AND FUTURE
DIRECTIONS

In 1580, the first consensus influenza pandemic occurred; yet the causative agent, IAV, remained a mystery for centuries. Following the 1918 pandemic, mounting efforts led to the isolation of the virus and, in 1933, a seminal study by Smith, Andrewes and Laidlaw used filtered throat washes from an infected human to transmit the disease to ferrets (504). In 1935, Sir Frank Macfarlane Burnet propagated IAV in the allantoic fluid of hen embryos for the first time (505), allowing for a boom in laboratory experimentation with the virus. Since then, decades of research have culminated in considerable understanding of the nature of the virus and the host's response to infection, helping to mould the paradigm that host defense to infectious disease is comprised of both **resistance** mechanisms (directly antiviral) and **tolerance** mechanisms (tissue damage prevention/repair) (506). But despite this, since its isolation, three other pandemics have arisen and yearly mortality still climbs to half a million per year in the absence of effective antivirals or vaccines. Thus, it was the goal of this work to further interrogate mechanisms of the immune response to influenza, in hopes of discovering novel targetable immunotherapies. The overarching findings of this thesis aim to enhance immunity against IAV infection at three levels: 1) host resistance, 2) disease tolerance and 3) trained immunity.

6.1: Phases of the immune response: resistance versus tolerance

The lung is a dynamic and intricate microenvironment with the indispensable function of providing oxygen to the entire body. As many pathogens are transmitted by respiratory droplets and/or aerosols like influenza, the lung faces the constant challenge of being exposed to invasion by pathogens. Thus, it is essential that the pulmonary immune response effectively “dials” to kill pathogens in the lung, while avoiding overt tissue damage and immunopathology. Although the interplay and overlap in kinetics involved in this regulation is appreciably complex due to nature of the immune response, conceptually, the magnitude of immunity can be stratified into an early resistance phase and a later tolerance phase (**Figure 6.1**).

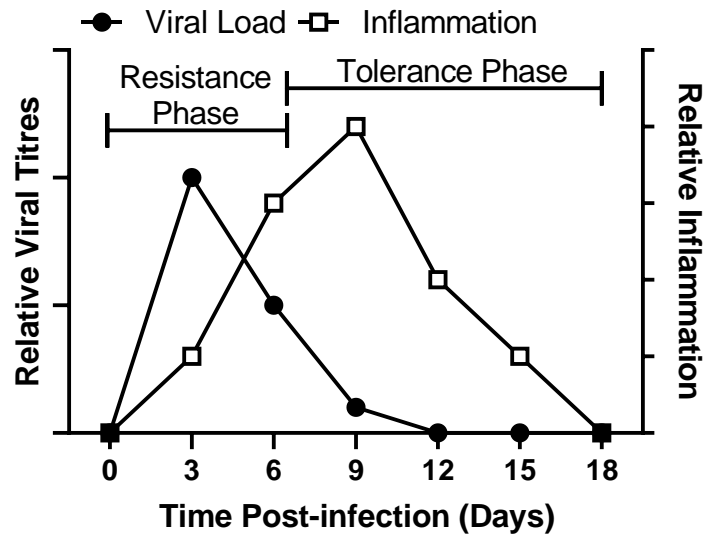


Figure 6.1: Two phases of immunity to IAV. Immunity to influenza can be conceptualized as two phases: 1) The host resistance phase that is concerned with viral clearance and 2) The disease tolerance phase where the tissue returns to homeostasis. Note the pivot point at ~day 6 post-infection.

Our studies in chapters 2 and 3 contribute to this notion of a phasic immune response to IAV. In chapter 2, we delineated a pathway of host resistance in pulmonary macrophages that was dependent upon RIPK3-mediated production of IFN-I (particularly IFN- β), which was important over the first six days of infection when viral titres are highest. In RIPK3-deficient mice, this initial reduction in pulmonary IFN-I led to elevated viral loads and susceptibility to infection. The IFN-I response by macrophages is a very well-established and broadly-studied resistance mechanism to influenza and other viruses (507). Classical induction of IFN-I to IAV proceeds via RNA sensing by the PRR RIG-I that interacts with MAVS at the mitochondrial membrane, followed by a cascade of TBK1/IRF3 signalling and the initial wave of IFN- β (507). Our results add RIP kinase family members as novel mediators of this pathway. Both RIPK1 and RIPK3 are critical regulators of programmed necrosis and can work synergistically or antagonistically in their varied cellular functions (436). Similarly, we observed antagonism of RIPK1 and RIPK3 at the MAVS/RIG-I interface, although our observations represented the first description of this interaction in the production of IFN-I.

Moreover, RIPK3-mediated necroptosis is also known to be highly antiviral and inflammatory, coordinating both innate and adaptive immune responses (508). During influenza

infection, this structural cell necroptosis is important in host resistance by rapidly removing the optimal niche of replication, during the first few hours to days of infection (222). This dual function in host resistance places RIPK3 at a unique evolutionary perspective in immunity to IAV. The IFN-I response is highly conserved phylogenetically, being expressed in ancient cartilaginous fish, while the necroptosis machinery is poorly conserved and confined to restricted classes of upper vertebrates. Interestingly, IFN-I is a known inducer of necroptosis in mammals (327) and while IAV encodes several levels of IFN-I antagonism, as introduced in chapter 1, no known inhibitors of necroptosis are expressed by IAV. We speculate that the necroptosis pathway may have evolved as a counter to IAV inhibition of IFN-I and cellular apoptosis, such that early IFN-I responses by macrophages promote necroptosis in structural cells with the goal of quick inhibition of viral replication. As such, the RIPK3/IFN-I/necroptosis pathway may represent a rapid host resistance strategy that provides an upper-hand against influenza infection.

An important caveat of our study is that we utilized a full-body RIPK3-deficient mouse, such that both the IFN-I and necroptotic pathways are compromised. Utilization of conditional knockout mice, such as RIPK3^{flox/flox}/LysM^{cre} to specifically knockout RIPK3 in the myeloid compartment, would serve to increase our knowledge of the interplay between RIPK3-mediated IFN-I production by myeloid cells and RIPK3-mediated necroptosis in structural cells. Furthermore, the IFN-III pathway is also confined to upper level vertebrates, suggesting more recent evolution than IFN-I. As mentioned in chapter 1, IFN-III production and signalling are primarily restricted to the upper airway epithelial cells, rather than leukocytes (117, 144). Neither a potential role for RIPK3 in IFN-III production nor the potential of IFN-III to induce necroptosis has been investigated; yet, because IFN-III signalling is not known to be potently inflammatory, we speculate that IFN-III is independent of these other pathways. This remains to be experimentally tested, however.

Our results in chapter 2 also outline the importance of regulated host resistance responses in setting the tone for subsequent disease tolerance responses. As early viral loads were elevated in *Ripk3*^{-/-} mice, the inflammatory response and virus-induced tissue damage from days 3 to 6 post-infection were also greater in magnitude. Thus, disease tolerance mechanisms were equally compromised, being insufficient to combat the exacerbated tissue damage caused by the attenuated

resistance responses, as illustrated by greater inflammation at day 9 post-infection in the *Ripk3*^{-/-} mice. This illustrates one way by which IAV infections can become fatal. By failing to restrict early viral replication, an overrun immune response unleashes a sequela of inflammation and respiratory insufficiency. Similarly, previous work in our lab showed that enhancing antiviral immunity through inhibition of MPGES-1 (the specific enzyme in the production of the lipid mediator PGE₂) led to elevated antiviral immunity shortly post-infection (day 3). This promoted better disease tolerance at later timepoints post-infection due to the faster viral clearance, such that there was reduced inflammation at day 12 and increased survival (154). Conceptually, these studies highlight the intimate tethering of early resistance responses and later tolerance responses, where there is a viral titre/inflammatory threshold that cannot be surpassed, or there is a break in disease tolerance and, ultimately, mortality (**Figure 6.2**).

In chapter 3, we described a previously unknown role for CypD in disease tolerance to influenza infection. In contrast to our RIPK3 model explored in chapter 2, for the first 6 days of

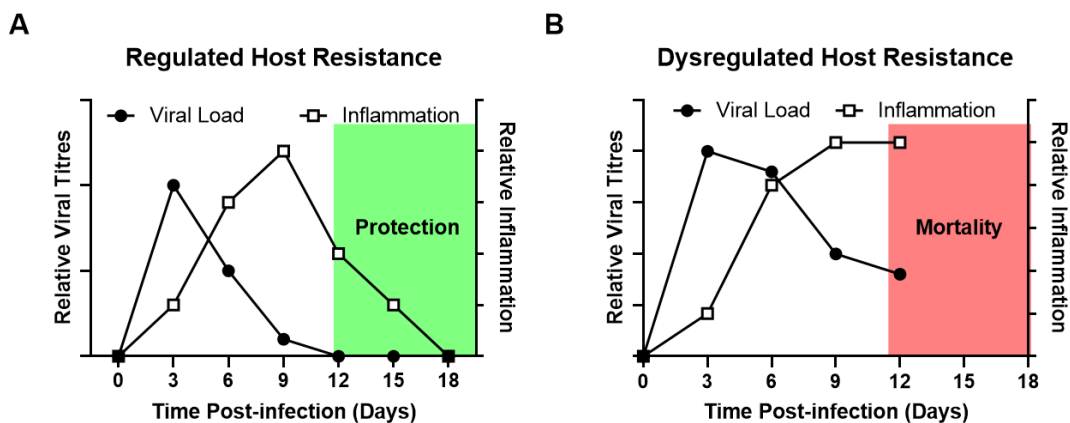


Figure 6.2: Mortality to IAV caused by insufficient host resistance responses. (A) Adequately regulated host resistance responses that resolve, or (B) insufficient and dysregulated resistance responses that cause prolonged elevated viral titres and fatal tissue damage. This scenario illustrates what we described in Chapter 2 in *Ripk3*^{-/-} mice.

infection we observed no significant changes between WT and *CypD*^{-/-} mice, as they exhibited equal pulmonary IFN- β production, viral loads and lung damage. However, beginning at day 7, *CypD*-deficient mice began to display enhanced epithelial cell damage, which was secondary to a loss of IL-22 production by NK cells. Other studies have shown that the epithelial protective cytokine IL-22 is required in disease tolerance to IAV infection and that NK cells represent a

necessary source (242, 243). However, our observation that mitochondrial CypD is required for its induction by NK cells provides a novel molecular mechanism of the NK cell/IL-22 axis in disease tolerance. How exactly CypD regulates the activation of NK cells and the production of IL-22 remains to be determined. Our finding that day 7 represented the timepoint where differences in lung damage were first pronounced fits into the conceptual framework of the duality of the immune response. Collectively, our data suggest that day 6/7 represents a critical pivot-point between these resistance and tolerance phases. This aligns well with clinical observations that suggest viral shedding occurs for the first 2-8 days post-infection (resistance phase) that can then be followed by weeks of resolving inflammation (tolerance phase) (509).

Bone marrow-residing HSCs and progenitors give rise to all circulating leukocytes and, therefore, represent ground zero of the immune response. In addition to its role in mature NK cells, we found that CypD facilitates NK cell lymphopoiesis by sequestering p53-dependent cell death in progenitors. We had previously established the importance of CypD in disease tolerance to *Mycobacterium tuberculosis* infection by regulating T-cell responses (352). Although the bone marrow was not investigated in the *Mtb* study, our work here hints at additional roles for CypD in lymphopoiesis (T cell and NK cell hematopoiesis) that have profound consequences on effector cell function. Similarly, in addition to their well-documented requirements in effector leukocyte responses, an emerging function for RIPK3, necroptosis and IFN-I in regulating hematopoiesis has been described (271). Our work in chapter 4 added to this emerging concept of hematopoietic and effector function of RIPK3. We found that *Mtb*-induced IFN-I responses in the bone marrow led to RIPK3-dependent necroptosis of myeloid progenitors (CMP/GMP) that suppressed myelopoiesis and contributed to *Mtb* pathogenesis. In addition, we had previously described a detrimental role for RIPK3 in immunity to *Mtb* through *Mtb*-induced macrophage necroptosis, which facilitated pulmonary bacterial dissemination (314). Thus, in contrast to its multi-protective role to IAV, RIPK3 contributes to TB progression through at least two distinct functions in the lung and the bone marrow, underscoring the complex specificity of host-pathogen interactions to pulmonary infections. In general, we propose greater investigation of protein function in both peripheral effector responses and centralized bone marrow hematopoiesis is warranted to gain more complete understanding of immune coordination.

Previous work by us (150) and others (229) has outlined the fundamental importance of maintaining the pulmonary epithelial/endothelial barrier in immunity to IAV and particularly in disease tolerance. We have recently delineated the requirement for the lipid mediator LTB₄ in potentiating the production of IFN-I (specifically IFN- α) to dampen the proliferation of inflammatory monocyte-derived cells. These inflammatory monocyte-derived cells damage the lung epithelium by secreting high levels of TNF- α and NO, such that by inhibiting proliferation of these cells, LTB₄ indirectly helps maintain the lung epithelial barrier by acting on myeloid cells (150). IL-22 signalling, on the other hand, is almost exclusively confined to structural cells, as immune cells are devoid of the receptor of IL-22 (IL-22R1). Following ligation, IL-22 induces a pro-survival, proliferative state in structural cells to repair the tissue (510). Thus, both immune and structural cell responses (i.e. LTB₄ versus IL-22) are needed in disease tolerance during the highly symptomatic late stages of influenza infection. Broadly, our work with the *CypD*^{-/-} mice adds to the mounting literature that suggests maintenance of the pulmonary epithelial/endothelial barrier is the crux of disease tolerance to influenza. Through this, our chapter 3 findings outline a second manner by which IAV infections can go from resolving to fatal. Although *CypD*-deficient mice have intact host resistance responses, they fail to properly promote disease tolerance and these

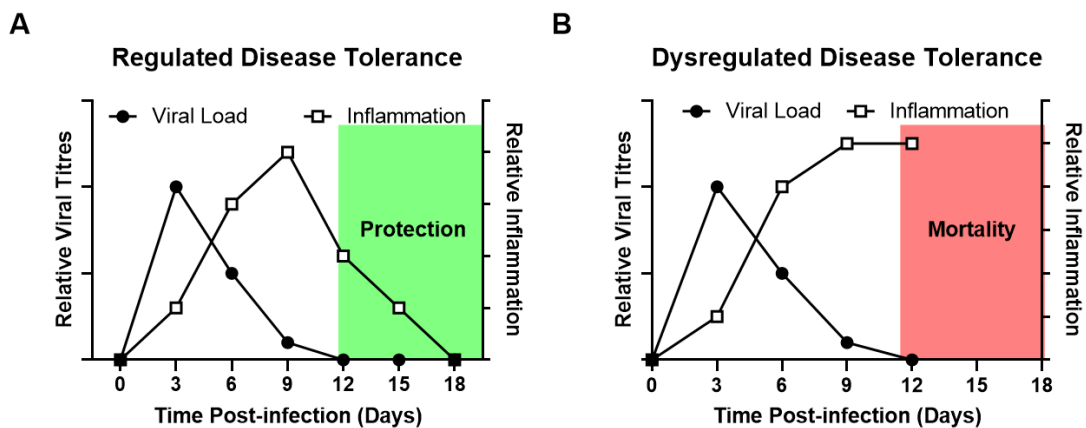


Figure 6.3: Mortality to IAV caused by insufficient disease tolerance responses. (A) Appropriately regulated disease tolerance responses that resolve and provide protection to IAV infection, or (B), despite identical virus clearance, a fatal immune response caused by dysregulated disease tolerance can occur. This situation was explored in Chapter 3 using *CypD*^{-/-} mice.

mice succumb to infection brought on directly by epithelial barrier destruction. Therefore, even if host resistance is intact, disease tolerance must be equally regulated (**Figure 6.3**).

Taken together, chapters 2 and 3 dictate how the time following infection orchestrates the magnitude of host resistance versus disease tolerance responses. Our results indicate that as viral loads begin to decline after day 6, host resistance responses wane and disease tolerance responses increase. A drop in viral shedding clinically, indicative of approximately 6 days post-infection, could represent an important timepoint for ceasing therapies that target resistance and substituting them for those that enhance tolerance. For example, intense study in our lab has centred around the kinetics of IFN-I over the course of IAV infection. Intriguingly, IFN-I acts in a biphasic manner to promote resistance then tolerance, assessed by the relative amounts of IFN- β (early stages, host resistance) and IFN- α (later stages, disease tolerance). We have shown how shortly following infection IFN- β is protective and contributes to antiviral immunity (1, 62, 154), while late-stage IFN- α had no effect on viral loads, but significant positive effect on disease tolerance (150). Therefore, it appears that close characterization of the nature of the IFN-I response (i.e. IFN- β versus IFN- α) may provide important insight into the phases of the immune response to IAV. In the same vein, in chapter 3, conventional NK cells were the critical source of IL-22 at day 7 post-infection. However, NK cells begin to accumulate in the lung as early as 2 days post-infection (356) and as discussed in chapter 3, it appears that NK cells are important switches of resistance versus tolerance responses. At early stages, NK cells predominantly lyse infected cells to contribute to virus elimination; while at later stages, their function changes to disease tolerance and IL-22 production. Interestingly, IFN-I signalling activates inflammatory monocytes to produce IL-18. IL-18 is a major activator of NK cells and causes them to produce IFN- γ and become highly cytotoxic during viral infection (511). However, IFN- α signalling directly on NK cells suppresses their expression of IFN- γ , which is associated with immunosuppression (512). This raises the question whether early IFN- β followed by late IFN- α signalling on NK cells may contribute to their resistance versus tolerance responses. Certainly, this requires formal investigation.

Finally, our findings in chapters 2 and 3 outline that RIPK3 and CypD each represent an attractive target of agonism for therapy against IAV. Collectively, the literature shows that the antiviral capacity of RIPK3 is at least two-fold, promoting IFN-I in macrophages and necroptosis of epithelial cells, with both mechanisms being protective. Similarly, CypD agonism in the lungs may contribute to enhanced NK cell activation and beneficial IL-22 production. However, targeting of these proteins has caveats. In addition to its role in NK cell maturation, CypD is a

critical regulator of leukocyte necrosis, which is highly inflammatory and potentially damaging. Thus, it can be envisioned that over-activation of CypD may, in fact, be detrimental by inducing pulmonary necrosis, as is often seen in fatal cases of IAV. Similarly, over-activation of RIPK3-dependent necroptosis could promote detrimental levels of tissue damage and inflammation. Potentially, these concerns could be mitigated by considering the kinetics of infection and our data suggest that day 6 is the critical flex point, where therapies that target antiviral pathways (i.e. resistance; RIPK3) are replaced by those that ameliorate tissue damage (i.e. tolerance, CypD). Similarly, it is known that early or prophylactic administration of Poly (I:C) protects against IAV by inducing an IFN-I dependent antiviral state in the lungs. This protection lasted for approximately a month and could be added to the standard vaccine program (310). However, this priming of the lungs with IFN-I, causes susceptibility to chronic *Mtb* infection (426, 513) and/or the promotion of autoimmune diseases (514). Therefore, understanding the cellular and molecular mechanisms of the early phase (host resistance) followed by later phase (disease tolerance) will provide novel targeted immunotherapy against IAV and other diseases.

Importantly, all the previously discussed therapies targeting the immune response only serve to attenuate disease severity, but cannot prevent infection. As we will discuss in the following section, improved vaccine design is the most effective strategy against infectious disease, as it entirely prevents disease.

6.2: Harnessing the power of immune training in vaccination against influenza

Vaccination is the only strategy for disease eradication. Smallpox remains the sole disease directly eradicated by human intervention, with polio considered the next and closest target. Both of these diseases have vaccines with nearly 100% efficacy that offer lifelong immunity and nearly complete global coverage. Despite extensive yearly vaccination campaigns and considerable population coverage, current influenza vaccines fail to provide consistent or even adequate protection, providing between 10-60% protection annually over the last 15 years (277). Furthermore, even if highly effective any given year, influenza vaccines do not readily convert into long-lasting immunity, due to the presence of multiple circulating strains and high mutation

rates of the globular hemagglutinin head, which is the target for the majority of anti-influenza neutralizing antibodies. Thus, contemporary strategies exhibit limited promise for eradication or even a significant drop in global infections and, thus, every year IAV kills between 300 000-500 000 people (27). Although, as we discussed in chapter 1, many promising strategies that improve upon the current vaccine and aim to develop a more universal vaccine are emerging. Yet, none have presently been approved, nor shown considerable increase in protection over the currently available vaccines. Collectively, this argues for a new strategy in vaccine design against influenza and potentially other pathogens.

Adaptive immunity provides specific protection against its cognate antigen, which has both pros and cons. On the one hand, these memory responses can be long-lived and render a host immune for life by eliminating a pathogen prior to the establishment of infection. This is particularly true of B-cell-derived antigen-specific neutralizing antibodies, if they target highly stable epitopes of pathogens. Generation of this type of antibody is the basis for the vast majority of protection afforded by current vaccinations in humans. On the other hand, this antigen-specificity fails to provide cross-protection and is susceptible to antigenic drift as seen in highly mutative viruses like influenza, being “blind” to dissimilar antigens even when they arise from the same pathogen or even protein. Interestingly, while innate immune cells respond to a multitude of PAMPs through various PRRs, they have been considered to possess no memory response and, therefore, offer little value in vaccine design. However, the vast majority of species (more than 95%) solely rely on innate immunity for host defense (515), and, thus, it is empirical that a critical evolutionary trait like immunological memory would have evolved in this primitive branch of our immune system. The realization that innate immune cells can exhibit long-term “memory-like” changes to their effector program provided new opportunities in vaccine design (516). This concept, known as trained innate immunity, is driven by epigenetic and metabolic reprogramming that allows “trained” innate cells to respond more robustly to a non-specific secondary infection and provide cross-protection. Although trained immunity was first established in cells of the mononuclear phagocyte lineage (i.e. monocytes and macrophages), these cells have a relatively short lifespan and are, thus, unlikely to transmit their memory phenotype to their progeny and provide sustainable protection. Therefore, current vaccine strategies that directly target monocytes/M ϕ may have limited capacity to generate sustained innate immune memory. One of

the goals of this thesis was to determine whether amplifying HSC reprogramming via trained immunity is a rational strategy for developing effective vaccines against influenza virus. We propose that harnessing trained immunity by reprogramming bone marrow HSCs/progenitors offers a novel approach for future vaccines against IAV and other pathogens. Our results in chapter 4 lend credence to this proposal by highlighting the importance of cellular and molecular mechanisms in host-pathogen interactions in the bone marrow in the induction of trained immunity, while chapter 5 provides proof-of-concept for the capacity of non-specific inducers of trained immunity to protect against IAV.

Seminal study on trained immunity revealed how intradermal delivery of the BCG vaccine trains peripheral blood monocytes of healthy human volunteers to respond more strongly to subsequent *ex vivo* and *in vivo* stimuli by a variety pathogens (302, 492). However, the longevity of monocyte training is limited by the short half-life of circulating classical monocytes, which has been experimentally validated to be approximately one day (303). We recently showed that by delivering BCG intravenously rather than subcutaneously, it accessed the bone marrow and reprogrammed HSCs. This BCG-dependent imprinting of HSCs was then transmitted to mature macrophages that more effectively controlled *Mtb* growth *in vitro* and *in vivo* (304). In the current study in chapter 4, we extended these observations by comparing the hematopoietic response to BCG and the related virulent *Mtb*. Importantly, in contrast to BCG, *Mtb* conferred a detrimental signature on HSCs that contributed to its pathogenesis. Additionally, we found that HSC imprinting in response to both mycobacteria was durable and long-lived, being maintained for at least one-year post-initial exposure. These findings highlight that HSC exposure to pathogens can continue to shape the host's immune response long after removal of the pathogen from the system. Taken together, our results argue for the importance of the HSC transcriptional signature in trained immunity and its consideration in vaccine design.

Interestingly, our bulk- and sc-RNA-Seq experiments on bone marrow HSCs and progenitor cells outlined the magnitude of the IFN-I versus IFN-II signature in HSCs/progenitors as the major determinant of the hematopoietic response to *Mtb* and BCG, respectively. Chronic IFN-I signalling is known to negatively impact HSC health and leads to exhaustion through cell death (271, 419), while this contrasts to what is observed in immunity to IAV. During IAV

infection, acute low-levels of IFN-I signalling in the bone marrow is beneficial, by promoting protective monopoiesis (123) and reprogramming monocytes with a pre-emptive antiviral signature (273) that is enhanced upon arrival at the IFN-I rich lung parenchyma (517). Thus, the magnitude and timeframe of IFN-I responses in the bone marrow have considerable impacts on disease outcome. Collectively, although the reprogramming of bone marrow HSCs shows substantial promise in future vaccination strategies, this area of research is still in its infancy. More effort must go into mapping the pathways involved in the long-term protective (i.e. BCG and β -Glucan) versus detrimental (e.g. *Mtb*) trained immunity.

Finally, in chapter 5, we provide important proof-of-concept of the potential usage of inducers of trained immunity against IAV, by showing that both BCG (live vaccine) and β -Glucan (adjuvant) protect against lethal IAV infection. Given the recent study of trained immunity in cross-protection to unrelated pathogens, we speculate that this can potentially explain the remarkable protection against IAV infection. Despite the fact that the mechanisms of protection were not fully elucidated in our study, we provide some candidates, as BCG induces trained BMDM responses to IAV, as well as generates a novel T-cell subset that rapidly mobilizes in the lung parenchyma and produces cytokines upon infection. β -Glucan, on the other hand, does not induce this α/β T-cell population, which is not surprising given that it is an adjuvant, implying that HSC-mediated trained macrophage responses is responsible for the observed protection, as we have seen in immunity to *Mtb* (395). However, more rigorous investigation is required to identify the interplay between BCG/ β -Glucan and trained immunity against IAV. Interestingly, our preliminary results suggest that BCG protects via IFN-I-mediated host resistance responses in the lung, while β -Glucan promotes disease tolerance. As vaccination has almost exclusively targeted host resistance mechanisms, these data provide impetus for the consideration of factors that boost disease tolerance in vaccine design. Thus, identifying agents that induce trained immunity with cross-protection capacity is a novel approach for developing vaccines against influenza and potentially other pulmonary infectious diseases, including coronaviruses.

6.3: Concluding remarks

To conclude, immunity to influenza infection is complex and highly regulated, with many pathways involved in this regulation remaining unknown. Here, we outlined the intricate balance between host resistance and disease tolerance in returning the lung to homeostasis following influenza infection. Collectively, the work presented in this thesis provides evidence for three novel mechanisms of immunity to IAV:

1. **Host Resistance** (RIPK3 interacts with MAVS to regulate type I IFN-mediated immunity to influenza A virus infection)
2. **Disease Tolerance** (Cyclophilin D promotes disease tolerance to influenza A virus infection by licensing NK cell development and function)
3. **Vaccination** (*M. tuberculosis* reprograms HSCs to limit myelopoiesis and impair trained immunity via a type I IFN/iron axis; Trained immunity as a vaccination strategy against influenza A virus infection)

Together, we highlight that these pathways are instrumental in a regulated and coordinated immune response to IAV. Future efforts will be focused on how we can better target these pathways therapeutically against IAV infection.

Globally, our work provides expansion of the important evolutionary concept of the immunological arms-race against infectious disease. Highly evolved pathogens like IAV provide constant, substantial pressure on the host's immune system to optimize its response and overcome viral immune subversion and manipulation. Better understanding of the entire landscape of the immune response will improve vaccination and clinical intervention to enhance the host's immunity to IAV. It is our hope that this and future study will help achieve this goal.

BIBLIOGRAPHY:

1. Downey J, Pernet E, Coulombe F, Allard B, Meunier I, Jaworska J, et al. RIPK3 interacts with MAVS to regulate type I IFN-mediated immunity to Influenza A virus infection. *PLoS Pathog.* 2017;13(4):e1006326.
2. Khan N, Downey J, Sanz J, Kaufmann E, Blankenhaus B, Pacis A, et al. M. tuberculosis Reprograms Hematopoietic Stem Cells to Limit Myelopoiesis and Impair Trained Immunity. *Cell.* 2020;183(3):752-70.e22.
3. Downey J, Pernet E, Coulombe F, and Divangahi M. Dissecting host cell death programs in the pathogenesis of influenza. *Microbes Infect.* 2018;20(9-10):560-9.
4. Mental Evolution in Animals. *Science.* 1884;4(74):16-9.
5. Nish S, and Medzhitov R. Host defense pathways: role of redundancy and compensation in infectious disease phenotypes. *Immunity.* 2011;34(5):629-36.
6. Sadd BM, and Schmid-Hempel P. Principles of ecological immunology. *Evol Appl.* 2009;2(1):113-21.
7. Dawkins R, and Krebs JR. Arms races between and within species. *Proc R Soc Lond B Biol Sci.* 1979;205(1161):489-511.
8. Paules C, and Subbarao K. Influenza. *Lancet.* 2017;390(10095):697-708.
9. Fontana J, and Steven AC. Influenza virus-mediated membrane fusion: Structural insights from electron microscopy. *Arch Biochem Biophys.* 2015;581:86-97.
10. Taubenberger JK, and Morens DM. Influenza: the once and future pandemic. *Public Health Rep.* 2010;125 Suppl 3:16-26.
11. Bouvier NM, and Palese P. The biology of influenza viruses. *Vaccine.* 2008;26 Suppl 4:D49-53.
12. Hause BM, Ducatez M, Collin EA, Ran Z, Liu R, Sheng Z, et al. Isolation of a novel swine influenza virus from Oklahoma in 2011 which is distantly related to human influenza C viruses. *PLoS Pathog.* 2013;9(2):e1003176.
13. White SK, Ma WJ, McDaniel CJ, Gray GC, and Lednicky JA. Serologic evidence of exposure to influenza D virus among persons with occupational contact with cattle. *J Clin Virol.* 2016;81:31-3.
14. Su S, Fu X, Li G, Kerlin F, and Veit M. Novel Influenza D virus: Epidemiology, pathology, evolution and biological characteristics. *Virulence.* 2017;8(8):1580-91.
15. Pleschka S. Overview of influenza viruses. *Curr Top Microbiol Immunol.* 2013;370:1-20.
16. Dou D, Revol R, Ostbye H, Wang H, and Daniels R. Influenza A Virus Cell Entry, Replication, Virion Assembly and Movement. *Front Immunol.* 2018;9:1581.

17. Mostafa A, Abdelwhab EM, Mettenleiter TC, and Pleschka S. Zoonotic Potential of Influenza A Viruses: A Comprehensive Overview. *Viruses*. 2018;10(9).
18. Chen W, Calvo PA, Malide D, Gibbs J, Schubert U, Bacik I, et al. A novel influenza A virus mitochondrial protein that induces cell death. *Nat Med*. 2001;7(12):1306-12.
19. Jagger BW, Wise HM, Kash JC, Walters KA, Wills NM, Xiao YL, et al. An overlapping protein-coding region in influenza A virus segment 3 modulates the host response. *Science*. 2012;337(6091):199-204.
20. Lazarowitz SG, Compans RW, and Choppin PW. Influenza Virus Structural and Nonstructural Proteins in Infected Cells and Their Plasma Membranes. *Virology*. 1971;46(3):830-+.
21. Ayllon J, and Garcia-Sastre A. The NS1 protein: a multitasking virulence factor. *Curr Top Microbiol Immunol*. 2015;386:73-107.
22. O'Neill RE, Talon J, and Palese P. The influenza virus NEP (NS2 protein) mediates the nuclear export of viral ribonucleoproteins. *The EMBO journal*. 1998;17(1):288-96.
23. Badham MD, and Rossman JS. Filamentous Influenza Viruses. *Curr Clin Microbiol*. 2016;3(3):155-61.
24. Cowling BJ, Ip DKM, Fang VJ, Suntarattiwong P, Olsen SJ, Levy J, et al. Aerosol transmission is an important mode of influenza A virus spread. *Nature Communications*. 2013;4.
25. Fukuyama S, and Kawaoka Y. The pathogenesis of influenza virus infections: the contributions of virus and host factors. *Curr Opin Immunol*. 2011;23(4):481-6.
26. Rossman JS, Leser GP, and Lamb RA. Filamentous influenza virus enters cells via macropinocytosis. *Journal of virology*. 2012;86(20):10950-60.
27. Krammer F, Smith GJD, Fouchier RAM, Peiris M, Kedzierska K, Doherty PC, et al. Influenza. *Nat Rev Dis Primers*. 2018;4(1):3.
28. Samji T. Influenza A: understanding the viral life cycle. *Yale J Biol Med*. 2009;82(4):153-9.
29. Steinhauer DA, and Skehel JJ. Genetics of influenza viruses. *Annu Rev Genet*. 2002;36:305-32.
30. Dobson J, Whitley RJ, Pocock S, and Monto AS. Oseltamivir treatment for influenza in adults: a meta-analysis of randomised controlled trials. *Lancet*. 2015;385(9979):1729-37.
31. Jefferson T, Jones MA, Doshi P, Del Mar CB, Hama R, Thompson MJ, et al. Neuraminidase inhibitors for preventing and treating influenza in healthy adults and children. *Cochrane Database Syst Rev*. 2014(4):CD008965.
32. Hung IFN, To KKW, Chan JFW, Cheng VCC, Liu KSH, Tam A, et al. Efficacy of Clarithromycin-Naproxen-Oseltamivir Combination in the Treatment of Patients Hospitalized for Influenza

- A(H3N2) Infection: An Open-label Randomized, Controlled, Phase IIb/III Trial. *Chest*. 2017;151(5):1069-80.
33. Garcia-Sastre A. Snatch-and-Grab Inhibitors to Fight the Flu. *Cell*. 2019;177(6):1367-.
 34. Rello J, and Pop-Vicas A. Clinical review: primary influenza viral pneumonia. *Crit Care*. 2009;13(6):235.
 35. Damjanovic D, Divangahi M, Kugathasan K, Small CL, Zganiacz A, Brown EG, et al. Negative regulation of lung inflammation and immunopathology by TNF-alpha during acute influenza infection. *Am J Pathol*. 2011;179(6):2963-76.
 36. Al-Garawi AA, Fattouh R, Walker TD, Jamula EB, Botelho F, Goncharova S, et al. Acute, but not resolved, influenza A infection enhances susceptibility to house dust mite-induced allergic disease. *J Immunol*. 2009;182(5):3095-104.
 37. Chang YJ, Kim HY, Albacker LA, Baumgarth N, McKenzie AN, Smith DE, et al. Innate lymphoid cells mediate influenza-induced airway hyper-reactivity independently of adaptive immunity. *Nat Immunol*. 2011;12(7):631-8.
 38. Obuchi M, Adachi Y, Takizawa T, and Sata T. Influenza A(H1N1)pdm09 virus and asthma. *Front Microbiol*. 2013;4:307.
 39. Herold S, Becker C, Ridge KM, and Budinger GR. Influenza virus-induced lung injury: pathogenesis and implications for treatment. *Eur Respir J*. 2015;45(5):1463-78.
 40. Simonsen L. The global impact of influenza on morbidity and mortality. *Vaccine*. 1999;17 Suppl 1:S3-10.
 41. Winternitz MC, and Lambert RA. Edema of the Lungs as a Cause of Death. *J Exp Med*. 1919;29(6):537-45.
 42. Taubenberger JK, and Morens DM. The pathology of influenza virus infections. *Annu Rev Pathol*. 2008;3:499-522.
 43. Taubenberger JK. The origin and virulence of the 1918 "Spanish" influenza virus. *P Am Philos Soc*. 2006;150(1):86-112.
 44. Bautista E, Chotpitayasunondh T, Gao Z, Harper SA, Shaw M, Uyeki TM, et al. Clinical aspects of pandemic 2009 influenza A (H1N1) virus infection. *N Engl J Med*. 2010;362(18):1708-19.
 45. Short KR, Kroeze E, Fouchier RAM, and Kuiken T. Pathogenesis of influenza-induced acute respiratory distress syndrome. *Lancet Infect Dis*. 2014;14(1):57-69.
 46. Sandbulte MR, Westgeest KB, Gao J, Xu X, Klimov AI, Russell CA, et al. Discordant antigenic drift of neuraminidase and hemagglutinin in H1N1 and H3N2 influenza viruses. *Proceedings of the National Academy of Sciences of the United States of America*. 2011;108(51):20748-53.

47. Pan D, Xue W, Wang X, Guo J, Liu H, and Yao X. Molecular mechanism of the enhanced virulence of 2009 pandemic influenza A (H1N1) virus from D222G mutation in the hemagglutinin: a molecular modeling study. *J Mol Model*. 2012;18(9):4355-66.
48. McCullers JA. The co-pathogenesis of influenza viruses with bacteria in the lung. *Nature reviews Microbiology*. 2014;12(4):252-62.
49. Xu Y, Peng R, Zhang W, Qi J, Song H, Liu S, et al. Avian-to-Human Receptor-Binding Adaptation of Avian H7N9 Influenza Virus Hemagglutinin. *Cell Rep*. 2019;29(8):2217-28 e5.
50. Tumpey TM, Basler CF, Aguilar PV, Zeng H, Solorzano A, Swayne DE, et al. Characterization of the reconstructed 1918 Spanish influenza pandemic virus. *Science*. 2005;310(5745):77-80.
51. Hsieh YC, Wu TZ, Liu DP, Shao PL, Chang LY, Lu CY, et al. Influenza pandemics: past, present and future. *J Formos Med Assoc*. 2006;105(1):1-6.
52. Garcia-Sastre A, Egorov A, Matassov D, Brandt S, Levy DE, Durbin JE, et al. Influenza A virus lacking the NS1 gene replicates in interferon-deficient systems. *Virology*. 1998;252(2):324-30.
53. Ivashkiv LB, and Donlin LT. Regulation of type I interferon responses. *Nat Rev Immunol*. 2014;14(1):36-49.
54. Pichlmair A, Schulz O, Tan CP, Naslund TI, Liljestrom P, Weber F, et al. RIG-I-mediated antiviral responses to single-stranded RNA bearing 5'-phosphates. *Science*. 2006;314(5801):997-1001.
55. Nemeroff ME, Barabino SM, Li Y, Keller W, and Krug RM. Influenza virus NS1 protein interacts with the cellular 30 kDa subunit of CPSF and inhibits 3' end formation of cellular pre-mRNAs. *Mol Cell*. 1998;1(7):991-1000.
56. Bergmann M, Garcia-Sastre A, Carnero E, Pehamberger H, Wolff K, Palese P, et al. Influenza virus NS1 protein counteracts PKR-mediated inhibition of replication. *Journal of virology*. 2000;74(13):6203-6.
57. Min JY, and Krug RM. The primary function of RNA binding by the influenza A virus NS1 protein in infected cells: Inhibiting the 2'-5' oligo (A) synthetase/RNase L pathway. *Proceedings of the National Academy of Sciences of the United States of America*. 2006;103(18):7100-5.
58. Chaimayo C, Dunagan M, Hayashi T, Santoso N, and Takimoto T. Specificity and functional interplay between influenza virus PA-X and NS1 shutoff activity. *Plos Pathogens*. 2018;14(11).
59. Ehrhardt C, Wolff T, Pleschka S, Planz O, Beermann W, Bode JG, et al. Influenza A virus NS1 protein activates the PI3K/Akt pathway to mediate antiapoptotic signaling responses. *Journal of virology*. 2007;81(7):3058-67.
60. Tripathi S, Batra J, Cao W, Sharma K, Patel JR, Ranjan P, et al. Influenza A virus nucleoprotein induces apoptosis in human airway epithelial cells: implications of a novel interaction between nucleoprotein and host protein Clusterin. *Cell death & disease*. 2013;4:e562.

61. Zamarin D, Garcia-Sastre A, Xiao X, Wang R, and Palese P. Influenza virus PB1-F2 protein induces cell death through mitochondrial ANT3 and VDAC1. *PLoS Pathog.* 2005;1(1):e4.
62. Jaworska J, Coulombe F, Downey J, Tzelepis F, Shalaby K, Tattoli I, et al. NLRX1 prevents mitochondrial induced apoptosis and enhances macrophage antiviral immunity by interacting with influenza virus PB1-F2 protein. *Proceedings of the National Academy of Sciences of the United States of America.* 2014;111(20):E2110-9.
63. Shieh WJ, Blau DM, Denison AM, DeLeon-Carnes M, Adem P, Bhatnagar J, et al. 2009 pandemic influenza A (H1N1): pathology and pathogenesis of 100 fatal cases in the United States. *Am J Pathol.* 2010;177(1):166-75.
64. Smith AM, and McCullers JA. Secondary bacterial infections in influenza virus infection pathogenesis. *Curr Top Microbiol Immunol.* 2014;385:327-56.
65. Jamieson AM, Pasman L, Yu S, Gamradt P, Homer RJ, Decker T, et al. Role of tissue protection in lethal respiratory viral-bacterial coinfection. *Science.* 2013;340(6137):1230-4.
66. Ghoneim HE, Thomas PG, and McCullers JA. Depletion of alveolar macrophages during influenza infection facilitates bacterial superinfections. *J Immunol.* 2013;191(3):1250-9.
67. Aegerter H, Kulikauskaite J, Crotta S, Patel H, Kelly G, Hessel EM, et al. Influenza-induced monocyte-derived alveolar macrophages confer prolonged antibacterial protection. *Nat Immunol.* 2020;21(2):145-57.
68. Nakamura S, Davis KM, and Weiser JN. Synergistic stimulation of type I interferons during influenza virus coinfection promotes *Streptococcus pneumoniae* colonization in mice. *J Clin Invest.* 2011;121(9):3657-65.
69. Belser JA, Katz JM, and Tumpey TM. The ferret as a model organism to study influenza A virus infection. *Dis Model Mech.* 2011;4(5):575-9.
70. Rodriguez L, Nogales A, and Martinez-Sobrido L. Influenza A Virus Studies in a Mouse Model of Infection. *J Vis Exp.* 2017(127).
71. Schulman JL, and Kilbourne ED. Experimental Transmission of Influenza Virus Infection in Mice .2. Some Factors Affecting Incidence of Transmitted Infection. *Journal of Experimental Medicine.* 1963;118(2):267-&.
72. Berry J. The Great Influenza: The Story of the Deadliest Pandemic in History. *Viking Books.* 2004.
73. Lofgren E, Fefferman NH, Naumov YN, Gorski J, and Naumova EN. Influenza seasonality: underlying causes and modeling theories. *Journal of virology.* 2007;81(11):5429-36.
74. Muscatello DJ. Redefining influenza seasonality at a global scale and aligning it to the influenza vaccine manufacturing cycle: A descriptive time series analysis. *The Journal of infection.* 2019;78(2):140-9.

75. Cauchemez S, Valleron AJ, Boelle PY, Flahault A, and Ferguson NM. Estimating the impact of school closure on influenza transmission from Sentinel data. *Nature*. 2008;452(7188):750-4.
76. Gruber-Bzura BM. Vitamin D and Influenza-Prevention or Therapy? *Int J Mol Sci*. 2018;19(8).
77. Shaman J, and Kohn M. Absolute humidity modulates influenza survival, transmission, and seasonality. *Proceedings of the National Academy of Sciences of the United States of America*. 2009;106(9):3243-8.
78. Lipsitch M, and Viboud C. Influenza seasonality: lifting the fog. *Proceedings of the National Academy of Sciences of the United States of America*. 2009;106(10):3645-6.
79. Lowen AC, Mubareka S, Steel J, and Palese P. Influenza virus transmission is dependent on relative humidity and temperature. *PLoS Pathog*. 2007;3(10):1470-6.
80. Kudo E, Song E, Yockey LJ, Rakib T, Wong PW, Homer RJ, et al. Low ambient humidity impairs barrier function and innate resistance against influenza infection. *Proceedings of the National Academy of Sciences of the United States of America*. 2019;116(22):10905-10.
81. Dolin R. Influenza--interpandemic as well as pandemic disease. *N Engl J Med*. 2005;353(24):2535-7.
82. Taubenberger JK, and Morens DM. 1918 Influenza: the mother of all pandemics. *Emerg Infect Dis*. 2006;12(1):15-22.
83. Cox NJ, and Subbarao K. Global epidemiology of influenza: past and present. *Annu Rev Med*. 2000;51:407-21.
84. Worobey M, Han GZ, and Rambaut A. Genesis and pathogenesis of the 1918 pandemic H1N1 influenza A virus. *Proceedings of the National Academy of Sciences of the United States of America*. 2014;111(22):8107-12.
85. Palese P. Influenza: old and new threats. *Nat Med*. 2004;10(12 Suppl):S82-7.
86. Morens DM, Taubenberger JK, and Fauci AS. Predominant role of bacterial pneumonia as a cause of death in pandemic influenza: implications for pandemic influenza preparedness. *J Infect Dis*. 2008;198(7):962-70.
87. Walker O. Pathology of influenza pneumonia. *J Lab Clin Med*. 1919(5):154-75.
88. Neumann G, Watanabe T, Ito H, Watanabe S, Goto H, Gao P, et al. Generation of influenza A viruses entirely from cloned cDNAs. *Proceedings of the National Academy of Sciences of the United States of America*. 1999;96(16):9345-50.
89. Kobasa D, Jones SM, Shinya K, Kash JC, Copps J, Ebihara H, et al. Aberrant innate immune response in lethal infection of macaques with the 1918 influenza virus. *Nature*. 2007;445(7125):319-23.

90. Garten RJ, Davis CT, Russell CA, Shu B, Lindstrom S, Balish A, et al. Antigenic and genetic characteristics of swine-origin 2009 A(H1N1) influenza viruses circulating in humans. *Science*. 2009;325(5937):197-201.
91. Hurt AC, Chotpitayasunondh T, Cox NJ, Daniels R, Fry AM, Gubareva LV, et al. Antiviral resistance during the 2009 influenza A H1N1 pandemic: public health, laboratory, and clinical perspectives. *Lancet Infect Dis*. 2012;12(3):240-8.
92. Itoh Y, Shinya K, Kiso M, Watanabe T, Sakoda Y, Hatta M, et al. In vitro and in vivo characterization of new swine-origin H1N1 influenza viruses. *Nature*. 2009;460(7258):1021-5.
93. Maines TR, Jayaraman A, Belser JA, Wadford DA, Pappas C, Zeng H, et al. Transmission and pathogenesis of swine-origin 2009 A(H1N1) influenza viruses in ferrets and mice. *Science*. 2009;325(5939):484-7.
94. Witkop CT, Duffy MR, Macias EA, Gibbons TF, Escobar JD, Burwell KN, et al. Novel Influenza A (H1N1) outbreak at the U.S. Air Force Academy: epidemiology and viral shedding duration. *Am J Prev Med*. 2010;38(2):121-6.
95. Fineberg HV. Pandemic Preparedness and Response - Lessons from the H1N1 Influenza of 2009. *New Engl J Med*. 2014;370(14):1335-42.
96. Mauad T, Hajjar LA, Callegari GD, da Silva LF, Schout D, Galas FR, et al. Lung pathology in fatal novel human influenza A (H1N1) infection. *Am J Respir Crit Care Med*. 2010;181(1):72-9.
97. Berera D, and Zambon M. Antivirals in the 2009 pandemic--lessons and implications for future strategies. *Influenza Other Respir Viruses*. 2013;7 Suppl 3:72-9.
98. Conly JM, and Johnston BL. Avian influenza - The next pandemic? *Can J Infect Dis Med Microbiol*. 2004;15(5):252-4.
99. Keidel. Ganong,Wf - Review of Medical Physiology. *Deut Med Wochenschr*. 1966;91(40):1807-&.
100. Quie PG. Lung defense against infection. *J Pediatr*. 1986;108(5 Pt 2):813-6.
101. Iwasaki A, Foxman EF, and Molony RD. Early local immune defences in the respiratory tract. *Nat Rev Immunol*. 2017;17(1):7-20.
102. Akira S, Uematsu S, and Takeuchi O. Pathogen recognition and innate immunity. *Cell*. 2006;124(4):783-801.
103. Medzhitov R. Toll-like receptors and innate immunity. *Nat Rev Immunol*. 2001;1(2):135-45.
104. Tipping PG. Toll-like receptors: the interface between innate and adaptive immunity. *J Am Soc Nephrol*. 2006;17(7):1769-71.
105. Netea MG, Joosten LA, Latz E, Mills KH, Natoli G, Stunnenberg HG, et al. Trained immunity: A program of innate immune memory in health and disease. *Science*. 2016;352(6284):aaf1098.

106. Medzhitov R, Schneider DS, and Soares MP. Disease tolerance as a defense strategy. *Science*. 2012;335(6071):936-41.
107. Iwasaki A, and Pillai PS. Innate immunity to influenza virus infection. *Nat Rev Immunol*. 2014;14(5):315-28.
108. Nicod LP. Lung defences: an overview. *Eur Respir Rev*. 2005;14(95):45-50.
109. Bals R. Epithelial antimicrobial peptides in host defense against infection. *Respiratory research*. 2000;1(3):141-50.
110. Rogan MP, Geraghty P, Greene CM, O'Neill SJ, Taggart CC, and McElvaney NG. Antimicrobial proteins and polypeptides in pulmonary innate defence. *Respiratory research*. 2006;7:29.
111. Hartshorn KL, White MR, Shepherd V, Reid K, Jensenius JC, and Crouch EC. Mechanisms of anti-influenza activity of surfactant proteins A and D: comparison with serum collectins. *Am J Physiol*. 1997;273(6):L1156-66.
112. Choi YS, and Baumgarth N. Dual role for B-1a cells in immunity to influenza virus infection. *J Exp Med*. 2008;205(13):3053-64.
113. Isaacs A, and Lindenmann J. Virus interference. I. The interferon. *Proc R Soc Lond B Biol Sci*. 1957;147(927):258-67.
114. Isaacs A, Lindenmann J, and Valentine RC. Virus interference. II. Some properties of interferon. *Proc R Soc Lond B Biol Sci*. 1957;147(927):268-73.
115. Kotenko SV, Gallagher G, Baurin VV, Lewis-Antes A, Shen ML, Shah NK, et al. IFN-lambda s mediate antiviral protection through a distinct class II cytokine receptor complex. *Nature Immunology*. 2003;4(1):69-77.
116. Sheppard P, Kindsvogel W, Xu WF, Henderson K, Schlutsmeyer S, Whitmore TE, et al. IL-28, IL-29 and their class II cytokine receptor IL-28R. *Nature Immunology*. 2003;4(1):63-8.
117. Lazear HM, Schoggins JW, and Diamond MS. Shared and Distinct Functions of Type I and Type III Interferons. *Immunity*. 2019;50(4):907-23.
118. Schreiber G. The molecular basis for differential type I interferon signaling. *The Journal of biological chemistry*. 2017;292(18):7285-94.
119. Ho HH, and Ivashkiv LB. Role of STAT3 in type I interferon responses. Negative regulation of STAT1-dependent inflammatory gene activation. *The Journal of biological chemistry*. 2006;281(20):14111-8.
120. Plataniias LC. Mechanisms of type-I- and type-II-interferon-mediated signalling. *Nat Rev Immunol*. 2005;5(5):375-86.

121. Koerner I, Kochs G, Kalinke U, Weiss S, and Staeheli P. Protective role of beta interferon in host defense against influenza A virus. *Journal of virology*. 2007;81(4):2025-30.
122. Arimori Y, Nakamura R, Yamada H, Shibata K, Maeda N, Kase T, et al. Type I interferon limits influenza virus-induced acute lung injury by regulation of excessive inflammation in mice. *Antiviral Res*. 2013;99(3):230-7.
123. Seo SU, Kwon HJ, Ko HJ, Byun YH, Seong BL, Uematsu S, et al. Type I interferon signaling regulates Ly6C(hi) monocytes and neutrophils during acute viral pneumonia in mice. *PLoS Pathog*. 2011;7(2):e1001304.
124. Shepardson KM, Larson K, Johns LL, Stanek K, Cho H, Wellham J, et al. IFNAR2 Is Required for Anti-influenza Immunity and Alters Susceptibility to Post-influenza Bacterial Superinfections. *Frontiers in Immunology*. 2018;9.
125. Szretter KJ, Gangappa S, Belser JA, Zeng H, Chen H, Matsuoka Y, et al. Early control of H5N1 influenza virus replication by the type I interferon response in mice. *Journal of virology*. 2009;83(11):5825-34.
126. Duerr CU, McCarthy CDA, Mindt BC, Rubio M, Meli AP, Pothlichet J, et al. Type I interferon restricts type 2 immunopathology through the regulation of group 2 innate lymphoid cells. *Nature Immunology*. 2016;17(1):65-+.
127. Garcia-Sastre A, Durbin RK, Zheng H, Palese P, Gertner R, Levy DE, et al. The role of interferon in influenza virus tissue tropism. *Journal of virology*. 1998;72(11):8550-8.
128. Sato M, Suemori H, Hata N, Asagiri M, Ogasawara K, Nakao K, et al. Distinct and essential roles of transcription factors IRF-3 and IRF-7 in response to viruses for IFN-alpha/beta gene induction. *Immunity*. 2000;13(4):539-48.
129. Staeheli P, Haller O, Boll W, Lindenmann J, and Weissmann C. Mx Protein - Constitutive Expression in 3t3-Cells Transformed with Cloned Mx Cdna Confers Selective Resistance to Influenza-Virus. *Cell*. 1986;44(1):147-58.
130. Verhelst J, Parthoens E, Schepens B, Fiers W, and Saelens X. Interferon-Inducible Protein Mx1 Inhibits Influenza Virus by Interfering with Functional Viral Ribonucleoprotein Complex Assembly. *Journal of virology*. 2012;86(24):13445-55.
131. Everitt AR, Clare S, Pertel T, John SP, Wash RS, Smith SE, et al. IFITM3 restricts the morbidity and mortality associated with influenza. *Nature*. 2012;484(7395):519-23.
132. Schulz O, Pichlmair A, Rehwinkel J, Rogers NC, Scheuner D, Kato H, et al. Protein kinase R contributes to immunity against specific viruses by regulating interferon mRNA integrity. *Cell Host Microbe*. 2010;7(5):354-61.
133. Chakrabarti A, Banerjee S, Franchi L, Loo YM, Gale M, Nunez G, et al. RNase L Activates the NLRP3 Inflammasome during Viral Infections. *Cell Host & Microbe*. 2015;17(4):466-77.

134. Pillai PS, Molony RD, Martinod K, Dong H, Pang IK, Tal MC, et al. Mx1 reveals innate pathways to antiviral resistance and lethal influenza disease. *Science*. 2016;352(6284):463-6.
135. Alspach E, Lussier DM, and Schreiber RD. Interferon gamma and Its Important Roles in Promoting and Inhibiting Spontaneous and Therapeutic Cancer Immunity. *Cold Spring Harb Perspect Biol*. 2019;11(3).
136. Stifter S, Bhattacharyya N, and Feng C. Functional Interplay between Type I and II Interferons Is Essential to Limit Influenza A Virus-Induced Tissue Inflammation. *Cytokine*. 2016;87:123-4.
137. Weiss ID, Wald O, Wald H, Beider K, Abraham M, Galun E, et al. IFN-gamma Treatment at Early Stages of Influenza Virus Infection Protects Mice from Death in a NK Cell-Dependent Manner. *J Interf Cytok Res*. 2010;30(6):439-49.
138. Califano D, Furuya Y, Roberts S, Avram D, McKenzie ANJ, and Metzger DW. IFN-gamma increases susceptibility to influenza A infection through suppression of group II innate lymphoid cells. *Mucosal Immunology*. 2018;11(1):209-19.
139. Graham MB, Dalton DK, Giltinan D, Braciale VL, Stewart TA, and Braciale TJ. Response to influenza infection in mice with a targeted disruption in the interferon gamma gene. *J Exp Med*. 1993;178(5):1725-32.
140. Muller U, Steinhoff U, Reis LFL, Hemmi S, Pavlovic J, Zinkernagel RM, et al. Functional-Role of Type-I and Type-II Interferons in Antiviral Defense. *Science*. 1994;264(5167):1918-21.
141. Bot A, Bot S, and Bona CA. Protective role of gamma interferon during the recall response to influenza virus. *Journal of virology*. 1998;72(8):6637-45.
142. Zhou JH, Wang YN, Chang QY, Ma P, Hu Y, and Cao X. Type III Interferons in Viral Infection and Antiviral Immunity. *Cell Physiol Biochem*. 2018;51(1):173-85.
143. An S, Jeon YJ, Jo A, Lim HJ, Han YE, Cho SW, et al. Initial Influenza Virus Replication Can Be Limited in Allergic Asthma Through Rapid Induction of Type III Interferons in Respiratory Epithelium. *Frontiers in Immunology*. 2018;9.
144. Klinkhammer J, Schnepf D, Ye L, Schwaderlapp M, Gad HH, Hartmann R, et al. IFN-lambda prevents influenza virus spread from the upper airways to the lungs and limits virus transmission. *Elife*. 2018;7.
145. Galani IE, Triantafyllia V, Eleminiadou EE, Koltsida O, Stavropoulos A, Manioudaki M, et al. Interferon-lambda Mediates Non-redundant Front-Line Antiviral Protection against Influenza Virus Infection without Compromising Host Fitness. *Immunity*. 2017;46(5):875-+.
146. Kato H, Sato S, Yoneyama M, Yamamoto M, Uematsu S, Matsui K, et al. Cell type-specific involvement of RIG-I in antiviral response. *Immunity*. 2005;23(1):19-28.

147. Onomoto K, Jogi M, Yoo JS, Narita R, Morimoto S, Takemura A, et al. Critical role of an antiviral stress granule containing RIG-I and PKR in viral detection and innate immunity. *PLoS One*. 2012;7(8):e43031.
148. Kandasamy M, Suryawanshi A, Tundup S, Perez JT, Schmolke M, Manicassamy S, et al. RIG-I Signaling Is Critical for Efficient Polyfunctional T Cell Responses during Influenza Virus Infection. *Plos Pathogens*. 2016;12(7).
149. Loo YM, Fornek J, Crochet N, Bajwa G, Perwitasari O, Martinez-Sobrido L, et al. Distinct RIG-I and MDA5 signaling by RNA viruses in innate immunity. *Journal of virology*. 2008;82(1):335-45.
150. Pernet E, Downey J, Vinh DC, Powell WS, and Divangahi M. Leukotriene B4-type I interferon axis regulates macrophage-mediated disease tolerance to influenza infection. *Nat Microbiol*. 2019;4(8):1389-400.
151. Koyama S, Ishii KJ, Kumar H, Tanimoto T, Coban C, Uematsu S, et al. Differential role of TLR- and RLR-signaling in the immune responses to influenza A virus infection and vaccination. *J Immunol*. 2007;179(7):4711-20.
152. Liu S, Cai X, Wu J, Cong Q, Chen X, Li T, et al. Phosphorylation of innate immune adaptor proteins MAVS, STING, and TRIF induces IRF3 activation. *Science*. 2015;347(6227):aaa2630.
153. Odendall C, Dixit E, Stavru F, Bierne H, Franz KM, Durbin AF, et al. Diverse intracellular pathogens activate type III interferon expression from peroxisomes. *Nat Immunol*. 2014;15(8):717-26.
154. Coulombe F, Jaworska J, Verway M, Tzelepis F, Massoud A, Gillard J, et al. Targeted prostaglandin E2 inhibition enhances antiviral immunity through induction of type I interferon and apoptosis in macrophages. *Immunity*. 2014;40(4):554-68.
155. Pang IK, Pillai PS, and Iwasaki A. Efficient influenza A virus replication in the respiratory tract requires signals from TLR7 and RIG-I. *Proceedings of the National Academy of Sciences of the United States of America*. 2013;110(34):13910-5.
156. Seo SU, Kwon HJ, Song JH, Byun YH, Seong BL, Kawai T, et al. MyD88 Signaling Is Indispensable for Primary Influenza A Virus Infection but Dispensable for Secondary Infection. *Journal of virology*. 2010;84(24):12713-22.
157. Le Goffic R, Balloy V, Lagranderie M, Alexopoulou L, Escriou N, Flavell R, et al. Detrimental contribution of the Toll-like receptor (TLR)3 to influenza A virus-induced acute pneumonia. *PLoS Pathog*. 2006;2(6):e53.
158. Prakash A, Smith E, Lee CK, and Levy DE. Tissue-specific positive feedback requirements for production of type I interferon following virus infection. *Journal of Biological Chemistry*. 2005;280(19):18651-7.
159. Wolf AI, Buehler D, Hensley SE, Cavanagh LL, Wherry EJ, Kastner P, et al. Plasmacytoid Dendritic Cells Are Dispensable during Primary Influenza Virus Infection. *Journal of Immunology*. 2009;182(2):871-9.

160. Kaminski MM, Ohnemus A, Cornitescu M, and Staeheli P. Plasmacytoid dendritic cells and Toll-like receptor 7-dependent signalling promote efficient protection of mice against highly virulent influenza A virus. *Journal of General Virology*. 2012;93:555-9.
161. Ciancanelli MJ, Huang SXL, Luthra P, Garner H, Itan Y, Volpi S, et al. Life-threatening influenza and impaired interferon amplification in human IRF7 deficiency. *Science*. 2015;348(6233):448-53.
162. Lim HK, Huang SXL, Chen J, Kerner G, Gilliaux O, Bastard P, et al. Severe influenza pneumonitis in children with inherited TLR3 deficiency. *J Exp Med*. 2019;216(9):2038-56.
163. Girardin SE, Boneca IG, Viala J, Chamaillard M, Labigne A, Thomas G, et al. Nod2 is a general sensor of peptidoglycan through muramyl dipeptide (MDP) detection. *Journal of Biological Chemistry*. 2003;278(11):8869-72.
164. Divangahi M, Mostowy S, Coulombe F, Kozak R, Guillot L, Veyrier F, et al. NOD2-Deficient Mice Have Impaired Resistance to Mycobacterium tuberculosis Infection through Defective Innate and Adaptive Immunity. *Journal of Immunology*. 2008;181(10):7157-65.
165. Sabbah A, Chang TH, Harnack R, Frohlich V, Tominaga K, Dube PH, et al. Activation of innate immune antiviral responses by Nod2. *Nature Immunology*. 2009;10(10):1073-U49.
166. Ranjan P, Singh N, Kumar A, Neerincx A, Kremmer E, Cao WP, et al. NLRC5 interacts with RIG-I to induce a robust antiviral response against influenza virus infection. *European Journal of Immunology*. 2015;45(3):758-72.
167. Lupfer CR, Stokes KL, Kuriakose T, and Kanneganti TD. Deficiency of the NOD-Like Receptor NLRC5 Results in Decreased CD8(+) T Cell Function and Impaired Viral Clearance. *Journal of virology*. 2017;91(17).
168. Allen IC, Moore CB, Schneider M, Lei Y, Davis BK, Scull MA, et al. NLRX1 Protein Attenuates Inflammatory Responses to Infection by Interfering with the RIG-I-MAVS and TRAF6-NF-kappa B Signaling Pathways. *Immunity*. 2011;34(6):854-65.
169. Rebsamen M, Vazquez J, Tardivel A, Guarda G, Curran J, and Tschopp J. NLRX1/NOD5 deficiency does not affect MAVS signalling. *Cell Death and Differentiation*. 2011;18(8):1387-.
170. Shiokawa M, Yamasaki S, and Saijo S. C-type lectin receptors in anti-fungal immunity. *Current opinion in microbiology*. 2017;40:123-30.
171. Londrigan SL, Tate MD, Brooks AG, and Reading PC. Cell-surface receptors on macrophages and dendritic cells for attachment and entry of influenza virus. *J Leukocyte Biol*. 2012;92(1):97-106.
172. Palomino-Segura M, Perez L, Farsakoglu Y, Virgilio T, Latino I, D'Antuono R, et al. Protection against influenza infection requires early recognition by inflammatory dendritic cells through C-type lectin receptor SIGN-R1. *Nat Microbiol*. 2019;4(11):1930-40.
173. Manicassamy B, Manicassamy S, Belicha-Villanueva A, Pisanelli G, Pulendran B, and Garcia-Sastre A. Analysis of in vivo dynamics of influenza virus infection in mice using a GFP reporter virus.

- Proceedings of the National Academy of Sciences of the United States of America*. 2010;107(25):11531-6.
174. Cline TD, Beck D, and Bianchini E. Influenza virus replication in macrophages: balancing protection and pathogenesis. *J Gen Virol*. 2017;98(10):2401-12.
 175. Schneider C, Nobs SP, Heer AK, Kurrer M, Klinke G, van Rooijen N, et al. Alveolar macrophages are essential for protection from respiratory failure and associated morbidity following influenza virus infection. *PLoS Pathog*. 2014;10(4):e1004053.
 176. Sever-Chroneos Z, Murthy A, Davis J, Florence JM, Kurdowska A, Krupa A, et al. GM-CSF modulates pulmonary resistance to influenza A infection. *Antiviral Res*. 2011;92(2):319-28.
 177. Cardani A, Boulton A, Kim TS, and Braciale TJ. Alveolar Macrophages Prevent Lethal Influenza Pneumonia By Inhibiting Infection Of Type-1 Alveolar Epithelial Cells. *PLoS Pathog*. 2017;13(1):e1006140.
 178. Kumagai Y, Takeuchi O, Kato H, Kumar H, Matsui K, Morii E, et al. Alveolar macrophages are the primary interferon-alpha producer in pulmonary infection with RNA viruses. *Immunity*. 2007;27(2):240-52.
 179. Doss M, White MR, Teclé T, Gantz D, Crouch EC, Jung G, et al. Interactions of alpha-, beta-, and theta-defensins with influenza A virus and surfactant protein D. *J Immunol*. 2009;182(12):7878-87.
 180. Narasaraju T, Yang E, Samy RP, Ng HH, Poh WP, Liew AA, et al. Excessive neutrophils and neutrophil extracellular traps contribute to acute lung injury of influenza pneumonitis. *Am J Pathol*. 2011;179(1):199-210.
 181. Schliehe C, Flynn EK, Vilagos B, Richson U, Swaminathan S, Bosnjak B, et al. The methyltransferase Setdb2 mediates virus-induced susceptibility to bacterial superinfection. *Nat Immunol*. 2015;16(1):67-74.
 182. Herold S, Steinmueller M, von Wulffen W, Cakarova L, Pinto R, Pleschka S, et al. Lung epithelial apoptosis in influenza virus pneumonia: the role of macrophage-expressed TNF-related apoptosis-inducing ligand. *J Exp Med*. 2008;205(13):3065-77.
 183. Dawson TC, Beck MA, Kuziel WA, Henderson F, and Maeda N. Contrasting effects of CCR5 and CCR2 deficiency in the pulmonary inflammatory response to influenza A virus. *Am J Pathol*. 2000;156(6):1951-9.
 184. Lin KL, Suzuki Y, Nakano H, Ramsburg E, and Gunn MD. CCR2+ monocyte-derived dendritic cells and exudate macrophages produce influenza-induced pulmonary immune pathology and mortality. *J Immunol*. 2008;180(4):2562-72.
 185. Aldridge JR, Jr., Moseley CE, Boltz DA, Negovetich NJ, Reynolds C, Franks J, et al. TNF/iNOS-producing dendritic cells are the necessary evil of lethal influenza virus infection. *Proceedings of the National Academy of Sciences of the United States of America*. 2009;106(13):5306-11.

186. Topham NJ, and Hewitt EW. Natural killer cell cytotoxicity: how do they pull the trigger? *Immunology*. 2009;128(1):7-15.
187. Mandelboim O, Lieberman N, Lev M, Paul L, Arnon TI, Bushkin Y, et al. Recognition of haemagglutinins on virus-infected cells by NKp46 activates lysis by human NK cells. *Nature*. 2001;409(6823):1055-60.
188. Gazit R, Gruda R, Elboim M, Arnon TI, Katz G, Achdout H, et al. Lethal influenza infection in the absence of the natural killer cell receptor gene *Ncr1*. *Nature Immunology*. 2006;7(5):517-23.
189. Stein-Streilein J, and Guffee J. In vivo treatment of mice and hamsters with antibodies to asialo GM1 increases morbidity and mortality to pulmonary influenza infection. *J Immunol*. 1986;136(4):1435-41.
190. Li T, Wang J, Wang Y, Chen Y, Wei H, Sun R, et al. Respiratory Influenza Virus Infection Induces Memory-like Liver NK Cells in Mice. *J Immunol*. 2017;198(3):1242-52.
191. Vashist N, Trittel S, Ebensen T, Chambers BJ, Guzman CA, and Riese P. Influenza-Activated ILC1s Contribute to Antiviral Immunity Partially Influenced by Differential GTR Expression. *Front Immunol*. 2018;9:505.
192. Artiaga BL, Yang G, Hutchinson TE, Loeb JC, Richt JA, Lednicky JA, et al. Rapid control of pandemic H1N1 influenza by targeting NKT-cells. *Sci Rep*. 2016;6:37999.
193. Matsuda JL, Mallevaey T, Scott-Browne J, and Gapin L. CD1d-restricted iNKT cells, the 'Swiss-Army knife' of the immune system. *Current Opinion in Immunology*. 2008;20(3):358-68.
194. Nielsen MM, Witherden DA, and Havran WL. gammadelta T cells in homeostasis and host defence of epithelial barrier tissues. *Nat Rev Immunol*. 2017;17(12):733-45.
195. Goldberg EL, Molony RD, Kudo E, Sidorov S, Kong Y, Dixit VD, et al. Ketogenic diet activates protective gammadelta T cell responses against influenza virus infection. *Sci Immunol*. 2019;4(41).
196. Braciale TJ, Sun J, and Kim TS. Regulating the adaptive immune response to respiratory virus infection. *Nat Rev Immunol*. 2012;12(4):295-305.
197. Waithman J, and Mintern JD. Dendritic cells and influenza A virus infection. *Virulence*. 2012;3(7):603-8.
198. Miller MA, Ganesan AP, Luckashenak N, Mendonca M, and Eisenlohr LC. Endogenous antigen processing drives the primary CD4+ T cell response to influenza. *Nat Med*. 2015;21(10):1216-22.
199. Bot A, Reichlin A, Isobe H, Bot S, Schulman J, Yokoyama WM, et al. Cellular mechanisms involved in protection and recovery from influenza virus infection in immunodeficient mice. *Journal of virology*. 1996;70(8):5668-72.

200. Fujimoto C, Takeda N, Matsunaga A, Sawada A, Tanaka T, Kimoto T, et al. Induction and maintenance of anti-influenza antigen-specific nasal secretory IgA levels and serum IgG levels after influenza infection in adults. *Influenza Other Respir Viruses*. 2012;6(6):396-403.
201. Wu H, Haist V, Baumgartner W, and Schughart K. Sustained viral load and late death in Rag2^{-/-} mice after influenza A virus infection. *Virology*. 2010;7:172.
202. Eichelberger M, Allan W, Zijlstra M, Jaenisch R, and Doherty PC. Clearance of influenza virus respiratory infection in mice lacking class I major histocompatibility complex-restricted CD8⁺ T cells. *J Exp Med*. 1991;174(4):875-80.
203. Lee BO, Rangel-Moreno J, Moyron-Quiroz JE, Hartson L, Makris M, Sprague F, et al. CD4 T cell-independent antibody response promotes resolution of primary influenza infection and helps to prevent reinfection. *J Immunol*. 2005;175(9):5827-38.
204. Topham DJ, and Doherty PC. Clearance of an influenza A virus by CD4(+) T cells is inefficient in the absence of B cells. *Journal of virology*. 1998;72(1):882-5.
205. Helft J, Manicassamy B, Guermonprez P, Hashimoto D, Silvin A, Agudo J, et al. Cross-presenting CD103⁺ dendritic cells are protected from influenza virus infection. *J Clin Invest*. 2012;122(11):4037-47.
206. Ballesteros-Tato A, Leon B, Lund FE, and Randall TD. Temporal changes in dendritic cell subsets, cross-priming and costimulation via CD70 control CD8⁺ T cell responses to influenza (vol 11, pg 216, 2010). *Nature Immunology*. 2010;11(7):644-.
207. GeurtsvanKessel CH, Willart MA, van Rijt LS, Muskens F, Kool M, Baas C, et al. Clearance of influenza virus from the lung depends on migratory langerin⁺CD11b⁻ but not plasmacytoid dendritic cells. *J Exp Med*. 2008;205(7):1621-34.
208. McGill J, Van Rooijen N, and Legge KL. Protective influenza-specific CD8 T cell responses require interactions with dendritic cells in the lungs. *J Exp Med*. 2008;205(7):1635-46.
209. Le Bon A, Durand V, Kamphuis E, Thompson C, Bulfone-Paus S, Rossmann C, et al. Direct stimulation of T cells by type I IFN enhances the CD8⁺ T cell response during cross-priming. *J Immunol*. 2006;176(8):4682-9.
210. Priest SO, and Baumgarth N. The role of innate signals in B cell immunity to influenza virus. *Front Biosci (Schol Ed)*. 2013;5:105-17.
211. Alimonti JB, Ball TB, and Fowke KR. Mechanisms of CD4⁺ T lymphocyte cell death in human immunodeficiency virus infection and AIDS. *J Gen Virol*. 2003;84(Pt 7):1649-61.
212. Behar SM, Divangahi M, and Remold HG. Evasion of innate immunity by Mycobacterium tuberculosis: is death an exit strategy? *Nature reviews Microbiology*. 2010;8(9):668-74.

213. Robinson N, McComb S, Mulligan R, Dudani R, Krishnan L, and Sad S. Type I interferon induces necroptosis in macrophages during infection with *Salmonella enterica* serovar Typhimurium. *Nat Immunol*. 2012;13(10):954-62.
214. Guarner J, and Falcon-Escobedo R. Comparison of the pathology caused by H1N1, H5N1, and H3N2 influenza viruses. *Archives of medical research*. 2009;40(8):655-61.
215. Elmore S. Apoptosis: a review of programmed cell death. *Toxicologic pathology*. 2007;35(4):495-516.
216. Hogner K, Wolff T, Pleschka S, Plog S, Gruber AD, Kalinke U, et al. Macrophage-expressed IFN-beta contributes to apoptotic alveolar epithelial cell injury in severe influenza virus pneumonia. *PLoS Pathog*. 2013;9(2):e1003188.
217. Wurzer WJ, Planz O, Ehrhardt C, Giner M, Silberzahn T, Pleschka S, et al. Caspase 3 activation is essential for efficient influenza virus propagation. *The EMBO journal*. 2003;22(11):2717-28.
218. McLean JE, Datan E, Matassov D, and Zakeri ZF. Lack of Bax prevents influenza A virus-induced apoptosis and causes diminished viral replication. *Journal of virology*. 2009;83(16):8233-46.
219. Wurzer WJ, Ehrhardt C, Pleschka S, Berberich-Siebelt F, Wolff T, Walczak H, et al. NF-kappaB-dependent induction of tumor necrosis factor-related apoptosis-inducing ligand (TRAIL) and Fas/FasL is crucial for efficient influenza virus propagation. *The Journal of biological chemistry*. 2004;279(30):30931-7.
220. Fujikura D, Chiba S, Muramatsu D, Kazumata M, Nakayama Y, Kawai T, et al. Type-I interferon is critical for FasL expression on lung cells to determine the severity of influenza. *PLoS One*. 2013;8(2):e55321.
221. Pasparakis M, and Vandenabeele P. Necroptosis and its role in inflammation. *Nature*. 2015;517(7534):311-20.
222. Nogusa S, Thapa RJ, Dillon CP, Liedmann S, Oguin TH, 3rd, Ingram JP, et al. RIPK3 Activates Parallel Pathways of MLKL-Driven Necroptosis and FADD-Mediated Apoptosis to Protect against Influenza A Virus. *Cell Host Microbe*. 2016;20(1):13-24.
223. Martins R, Carlos AR, Braza F, Thompson JA, Bastos-Amador P, Ramos S, et al. Disease Tolerance as an Inherent Component of Immunity. *Annu Rev Immunol*. 2019;37:405-37.
224. Schneider DS, and Ayres JS. Two ways to survive infection: what resistance and tolerance can teach us about treating infectious diseases. *Nature Reviews Immunology*. 2008;8(11):889-95.
225. Brandes M, Klauschen F, Kuchen S, and Germain RN. A systems analysis identifies a feedforward inflammatory circuit leading to lethal influenza infection. *Cell*. 2013;154(1):197-212.
226. Hwang SY, Hertzog PJ, Holland KA, Sumarsono SH, Tymms MJ, Hamilton JA, et al. A null mutation in the gene encoding a type I interferon receptor component eliminates antiproliferative and

- antiviral responses to interferons alpha and beta and alters macrophage responses. *Proceedings of the National Academy of Sciences of the United States of America*. 1995;92(24):11284-8.
227. Hussell T, and Bell TJ. Alveolar macrophages: plasticity in a tissue-specific context. *Nat Rev Immunol*. 2014;14(2):81-93.
228. Snelgrove RJ, Goulding J, Didierlaurent AM, Lyonga D, Vekaria S, Edwards L, et al. A critical function for CD200 in lung immune homeostasis and the severity of influenza infection. *Nat Immunol*. 2008;9(9):1074-83.
229. Talmi-Frank D, Altboum Z, Solomonov I, Udi Y, Jaitin DA, Klepfish M, et al. Extracellular Matrix Proteolysis by MT1-MMP Contributes to Influenza-Related Tissue Damage and Mortality. *Cell Host Microbe*. 2016;20(4):458-70.
230. Teijaro JR, Walsh KB, Cahalan S, Fremgen DM, Roberts E, Scott F, et al. Endothelial cells are central orchestrators of cytokine amplification during influenza virus infection. *Cell*. 2011;146(6):980-91.
231. Monticelli LA, Sonnenberg GF, Abt MC, Alenghat T, Ziegler CGK, Doering TA, et al. Innate lymphoid cells promote lung-tissue homeostasis after infection with influenza virus. *Nature Immunology*. 2011;12(11):1045-U47.
232. Gorski SA, Hahn YS, and Braciale TJ. Group 2 Innate Lymphoid Cell Production of IL-5 Is Regulated by NKT Cells during Influenza Virus Infection. *Plos Pathogens*. 2013;9(9).
233. Hussell T, Pennycook A, and Openshaw PJ. Inhibition of tumor necrosis factor reduces the severity of virus-specific lung immunopathology. *Eur J Immunol*. 2001;31(9):2566-73.
234. Guo XZJ, Dash P, Crawford JC, Allen EK, Zamora AE, Boyd DF, et al. Lung gamma delta T Cells Mediate Protective Responses during Neonatal Influenza Infection that Are Associated with Type 2 Immunity. *Immunity*. 2018;49(3):531-+.
235. Wang J, Li FQ, Wei HM, Lian ZX, Sun R, and Tian ZG. Respiratory influenza virus infection induces intestinal immune injury via microbiota-mediated Th17 cell-dependent inflammation (vol 211, pg 2397, 2014). *Journal of Experimental Medicine*. 2014;211(13):2683-.
236. Crowe CR, Chen K, Pociask DA, Alcorn JF, Krivich C, Enelow RI, et al. Critical Role of IL-17RA in Immunopathology of Influenza Infection. *Journal of Immunology*. 2009;183(8):5301-10.
237. Godfrey DI, Koay HF, McCluskey J, and Gherardin NA. The biology and functional importance of MAIT cells. *Nature Immunology*. 2019;20(9):1110-28.
238. van Wilgenburg B, Loh L, Chen ZJ, Pediongco TJ, Wang HM, Shi M, et al. MAIT cells contribute to protection against lethal influenza infection in vivo. *Nature Communications*. 2018;9.
239. Loh L, Wang ZF, Sant S, Koutsakos M, Jegaskanda S, Corbett AJ, et al. Human mucosal-associated invariant T cells contribute to antiviral influenza immunity via IL-18-dependent activation. *Proceedings of the National Academy of Sciences of the United States of America*. 2016;113(36):10133-8.

240. Parks OB, Pociask DA, Hodzic Z, Kolls JK, and Good M. Interleukin-22 Signaling in the Regulation of Intestinal Health and Disease. *Front Cell Dev Biol.* 2016;3.
241. Pociask DA, Scheller EV, Mandalapu S, McHugh KJ, Enelow RI, Fattman CL, et al. IL-22 Is Essential for Lung Epithelial Repair following Influenza Infection. *American Journal of Pathology.* 2013;182(4):1286-96.
242. Guo HL, and Topham DJ. Interleukin-22 (IL-22) Production by Pulmonary Natural Killer Cells and the Potential Role of IL-22 during Primary Influenza Virus Infection. *Journal of virology.* 2010;84(15):7750-9.
243. Kumar P, Thakar MS, Ouyang W, and Malarkannan S. IL-22 from conventional NK cells is epithelial regenerative and inflammation protective during influenza infection. *Mucosal Immunology.* 2013;6(1):69-82.
244. Barthelemy A, Sencio V, Soulard D, Deruyter L, Faveeuw C, Le Goffic R, et al. Interleukin-22 Immunotherapy during Severe Influenza Enhances Lung Tissue Integrity and Reduces Secondary Bacterial Systemic Invasion. *Infection and Immunity.* 2018;86(7).
245. Ivanov S, Renneson J, Fontaine J, Barthelemy A, Paget C, Fernandez EM, et al. Interleukin-22 Reduces Lung Inflammation during Influenza A Virus Infection and Protects against Secondary Bacterial Infection. *Journal of virology.* 2013;87(12):6911-24.
246. Paget C, Ivanov S, Fontaine J, Renneson J, Blanc F, Pichavant M, et al. Interleukin-22 Is Produced by Invariant Natural Killer T Lymphocytes during Influenza A Virus Infection POTENTIAL ROLE IN PROTECTION AGAINST LUNG EPITHELIAL DAMAGES. *Journal of Biological Chemistry.* 2012;287(12):8816-29.
247. Betts RJ, Prabhu N, Ho AW, Lew FC, Hutchinson PE, Rotzschke O, et al. Influenza A virus infection results in a robust, antigen-responsive, and widely disseminated Foxp3+ regulatory T cell response. *Journal of virology.* 2012;86(5):2817-25.
248. Sun J, Madan R, Karp CL, and Braciale TJ. Effector T cells control lung inflammation during acute influenza virus infection by producing IL-10. *Nature Medicine.* 2009;15(3):277-84.
249. Bergsbaken T, Fink SL, and Cookson BT. Pyroptosis: host cell death and inflammation. *Nature reviews Microbiology.* 2009;7(2):99-109.
250. Kuriakose T, Man SM, Malireddi RK, Karki R, Kesavardhana S, Place DE, et al. ZBP1/DAI is an innate sensor of influenza virus triggering the NLRP3 inflammasome and programmed cell death pathways. *Sci Immunol.* 2016;1(2).
251. Thomas PG, Dash P, Aldridge JR, Jr., Ellebedy AH, Reynolds C, Funk AJ, et al. The intracellular sensor NLRP3 mediates key innate and healing responses to influenza A virus via the regulation of caspase-1. *Immunity.* 2009;30(4):566-75.
252. Ichinohe T, Lee HK, Ogura Y, Flavell R, and Iwasaki A. Inflammasome recognition of influenza virus is essential for adaptive immune responses. *J Exp Med.* 2009;206(1):79-87.

253. Heaton NS, Langlois RA, Sachs D, Lim JK, Palese P, and tenOever BR. Long-term survival of influenza virus infected club cells drives immunopathology. *J Exp Med*. 2014;211(9):1707-14.
254. Hamilton JR, Sachs D, Lim JK, Langlois RA, Palese P, and Heaton NS. Club cells surviving influenza A virus infection induce temporary nonspecific antiviral immunity. *Proceedings of the National Academy of Sciences of the United States of America*. 2016;113(14):3861-6.
255. Cooper B. The origins of bone marrow as the seedbed of our blood: from antiquity to the time of Osler. *Proc (Bayl Univ Med Cent)*. 2011;24(2):115-8.
256. Osler W. VI. An account of certain organisms occurring in the liquor sanguinis. *Proceedings of the Royal Society of London*. 1874;22(148-155):391-8.
257. Orkin SH, and Zon LI. Hematopoiesis: an evolving paradigm for stem cell biology. *Cell*. 2008;132(4):631-44.
258. Cheng H, Zheng Z, and Cheng T. New paradigms on hematopoietic stem cell differentiation. *Protein Cell*. 2020;11(1):34-44.
259. Mezey E. On the origin of blood cells--hematopoiesis revisited. *Oral Dis*. 2016;22(4):247-8.
260. Liu ZY, Gu YQ, Chakarov S, Bleriot C, Kwok I, Chen X, et al. Fate Mapping via Ms4a3-Expression History Traces Monocyte-Derived Cells. *Cell*. 2019;178(6):1509-+.
261. Beerman I, Bhattacharya D, Zandi S, Sigvardsson M, Weissman IL, Bryder D, et al. Functionally distinct hematopoietic stem cells modulate hematopoietic lineage potential during aging by a mechanism of clonal expansion. *Proceedings of the National Academy of Sciences of the United States of America*. 2010;107(12):5465-70.
262. Pietras EM, Reynaud D, Kang YA, Carlin D, Calero-Nieto FJ, Leavitt AD, et al. Functionally Distinct Subsets of Lineage-Biased Multipotent Progenitors Control Blood Production in Normal and Regenerative Conditions. *Cell Stem Cell*. 2015;17(1):35-46.
263. Yamashita M, and Passegue E. TNF-alpha Coordinates Hematopoietic Stem Cell Survival and Myeloid Regeneration. *Cell Stem Cell*. 2019;25(3):357-72 e7.
264. Maeda K, Baba Y, Nagai Y, Miyazaki K, Malykhin A, Nakamura K, et al. IL-6 blocks a discrete early step in lymphopoiesis. *Blood*. 2005;106(3):879-85.
265. Baldridge MT, King KY, Boles NC, Weksberg DC, and Goodell MA. Quiescent haematopoietic stem cells are activated by IFN-gamma in response to chronic infection. *Nature*. 2010;465(7299):793-7.
266. Sato T, Onai N, Yoshihara H, Arai F, Suda T, and Ohteki T. Interferon regulatory factor-2 protects quiescent hematopoietic stem cells from type I interferon-dependent exhaustion. *Nat Med*. 2009;15(6):696-700.

267. Essers MA, Offner S, Blanco-Bose WE, Waibler Z, Kalinke U, Duchosal MA, et al. IFNalpha activates dormant haematopoietic stem cells in vivo. *Nature*. 2009;458(7240):904-8.
268. Matatall KA, Jeong M, Chen S, Sun D, Chen F, Mo Q, et al. Chronic Infection Depletes Hematopoietic Stem Cells through Stress-Induced Terminal Differentiation. *Cell Rep*. 2016;17(10):2584-95.
269. Shinohara ML, Lu LR, Bu J, Werneck MBF, Kobayashi KS, Glimcher LH, et al. Osteopontin expression is essential for interferon-alpha production by plasmacytoid dendritic cells. *Nature Immunology*. 2006;7(5):498-506.
270. Kanayama M, Xu S, Danzaki K, Gibson JR, Inoue M, Gregory SG, et al. Skewing of the population balance of lymphoid and myeloid cells by secreted and intracellular osteopontin. *Nat Immunol*. 2017;18(9):973-84.
271. Smith JNP, Zhang Y, Li JJ, McCabe A, Jo HJ, Maloney J, et al. Type I IFNs drive hematopoietic stem and progenitor cell collapse via impaired proliferation and increased RIPK1-dependent cell death during shock-like ehrlichial infection. *PLoS Pathog*. 2018;14(8):e1007234.
272. Ramos-Casals M, Garcia-Carrasco M, Lopez-Medrano F, Trejo O, Forns X, Lopez-Guillermo A, et al. Severe autoimmune cytopenias in treatment-naive hepatitis C virus infection: clinical description of 35 cases. *Medicine (Baltimore)*. 2003;82(2):87-96.
273. Hermesh T, Moltedo B, Moran TM, and Lopez CB. Antiviral instruction of bone marrow leukocytes during respiratory viral infections. *Cell Host Microbe*. 2010;7(5):343-53.
274. Trompette A, Gollwitzer ES, Pattaroni C, Lopez-Mejia IC, Riva E, Pernot J, et al. Dietary Fiber Confers Protection against Flu by Shaping Ly6c(-) Patrolling Monocyte Hematopoiesis and CD8(+) T Cell Metabolism. *Immunity*. 2018;48(5):992-+.
275. Rajao DS, and Perez DR. Universal Vaccines and Vaccine Platforms to Protect against Influenza Viruses in Humans and Agriculture. *Front Microbiol*. 2018;9:123.
276. Yamayoshi S, and Kawaoka Y. Current and future influenza vaccines. *Nat Med*. 2019;25(2):212-20.
277. Vaccination C. <https://www.cdc.gov/flu/prevent/vaccinations.htm>. 2019.
278. Hoft DF, Lottenbach KR, Blazevic A, Turan A, Blevins TP, Pacatte TP, et al. Comparisons of the Humoral and Cellular Immune Responses Induced by Live Attenuated Influenza Vaccine and Inactivated Influenza Vaccine in Adults. *Clin Vaccine Immunol*. 2017;24(1).
279. Wu NC, Zost SJ, Thompson AJ, Oyen D, Nycholat CM, McBride R, et al. A structural explanation for the low effectiveness of the seasonal influenza H3N2 vaccine. *PLoS Pathog*. 2017;13(10):e1006682.
280. Cox MM, and Hollister JR. FluBlok, a next generation influenza vaccine manufactured in insect cells. *Biologicals*. 2009;37(3):182-9.

281. Hodgins B, Yam KK, Winter K, Pillet S, Landry N, and Ward BJ. A Single Intramuscular Dose of a Plant-Made Virus-Like Particle Vaccine Elicits a Balanced Humoral and Cellular Response and Protects Young and Aged Mice from Influenza H1N1 Virus Challenge despite a Modest/Absent Humoral Response. *Clin Vaccine Immunol.* 2017;24(12).
282. Pillet S, Couillard J, Trepanier S, Poulin JF, Yassine-Diab B, Guy B, et al. Immunogenicity and safety of a quadrivalent plant-derived virus like particle influenza vaccine candidate—Two randomized Phase II clinical trials in 18 to 49 and ≥ 50 years old adults. *PLoS One.* 2019;14(6):e0216533.
283. Corti D, Voss J, Gamblin SJ, Codoni G, Macagno A, Jarrossay D, et al. A neutralizing antibody selected from plasma cells that binds to group 1 and group 2 influenza A hemagglutinins. *Science.* 2011;333(6044):850-6.
284. Impagliazzo A, Milder F, Kuipers H, Wagner MV, Zhu XY, Hoffman RMB, et al. A stable trimeric influenza hemagglutinin stem as a broadly protective immunogen. *Science.* 2015;349(6254):1301-6.
285. Stadlbauer D, Zhu XY, McMahon M, Turner JS, Wohlbold TJ, Schmitz AJ, et al. Broadly protective human antibodies that target the active site of influenza virus neuraminidase. *Science.* 2019;366(6464):499-+.
286. Kolpe A, Schepens B, Fiers W, and Saelens X. M2-based influenza vaccines: recent advances and clinical potential. *Expert Rev Vaccines.* 2017;16(2):123-36.
287. Murasko DM, Bernstein ED, Gardner EM, Gross P, Munk G, Dran S, et al. Role of humoral and cell-mediated immunity in protection from influenza disease after immunization of healthy elderly. *Exp Gerontol.* 2002;37(2-3):427-39.
288. Lillie PJ, Berthoud TK, Powell TJ, Lambe T, Mullarkey C, Spencer AJ, et al. Preliminary assessment of the efficacy of a T-cell-based influenza vaccine, MVA-NP+M1, in humans. *Clinical infectious diseases : an official publication of the Infectious Diseases Society of America.* 2012;55(1):19-25.
289. Chester KS. The problem of acquired physiological immunity in plants. *The Quarterly Review of Biology.* 1933;8(3):275-324.
290. Sticher L, Mauch-Mani B, Métraux, and JP. Systemic acquired resistance. *Annual review of phytopathology.* 1997;35(1):235-70.
291. Kurtz J. Specific memory within innate immune systems. *Trends in Immunology.* 2005;26(4):186-92.
292. Netea MG, Quintin J, and van der Meer JW. Trained immunity: a memory for innate host defense. *Cell Host Microbe.* 2011;9(5):355-61.
293. Foster SL, Hargreaves DC, and Medzhitov R. Gene-specific control of inflammation by TLR-induced chromatin modifications. *Nature.* 2007;447(7147):972-8.

294. Yoshida K, Maekawa T, Zhu Y, Renard-Guillet C, Chatton B, Inoue K, et al. The transcription factor ATF7 mediates lipopolysaccharide-induced epigenetic changes in macrophages involved in innate immunological memory. *Nature Immunology*. 2015;16(10):1034-+.
295. Cheng SC, Quintin J, Cramer RA, Shepardson KM, Saeed S, Kumar V, et al. mTOR- and HIF-1 α -mediated aerobic glycolysis as metabolic basis for trained immunity. *Science*. 2014;345(6204):1250684.
296. Mitroulis I, Ruppova K, Wang B, Chen LS, Grzybek M, Grinenko T, et al. Modulation of Myelopoiesis Progenitors Is an Integral Component of Trained Immunity. *Cell*. 2018;172(1-2):147-61 e12.
297. Yao YS, Jeyanathan M, Haddadi S, Barra NG, Vaseghi-Shanjani M, Damjanovic D, et al. Induction of Autonomous Memory Alveolar Macrophages Requires T Cell Help and Is Critical to Trained Immunity. *Cell*. 2018;175(6):1634-+.
298. Hamada A, Torre C, Drancourt M, and Ghigo E. Trained Immunity Carried by Non-immune Cells. *Front Microbiol*. 2018;9:3225.
299. Wlodarczyk M, Druszczynska M, and Fol M. Trained Innate Immunity Not Always Amicable. *Int J Mol Sci*. 2019;20(10).
300. Khader SA, Divangahi M, Hanekom W, Hill PC, Maeurer M, Makar KW, et al. Targeting innate immunity for tuberculosis vaccination. *J Clin Invest*. 2019;129(9):3482-91.
301. Gow NA, Netea MG, Munro CA, Ferwerda G, Bates S, Mora-Montes HM, et al. Immune recognition of *Candida albicans* beta-glucan by dectin-1. *J Infect Dis*. 2007;196(10):1565-71.
302. Kleinnijenhuis J, Quintin J, Preijers F, Joosten LA, Ifrim DC, Saeed S, et al. Bacille Calmette-Guerin induces NOD2-dependent nonspecific protection from reinfection via epigenetic reprogramming of monocytes. *Proceedings of the National Academy of Sciences of the United States of America*. 2012;109(43):17537-42.
303. Patel AA, Zhang Y, Fullerton JN, Boelen L, Rongvaux A, Maini AA, et al. The fate and lifespan of human monocyte subsets in steady state and systemic inflammation. *J Exp Med*. 2017;214(7):1913-23.
304. Kaufmann E, Sanz J, Dunn JL, Khan N, Mendonca LE, Pacis A, et al. BCG Educates Hematopoietic Stem Cells to Generate Protective Innate Immunity against Tuberculosis. *Cell*. 2018;172(1-2):176-90 e19.
305. Divangahi M. Are tolerance and training required to end TB? *Nat Rev Immunol*. 2018;18(11):661-3.
306. Darrah PA, Zeppa JJ, Maiello P, Hackney JA, Wadsworth MH, 2nd, Hughes TK, et al. Prevention of tuberculosis in macaques after intravenous BCG immunization. *Nature*. 2020;577(7788):95-102.

307. Wong JP, Saravolac EG, Sabuda D, Levy HB, and Kende M. Prophylactic and therapeutic efficacies of poly(I:C) against respiratory influenza A virus infection in mice. *Antimicrob Agents Chemother.* 1995;39(11):2574-6.
308. Wong JP, Christopher ME, Viswanathan S, Karpoff N, Dai X, Das D, et al. Activation of toll-like receptor signaling pathway for protection against influenza virus infection. *Vaccine.* 2009;27(25-26):3481-3.
309. Baer GM, Shaddock JH, Moore SA, Yager PA, Baron SS, and Levy HB. Successful prophylaxis against rabies in mice and Rhesus monkeys: the interferon system and vaccine. *J Infect Dis.* 1977;136(2):286-91.
310. Ichinohe T, Watanabe I, Ito S, Fujii H, Moriyama M, Tamura S-i, et al. Synthetic Double-Stranded RNA Poly(I:C) Combined with Mucosal Vaccine Protects against Influenza Virus Infection. *Journal of virology.* 2005;79(5):2910-9.
311. Malcolm BA, Aerts CA, Dubois KJ, Geurts FJ, Marien K, Rusch S, et al. PrEP-001 prophylactic effect against rhinovirus and influenza virus - RESULTS of 2 randomized trials. *Antiviral Res.* 2018;153:70-7.
312. Hinshaw VS, Olsen CW, Dybdahl-Sissoko N, and Evans D. Apoptosis: a mechanism of cell killing by influenza A and B viruses. *Journal of virology.* 1994;68(6):3667-73.
313. Cho YS, Challa S, Moquin D, Genga R, Ray TD, Guildford M, et al. Phosphorylation-driven assembly of the RIP1-RIP3 complex regulates programmed necrosis and virus-induced inflammation. *Cell.* 2009;137(6):1112-23.
314. Zhao X, Khan N, Gan H, Tzelepis F, Nishimura T, Park SY, et al. Bcl-xL mediates RIPK3-dependent necrosis in M. tuberculosis-infected macrophages. *Mucosal Immunol.* 2017;10(6):1553-68.
315. Wang J, Nikrad MP, Travanty EA, Zhou B, Phang T, Gao B, et al. Innate immune response of human alveolar macrophages during influenza A infection. *PLoS One.* 2012;7(3):e29879.
316. Goritzka M, Makris S, Kausar F, Durant LR, Pereira C, Kumagai Y, et al. Alveolar macrophage-derived type I interferons orchestrate innate immunity to RSV through recruitment of antiviral monocytes. *J Exp Med.* 2015;212(5):699-714.
317. Balachandran S, Roberts PC, Brown LE, Truong H, Pattnaik AK, Archer DR, et al. Essential role for the dsRNA-dependent protein kinase PKR in innate immunity to viral infection. *Immunity.* 2000;13(1):129-41.
318. Hashimoto D, Chow A, Noizat C, Teo P, Beasley MB, Leboeuf M, et al. Tissue-resident macrophages self-maintain locally throughout adult life with minimal contribution from circulating monocytes. *Immunity.* 2013;38(4):792-804.
319. McAuley JL, Hornung F, Boyd KL, Smith AM, McKeon R, Bennink J, et al. Expression of the 1918 influenza A virus PB1-F2 enhances the pathogenesis of viral and secondary bacterial pneumonia. *Cell Host Microbe.* 2007;2(4):240-9.

320. Upton JW, Kaiser WJ, and Mocarski ES. Virus inhibition of RIP3-dependent necrosis. *Cell Host Microbe*. 2010;7(4):302-13.
321. Vince JE, Wong WW, Gentle I, Lawlor KE, Allam R, O'Reilly L, et al. Inhibitor of apoptosis proteins limit RIP3 kinase-dependent interleukin-1 activation. *Immunity*. 2012;36(2):215-27.
322. Moriwaki K, Balaji S, McQuade T, Malhotra N, Kang J, and Chan FK. The necroptosis adaptor RIPK3 promotes injury-induced cytokine expression and tissue repair. *Immunity*. 2014;41(4):567-78.
323. England H, Summersgill HR, Edye ME, Rothwell NJ, and Brough D. Release of interleukin-1alpha or interleukin-1beta depends on mechanism of cell death. *The Journal of biological chemistry*. 2014;289(23):15942-50.
324. Cullen SP, Kearney CJ, Clancy DM, and Martin SJ. Diverse Activators of the NLRP3 Inflammasome Promote IL-1beta Secretion by Triggering Necrosis. *Cell Reports*. 2015;11(10):1535-48.
325. Christofferson DE, Li Y, Hitomi J, Zhou W, Upperman C, Zhu H, et al. A novel role for RIP1 kinase in mediating TNFalpha production. *Cell death & disease*. 2012;3:e320.
326. Nogusa S, Slifker MJ, Ingram JP, Thapa RJ, and Balachandran S. RIPK3 Is Largely Dispensable for RIG-I-Like Receptor- and Type I Interferon-Driven Transcriptional Responses to Influenza A Virus in Murine Fibroblasts. *PLoS One*. 2016;11(7):e0158774.
327. McComb S, Cessford E, Alturki NA, Joseph J, Shutinoski B, Startek JB, et al. Type-I interferon signaling through ISGF3 complex is required for sustained Rip3 activation and necroptosis in macrophages. *Proceedings of the National Academy of Sciences of the United States of America*. 2014;111(31):E3206-13.
328. Williams BR. Signal integration via PKR. *Sci STKE*. 2001;2001(89):re2.
329. Barry G, Breakwell L, Fragkoudis R, Attarzadeh-Yazdi G, Rodriguez-Andres J, Kohl A, et al. PKR acts early in infection to suppress Semliki Forest virus production and strongly enhances the type I interferon response. *Journal of General Virology*. 2009;90(Pt 6):1382-91.
330. McAllister CS, Taghavi N, and Samuel CE. Protein kinase PKR amplification of interferon beta induction occurs through initiation factor eIF-2alpha-mediated translational control. *The Journal of biological chemistry*. 2012;287(43):36384-92.
331. Kaiser WJ, Upton JW, Long AB, Livingston-Rosanoff D, Daley-Bauer LP, Hakem R, et al. RIP3 mediates the embryonic lethality of caspase-8-deficient mice. *Nature*. 2011;471(7338):368-72.
332. Dillon CP, Weinlich R, Rodriguez DA, Cripps JG, Quarato G, Gurung P, et al. RIPK1 blocks early postnatal lethality mediated by caspase-8 and RIPK3. *Cell*. 2014;157(5):1189-202.
333. Wang X, Jiang W, Yan Y, Gong T, Han J, Tian Z, et al. RNA viruses promote activation of the NLRP3 inflammasome through a RIP1-RIP3-DRP1 signaling pathway. *Nat Immunol*. 2014;15(12):1126-33.

334. Rodrigue-Gervais IG, Labbe K, Dagenais M, Dupaul-Chicoine J, Champagne C, Morizot A, et al. Cellular inhibitor of apoptosis protein cIAP2 protects against pulmonary tissue necrosis during influenza virus infection to promote host survival. *Cell Host Microbe*. 2014;15(1):23-35.
335. Lu JV, Weist BM, van Raam BJ, Marro BS, Nguyen LV, Srinivas P, et al. Complementary roles of Fas-associated death domain (FADD) and receptor interacting protein kinase-3 (RIPK3) in T-cell homeostasis and antiviral immunity. *Proceedings of the National Academy of Sciences of the United States of America*. 2011;108(37):15312-7.
336. Ch'en IL, Tsau JS, Molkenin JD, Komatsu M, and Hedrick SM. Mechanisms of necroptosis in T cells. *J Exp Med*. 2011;208(4):633-41.
337. Weng D, Marty-Roix R, Ganesan S, Proulx MK, Vladimer GI, Kaiser WJ, et al. Caspase-8 and RIP kinases regulate bacteria-induced innate immune responses and cell death. *Proceedings of the National Academy of Sciences of the United States of America*. 2014;111(20):7391-6.
338. Balachandran S, Thomas E, and Barber GN. A FADD-dependent innate immune mechanism in mammalian cells. *Nature*. 2004;432(7015):401-5.
339. Meylan E, Burns K, Hofmann K, Blancheteau V, Martinon F, Kelliher M, et al. RIP1 is an essential mediator of Toll-like receptor 3-induced NF-kappa B activation. *Nat Immunol*. 2004;5(5):503-7.
340. Cusson-Hermance N, Khurana S, Lee TH, Fitzgerald KA, and Kelliher MA. Rip1 mediates the Trif-dependent toll-like receptor 3- and 4-induced NF- κ B activation but does not contribute to interferon regulatory factor 3 activation. *The Journal of biological chemistry*. 2005;280(44):36560-6.
341. Hyun J, Ramos JC, Toomey N, Balachandran S, Lavorgna A, Harhaj E, et al. Oncogenic human T-cell lymphotropic virus type 1 tax suppression of primary innate immune signaling pathways. *Journal of virology*. 2015;89(9):4880-93.
342. Michallet MC, Meylan E, Ermolaeva MA, Vazquez J, Rebsamen M, Curran J, et al. TRADD protein is an essential component of the RIG-like helicase antiviral pathway. *Immunity*. 2008;28(5):651-61.
343. Rajput A, Kovalenko A, Bogdanov K, Yang SH, Kang TB, Kim JC, et al. RIG-I RNA helicase activation of IRF3 transcription factor is negatively regulated by caspase-8-mediated cleavage of the RIP1 protein. *Immunity*. 2011;34(3):340-51.
344. Wong WW, Vince JE, Lalaoui N, Lawlor KE, Chau D, Bankovacki A, et al. cIAPs and XIAP regulate myelopoiesis through cytokine production in an RIPK1- and RIPK3-dependent manner. *Blood*. 2014;123(16):2562-72.
345. Thapa RJ, Ingram JP, Ragan KB, Nogusa S, Boyd DF, Benitez AA, et al. DAI Senses Influenza A Virus Genomic RNA and Activates RIPK3-Dependent Cell Death. *Cell Host Microbe*. 2016;20(5):674-81.
346. Takaoka A, Wang Z, Choi MK, Yanai H, Negishi H, Ban T, et al. DAI (DLM-1/ZBP1) is a cytosolic DNA sensor and an activator of innate immune response. *Nature*. 2007;448(7152):501-5.

347. Tzelepis F, Verway M, Daoud J, Gillard J, Hassani-Ardakani K, Dunn J, et al. Annexin1 regulates DC efferocytosis and cross-presentation during Mycobacterium tuberculosis infection. *J Clin Invest*. 2015;125(2):752-68.
348. Gaush CR, and Smith TF. Replication and plaque assay of influenza virus in an established line of canine kidney cells. *Appl Microbiol*. 1968;16(4):588-94.
349. Coulombe F, Fiola S, Akira S, Cormier Y, and Gosselin J. Muramyl dipeptide induces NOD2-dependent Ly6C(high) monocyte recruitment to the lungs and protects against influenza virus infection. *PLoS One*. 2012;7(5):e36734.
350. Kaiser WJ, Sridharan H, Huang C, Mandal P, Upton JW, Gough PJ, et al. Toll-like receptor 3-mediated necrosis via TRIF, RIP3, and MLKL. *The Journal of biological chemistry*. 2013;288(43):31268-79.
351. Meunier I, Kaufmann E, Downey J, and Divangahi M. Unravelling the networks dictating host resistance versus tolerance during pulmonary infections. *Cell Tissue Res*. 2017;367(3):525-36.
352. Tzelepis F, Blagih J, Khan N, Gillard J, Mendonca L, Roy DG, et al. Mitochondrial cyclophilin D regulates T cell metabolic responses and disease tolerance to tuberculosis. *Sci Immunol*. 2018;3(23).
353. Perrone LA, Plowden JK, Garcia-Sastre A, Katz JM, and Tumpey TM. H5N1 and 1918 pandemic influenza virus infection results in early and excessive infiltration of macrophages and neutrophils in the lungs of mice. *PLoS Pathog*. 2008;4(8):e1000115.
354. Leung NH, Xu C, Ip DK, and Cowling BJ. Review Article: The Fraction of Influenza Virus Infections That Are Asymptomatic: A Systematic Review and Meta-analysis. *Epidemiology*. 2015;26(6):862-72.
355. Zou L, Ruan F, Huang M, Liang L, Huang H, Hong Z, et al. SARS-CoV-2 Viral Load in Upper Respiratory Specimens of Infected Patients. *N Engl J Med*. 2020;382(12):1177-9.
356. Carlin LE, Hemann EA, Zacharias ZR, Heusel JW, and Legge KL. Natural Killer Cell Recruitment to the Lung During Influenza A Virus Infection Is Dependent on CXCR3, CCR5, and Virus Exposure Dose. *Frontiers in Immunology*. 2018;9(781).
357. Vivier E, Tomasello E, Baratin M, Walzer T, and Ugolini S. Functions of natural killer cells. *Nat Immunol*. 2008;9(5):503-10.
358. Glasner A, Zurunic A, Meningher T, Lenac Rovis T, Tsukerman P, Bar-On Y, et al. Elucidating the mechanisms of influenza virus recognition by Ncr1. *PLoS One*. 2012;7(5):e36837.
359. McAleer JP, and Kolls JK. Directing traffic: IL-17 and IL-22 coordinate pulmonary immune defense. *Immunol Rev*. 2014;260(1):129-44.

360. Baines CP, Kaiser RA, Purcell NH, Blair NS, Osinska H, Hambleton MA, et al. Loss of cyclophilin D reveals a critical role for mitochondrial permeability transition in cell death. *Nature*. 2005;434(7033):658-62.
361. Nakagawa T, Shimizu S, Watanabe T, Yamaguchi O, Otsu K, Yamagata H, et al. Cyclophilin D-dependent mitochondrial permeability transition regulates some necrotic but not apoptotic cell death. *Nature*. 2005;434(7033):652-8.
362. Schinzel AC, Takeuchi O, Huang Z, Fisher JK, Zhou Z, Rubens J, et al. Cyclophilin D is a component of mitochondrial permeability transition and mediates neuronal cell death after focal cerebral ischemia. *Proceedings of the National Academy of Sciences of the United States of America*. 2005;102(34):12005-10.
363. Fayaz SM, Raj YV, and Krishnamurthy RG. CypD: The Key to the Death Door. *CNS Neurol Disord Drug Targets*. 2015;14(5):654-63.
364. Condotta SA, Downey J, Pardy RD, Valbon SF, Tarrab E, Lamarre A, et al. Cyclophilin D Regulates Antiviral CD8(+) T Cell Survival in a Cell-Extrinsic Manner. *Immunohorizons*. 2020;4(4):217-30.
365. Soares MP, Teixeira L, and Moita LF. Disease tolerance and immunity in host protection against infection. *Nat Rev Immunol*. 2017;17(2):83-96.
366. Sengupta S, Tang SY, Devine JC, Anderson ST, Nayak S, Zhang SL, et al. Circadian control of lung inflammation in influenza infection. *Nat Commun*. 2019;10(1):4107.
367. Chiossone L, Chaix J, Fuseri N, Roth C, Vivier E, and Walzer T. Maturation of mouse NK cells is a 4-stage developmental program. *Blood*. 2009;113(22):5488-96.
368. Collin R, St-Pierre C, Guilbault L, Mullins-Dansereau V, Policheni A, Guimont-Desrochers F, et al. An Unbiased Linkage Approach Reveals That the p53 Pathway Is Coupled to NK Cell Maturation. *J Immunol*. 2017;199(4):1490-504.
369. Fu B, Wang F, Sun R, Ling B, Tian Z, and Wei H. CD11b and CD27 reflect distinct population and functional specialization in human natural killer cells. *Immunology*. 2011;133(3):350-9.
370. Crinier A, Milpied P, Escaliere B, Piperoglou C, Galluso J, Balsamo A, et al. High-Dimensional Single-Cell Analysis Identifies Organ-Specific Signatures and Conserved NK Cell Subsets in Humans and Mice. *Immunity*. 2018;49(5):971-86 e5.
371. Gautier EL, Shay T, Miller J, Greter M, Jakubzick C, Ivanov S, et al. Gene-expression profiles and transcriptional regulatory pathways that underlie the identity and diversity of mouse tissue macrophages. *Nat Immunol*. 2012;13(11):1118-28.
372. van Helden MJ, Zaiss DM, and Sijts AJ. CCR2 defines a distinct population of NK cells and mediates their migration during influenza virus infection in mice. *PLoS One*. 2012;7(12):e52027.

373. Peng H, Jiang X, Chen Y, Sojka DK, Wei H, Gao X, et al. Liver-resident NK cells confer adaptive immunity in skin-contact inflammation. *The Journal of Clinical Investigation*. 2013;123(4):1444-56.
374. Sojka DK, Plougastel-Douglas B, Yang L, Pak-Wittel MA, Artyomov MN, Ivanova Y, et al. Tissue-resident natural killer (NK) cells are cell lineages distinct from thymic and conventional splenic NK cells. *Elife*. 2014;3:e01659.
375. Abel AM, Yang C, Thakar MS, and Malarkannan S. Natural Killer Cells: Development, Maturation, and Clinical Utilization. *Frontiers in Immunology*. 2018;9(1869).
376. Brady CA, and Attardi LD. p53 at a glance. *J Cell Sci*. 2010;123(Pt 15):2527-32.
377. Vaseva AV, Marchenko ND, Ji K, Tsrirka SE, Holzmann S, and Moll UM. p53 opens the mitochondrial permeability transition pore to trigger necrosis. *Cell*. 2012;149(7):1536-48.
378. Bigi A, Beltrami E, Trinei M, Stendardo M, Pelicci PG, and Giorgio M. Cyclophilin D counteracts P53-mediated growth arrest and promotes Ras tumorigenesis. *Oncogene*. 2016;35(39):5132-43.
379. Belle JI, Langlais D, Petrov JC, Pardo M, Jones RG, Gros P, et al. p53 mediates loss of hematopoietic stem cell function and lymphopenia in Mym1 deficiency. *Blood*. 2015;125(15):2344-8.
380. Mendrysa SM, McElwee MK, Michalowski J, O'Leary KA, Young KM, and Perry ME. mdm2 Is critical for inhibition of p53 during lymphopoiesis and the response to ionizing irradiation. *Mol Cell Biol*. 2003;23(2):462-72.
381. Stegemann-Koniszewski S, Behrens S, Boehme JD, Hochnadel I, Riese P, Guzmán CA, et al. Respiratory Influenza A Virus Infection Triggers Local and Systemic Natural Killer Cell Activation via Toll-Like Receptor 7. *Front Immunol*. 2018;9:245.
382. Long BR, Michaelsson J, Loo CP, Ballan WM, Vu B-AN, Hecht FM, et al. Elevated Frequency of Gamma Interferon-Producing NK Cells in Healthy Adults Vaccinated against Influenza Virus. *Clinical and Vaccine Immunology*. 2008;15(1):120-30.
383. Herold S, Becker C, Ridge KM, and Budinger GRS. Influenza virus-induced lung injury: pathogenesis and implications for treatment. *European Respiratory Journal*. 2015;45(5):1463-78.
384. To KK, Hung IF, Li IW, Lee KL, Koo CK, Yan WW, et al. Delayed clearance of viral load and marked cytokine activation in severe cases of pandemic H1N1 2009 influenza virus infection. *Clinical infectious diseases : an official publication of the Infectious Diseases Society of America*. 2010;50(6):850-9.
385. Kover PX, and Schaal BA. Genetic variation for disease resistance and tolerance among *Arabidopsis thaliana* accessions. *Proceedings of the National Academy of Sciences of the United States of America*. 2002;99(17):11270-4.
386. King IL, and Li Y. Host-Parasite Interactions Promote Disease Tolerance to Intestinal Helminth Infection. *Frontiers in Immunology*. 2018;9(2128).

387. West AP, Shadel GS, and Ghosh S. Mitochondria in innate immune responses. *Nat Rev Immunol*. 2011;11(6):389-402.
388. Wu D, Sanin DE, Everts B, Chen Q, Qiu J, Buck MD, et al. Type 1 Interferons Induce Changes in Core Metabolism that Are Critical for Immune Function. *Immunity*. 2016;44(6):1325-36.
389. Zhou G, Juang SW, and Kane KP. NK cells exacerbate the pathology of influenza virus infection in mice. *Eur J Immunol*. 2013;43(4):929-38.
390. Netea MG, Domínguez-Andrés J, Barreiro LB, Chavakis T, Divangahi M, Fuchs E, et al. Defining trained immunity and its role in health and disease. *Nat Rev Immunol*. 2020.
391. Kleinnijenhuis J, Quintin J, Preijers F, Joosten LA, Jacobs C, Xavier RJ, et al. BCG-induced trained immunity in NK cells: Role for non-specific protection to infection. *Clin Immunol*. 2014;155(2):213-9.
392. Tay MZ, Poh CM, Renia L, MacAry PA, and Ng LFP. The trinity of COVID-19: immunity, inflammation and intervention. *Nat Rev Immunol*. 2020;20(6):363-74.
393. Ayres JS. Surviving COVID-19: A disease tolerance perspective. *Sci Adv*. 2020;6(18):eabc1518.
394. Hartner JC, Walkley CR, Lu J, and Orkin SH. ADAR1 is essential for the maintenance of hematopoiesis and suppression of interferon signaling. *Nat Immunol*. 2009;10(1):109-15.
395. Moorlag S, Khan N, Novakovic B, Kaufmann E, Jansen T, van Crevel R, et al. beta-Glucan Induces Protective Trained Immunity against Mycobacterium tuberculosis Infection: A Key Role for IL-1. *Cell Rep*. 2020;31(7):107634.
396. Lemaitre B, Reichhart JM, and Hoffmann JA. Drosophila host defense: differential induction of antimicrobial peptide genes after infection by various classes of microorganisms. *Proc Natl Acad Sci U S A*. 1997;94(26):14614-9.
397. Leentjens J, Bekkering S, Joosten LAB, Netea MG, Burgner DP, and Riksen NP. Trained Innate Immunity as a Novel Mechanism Linking Infection and the Development of Atherosclerosis. *Circ Res*. 2018;122(5):664-9.
398. Bekkering S, Quintin J, Joosten LA, van der Meer JW, Netea MG, and Riksen NP. Oxidized low-density lipoprotein induces long-term proinflammatory cytokine production and foam cell formation via epigenetic reprogramming of monocytes. *Arterioscler Thromb Vasc Biol*. 2014;34(8):1731-8.
399. Wendeln AC, Degenhardt K, Kaurani L, Gertig M, Ulas T, Jain G, et al. Innate immune memory in the brain shapes neurological disease hallmarks. *Nature*. 2018;556(7701):332-8.
400. Belyaev NN, Brown DE, Diaz AI, Rae A, Jarra W, Thompson J, et al. Induction of an IL7-R(+)c-Kit(hi) myelolymphoid progenitor critically dependent on IFN-gamma signaling during acute malaria. *Nat Immunol*. 2010;11(6):477-85.

401. Kamada R, Yang W, Zhang Y, Patel MC, Yang Y, Ouda R, et al. Interferon stimulation creates chromatin marks and establishes transcriptional memory. *Proc Natl Acad Sci U S A*. 2018;115(39):E9162-E71.
402. Dolznig H, Habermann B, Stangl K, Deiner EM, Moriggl R, Beug H, et al. Apoptosis protection by the Epo target Bcl-X(L) allows factor-independent differentiation of primary erythroblasts. *Curr Biol*. 2002;12(13):1076-85.
403. Akashi K, Kondo M, von Freeden-Jeffry U, Murray R, and Weissman IL. Bcl-2 rescues T lymphopoiesis in interleukin-7 receptor-deficient mice. *Cell*. 1997;89(7):1033-41.
404. Nunez G, Sakamoto K, and Soares MP. Innate Nutritional Immunity. *J Immunol*. 2018;201(1):11-8.
405. Wang J, and Pantopoulos K. Regulation of cellular iron metabolism. *Biochem J*. 2011;434(3):365-81.
406. Dixon SJ, Lemberg KM, Lamprecht MR, Skouta R, Zaitsev EM, Gleason CE, et al. Ferroptosis: an iron-dependent form of nonapoptotic cell death. *Cell*. 2012;149(5):1060-72.
407. Verbon EH, Trapet PL, Stringlis IA, Kruijs S, Bakker P, and Pieterse CMJ. Iron and Immunity. *Annu Rev Phytopathol*. 2017;55:355-75.
408. Hood MI, and Skaar EP. Nutritional immunity: transition metals at the pathogen-host interface. *Nat Rev Microbiol*. 2012;10(8):525-37.
409. Soares MP, and Weiss G. The Iron age of host-microbe interactions. *EMBO Rep*. 2015;16(11):1482-500.
410. Palmer LD, and Skaar EP. Transition Metals and Virulence in Bacteria. *Annu Rev Genet*. 2016;50:67-91.
411. Parrow NL, Fleming RE, and Minnick MF. Sequestration and scavenging of iron in infection. *Infect Immun*. 2013;81(10):3503-14.
412. Olakanmi O, Schlesinger LS, and Britigan BE. Hereditary hemochromatosis results in decreased iron acquisition and growth by Mycobacterium tuberculosis within human macrophages. *J Leukoc Biol*. 2007;81(1):195-204.
413. Gangaidzo IT, Moyo VM, Mvundura E, Aggrey G, Murphree NL, Khumalo H, et al. Association of pulmonary tuberculosis with increased dietary iron. *J Infect Dis*. 2001;184(7):936-9.
414. Murray MJ, Murray AB, Murray MB, and Murray CJ. The adverse effect of iron repletion on the course of certain infections. *Br Med J*. 1978;2(6145):1113-5.
415. Muto Y, Nishiyama M, Nita A, Moroishi T, and Nakayama KI. Essential role of FBXL5-mediated cellular iron homeostasis in maintenance of hematopoietic stem cells. *Nat Commun*. 2017;8:16114.

416. Jin X, He X, Cao X, Xu P, Xing Y, Sui S, et al. Iron overload impairs normal hematopoietic stem and progenitor cells through reactive oxygen species and shortens survival in myelodysplastic syndrome mice. *Haematologica*. 2018;103(10):1627-34.
417. Das B, Kashino SS, Pulu I, Kalita D, Swami V, Yeger H, et al. CD271(+) bone marrow mesenchymal stem cells may provide a niche for dormant Mycobacterium tuberculosis. *Sci Transl Med*. 2013;5(170):170ra13.
418. Lai AY, and Kondo M. Asymmetrical lymphoid and myeloid lineage commitment in multipotent hematopoietic progenitors. *J Exp Med*. 2006;203(8):1867-73.
419. Pietras EM, Lakshminarasimhan R, Techner JM, Fong S, Flach J, Binnewies M, et al. Re-entry into quiescence protects hematopoietic stem cells from the killing effect of chronic exposure to type I interferons. *J Exp Med*. 2014;211(2):245-62.
420. Kondo M, Weissman IL, and Akashi K. Identification of clonogenic common lymphoid progenitors in mouse bone marrow. *Cell*. 1997;91(5):661-72.
421. Lewis KN, Liao R, Guinn KM, Hickey MJ, Smith S, Behr MA, et al. Deletion of RD1 from Mycobacterium tuberculosis Mimics Bacille Calmette-Guérin Attenuation. *The Journal of Infectious Diseases*. 2003;187(1):117-23.
422. Sherman DR, Guinn KM, Hickey MJ, Mathur SK, Zakel KL, and Smith S. Mycobacterium tuberculosis H37Rv:ΔRD1 Is More Virulent than M. bovis Bacille Calmette-Guérin in Long-Term Murine Infection. *The Journal of Infectious Diseases*. 2004;190(1):123-6.
423. Bronte V, and Pittet MJ. The spleen in local and systemic regulation of immunity. *Immunity*. 2013;39(5):806-18.
424. Silva-Gomes S, Appelberg R, Larsen R, Soares MP, and Gomes MS. Heme catabolism by heme oxygenase-1 confers host resistance to Mycobacterium infection. *Infect Immun*. 2013;81(7):2536-45.
425. Amaral EP, Costa DL, Namasivayam S, Riteau N, Kamenyeva O, Mittereder L, et al. A major role for ferroptosis in Mycobacterium tuberculosis-induced cell death and tissue necrosis. *J Exp Med*. 2019;216(3):556-70.
426. Mayer-Barber KD, Andrade BB, Oland SD, Amaral EP, Barber DL, Gonzales J, et al. Host-directed therapy of tuberculosis based on interleukin-1 and type I interferon crosstalk. *Nature*. 2014;511(7507):99-103.
427. Martin CJ, Booty MG, Rosebrock TR, Nunes-Alves C, Desjardins DM, Keren I, et al. Efferocytosis is an innate antibacterial mechanism. *Cell Host Microbe*. 2012;12(3):289-300.
428. Fortune SM, Solache A, Jaeger A, Hill PJ, Belisle JT, Bloom BR, et al. Mycobacterium tuberculosis inhibits macrophage responses to IFN-gamma through myeloid differentiation factor 88-dependent and -independent mechanisms. *J Immunol*. 2004;172(10):6272-80.

429. Chackerian AA, Alt JM, Perera TV, Dascher CC, and Behar SM. Dissemination of Mycobacterium tuberculosis is influenced by host factors and precedes the initiation of T-cell immunity. *Infect Immun.* 2002;70(8):4501-9.
430. Wolf AJ, Desvignes L, Linas B, Banaiee N, Tamura T, Takatsu K, et al. Initiation of the adaptive immune response to Mycobacterium tuberculosis depends on antigen production in the local lymph node, not the lungs. *J Exp Med.* 2008;205(1):105-15.
431. Samstein M, Schreiber HA, Leiner IM, Susac B, Glickman MS, and Pamer EG. Essential yet limited role for CCR2(+) inflammatory monocytes during Mycobacterium tuberculosis-specific T cell priming. *Elife.* 2013;2:e01086.
432. Zheng GXY, Terry JM, Belgrader P, Ryvkin P, Bent ZW, Wilson R, et al. Massively parallel digital transcriptional profiling of single cells. *Nature Communications.* 2017;8(1):14049.
433. Cabezas-Wallscheid N, Klimmeck D, Hansson J, Lipka DB, Reyes A, Wang Q, et al. Identification of regulatory networks in HSCs and their immediate progeny via integrated proteome, transcriptome, and DNA methylome analysis. *Cell Stem Cell.* 2014;15(4):507-22.
434. Nandi B, and Behar SM. Regulation of neutrophils by interferon-gamma limits lung inflammation during tuberculosis infection. *J Exp Med.* 2011;208(11):2251-62.
435. Antonelli LR, Gigliotti Rothfuchs A, Goncalves R, Roffe E, Cheever AW, Bafica A, et al. Intranasal Poly-IC treatment exacerbates tuberculosis in mice through the pulmonary recruitment of a pathogen-permissive monocyte/macrophage population. *J Clin Invest.* 2010;120(5):1674-82.
436. Vandenabeele P, Galluzzi L, Vanden Berghe T, and Kroemer G. Molecular mechanisms of necroptosis: an ordered cellular explosion. *Nat Rev Mol Cell Biol.* 2010;11(10):700-14.
437. Roca FJ, and Ramakrishnan L. TNF dually mediates resistance and susceptibility to mycobacteria via mitochondrial reactive oxygen species. *Cell.* 2013;153(3):521-34.
438. Martin-Sanchez D, Gallegos-Villalobos A, Fontecha-Barriuso M, Carrasco S, Sanchez-Nino MD, Lopez-Hernandez FJ, et al. Deferasirox-induced iron depletion promotes BclxL downregulation and death of proximal tubular cells. *Sci Rep.* 2017;7:41510.
439. al-Rafaie FN, Wilkes S, Wonke B, and Hoffbrand AV. The effect of deferiprone (L1) and desferrioxamine on myelopoiesis using a liquid culture system. *Br J Haematol.* 1994;87(1):196-8.
440. Ganz T. Systemic iron homeostasis. *Physiol Rev.* 2013;93(4):1721-41.
441. Blankenhaus B, Braza F, Martins R, Bastos-Amador P, Gonzalez-Garcia I, Carlos AR, et al. Ferritin regulates organismal energy balance and thermogenesis. *Mol Metab.* 2019;24:64-79.
442. Reddy VP, Chinta KC, Saini V, Glasgow JN, Hull TD, Traylor A, et al. Ferritin H Deficiency in Myeloid Compartments Dysregulates Host Energy Metabolism and Increases Susceptibility to Mycobacterium tuberculosis Infection. *Front Immunol.* 2018;9:860.

443. Hunt BJ, Andrews V, and Pettingale KW. The significance of pancytopenia in military tuberculosis. *Postgrad Med J.* 1987;63(743):801-4.
444. Liberzon A, Birger C, Thorvaldsdottir H, Ghandi M, Mesirov JP, and Tamayo P. The Molecular Signatures Database (MSigDB) hallmark gene set collection. *Cell Syst.* 2015;1(6):417-25.
445. Polager S, and Ginsberg D. p53 and E2f: partners in life and death. *Nature reviews Cancer.* 2009;9(10):738-48.
446. Altare F, Durandy A, Lammas D, Emile JF, Lamhamedi S, Le Deist F, et al. Impairment of mycobacterial immunity in human interleukin-12 receptor deficiency. *Science.* 1998;280(5368):1432-5.
447. Kee BL. A comprehensive transcriptional landscape of human hematopoiesis. *Cell Stem Cell.* 2011;8(2):122-4.
448. Novershtern N, Subramanian A, Lawton LN, Mak RH, Haining WN, McConkey ME, et al. Densely interconnected transcriptional circuits control cell states in human hematopoiesis. *Cell.* 2011;144(2):296-309.
449. Lauridsen FKB, Jensen TL, Rapin N, Aslan D, Wilhelmson AS, Punthir S, et al. Differences in Cell Cycle Status Underlie Transcriptional Heterogeneity in the HSC Compartment. *Cell Rep.* 2018;24(3):766-80.
450. Regev D, Surolia R, Karki S, Zolak J, Montes-Worboys A, Oliva O, et al. Heme oxygenase-1 promotes granuloma development and protects against dissemination of mycobacteria. *Lab Invest.* 2012;92(11):1541-52.
451. Reddy PV, Puri RV, Khera A, and Tyagi AK. Iron storage proteins are essential for the survival and pathogenesis of Mycobacterium tuberculosis in THP-1 macrophages and the guinea pig model of infection. *J Bacteriol.* 2012;194(3):567-75.
452. Marcela Rodriguez G, and Neyrolles O. Metallobiology of Tuberculosis. *Microbiol Spectr.* 2014;2(3).
453. Rickard JA, O'Donnell JA, Evans JM, Lalaoui N, Poh AR, Rogers T, et al. RIPK1 regulates RIPK3-MLKL-driven systemic inflammation and emergency hematopoiesis. *Cell.* 2014;157(5):1175-88.
454. Roderick JE, Hermance N, Zelic M, Simmons MJ, Polykratis A, Pasparakis M, et al. Hematopoietic RIPK1 deficiency results in bone marrow failure caused by apoptosis and RIPK3-mediated necroptosis. *Proc Natl Acad Sci U S A.* 2014;111(40):14436-41.
455. Divangahi M, Chen M, Gan H, Desjardins D, Hickman TT, Lee DM, et al. Mycobacterium tuberculosis evades macrophage defenses by inhibiting plasma membrane repair. *Nat Immunol.* 2009;10(8):899-906.
456. Riccardi G, Milano A, Pasca MR, and Nies DH. Genomic analysis of zinc homeostasis in Mycobacterium tuberculosis. *FEMS Microbiol Lett.* 2008;287(1):1-7.

457. King LE, and Fraker PJ. Zinc deficiency in mice alters myelopoiesis and hematopoiesis. *J Nutr.* 2002;132(11):3301-7.
458. Weinberg ED. Nutritional immunity. Host's attempt to withhold iron from microbial invaders. *JAMA.* 1975;231(1):39-41.
459. Ioannou S, Hatzis G, Vlahadami I, and Voulgarelis M. Aplastic anemia associated with interferon alpha 2a in a patient with chronic hepatitis C virus infection: a case report. *J Med Case Rep.* 2010;4:268.
460. Plataniias LC, and Fish EN. Signaling pathways activated by interferons. *Exp Hematol.* 1999;27(11):1583-92.
461. de Bruin AM, Demirel O, Hooibrink B, Brandts CH, and Nolte MA. Interferon-gamma impairs proliferation of hematopoietic stem cells in mice. *Blood.* 2013;121(18):3578-85.
462. Novakovic B, Habibi E, Wang SY, Arts RJW, Davar R, Megchelenbrink W, et al. beta-Glucan Reverses the Epigenetic State of LPS-Induced Immunological Tolerance. *Cell.* 2016;167(5):1354-68 e14.
463. Bauer H, Paronetto F, Burns WA, and Einheber A. The enhancing effect of the microbial flora on macrophage function and the immune response. A study in germfree mice. *J Exp Med.* 1966;123(6):1013-24.
464. Gorjifard S, and Goldszmid RS. Microbiota-myeloid cell crosstalk beyond the gut. *J Leukoc Biol.* 2016;100(5):865-79.
465. Domingo-Gonzalez R, and Moore BB. Innate Immunity Post-Hematopoietic Stem Cell Transplantation: Focus on Epigenetics. *Adv Neuroimmune Biol.* 2014;5(3):189-97.
466. Comas I, Chakravarti J, Small PM, Galagan J, Niemann S, Kremer K, et al. Human T cell epitopes of Mycobacterium tuberculosis are evolutionarily hyperconserved. *Nat Genet.* 2010;42(6):498-503.
467. Genewein A, Telenti A, Bernasconi C, Mordasini C, Weiss S, Maurer AM, et al. Molecular approach to identifying route of transmission of tuberculosis in the community. *Lancet.* 1993;342(8875):841-4.
468. Rodrigo T, Cayla JA, Garcia de Olalla P, Galdos-Tanguis H, Jansa JM, Miranda P, et al. Characteristics of tuberculosis patients who generate secondary cases. *Int J Tuberc Lung Dis.* 1997;1(4):352-7.
469. Ip WKE, Hoshi N, Shouval DS, Snapper S, and Medzhitov R. Anti-inflammatory effect of IL-10 mediated by metabolic reprogramming of macrophages. *Science.* 2017;356(6337):513-9.
470. Bray NL, Pimentel H, Melsted P, and Pachter L. Near-optimal probabilistic RNA-seq quantification. *Nat Biotechnol.* 2016;34(5):525-7.

471. Robinson MD, McCarthy DJ, and Smyth GK. edgeR: a Bioconductor package for differential expression analysis of digital gene expression data. *Bioinformatics*. 2010;26(1):139-40.
472. Ritchie ME, Phipson B, Wu D, Hu Y, Law CW, Shi W, et al. limma powers differential expression analyses for RNA-sequencing and microarray studies. *Nucleic Acids Res*. 2015;43(7):e47.
473. Lun AT, McCarthy DJ, and Marioni JC. A step-by-step workflow for low-level analysis of single-cell RNA-seq data with Bioconductor. *F1000Res*. 2016;5:2122.
474. Paul F, Arkin Y, Giladi A, Jaitin DA, Kenigsberg E, Keren-Shaul H, et al. Transcriptional Heterogeneity and Lineage Commitment in Myeloid Progenitors. *Cell*. 2015;163(7):1663-77.
475. Stuart T, Butler A, Hoffman P, Hafemeister C, Papalexi E, Mauck WM, 3rd, et al. Comprehensive Integration of Single-Cell Data. *Cell*. 2019;177(7):1888-902.e21.
476. Satija R, Farrell JA, Gennert D, Schier AF, and Regev A. Spatial reconstruction of single-cell gene expression data. *Nat Biotechnol*. 2015;33(5):495-502.
477. Shannon P, Markiel A, Ozier O, Baliga NS, Wang JT, Ramage D, et al. Cytoscape: a software environment for integrated models of biomolecular interaction networks. *Genome Res*. 2003;13(11):2498-504.
478. Bindea G, Mlecnik B, Hackl H, Charoentong P, Tosolini M, Kirilovsky A, et al. ClueGO: a Cytoscape plug-in to decipher functionally grouped gene ontology and pathway annotation networks. *Bioinformatics*. 2009;25(8):1091-3.
479. Benjamini Y, and Hochberg Y. Controlling the False Discovery Rate - a Practical and Powerful Approach to Multiple Testing. *J R Stat Soc B*. 1995;57(1):289-300.
480. Uthayakumar D, Paris S, Chapat L, Freyburger L, Poulet H, and De Luca K. Non-specific Effects of Vaccines Illustrated Through the BCG Example: From Observations to Demonstrations. *Front Immunol*. 2018;9:2869.
481. Shaw MW, Xu X, Li Y, Normand S, Ueki RT, Kunimoto GY, et al. Reappearance and global spread of variants of influenza B/Victoria/2/87 lineage viruses in the 2000-2001 and 2001-2002 seasons. *Virology*. 2002;303(1):1-8.
482. Control CfD. Influenza vaccination coverage. 2018.
483. Gavigan P, and McCullers JA. Influenza: annual seasonal severity. *Current Opinion in Pediatrics*. 2019;31(1):112-8.
484. Lord JM. The effect of ageing of the immune system on vaccination responses. *Hum Vaccin Immunother*. 2013;9(6):1364-7.
485. McElhaney JE, and Dutz JP. Better Influenza Vaccines for Older People: What Will It Take? *The Journal of Infectious Diseases*. 2008;198(5):632-4.

486. Osterhaus A, Fouchier R, and Rimmelzwaan G. Towards universal influenza vaccines? *Philos Trans R Soc Lond B Biol Sci.* 2011;366(1579):2766-73.
487. Yassine HM, Boyington JC, McTamney PM, Wei C-J, Kanekiyo M, Kong W-P, et al. Hemagglutinin-stem nanoparticles generate heterosubtypic influenza protection. *Nature Medicine.* 2015;21(9):1065-70.
488. Jensen KJ, Larsen N, Biering-Sørensen S, Andersen A, Eriksen HB, Monteiro I, et al. Heterologous immunological effects of early BCG vaccination in low-birth-weight infants in Guinea-Bissau: a randomized-controlled trial. *J Infect Dis.* 2015;211(6):956-67.
489. Spencer JC, Ganguly R, and Waldman RH. Nonspecific protection of mice against influenza virus infection by local or systemic immunization with Bacille Calmette-Guérin. *J Infect Dis.* 1977;136(2):171-5.
490. Vetvicka V, and Vetvickova J. Glucan supplementation enhances the immune response against an influenza challenge in mice. *Ann Transl Med.* 2015;3(2):22.
491. Moorlag S, Arts RJW, van Crevel R, and Netea MG. Non-specific effects of BCG vaccine on viral infections. *Clin Microbiol Infect.* 2019;25(12):1473-8.
492. Arts RJW, Moorlag SJCFM, Novakovic B, Li Y, Wang SY, Oosting M, et al. BCG Vaccination Protects against Experimental Viral Infection in Humans through the Induction of Cytokines Associated with Trained Immunity. *Cell Host & Microbe.* 2018;23(1):89-+.
493. O'Neill LAJ, and Netea MG. BCG-induced trained immunity: can it offer protection against COVID-19? *Nature Reviews Immunology.* 2020;20(6):335-7.
494. Sakai S, Kauffman KD, Schenkel JM, McBerry CC, Mayer-Barber KD, Masopust D, et al. Cutting Edge: Control of Mycobacterium tuberculosis Infection by a Subset of Lung Parenchyma-Homing CD4 T Cells. *Journal of Immunology.* 2014;192(7):2965-9.
495. Böttcher JP, Beyer M, Meissner F, Abdullah Z, Sander J, Höchst B, et al. Functional classification of memory CD8+ T cells by CX3CR1 expression. *Nature Communications.* 2015;6(1):8306.
496. Gerlach C, Moseman EA, Loughhead SM, Alvarez D, Zwijnenburg AJ, Waanders L, et al. The Chemokine Receptor CX3CR1 Defines Three Antigen-Experienced CD8 T Cell Subsets with Distinct Roles in Immune Surveillance and Homeostasis. *Immunity.* 2016;45(6):1270-84.
497. Anderson KG, Mayer-Barber K, Sung H, Beura L, James BR, Taylor JJ, et al. Intravascular staining for discrimination of vascular and tissue leukocytes. *Nat Protoc.* 2014;9(1):209-22.
498. Geerman S, Brassier G, Bhushal S, Salerno F, Kragten NA, Hoogenboezem M, et al. Memory CD8(+) T cells support the maintenance of hematopoietic stem cells in the bone marrow. *Haematologica.* 2018;103(6):e230-e3.
499. de Bruin AM, Voermans C, and Nolte MA. Impact of interferon- γ on hematopoiesis. *Blood.* 2014;124(16):2479-86.

500. Kleinnijenhuis J, Quintin J, Preijers F, Benn CS, Joosten LA, Jacobs C, et al. Long-lasting effects of BCG vaccination on both heterologous Th1/Th17 responses and innate trained immunity. *J Innate Immun.* 2014;6(2):152-8.
501. Dos Santos JC, Barroso de Figueiredo AM, Teodoro Silva MV, Cirovic B, de Bree LCJ, Damen M, et al. beta-Glucan-Induced Trained Immunity Protects against *Leishmania braziliensis* Infection: a Crucial Role for IL-32. *Cell Rep.* 2019;28(10):2659-72 e6.
502. Cirovic B, de Bree LCJ, Groh L, Blok BA, Chan J, van der Velden W, et al. BCG Vaccination in Humans Elicits Trained Immunity via the Hematopoietic Progenitor Compartment. *Cell Host Microbe.* 2020.
503. de Bree LCJ, Marijnissen RJ, Kel JM, Rosendahl Huber SK, Aaby P, Benn CS, et al. Bacillus Calmette-Guerin-Induced Trained Immunity Is Not Protective for Experimental Influenza A/Anhui/1/2013 (H7N9) Infection in Mice. *Front Immunol.* 2018;9:869.
504. Smith W, Andrewes CH, and Laidlaw PP. A virus obtained from influenza patients. *Lancet.* 1933;2:66-8.
505. Burnet FM. Influenza virus infections of the chick embryo lung. *Brit J Exp Pathol.* 1940;21(3):147-53.
506. Ayres JS, and Schneider DS. Tolerance of infections. *Annu Rev Immunol.* 2012;30:271-94.
507. Killip MJ, Fodor E, and Randall RE. Influenza virus activation of the interferon system. *Virus Research.* 2015;209:11-22.
508. Balachandran S, and Rall GF. Benefits and Perils of Necroptosis in Influenza Virus Infection. *Journal of virology.* 2020;94(9):e01101-19.
509. Fielding JE, Kelly HA, Mercer GN, and Glass K. Systematic review of influenza A(H1N1)pdm09 virus shedding: duration is affected by severity, but not age. *Influenza Other Respir Viruses.* 2014;8(2):142-50.
510. Wolk K, Kunz S, Witte E, Friedrich M, Asadullah K, and Sabat R. IL-22 increases the innate immunity of tissues. *Immunity.* 2004;21(2):241-54.
511. Lee AJ, Chen B, Chew MV, Barra NG, Shenouda MM, Nham T, et al. Inflammatory monocytes require type I interferon receptor signaling to activate NK cells via IL-18 during a mucosal viral infection. *J Exp Med.* 2017;214(4):1153-67.
512. Nguyen KB, Cousens LP, Doughty LA, Pien GC, Durbin JE, and Biron CA. Interferon α/β -mediated inhibition and promotion of interferon γ : STAT1 resolves a paradox. *Nature Immunology.* 2000;1(1):70-6.
513. Redford PS, Mayer-Barber KD, McNab FW, Stavropoulos E, Wack A, Sher A, et al. Influenza A Virus Impairs Control of Mycobacterium tuberculosis Coinfection Through a Type I Interferon Receptor-Dependent Pathway. *The Journal of Infectious Diseases.* 2013;209(2):270-4.

514. Crow MK, Olfertiev M, and Kirou KA. Type I Interferons in Autoimmune Disease. *Annu Rev Pathol.* 2019;14:369-93.
515. Flajnik MF, and Kasahara M. Origin and evolution of the adaptive immune system: genetic events and selective pressures. *Nat Rev Genet.* 2010;11(1):47-59.
516. Sánchez-Ramón S, Conejero L, Netea MG, Sancho D, Palomares Ó, and Subiza JL. Trained Immunity-Based Vaccines: A New Paradigm for the Development of Broad-Spectrum Anti-infectious Formulations. *Frontiers in Immunology.* 2018;9(2936).
517. Uccellini MB, and García-Sastre A. ISRE-Reporter Mouse Reveals High Basal and Induced Type I IFN Responses in Inflammatory Monocytes. *Cell Rep.* 2018;25(10):2784-96.e3.

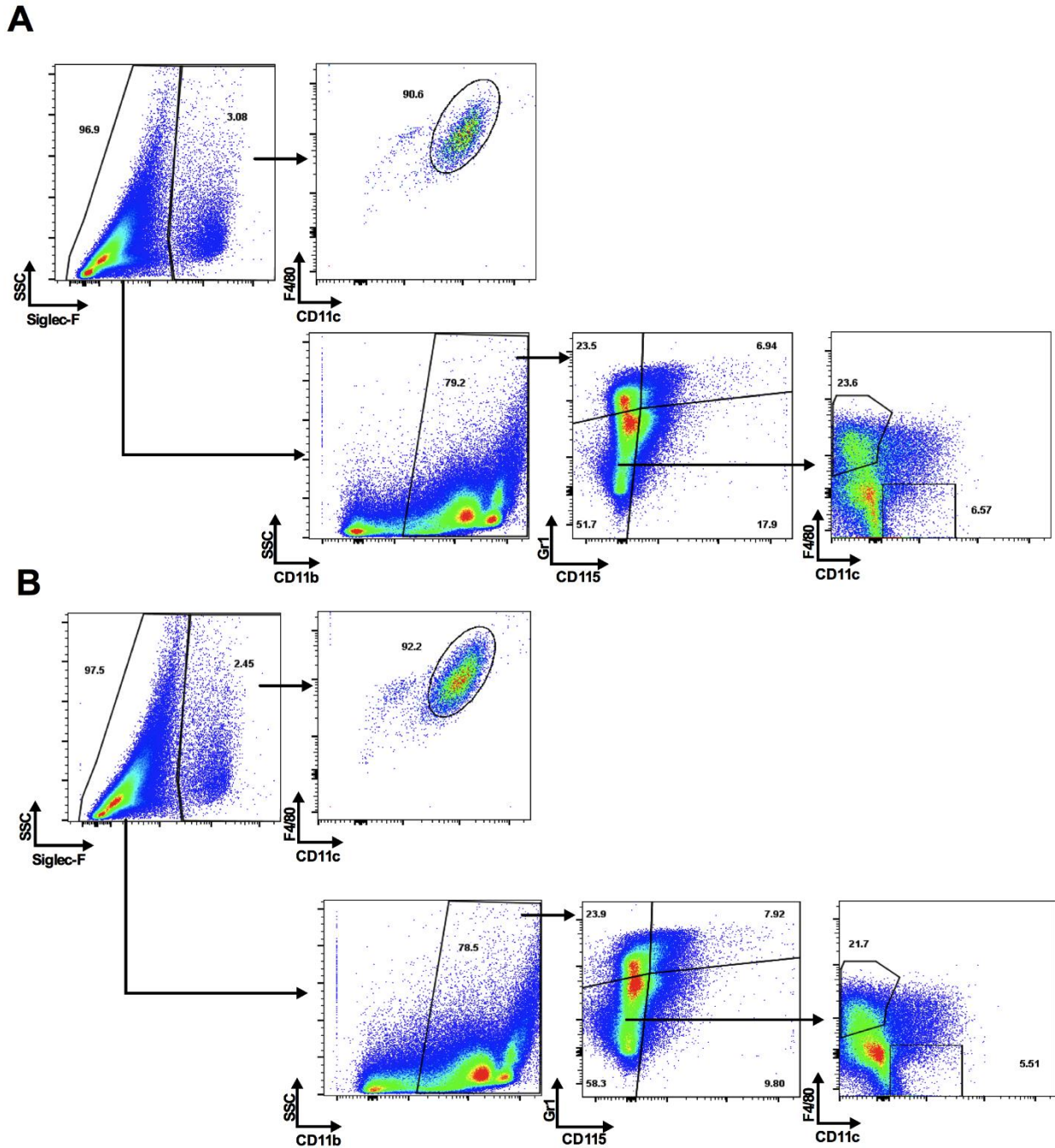
APPENDICES:

Appendix 1: Supplementary Figures for Chapter 2 (1.1-1.5)

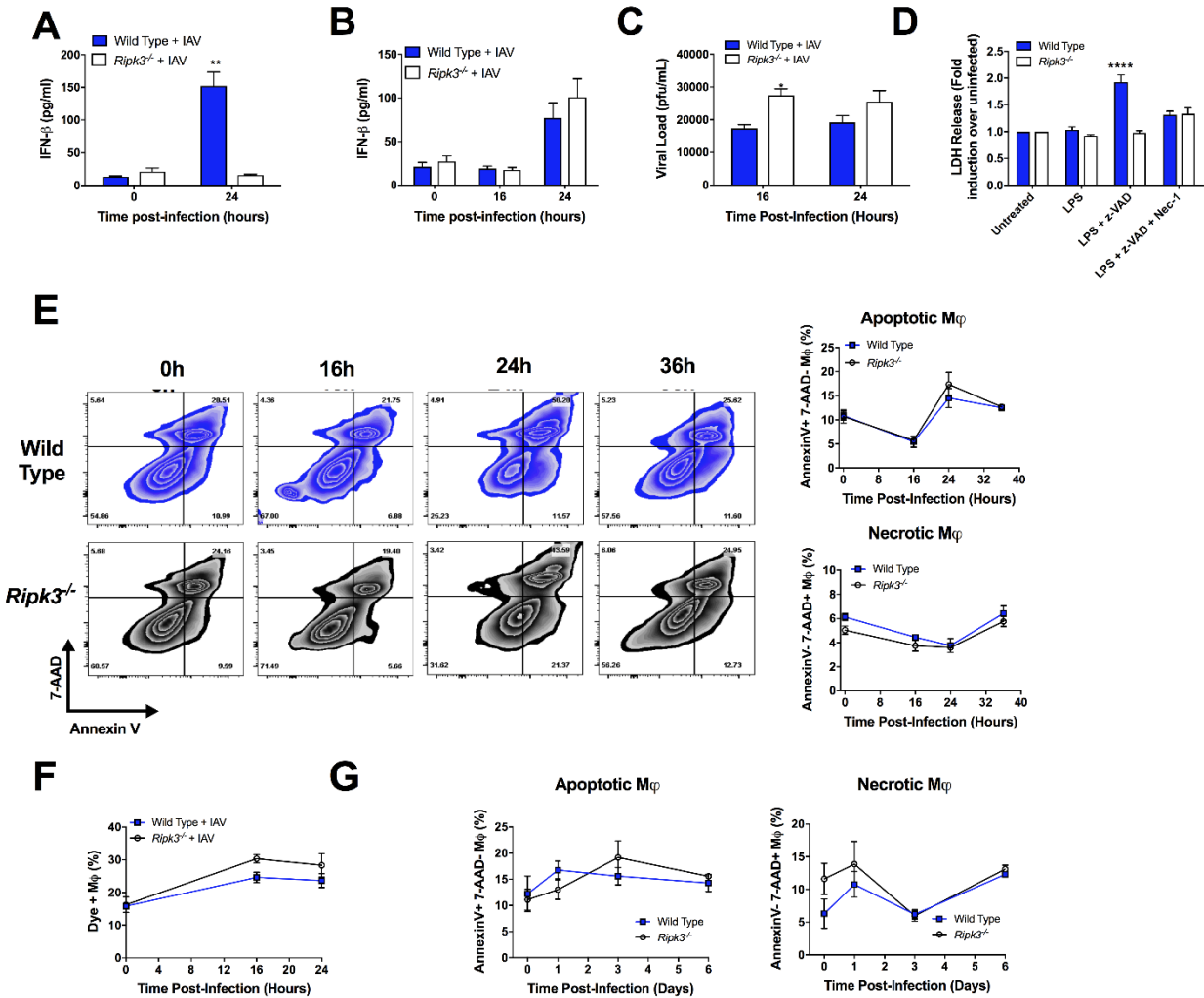
Appendix 2: Supplementary Figures for Chapter 3 (2.1-2.5)

Appendix 3: Supplementary Figures for Chapter 4 (3.1-3.7)

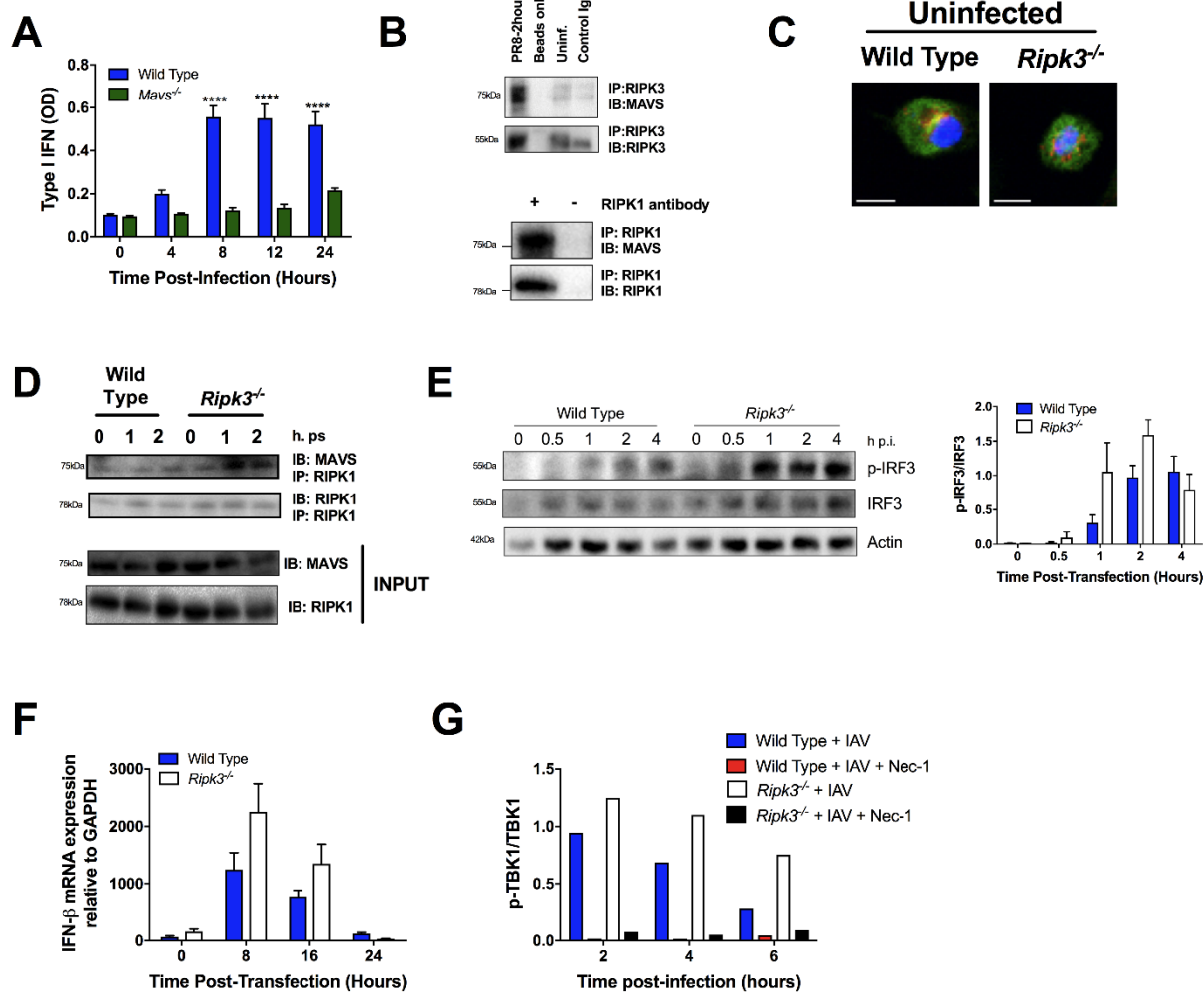
Appendix 4: Supplementary Figures for Chapter 5 (4.1)



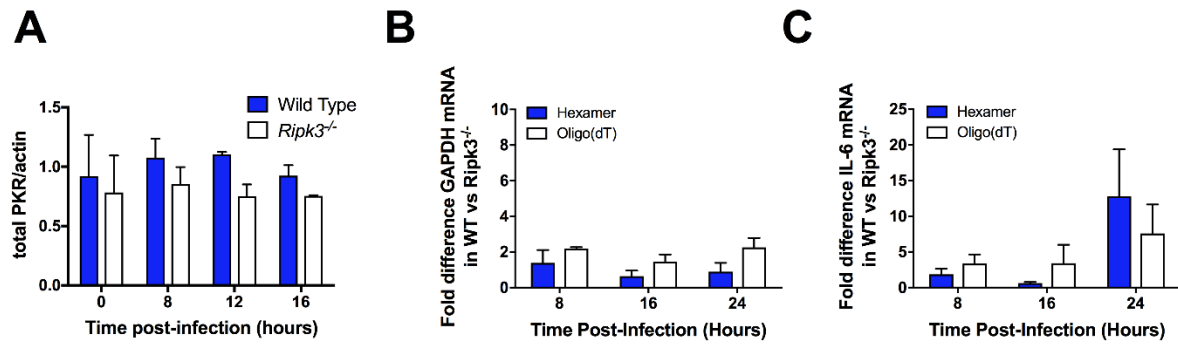
Appendix 1.2. Gating strategy to identify innate immune cells in the BAL of infected mice. Representative pseudocolor plots of the flow cytometry gating strategy of various innate leukocytes of the BAL of WT (A) and *Ripk3*^{-/-} (B) mice at 3 days post-infection with a sublethal dose of IAV. Total cell counts are quantified in Fig 1F. Numbers in proximity to each gate are the percentage of cells within that gate. M ϕ are described as AM (Siglec F⁺, CD11c⁺, F4/80⁺) or IM (Siglec F⁻, CD11b⁺, Gr1⁻, CD115⁻, F4/80⁺, CD11c⁻). Dendritic cells are considered Siglec F⁻, CD11b⁺, Gr1⁻, CD115⁻, F4/80⁻, CD11c⁺ and neutrophils are Siglec F⁻, CD11b⁺, Gr1⁺, CD115⁻. Monocytes are inflammatory (“Inflam Mono” Siglec F⁻, CD11b⁺, Gr1⁺, CD115⁺) or residential (“Res Mono” Siglec F⁻, CD11b⁺, Gr1⁻, CD115⁺).



Appendix 1.3. *Ripk3*^{-/-} MΦ are impaired in their anti-viral capacity, independent of cell death. (A) AMΦ from WT and *Ripk3*^{-/-} mice were infected with IAV (MOI 5) and IFN-β levels were assessed in supernatants 24 hours post infection by ELISA. (B) BMDC from WT and *Ripk3*^{-/-} mice were infected with IAV (MOI 1) and IFN-β levels were assessed in supernatants by ELISA. (C) The viral load in culture supernatants of infected BMD-MΦ (MOI 1) was determined by standard plaque assay. (D) WT and RIPK3-deficient BMD-MΦ were pretreated with various combinations of zVAD (25μM) and Nec-1 (10μM) and LPS (100 ng/mL) for 24 hours. Cell death levels were assessed by LDH assay in cell culture supernatants. (E) The frequency of IAV-infected (MOI 1) MΦ undergoing apoptosis (Annexin V⁺, 7-AAD⁻) (top panel), or necrosis (Annexin V⁺, 7-AAD⁺) (bottom panel) was determined by flow cytometry, with representative zebra plots shown (left panels). The frequency of dead WT or *Ripk3*^{-/-} BMD-MΦ infected with IAV (MOI 1) was measured by flow cytometry, following staining with LIVE/DEAD dye (F). (G) WT and *Ripk3*^{-/-} mice were infected with IAV (50 pfu) and the percentage of MΦ (F4/80⁺, CD19⁻) undergoing apoptosis (left panel) or necrosis (right panel) was determined in the BAL using the same assay as in E. Refers to Fig 2.

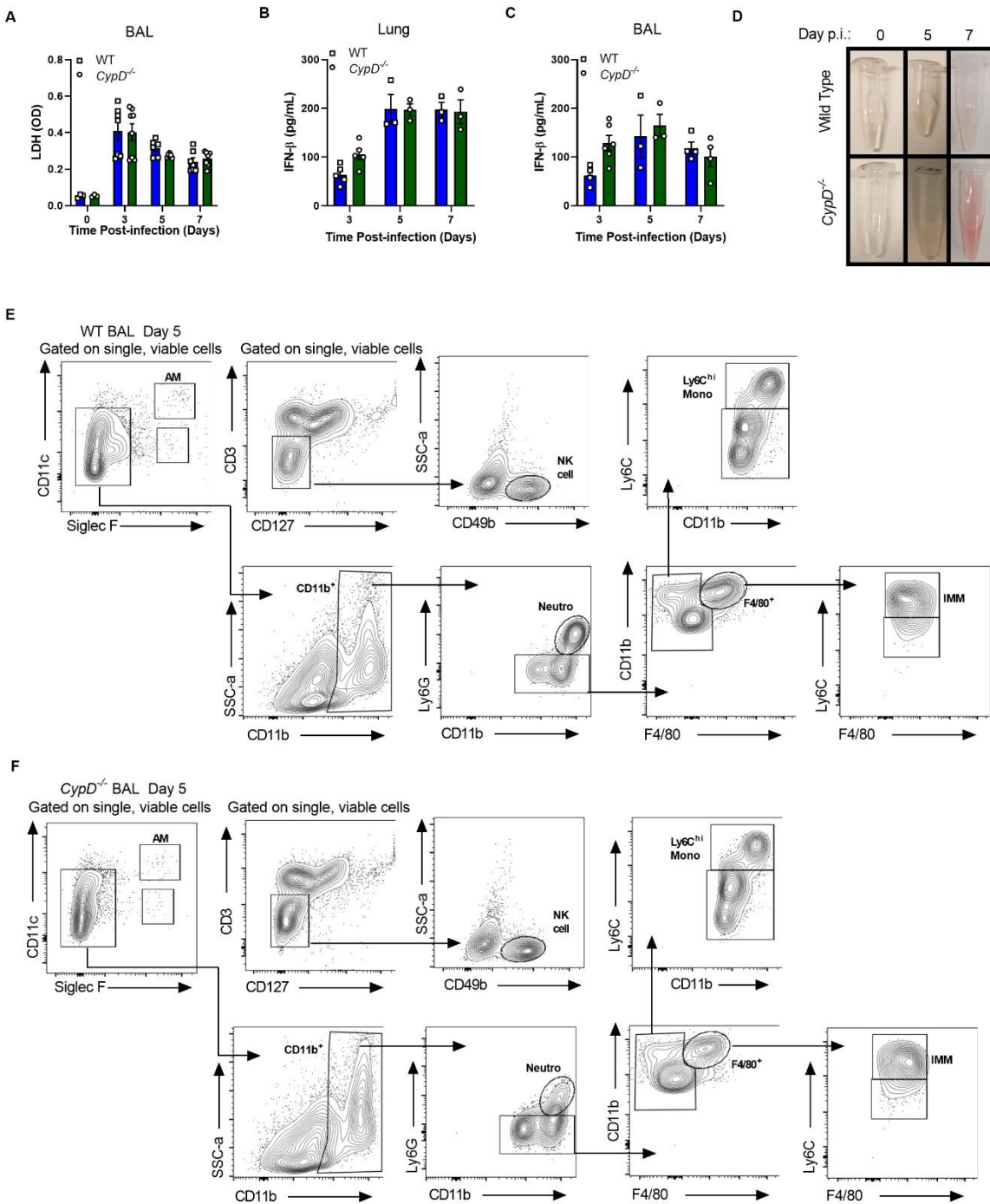


Appendix 1.4. RIPK3 regulates MAVS-dependent type IFN pathway activation. (A) WT and *Mavs*^{-/-} BMD-Mφ were infected with IAV at MOI of 5. Supernatants were collected for relative quantification of total active type I IFN (α and β) using B16-blue reporter cells. (B) Immunoprecipitations were performed with beads only or control IgG to ensure specificity. (C) Immunofluorescence analysis of colocalization of RIPK1 (green) and mitochondria (red) in uninfected WT and *Ripk3*^{-/-} BMD-Mφ. Nuclei were stained with Hoechst (blue). Scale bar = 10 μ m in relation to Fig 3C-E. (D-F) WT and *Ripk3*^{-/-} BMD-Mφ were transfected, or not, with 1 μ g/mL of the RIG-I ligand 5'ppp dsRNA. (D) Following transfection, interaction of RIPK1 with MAVS was determined as in Fig 3E. (E) Phosphorylation of IRF3 was determined by western blot (n=3) and densitometry analysis of the ratio of pIRF3 on total IRF3 is shown on right panel. (F) Expression of antiviral IFN- β mRNA was assessed by qPCR. (G) Densitometry analysis of the ratio of pTBK1 on total TBK1 related to Fig 3H.

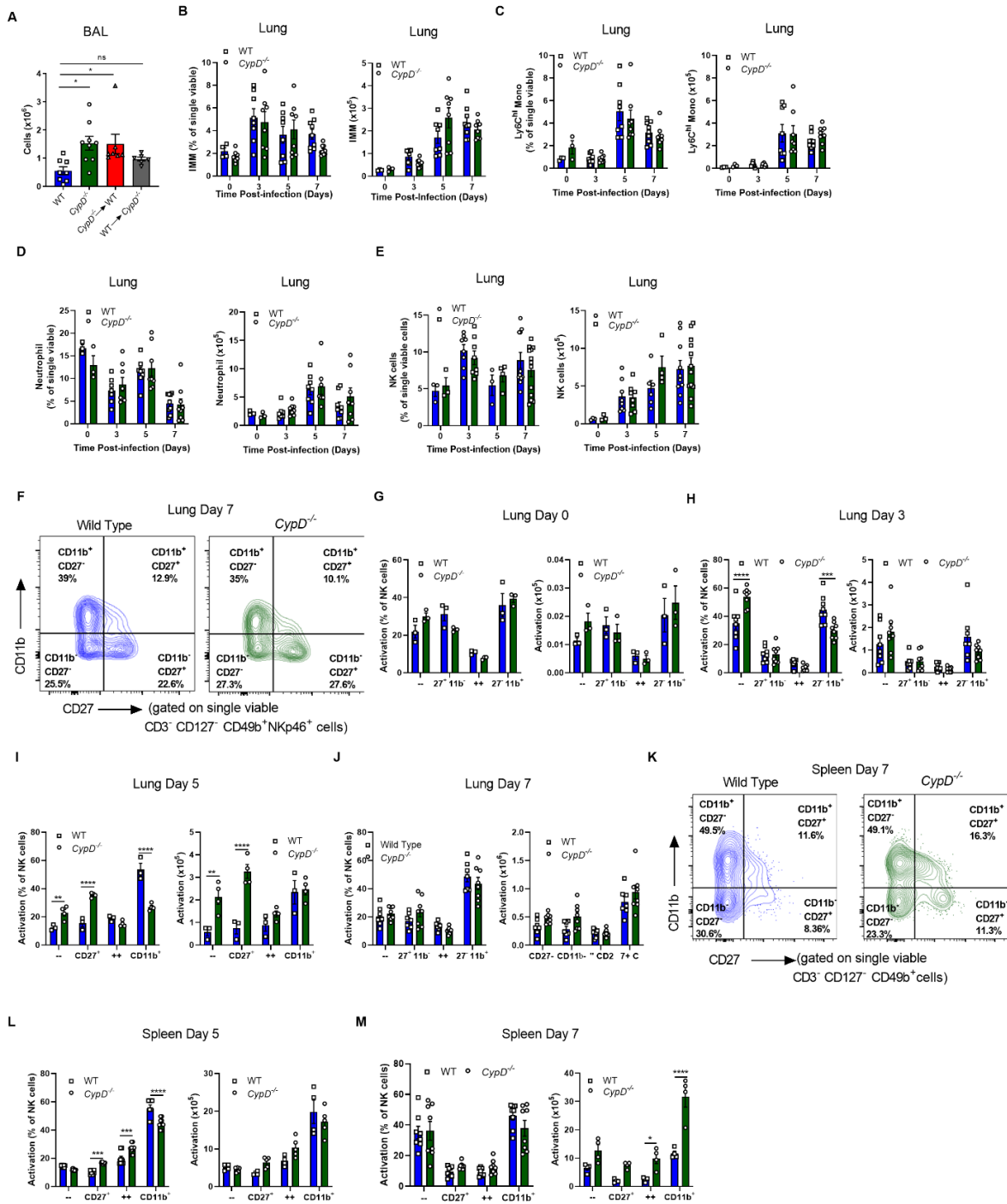


Appendix 1.5. RIPK3 activates PKR in IAV-infected M Φ to stabilize IFN- β mRNA. (A) Densitometry analysis of the expression of PKR at different time points in WT and *Ripk3*^{-/-} BMD-M Φ infected with IAV (MOI 5). (B-C) Difference in the expression of *GAPDH* (B) and *IL-6* (C) between WT and *Ripk3*^{-/-} BMD-M Φ infected with IAV. Gene expression was analyzed by qPCR following cDNA generation using random hexamers (blue bars) or oligo(dT) primers (white bars), as in Fig 4F.

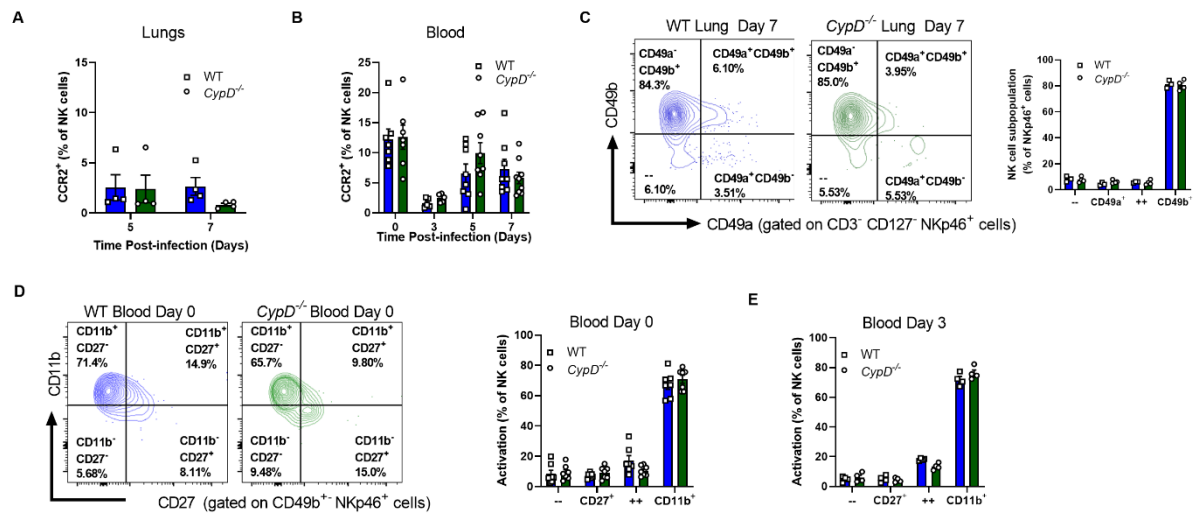
APPENDIX 2:



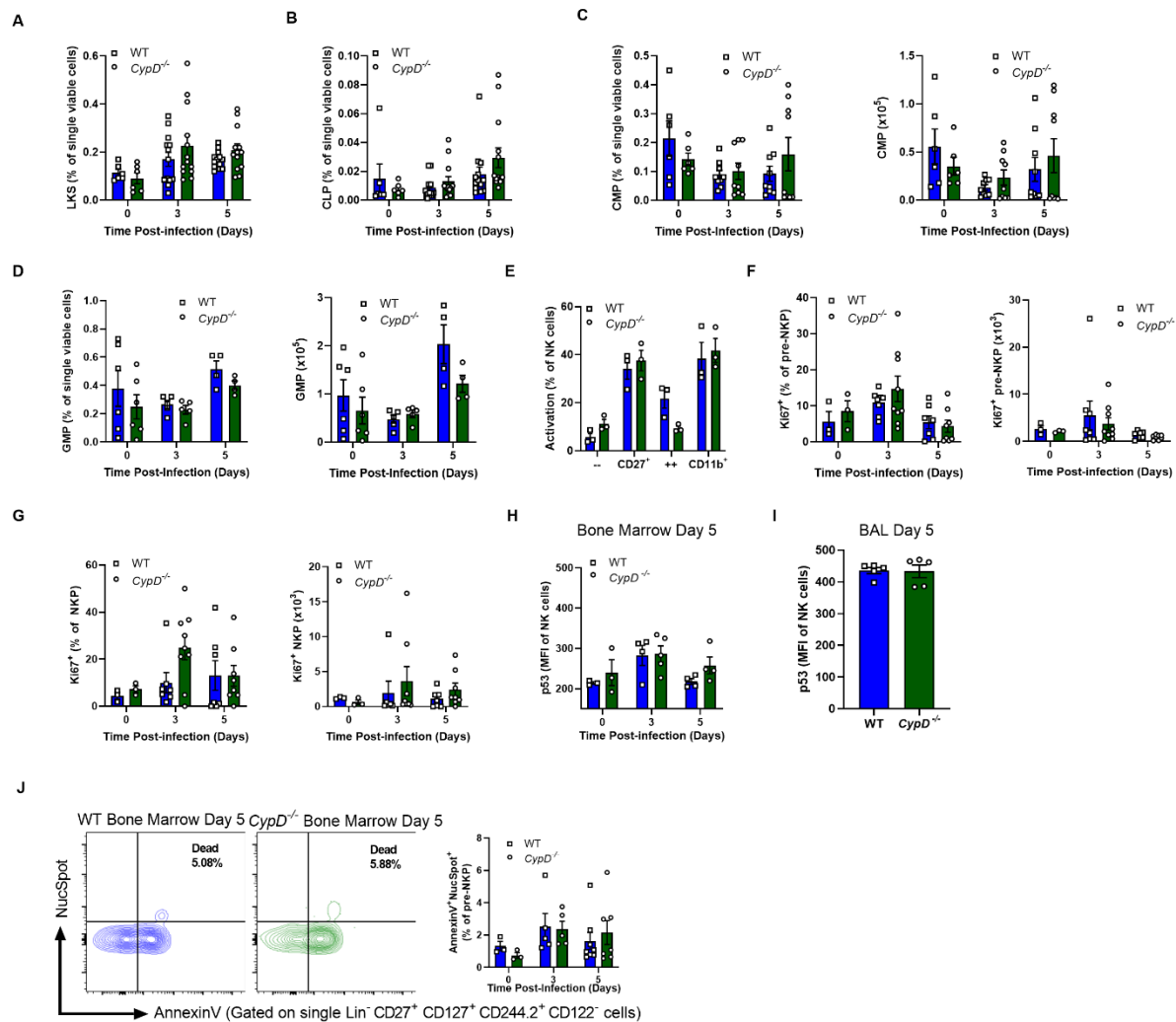
Appendix 2.1: Susceptibility of *CypD*-deficient is due to disease tolerance and not host resistance mechanisms. (A-D) Mice were infected with 50 PFU of IAV and levels of LDH in the BAL (A), IFN- β in the lung (B) or BAL (C) were quantified. (D) Representative pictures of the BAL of mice over the course of infection as quantified in **Figure 1H**. Gating strategy for WT (E) and *CypD*^{-/-} mice used to quantify innate cells in the study. In panels A-C, each symbol indicates a separate mouse. Panel A is a compilation of two independent experiments and B-C are from one experiment. In panels A-C differences were assessed by Two-way ANOVA followed by Sidak's multiple comparisons test.



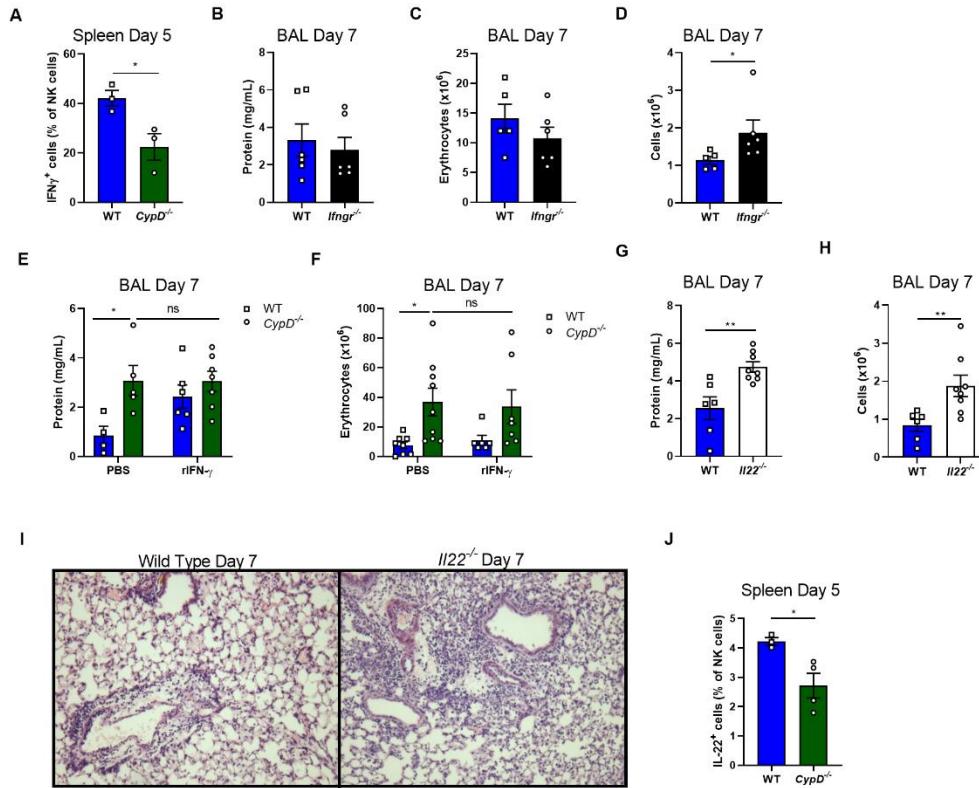
Appendix 2.2: Kinetics and activation of NK cells. (A-M) Mice were infected with 50 PFU of IAV. (A) Total cell counts in the BAL of chimeric mice at 7 days post-infection. (B-E) Frequencies (left panels) and total cell counts (right panels) of (IMM), Ly6C^{hi} monocytes (D), neutrophils (E) and NK cells (F) in the lung. (F-J) Activation states of NK cells in the lung taken at steady-state (G), day 3 (H), day 5 (I) and day 7 (J) post-infection, with frequencies in the left panels and total cell counts on the right. (F) Representative FACS plots of day 7 and quantified as part of J. (K) Representative FACS plot of the CD11b versus CD27 expression on splenic NK cells at day 7 post-infection. Frequencies (left panels) and total cell counts (right panels) of NK cell activation in the spleen at day 5 (L) and day 7 (M). In each panel, each shape represents an individual mouse. Each panel is a compilation of two individual experiments, except G and I which are one individual experiment. Statistical differences were determined by One-way ANOVA followed by Dunnett's test in A, or Two-way ANOVA followed by Sidak's multiple comparisons test in all other panels.



Appendix 2.3: Kinetics of recruited NK cells in the lung and blood. (A-E) Mice were infected with 50 PFU of IAV. The percentage of CCR2-expressing NK cells in the lung (A) and blood (B). (C) Differential expression of CD49b and CD49a in the lung, with a representative FACS plot on the left and quantified on the right. (D-E) Activation status of NK cells in the blood in uninfected (D; representative FACS plot on the left) and day 3 (E) post-infection. Symbols indicate an individual mouse and B-D are compilations of two individual experiments and A, C and E are one representative experiment of two. Statistical differences were assessed by Two-way ANOVA followed by Sidak's multiple comparisons test for all panels.

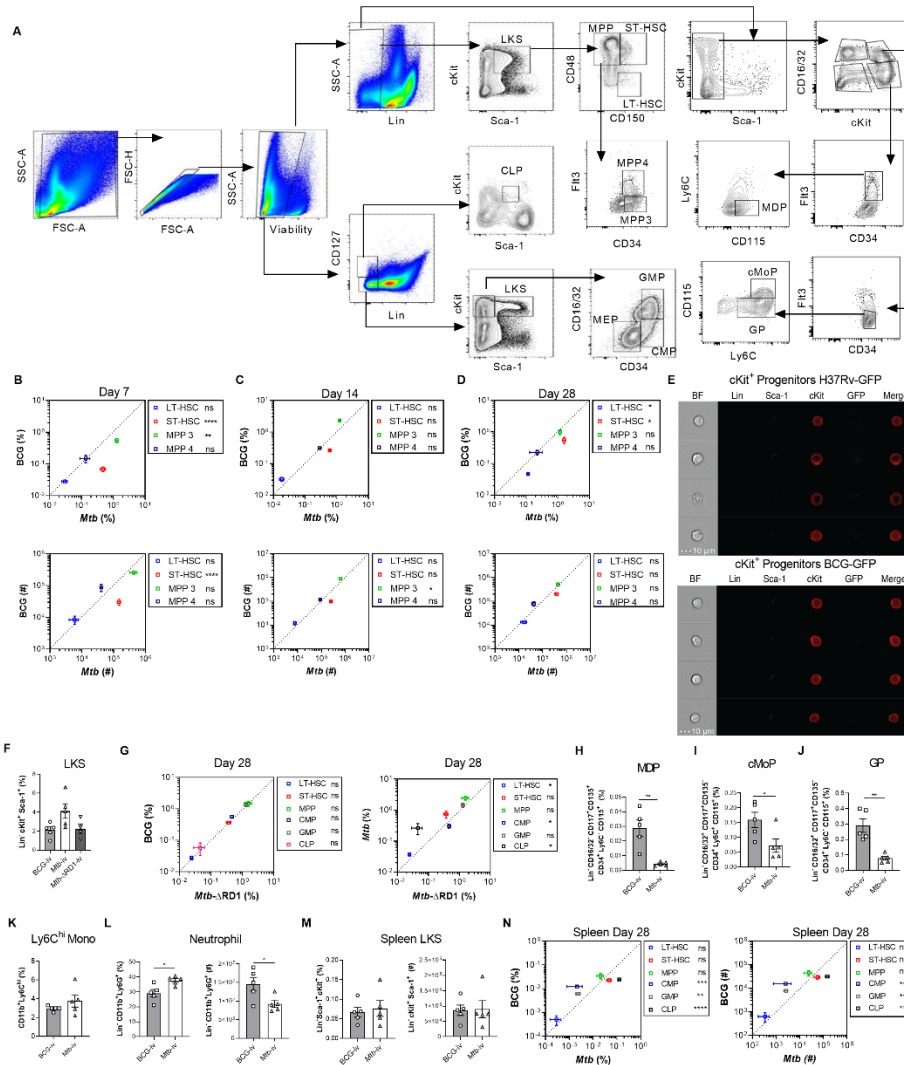


Appendix 2.4: NK cell hematopoiesis in the bone marrow of WT and *CypD*-deficient mice. (A-J) Mice were infected with 50 PFU of IAV and phenotyped by flow cytometry. Frequencies of LKS (B) and CLPs (C) following infection. Frequencies (left panels) and total cell counts (right panels) of CMPs (C) and GMPs (D). Relative activation states of NK cells in the BM (E) as well as the percentage (left panels) and total cell counts (right panels) of Ki67-expressing pre-NKPs (F) and NKPs (G). Level of expression of p53 in mature NK cells in the bone marrow (H) and BAL (I) at day 5 post-infection. (J) Representative FACS plot (left panel) and quantification (right panel) of cell death in pre-NKPs as determined by AnnexinV and NucSpot staining. In all panels, each symbol is data from one individual mouse; in panels A-D, F, G and J, data are compilations from at least 2 experiments and in E, H and I data are representative of one experiment of two unique experiments. In figures A-H and J, differences were investigated by Two-way ANOVA followed by Sidak's multiple comparisons test and in I by Two-tailed Student's T-test.

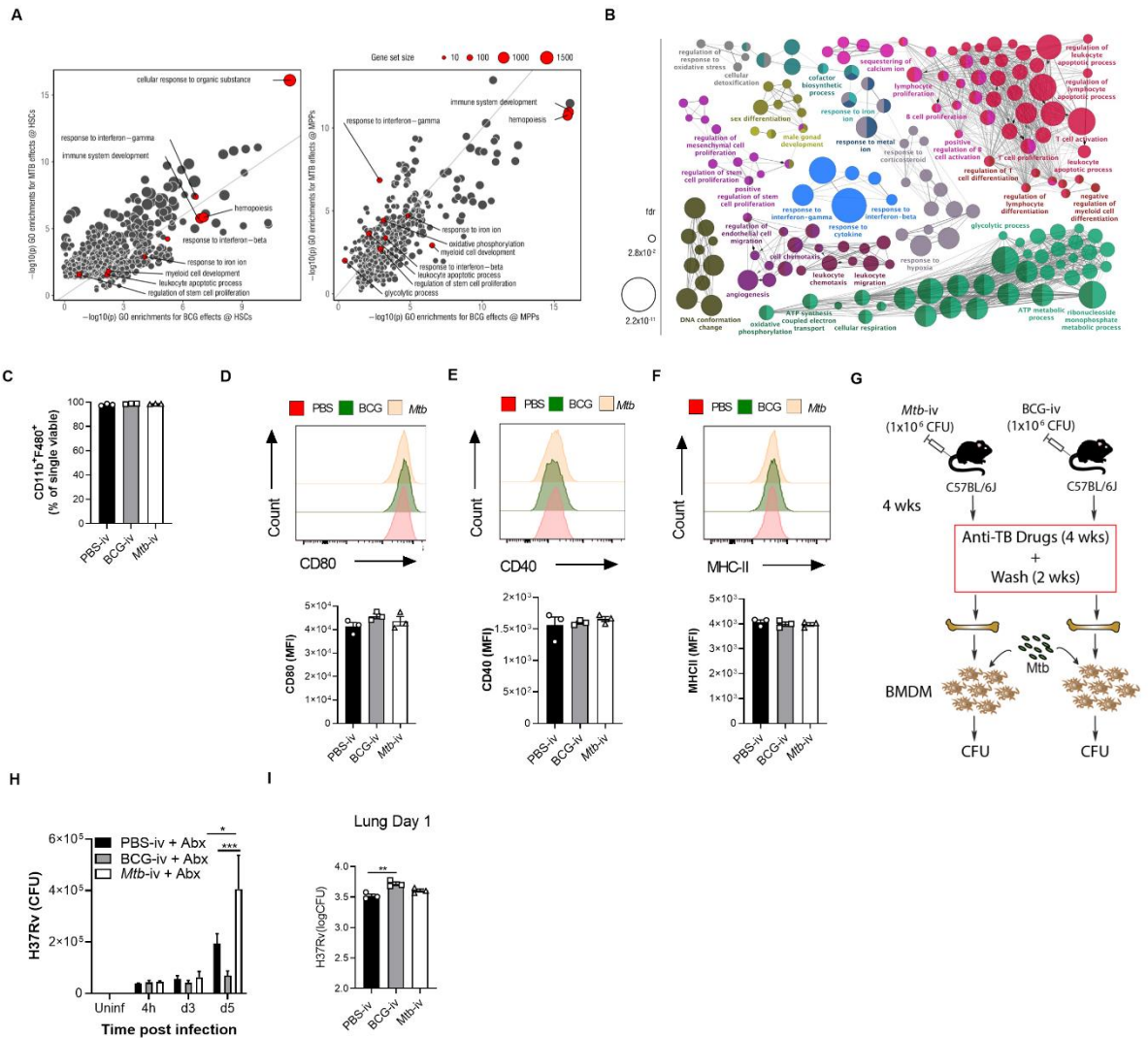


Appendix 2.5: Disease tolerance is mediated by IL-22 and not IFN- γ following IAV infection. (A-K) Mice were infected with 50 PFU of IAV. (A) The frequency of IFN- γ -producing splenic NK cells at day 5 post-infection. (B-D) WT and *Ifngr*^{-/-} mice were infected and the levels of protein (B), erythrocytes (C) and total cells (D) in the BAL at 7 days post-infection were determined. Following administration of recombinant IFN- γ , levels of protein (E) and erythrocytes (F) were assessed in the BAL. (G-I) WT and IL-22-deficient mice were infected and amount of protein (G) and number of cells (H) were enumerated, as well as pulmonary inflammation by hematoxylin and eosin staining (I). (J) Frequency of IL-22-producing NK cells in the spleens of WT and *CypD*-deficient mice at 5 days post-IAV infection. In all panels except I, symbols represent an individual mouse. In I, micrographs are a representative image taken from one of four mice. In A and J, data are taken from one experiment that is representative of three. In B-I, panels are a compilation of two individual experiments. Differences were determined as follows: in A-D, G-H and J Two-tailed Student's T-test; in E and F Two-way ANOVA followed by Tukey's multiple comparisons test.

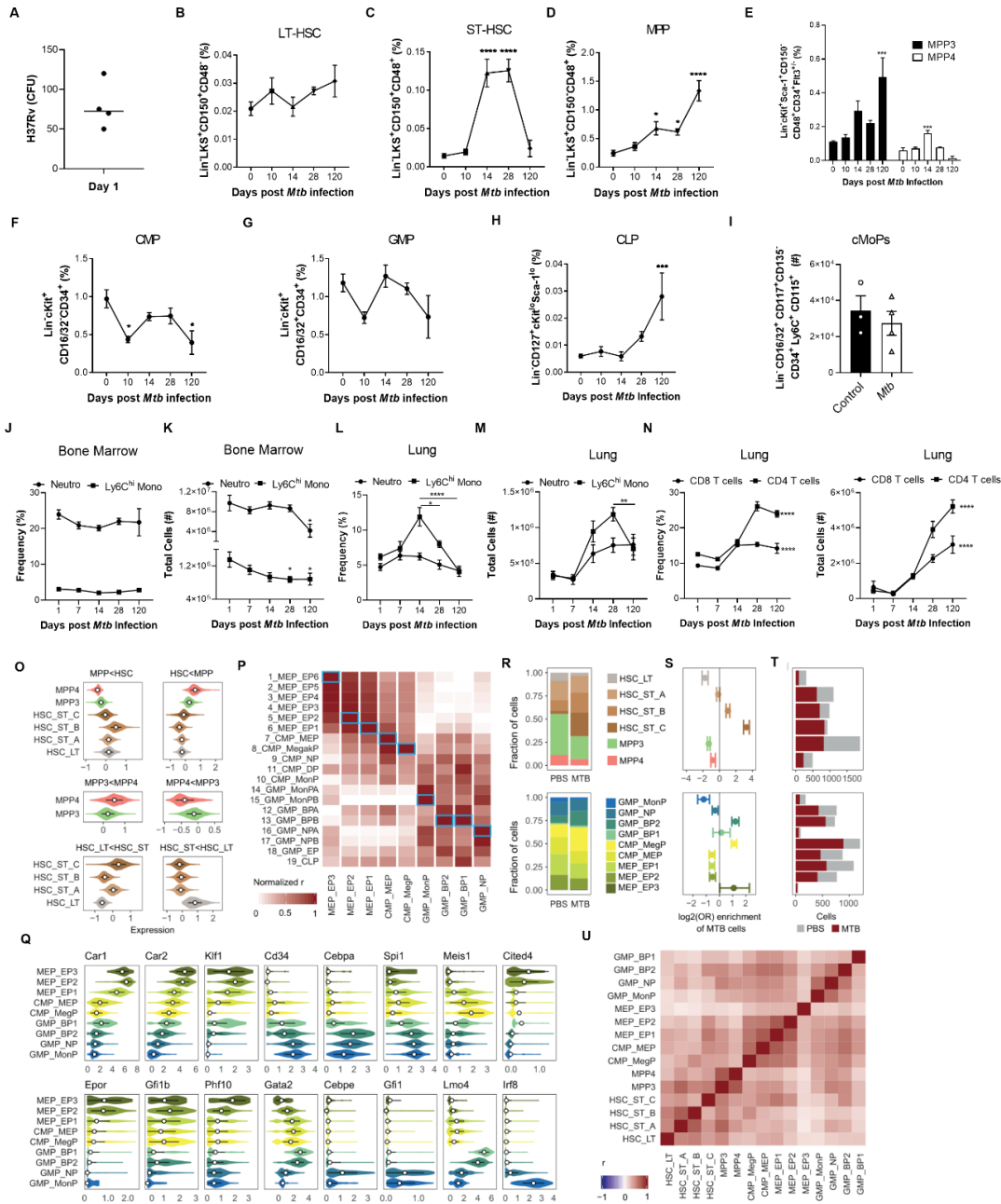
APPENDIX 3:



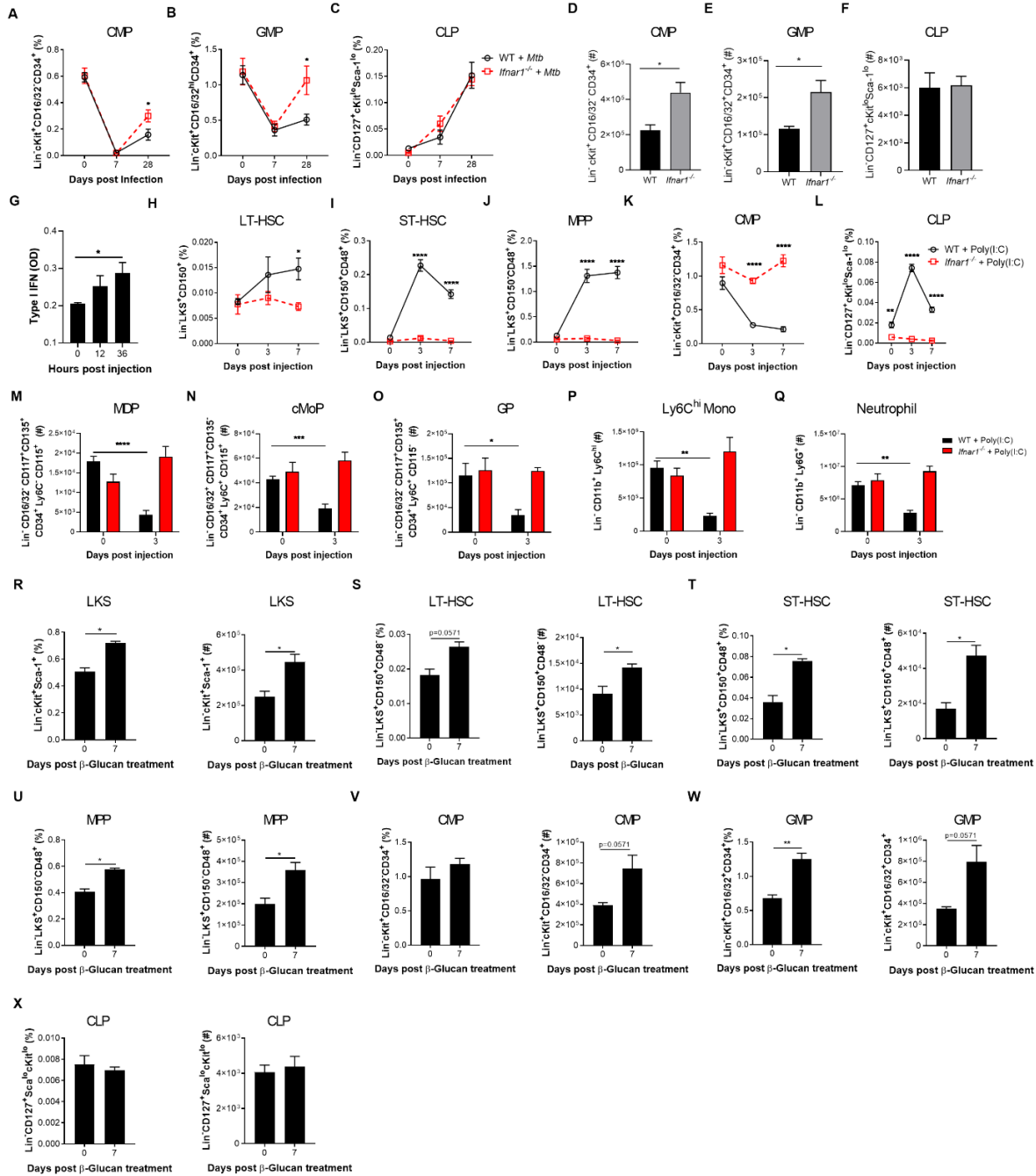
Appendix 3.1: Gating strategy for HSCs and progenitors and their kinetics post-infection. (A) Cells were gated for FSC-A against SSC-A. Doublets were excluded using FSC-H against FSC-A and subsequently SSC-H against SSC-A. Viable cells were gated and lineage-committed cells were excluded. Within the lineage-negative population, cells were gated as LKS-defined as cKit and Sca-1. Gated on the LKS population, cells were divided into LT-HSC, ST-HSC and MPP based on CD150 and CD48 expression. MPPs were characterized as MPP3 or MPP4 by their surface expression of CD34 and Flt3. In a second strategy, lineage negative cells were gated based on CD127⁺ and CD127⁻. Lin⁻ CD127⁻ population was further defined by Sca-1 and c-Kit. c-Kit⁺ Sca-1⁻ cells were further gated based on CD34 and CD16/32 to define CMP, GMP and MEP. Lineage⁻ and CD127⁺ cells are defined as CLPs based on Sca-1^{lo} and c-Kit^{lo} expression. Finally, in another set of experiments, Lineage⁺ cells and then Sca-1⁺ cells were excluded. The remaining cells were further subdivided into cKit⁺ CD16/32⁺ and cKit⁺ CD16/32⁻ groups. In the cKit⁺ CD16/32⁻ group, CD34⁺ Flt3⁺ cells were denoted as MDP by being CD115⁺ but Ly6C⁻. cKit⁺ CD16/32⁻ cells were further gated on CD34⁺ Flt3⁻ cells. Within this fraction, Ly6C⁺ CD115⁻ cells were the GP and Ly6C⁺ CD115⁺ were cMoP. (B-D) Kinetics of the frequency among single viable BM cells (top panel) and total cell counts (bottom panel) of LT-HSC, ST-HSC, MPP3/MPP4 in the BM of BCG-iv vaccinated or *Mtb*-iv infected mice. (E) BM cells from WT mice were infected with BCG-GFP or H37Rv-GFP for 4 hours *in vitro* (MOI 3). ImageStream analysis of H37Rv-GFP infection (top panel) and BCG-GFP (bottom panel) in Lin⁻ cKit⁺ Sca-1⁻ progenitors. (F-G) Mice were intravenously infected with 1x10⁶ CFU of BCG, *Mtb* or *Mtb*-ARD-1 for 28 days. Frequency of LKS in each group (F) and HSC/progenitor subsets of BCG versus *Mtb*-ARD-1 (G; left panel) or *Mtb* versus *Mtb*-ARD-1 (G; right panel). (H-N) 1x10⁶ CFU of BCG or *Mtb* were delivered intravenously for 28 days. Percentage of MDP (H), cMoP (I), GP (J) and Ly6C^{hi} monocytes (K) in the BM and frequency and total numbers of neutrophils (L). (M-N) Frequency and total LKS cells (M), as well as the frequency and total cell number of the HSC/progenitor fractions in BCG versus *Mtb*-infected mice in the spleen after 28 days (N). All data are expressed as mean ± SEM. *p<0.05, **p<0.01, ***p<0.001, ****p<0.0001 as assessed by Two-tailed Student's T-Test for each individual cell population in B-D and G-N or One-way ANOVA followed by Tukey's Multiple Comparisons Test in F.



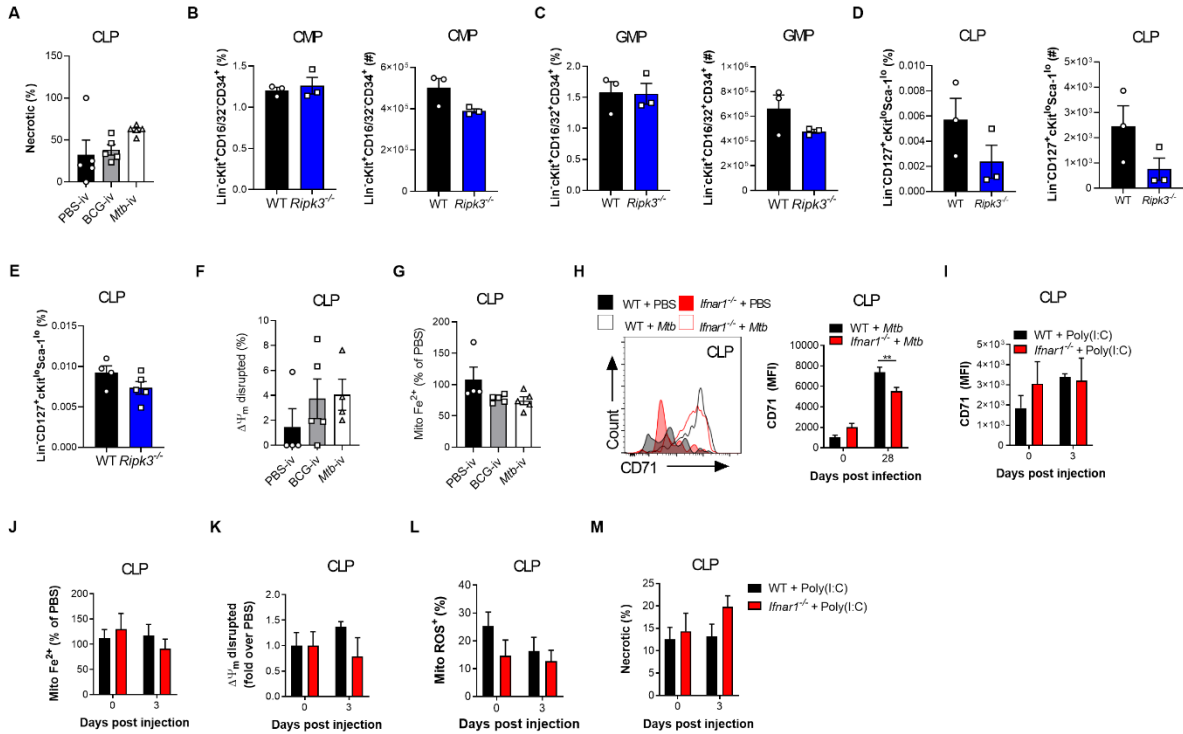
Appendix 3.2: HSC imprinting by BCG and *Mtb-iv* and subsequent antimycobacterial responses by macrophages to *Mtb* infection *in vitro*. (A) Scatter plot for significance levels ($-\log_{10}(p \text{ value})$) of gene ontology enrichment analyses conducted among DE genes upon BCG vs *Mtb* infections in HSC (left) and MPP (right). (B) Gene ontology terms enriched among genes differentially expressed in response to *Mtb* in MPP (at $FDR < 0.01$). (C-F) BMDM from PBS control, BCG-iv and *Mtb-iv* groups were generated. Purity of BMDM cultures was determined by flow cytometry using expression of BMDM markers CD11b and F4/80 (C). Activation of mature BMDM was assessed by flow cytometry via MFIs of CD80 (D), CD40 (E) and MHC-II (F) with representative histograms in the top panels. Model of *in vivo* antibiotic treatment (G). BMDM-derived from the BM cells of these mice were infected with *Mtb* (H37Rv; MOI 1) and the number of CFU was determined at different time points after infection (H). (I) BMDM CFU prior to intratracheal transfer, as detailed in **Figure 2H-I**. Means are represented \pm SEM. * $p < 0.05$, ** $p < 0.01$, *** $p < 0.001$ as determined by One-way ANOVA followed by Tukey's Multiple Comparisons Test in C-F and I; Two-way ANOVA followed by Tukey's Multiple Comparisons Test in H.



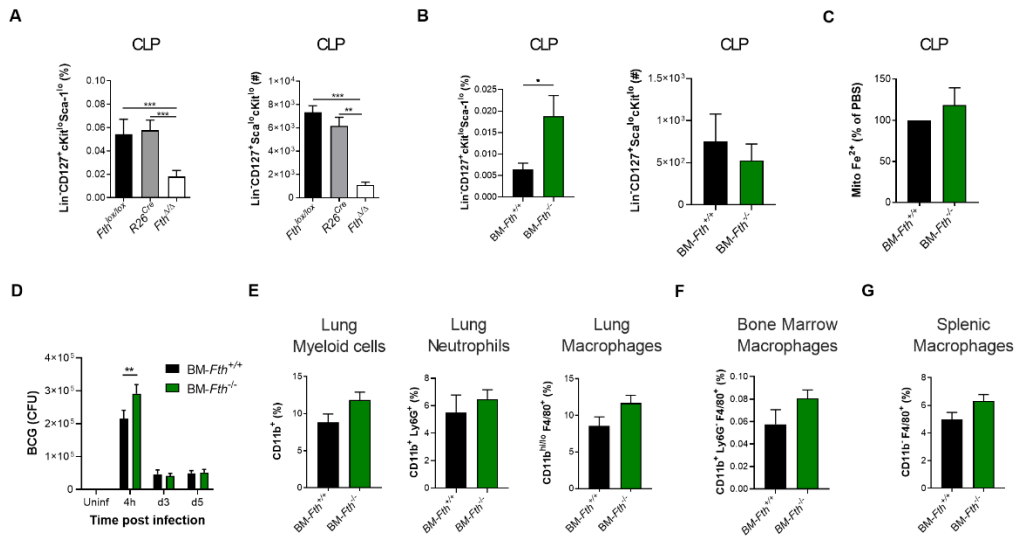
Appendix 3.3: HSC and progenitor kinetics following aerosolized *Mtb* infection. (A-O) WT mice were infected with aerosolized *Mtb*. (A) Day 1 lung CFU following aerosol infection. (B-H) Kinetics of the frequencies among BM cells of LT-HSC (B), ST-HSC (C), MPP (D), MPP3/MPP4 (E), CMP (F), GMP (G), CLP (H) in *Mtb* infected WT mice. (I) Total cell counts cMoPs in the BM of WT mice at 120 days post-infection. Kinetics of the frequencies and total numbers of neutrophils and Ly6C^{hi} monocytes in the BM (J-K) and lung (L-M) as well as the frequencies (N) and total cell counts (O) of adaptive CD8 and CD4 T-cells in the lung. (P) Average expression of cell-type markers across clusters. (Q) Correlations between genome-wide expression patterns of our myeloid progenitor data and results published in Paul et al. 2015. In each column, Spearman correlations are normalized to cover the range [0-1]. Blue boxes mark the best fit (i.e. candidate identity match) for each of our clusters. (R) Expression patterns across clusters for some marker genes associated to commitment to the different lineages characterized in this study. (S) Proportion of cells per cluster in both sub-populations (LKS and myeloid progenitors), for cells coming from PBS vs *Mtb* treated mice. (T) Fisher exact test enrichments (log2 odds ratios) for the fraction of *Mtb* cells in each cluster. (U) Number of PBS vs *Mtb* cells in each cluster. (V) Genome wide correlation of *Mtb* effect sizes (logFC) across clusters. Means are represented \pm SEM. * $p < 0.05$, ** $p < 0.01$, *** $p < 0.001$, **** $p < 0.0001$. (B-H, J-O) One-way ANOVA followed by Tukey's Multiple Comparisons Test with significance shown compared to day 0 or day 1 post-infection mice for each cell type and Two-tailed Student's T-test (I).



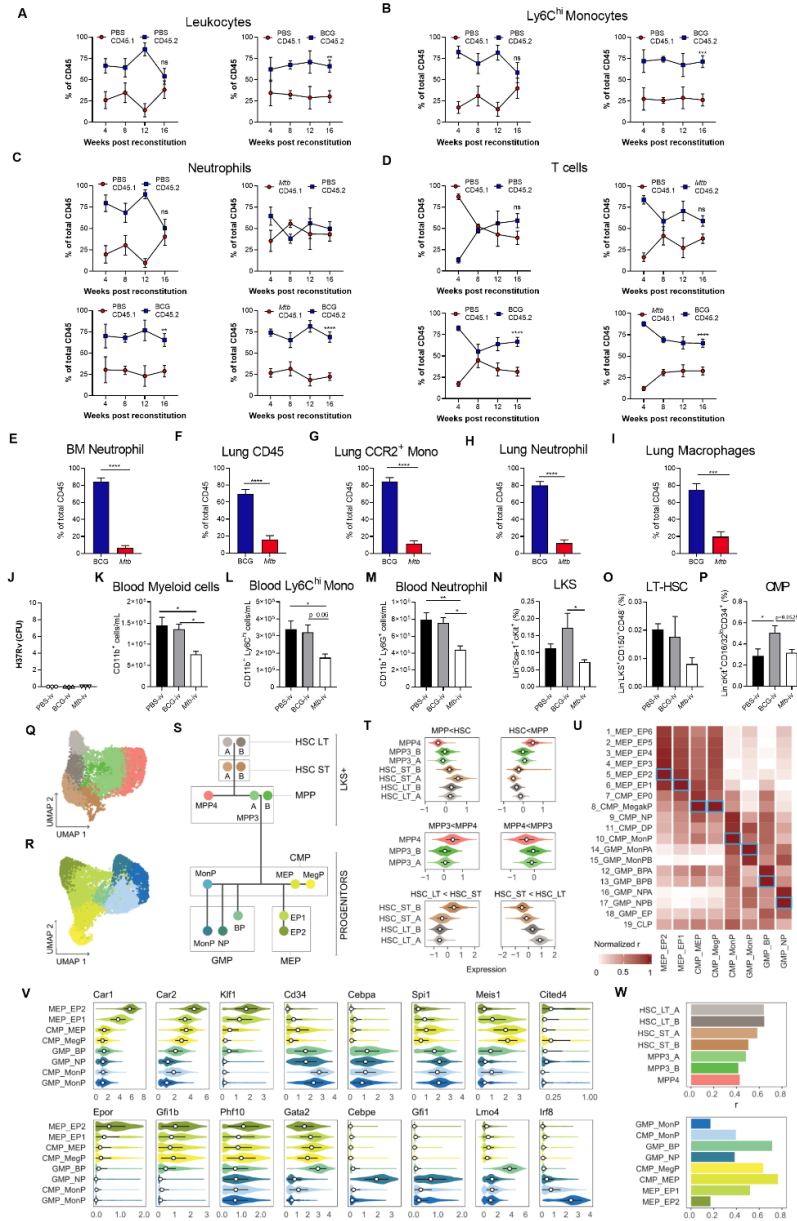
Appendix 3.4: IFN-I signaling impairs myelopoiesis and trained immunity during *Mtb* infection. (A-C) WT and *Ifnar1*^{-/-} mice were infected with *Mtb*-iv with 1x10⁶ bacteria. Kinetics of the frequencies among single viable BM cells of CMP (A), GMP (B) and CLP (C). (D-F) mice were infected with *Mtb* via the aerosol route. Percentages of CMP (D), GMP (E) and CLP (F) in the BM at day 60. (G) Active IFN-I was measured in the BM collected after 12, 24, and 36 hours after Poly (I:C) treatment by B16-Blue Reporter Cells. (H-Q) WT and *Ifnar1*^{-/-} mice were treated with Poly (I:C), or not, at day 0, 2, 4, 6. Frequencies among single viable BM cells of LT-HSC (H), ST-HSC (I), MPP (J), CMP (K) and CLP (L) at days 0, 3 and 7, as well as the total number of MDP (M), cMoP (N), GP (O), Ly6C^{hi} monocytes (P) and neutrophils (Q) at day 3 post-Poly-(I:C) treatment. (R-X) WT mice were treated with β-glucan at day 0 and day 3. Frequencies among BM cells (left panel) and total cell counts (right panel) of LKS (R), LT-HSC (S), ST-HSC (T), MPP (U), CMP (V), GMP (W) and CLP (X) in PBS (day 0) or β-glucan i.p. at day 7 post-treatment in the BM. Means are represented ± SEM. *p<0.05, **p<0.01, ***p<0.001, ****p<0.0001 as determined by Two-way ANOVA followed by Sidak's Multiple Comparisons Test in A-C, H-Q, Two-Tailed Student's T-Test in D-F, Non-Parametric Mann-Whitney Test R-X and One-way ANOVA followed by Dunnett's Multiple Comparisons Test in G.



Appendix 3.5: IFN-I/iron axis regulates cell death of myeloid progenitors. Frequency of necrotic (NucSpot⁺ AnnexinV⁻) CLP (A) in the BM of BCG-iv and *Mtb*-iv infected mice at day 7. (B-D) Frequency among single viable BM cells (left panels) and total cell counts (right panels) of CMP (B), GMP (C), CLP (D) of naïve WT and *Ripk3*^{-/-} mice. (E) Frequency among BM cells of CLP in WT and *Ripk3*^{-/-} *Mtb*-iv infected mice at day 7. (F) Frequency of CLP with disrupted mitochondria in the BM of BCG-iv and *Mtb*-iv infected mice at day 7. (G) Relative levels of mitochondrial iron (Fe²⁺) in CLP of BCG-iv and *Mtb*-iv infected mice at day 7. (H) Representative histogram of expression of CD71 (left panel) and quantification of CD71 expression (right panel) on CLP in the BM of *Mtb*-iv infected WT and *Ifnar1*^{-/-} mice at day 28. (I) Expression of CD71 on CLP in the BM of WT and Poly (I:C)-treated WT and *Ifnar1*^{-/-} mice. (J) Relative proportion of mitochondrial iron dye (Fe²⁺) in the CLP of Poly (I:C)-treated WT and *Ifnar1*^{-/-} mice. Frequency of CLPs with a disrupted mitochondrial potential (K), high mitochondrial ROS (L), or those that are necrotic (M). Means are represented as ± SEM. **p<0.01. One-way ANOVA followed by Tukey’s Multiple Comparison Test (A; F-G), Two-tailed Student’s T-Test (B-E), Two-way ANOVA followed by Sidak’s Multiple Comparisons Test (H-M).

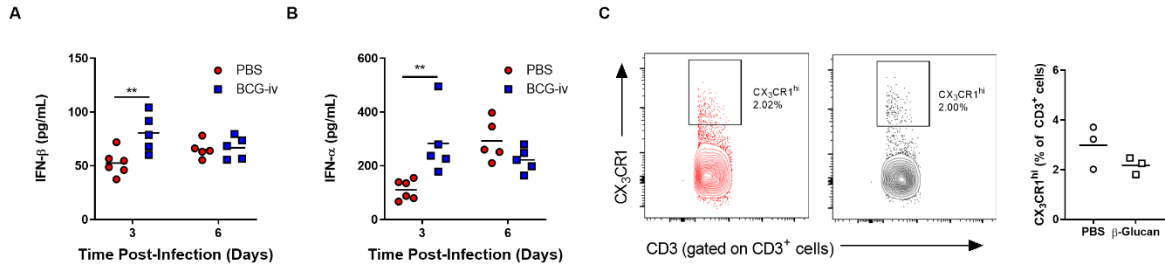


Appendix 3.6: A loss of iron homeostasis disrupts myelopoiesis. (A) Frequency (left panel) and total cell count (right panel) of CLP in *Fth^{ΔΔ}*, *R26^{cre}* or *Fth^{lox/lox}* mice as generated in **Figure 6A**. (B-G) BM-*Fth^{+/+}* or BM-*Fth^{-/-}* chimeric mice were generated as described in **Figure 6D**. Frequency (left panel) and total cell count (right panel) of CLP in BM-*Fth^{+/+}* or BM-*Fth^{-/-}* chimeric mice (B). (C) Relative percentage of iron (Fe²⁺) specific dye in the mitochondria of CLP in the BM of BM-*Fth^{-/-}* compared to BM-*Fth^{+/+}* mice. (D) BCG CFU (infection at MOI 10) in BMDM from BM-*Fth^{+/+}* or BM-*Fth^{-/-}* mice at the indicated timepoints. Frequency of myeloid cell populations in the lungs (E), BM (F) and spleen (G) in naïve BM-*Fth^{+/+}* and BM-*Fth^{-/-}* mice. Means are represented ± SEM. *p < 0.05, **p < 0.01, ***p < 0.001 by One-way ANOVA followed by Tukey's Multiple Comparisons Test (A), Two-tailed Student's T-Test (B-C and E-G), or Two-way ANOVA followed by Sidak's Multiple Comparisons Test (D).



Appendix 3.7: *Mtb*-imprinted HSCs have impaired engraftment up to at least one-year post-exposure. (A-I) Mixed chimeric mice were generated as described in **Figure 7A**. At 4-week intervals post-reconstitution, peripheral blood was sampled. Percentages of CD45.1⁺ versus CD45.2⁺ leukocytes (A), Ly6C^{hi} monocytes (B), neutrophils (C) or T-cells (D) in the blood. At 16 weeks post-reconstitution, BCG:*Mtb* mixed chimera mice were sacrificed. Frequency of neutrophils in the BM (E), as well as pulmonary leukocytes (F), CCR2⁺ monocytes (G), neutrophils (H) and macrophages (I). (J-O) Secondary engraftment experiments were performed as in **Figure 7M**. *Mtb* CFU in the BM cells prior to adoptive transfer to do second engraftment (J). In the peripheral blood, total cell counts of CD11b⁺ cells (K), Ly6C^{hi} monocytes (L) and neutrophils (M) were assessed by flow cytometry. LKS (N), LT-HSC (O) and CMP (P) frequencies were assayed as a percentage of single viable BM cells. (Q-R) UMAP dimensionality reduction plots for LKS and myeloid progenitor cells, respectively, for the serial engraftment experiment. (S) Schematic hematopoietic tree diagram showing the approximated position of the different clusters identified (cluster specific color code common to panels Q-R). (T) Average expression of cell-type markers across clusters. (U) Correlations between genome-wide expression patterns of our myeloid progenitor data and results published in Paul et al. 2015. In each column, Spearman correlations are normalized to cover the range [0-1]. Blue boxes mark the best fit (i.e. candidate identity match) for each of our clusters. (V) Expression patterns across clusters for some marker genes associated to commitment to the different lineages characterized in this study. (W) Genome wide correlation of *Mtb* vs BCG effect sizes (logFC) in each cluster. Means are represented \pm SEM. * $p < 0.05$, ** $p < 0.01$, *** $p < 0.001$ and **** $p < 0.0001$ via Two-Way ANOVA followed by Sidak's Multiple Comparison Test (A-D), Student's Two-tailed T-Test (E-I) and One-Way ANOVA followed by Tukey's Multiple Comparisons Test in (J-O). In A-D, only significant differences at 16 weeks were labelled.

APPENDIX 4:



Appendix 4.1: Immunological readouts in BCG and β -Glucan treated mice. (A-B) Mice were vaccinated with BCG for 28 days and then infected with IAV. After 3 or 6 days of infection mice were sacrificed and the levels of IFN- β (A) or IFN- α (B) were assessed by ELISA in lung homogenates. (C) CX₃CR1 expression on T-cells 7 days post- β -Glucan treatment. Means are represented \pm SEM and differences were assessed by two-way ANOVA followed by Sidak's multiple comparisons test in A and B, or two-tailed Student's T-test in C.